

Surfaces of intermetallics: Quasicrystals and beyond

by

Chad David Yuen

A dissertation submitted to the graduate faculty
in partial fulfillment of the requirements for the degree of
DOCTOR OF PHILOSOPHY

Major: Physical Chemistry

Program of Study Committee:
Patricia A. Thiel, Major Professor
James W. Evans
Gordon J. Miller
Thomas Greenbowe
Mark Gordon

Iowa State University

Ames, Iowa

2012

Copyright © Chad David Yuen, 2012. All rights reserved.

Dedicated to my wonderful family, friends, and everybody who had played a crucial role
in my life.

TABLE OF CONTENTS

CHAPTER 1. General Introduction	1
Dissertation Organization	4
References	4
CHAPTER 2. Weak Bonding of Zn in an Al-Based Approximant, Based on Surface Measurements	6
Abstract	6
1. Introduction	7
2. Experimental Details	9
3. Clean Surface: Experimental Results and Interpretation	13
3.1 Depth profiling with XPS at room temperature	13
3.2 Annealing	14
3.2.1 Variable temperature annealing: Compositional evolution from XPS	15
3.2.2 Constant temperature annealing: Compositional evolution from XPS	16
3.3 STM	17
3.3.1 STM image features	17
3.3.2 Sample roughness from STM	19
4. Surface Oxidation	20
4.1 Oxidation in UHV	21
4.2 Air-oxidized samples	23
4.3 Comparison between oxidation conditions	24
5. Conclusions	25
Acknowledgements	27

References	28
Figure Captions	31
Tables	33
Figures	38
CHAPTER 3. Structure of the Clean Gd ₅ Ge ₄ (010) Surface	60
Abstract	60
1. Introduction	61
2. Experimental Procedures	62
3. Background: Bulk Phases	66
3.1 Gd ₅ Ge ₄	66
3.2 Gd ₅ Ge ₃ Thin Plates	67
4. Experimental Results	67
4.1 XPS	67
4.1.1 XPS: Initial Depth-Profiling after Air Exposure (Sample #1)	67
4.1.2 XPS: Surface Composition as a Function of Annealing Temperature in UHV (Sample #1, #2, and #3)	68
4.1.3 XPS: Depth-Profiling after Annealing at Different Temperatures in UHV (Samples #1, #2, and #3)	69
4.1.4 Summary and Analysis of XPS Data	71
4.2 STM	72
4.2.1 STM: General Comments	72
4.2.2 STM: Sample #1	73
4.2.2.1 STM Images after Sputtering at Room Temperature (Sample #1)	73
4.2.2.2 STM Images after Annealing at 900 K (Sample #1)	74

4.2.2.3 STM Images after Annealing above 900 K (Sample #1)	75
4.2.3 STM: Sample #2	75
4.2.3.1 STM Images after Annealing to 900 K (Sample #2)	75
4.2.3.2 STM Images after Annealing Above 900 K (Sample #2)	77
4.2.4 Summary of STM Data	80
5. Comparison of STM Results (Section 4.2) with Bulk Structure	81
6. Characterizing Gd ₅ Ge ₃ Thin Plates (Samples #2 and #4)	85
6.1 Characterizing Gd ₅ Ge ₃ Thin Plates: Optical Microscopy (Sample #4)	85
6.2 Characterizing Gd ₅ Ge ₃ Thin Plates: SEM, AES and SAM (Sample #4)	85
6.3 Characterizing Gd ₅ Ge ₃ Thin Plates: SEM (Sample #2)	88
6.4 Characterizing Gd ₅ Ge ₃ Thin Plates: STM (Sample #2)	89
7. Conclusions	91
Acknowledgements	91
References	92
Figure Captions	95
Tables	101
Figures	109
Appendix	145
CHAPTER 4. Preferential Surface Oxidation of Gd in Gd ₅ Ge ₄	153
Abstract	153
1. Introduction	153
2. Materials and methods	154

3. Results	155
4. Discussion	157
5. Conclusions	159
Acknowledgements	159
References	159
Figure Captions	162
Figures	163
Appendix	167
CHAPTER 5. Interaction of Au with the NiAl (110) Surface	175
1. Introduction	175
2. Experimental Procedures	177
3. Experimental Results and Discussion	180
3.1 Growth at 200 K and 300 K	181
3.2 Thermal Treatments above 300 K	182
4. Discussion	184
4.1 Growth at 200 K and 300 K	184
4.2 Thermal effects above 300 K	186
5. Conclusions	188
Acknowledgements	188
References	189
Figure Captions	192
Tables	195
Figures	198

CHAPTER 6. A Comparison of the Ag and Au Structures on NiAl (110) using XPD and STM	224
1. Introduction	224
2. Experimental Details	225
3. Experimental Results: Ag on NiAl (110)	228
3.1 STM, XPD, and LEED for Ag on NiAl (110)	228
3.2 Comparing SSC Models with XPD Patterns for Ag on NiAl (110)	230
4. Experimental Results: Au on NiAl (110)	232
4.1 STM, XPD, and LEED for Au on NiAl (110)	232
4.2 SSC Models	232
5. Conclusions	233
Acknowledgements	233
References	234
Figure Captions	235
Figures	237
APPENDIX A. Using CasaXPS Software	252
APPENDIX B. Experimental Database	280
ACKNOWLEDGEMENTS	354

CHAPTER 1

General Introduction

The goal of this work is to characterize surfaces of intermetallics, including quasicrystals. Achieving this goal requires techniques to determine surface composition and surface structure of these materials. However, there is very little work in characterizing such surfaces (other than quasicrystals and closely-related periodic systems), and so there are new opportunities in this direction.

Intermetallics are usually metal rich compounds where the stoichiometry is fixed (or can vary over a very narrow range), corresponding to a specific chemical identity of an atom occupying any given site [1]. However, their mechanical, catalytic, magnetic, and surface properties are highly desirable for certain applications. For instance, aluminides have high strength and stiffness at elevated temperatures [2], Gd-Ge compounds exhibit magnetocaloric properties that may lead to new refrigeration and other energy conversion technologies [3], and $\text{Al}_{13}\text{Fe}_4$ holds promise as a cheap and environmentally friendly hydrogenation catalyst [4].

A particularly interesting subset of intermetallics are quasicrystals. They were first discovered by Daniel J. Shechtman in 1982 [5]. They are aperiodic structures that usually have forbidden rotational symmetries, such as fivefold or tenfold axes [6]. The first materials discovered were icosahedral. Later, decagonal quasicrystals were discovered by Chattopadhyay et al. [7] and Bendersky [8]. Surface studies of quasicrystals are important because they shed light on the atomic and electronic surface

structures, and how those may be related to phenomena such as epitaxy [6; 9; 10], low friction [11], wetting by liquids [12], and resistance to oxidation [13] – in all of which the quasicrystals exhibit unusual and potentially useful surface properties.

In this work, surface characterization is primarily focused on composition and structure using X-ray photoelectron spectroscopy (XPS) and scanning tunneling microscopy (STM) performed under ultrahigh vacuum (UHV) conditions. XPS provides critical information on the surface composition and the chemical state of the elements. STM is used to characterize the surface structure by determining the topography of the surface. Surfaces need to be studied in UHV conditions because it is the only possible environment where such surfaces can be prepared and maintained from outside contamination such as oxygen and carbon.

Surface composition can be determined from the area underneath the curve of a photoelectron peak in XPS. We can apply this value to a general expression in determining the atomic concentration, C_x , in the sample,

$$C_x = \frac{A_x/S_x}{\sum A_i/S_i} \quad (1)$$

A corresponds to the area underneath the curve of the photoelectron peak, S corresponds to the atomic sensitivity factor of the photoelectron peak to scale the measured intensities, these values were taken from [14], the subscript “ x ” corresponds to the element of interest and “ i ” is an index that runs over all of the elements in the sample. Equation (1), enables the determination of surface chemical composition, which is useful in comparing surfaces versus bulk composition.

Chemical states of the elements are shown by the variations in binding energies of the photoelectron peaks as determined by XPS. For instance, pure metals typically tend to have lower binding energies than oxide metals. Therefore, we can measure the difference in binding energies of a photoelectron peak from a clean metal and an oxidized metal and see if the metal oxidizes.

STM complements XPS in characterizing surfaces. The surface topography provided by STM is most useful when scanning smooth surfaces, i.e. a step-terrace morphology. In general, step-terraces can be achieved after several cleaning cycles. Studying clean surfaces is ideal in finding the correct atomic structure without being contaminated by outside environment. A cleaning cycle is defined as sputtering and annealing [15]. In such a cycle, sputtering is a process of removing material from the surface by ion bombardment [15] and annealing is heating the sample to a specific temperature for an amount of time to repair the surface damage from sputtering [15]. With preparation of a step-terrace morphology using a sputter-annealing regimen in UHV, the surface can be used to determine the atomic structure with STM.

We apply these techniques generally on the clean surface, but in some cases, we can also apply these techniques after an adsorption of a molecule or a metal on surfaces as well. This can help us understand the chemical interaction between the molecule or metal and the surface. With metal adsorption, we can also study the self-assembly of metal nanostructures on surfaces. Self-assembly involves spontaneous arrangement into ordered structures [16]. In this work, it means that a nanostructure builds itself on surfaces. This may provide practical insights into creating useful nanostructures.

Dissertation Organization

In this dissertation, five chapters focus on characterizing clean surfaces and other types of systems on surfaces. They are: (1) Weak bonding of Zn in an Al-Based approximant, based on surface measurements (a part of this chapter was published in Philosophical Magazine in 2010); (2) Structure of the clean Gd₅Ge₄ (010) surface; (3) Preferential surface oxidation of Gd in Gd₅Ge₄ (a part of this chapter was published in Applied Surface Science in 2012); (4) The interaction of Au on the binary NiAl (110) surface; and (5) A comparison of the Ag and Au structures on NiAl (110) using XPD and STM. Following the five chapters are appendices that document a standard procedure for using CasaXPS software, and an experimental database of STM, XPS, SEM, AES, SAM, XPD, and LEED.

References

- [1] C.D. Yuen, B. Unal, D. Jing, P.A. Thiel, Philosophical Magazine 91 2879-2888.
- [2] T. Duguet, P.A. Thiel, Progress in Surface Science 87 47-62.
- [3] V.K. Pecharsky, J.K.A. Gschneidner, Physical Review Letters 78 (1997) 4494-4497.
- [4] M. Armbruster, et al., Nature Materials 11 (2012) 690-693.
- [5] P.A. Thiel, Progress in Surface Science 75 (2004) 69-86.
- [6] H.R. Sharma, M. Shimoda, A.P. Tsai, Advances in Physics 56 (2007) 403-464.
- [7] K. Chattopadhyay, S. Ranganathan, G.N. Subbanna, N. Thangaraj, Scripta Metallurgica 19 (1985) 767-771.
- [8] L. Bendersky, Physical Review Letters 55 (1985) 1461-1463.

- [9] V. Fournee, P.A. Thiel, *Journal of Physics D-Applied Physics* 38 (2005) R83-R106.
- [10] V. Fournée, J. Ledieu, P.A. Thiel, *Journal of Physics: Condensed Matter* 20 (2008).
- [11] J.Y. Park, P.A. Thiel, *Journal of Physics-Condensed Matter* 20 (2008) -.
- [12] J.M. Dubois, V. Fournee, P.A. Thiel, E. Belin-Ferre, *Journal of Physics-Condensed Matter* 20 (2008) -.
- [13] D. Rouxel, P. Pigeat, *Progress in Surface Science* 81 (2006) 488-514.
- [14] J.F. Moulder, J. Chastain, W.F. Stickle, P.E. Sobol, K.D. Bomben, *Handbook of x-ray photoelectron spectroscopy: a reference book of standard spectra for identification and interpretation of XPS data*, Physical Electronics, 1995.
- [15] K. Oura, V.G. Lifshits, A.A. Saranin, A.V. Zotov, M. Katayama, *Surface Science: An Introduction*, Springer, Verlag, 2003.
- [16] G.M. Whitesides, B. Grzybowski, *Science* 295 (2002) 2418-2421.

CHAPTER 2

Weak Bonding of Zn in an Al-Based Approximant, Based on Surface Measurements

Chad D. Yuen,^{1,2} Baris Unal,^{1,3,4} Dapeng Jing,^{1,2} and Patricia A. Thiel^{1,2,3,}

¹Ames Laboratory, Iowa State University, Ames, Iowa 50011

²Department of Chemistry, Iowa State University, Ames, Iowa 50011

³Department of Material Science and Engineering, Iowa State University, Ames, Iowa 50011

⁴Present address: Department of Chemical Engineering, Massachusetts Institute of Technology, Boston, Massachusetts

*Parts of this chapter was published in “Philosophical Magazine, 2010”

Abstract

We have studied two surfaces of a new Al-Pd-Zn approximant using mass spectrometry, X-ray photoemission spectroscopy (XPS) and scanning tunneling microscopy (STM). Zn is bonded weakly in this approximant, perhaps as weakly as in elemental Zn. This is based upon three observations: the high vapor pressure of Zn above the approximant (detectable in the gas phase at 600 K); preferential sputtering of Zn (contrary to the usual preferential sputtering of Al in Al-rich quasicrystals); and preferential surface segregation of Zn. We further show that preferential segregation – and perhaps incipient evaporation – causes the surface to roughen, preventing it from forming a terrace-step morphology. Finally, our data show that at low O₂ pressures, Al oxidizes. In air, Zn oxidizes as well. All results and conclusions are similar for the two-fold and pseudo-ten-fold surfaces.

1. Introduction

In 1982, quasicrystals were discovered by Daniel J. Shechtman [1]. They are aperiodic structures that usually have forbidden rotational symmetries, such as fivefold or tenfold axes [2]. The first materials discovered were icosahedral. Later, decagonal quasicrystals were discovered by Chattopadhyay et al. [3] and Bendersky [4]. Surface studies of quasicrystals are important because they shed light on the atomic and electronic surface structures, and how those may be related to phenomena such as epitaxy [2; 5; 6], friction [7], wetting by liquids [8], and oxidation [9]—in all of which the quasicrystals exhibit unusual and potentially useful properties.

In this work, we studied a newly-discovered $\text{Al}_{57}\text{Pd}_{30}\text{Zn}_{13}$ approximant, which is an approximant to a quasicrystal. Approximant is defined as periodic crystals that are closely related to quasicrystalline phases and the local clusters of atoms are common to both the approximant and quasicrystal [10]. This approximant had been found by Dr. Srinivasa Thimmaiah, in the group of Prof. Gordon Miller, while working on a project supported by the Department of Energy at the Ames Laboratory.

Structurally, a decagonal quasicrystal has three families of high-symmetry axes [2]: a single periodic tenfold (10f) axis and two groups of five aperiodic twofold (2f) axes. As shown in Fig. 1, the 10f axis is along the decagonal rod while the 2f axes are perpendicular to the 10f. In the plane of the 2f axes, five of the 2f axes are perpendicular to the faces of the decagonal rod, while the other five bisect the angle between each pair in the first family, i.e. the second set is rotated by approximately 18° with respect to the first, in the 2f plane. The growth facets along the sides of the rod are perpendicular to one

set of 2f axes. In the approximant, we studied two samples, the pseudo-ten-fold (10f) surface and the two-fold (2f) surface.

Our goal was to determine the composition and structure of this surface under conditions typically applied to prepare a clean surface in ultrahigh vacuum, i.e. sputtering followed by annealing. The optimal outcome would have been to observe a terrace-step structure under conditions of annealing that did not cause significant segregation or evaporation of any of the constituent elements. The terrace-step structure could then have been analyzed in terms of its atomic structure, and this structure compared with the bulk structure model to shed light on the surface terminations. This approach has been carried out for several of the Al-rich quasicrystals [11-14]. Regarding the Al-Pd-Zn material, however, a major concern was the high vapor pressure of elemental Zn. This normally precludes Zn and its alloys from being used or studied in ultrahigh vacuum, because Zn can evaporate and contaminate the chamber, leading to spurious detection of Zn in subsequent samples. This fear of instrument degradation has prevented surface scientists from analyzing Zn and its alloys with some of the most powerful surface probes, such as X-ray photoemission spectroscopy (XPS) and scanning tunneling microscopy (STM). Our hope a priori was that the chemical potential of Zn in the Al-Pd-Zn approximant would be significantly lower than that of elemental Zn. Indeed, the surface of quasicrystalline Ag-In-Yb has been annealed and characterized successfully in UHV, despite the rather high vapor pressure of elemental Yb [15].

The Al-Pd-Zn phase is an orthorhombic $5/3$ approximant, with bulk lattice constants of $a = 2.36$ nm, $b = 3.24$ nm, and $c = 1.67$ nm. Its bulk composition is 57 at% Al, 30 at% Pd, and 13 at% Zn. It is structurally similar to a known Al-Os-Ir phase. It

melts congruently at 1045 K. The synthesis and analysis of this material will be reported elsewhere.

2. Experimental Details

We first measured the effective pressure of Zn over an Al-Pd-Zn sample as a function of sample temperature. A small piece of the two-fold Al-Pd-Zn sample was used to perform this experiment. It was characterized by Energy Dispersive Spectroscopy (EDS) by Jim Anderegg and William Yuhasz. A detailed description of how it was oriented and grown is discussed below. This was done using a UTI 100C quadrupole mass spectrometer in a test chamber with a total base pressure of about 1×10^{-7} Torr, and with the sample in a Knudsen-type cell with a 0.8 mm diameter orifice. The distance between the cell and the quadrupole is 300 mm. As we started to increase the temperature, the sample was being held roughly 2 minutes per degree. As shown in Fig. 2, the gas-phase Zn level first rose above its baseline reading of 5×10^{-10} Torr when the sample reached a temperature of 600 K, thereby setting an upper limit on the temperature to be used in UHV work. Given the configuration of the test chamber, we can estimate that a net Zn pressure of 2×10^{-10} Torr above baseline (the detection limit) corresponds to a pressure at the Knudsen cell of about $10^{-4 \pm 1}$ Torr, which is close to the equilibrium vapor pressure of elemental Zn (10^{-3} Torr) at 600 K. Thus, the vapor pressure of Zn in the approximant is about the same as that in the elemental metal, to within about one order of magnitude.

The Al-Pd-Zn specimens used for UHV studies were synthesized by William Yuhasz, working at the Materials Preparation Center at Ames Laboratory DOE [16]. The sample numbers for the pseudo-ten-fold (10f) and two-fold (2f) Al-Pd-Zn approximant is HTB-3-108 and WMY-1-134a. Ingots were grown using two techniques. These were the flux-growth technique and the Bridgman technique.

The Bridgman technique produced a large ingot. However, the area of single grains within the ingot proved to be no larger than 1 mm^2 , based on Laue. A circular sample, 12 mm wide and 1.5 mm thick, was prepared from the Bridgman ingot. This sample contained a grain whose surface was perpendicular to the 10f axis, and whose position was marked with electrical discharge machining. See Fig. 3a. Based on Laue, the grain was oriented within ± 1 degree of the 10f axis. The other grains were within ± 10 degrees of each other.

Flux growth produced smaller specimens. Because they tended to grow fast in the 10f direction, they were elongated (as shown in Fig. 1) and hence large enough for preparing 2f samples but not 10f samples. A rectangular 2f sample, 0.7 mm in length by 0.3 mm in width by 0.2 mm in thickness was prepared from the flux-grown specimen. Based on Laue, this sample had a uniform 2f orientation within ± 1 degree.

The samples were polished using standard metallographic techniques, down to $0.25 \mu\text{m}$ diamond paste. Both samples were then sonicated with acetone and methanol, and fixed on tantalum plates. They were held in place with spot-welded tantalum wires. When the 2f sample was fixed onto the sample plate, a fracture line appeared in the middle, probably at a pre-existing grain boundary. In order to distinguish between the

two grains, the left region will be called “Side A” and the right “Side B,” as shown in Fig. 3b.

The samples were then transferred to an UHV chamber that was equipped with a sputter gun, Omicron x-ray source (Mg K α), Omicron EA 125 hemispherical electron energy analyzer, and an Omicron variable-temperature STM. The base pressure of the chamber was below 7.7×10^{-11} Torr throughout the experiments. The sample was sputtered with Ar^+ ions at 0.5 to 1.5 keV energy, with the incident beam at an angle of 45° to the surface plane and the sample at $T = 300$ K. The 10f sample was sputtered at three different positions (each position was sputtered at constant time) in order to cover the entire area, while the 2f sample was sputtered at one position since the sample was small. The sputter beam diameter is in the range of 3 mm to 18 mm FWHM. Sputtering procedures of the sample are listed in section 3 below.

The sample plate temperature was measured using chromel-alumel thermocouple wires that were connected to the stainless steel sample plate. The voltage output was measured without using an ice-water reference. The voltages were converted to temperatures using standard K-type thermocouple data [17] and adding 25 degrees to compensate for room temperature.

STM was used to study the surface morphology and surface roughness of the Al-Pd-Zn approximant. The RMS roughness values were calculated from the STM images using WSxM scanning probe microscopy software [18]. A tungsten tip was used to scan the images with a bias voltage of -1 V. The tunneling current was set at 0.2 nA and 0.5 nA. A single STM image takes 2 minutes. All STM images were acquired with the sample at room temperature. In the annealing experiments, after desired annealing time,

the heating power is shutdown to let the sample cool down to room temperature. STM was used after the sample was cooled for 45 minutes.

Gas exposures are reported in units of Langmuir, L ($1 \text{ L} \equiv 1 \times 10^{-6} \text{ Torr s}$). Oxygen exposure was achieved by backfilling the Omicron chamber with research grade oxygen (99.99%) to a constant pressure of 10^{-8} Torr to 10^{-7} Torr, as needed.

XPS data were analyzed using CasaXPS software [19]. The CasaXPS software analyzes both spectral and imaging data from quantifying surface composition to thickness measurements for spectra and images. It is mainly designed for XPS and Auger data but can also be used for other techniques such as SIMS. The XPS source was perpendicular to the sample plate, and the take-off angle (defined as the angle between the entrance axis of the analyzer and the sample surface) was 45° . Spectra were acquired in one of two ways: Over a broad energy range, 1150 eV to 0 eV, with low energy resolution (“survey”); or over smaller energy ranges with higher resolution. These ranges were tailored to reveal the Zn 2p binding energy from 1075 eV to 1000 eV, the Pd 3d binding energy from 400 eV to 300 eV, the Pd 3p and O 1s binding energy from 570 eV to 510 eV or the Al 2p binding energy from 100 eV to 50 eV. The analysis size in our XPS was less than 1.5 mm in diameter. The angular acceptance angle was $\pm 8^\circ$. The aperture size that was used in the EA 125 analyzer was 6 mm x 12 mm.

The reported surface compositions from the XPS data was taken from the smaller energy ranges of the individual peaks. The reason why we chose the individual peak spectra was due to the uncertainty when comparing to the survey spectra. The uncertainty of the surface composition between the survey spectra and the smaller energy ranges of the individual peak spectra were 1.15% Al, 5.23% Pd, and 21.8% Zn,

respectively. These uncertainties were calculated by taking the ratio of the composition between the survey spectra and the individual peak spectra.

3. Clean Surface: Experimental Results and Interpretation

3.1 Depth profiling with XPS at room temperature

Our first goal was to determine the asymptotic composition of the surface during sputtering. To this end, we started with samples that had been introduced from air to UHV, without any prior UHV treatment. Figure 4a shows the initial overview spectrum. The initial overview spectrum shows high intensity contamination peaks such as carbon and oxygen. Other contaminants such as S and Ag were also not detected by XPS. The metal peaks such as Al, Pd, and Zn showed low concentrations. This was expected since the sample was exposed to air. The sample was then sputtered at 300 K for two minutes. XPS was measured again, and this process was repeated several times until the sample had been sputtered a total of 24 minutes. After this period, the sputtering process was increased from two to five minutes in between the XPS runs until the surface had been sputtered a total of 54 minutes. At this point the sputter time was increased again between XPS runs from five minutes to ten minutes, until the sample was clean by XPS. XPS did not detect contamination peaks such as C and O after several sputtering cycles. The O peak, however, was more difficult to detect since it overlaps with the Pd 3p_{3/2} peak. A ratio was taken between the (O 1s and the Pd 3p_{3/2} peak) with the pure Pd 3d peak. As expected, the ratio decreased throughout several cycles of sputtering until the ratio held constant. This indicates there was only Pd. While the contamination peaks

were gone, the Pd peak intensities increased dramatically while the Al and Zn peaks decreased slightly due to sputtering. This will be discussed below. The total sputtering time was 204 minutes. Figure 4b shows the final overview spectrum at the end of the experiment, for the 10f sample.

A similar sequence was employed to clean the two-fold sample, where the initial sputtering time was five minutes. Again, XP spectra were acquired between sputtering. The sputtering time was then increased to 10 minutes between spectra. The total sputtering time required to clean the two-fold sample was 40 minutes according to XPS. Initial and final overview spectra are shown in Fig. 4c,d.

The depth profile itself is shown in Fig. 5. After extensive sputtering, the surface compositions of the two samples approached asymptotic limits in the range of $\text{Al}_{62-67}\text{Pd}_{29-32}\text{Zn}_{3-6}$, which is Al-rich by 5-10 at% and Zn-poor by 7-10 at%, relative to the bulk composition of $\text{Al}_{57}\text{Pd}_{30}\text{Zn}_{13}$. These results are shown in Table 1, along with the bulk composition for reference. This reveals preferential sputtering of Zn, contrary to the preferential sputtering of Al that is usually seen in Al-rich quasicrystals. Light atomic weight and weak interatomic bonding are known to favor preferential sputtering [20]. Since Zn is heavier than Al, its preferential sputtering most likely reflects weaker bonding in the solid.

3.2 Annealing

Our second goal was to determine the effect of heating on surface composition. Two types of temperature programs were employed. The first consisted of heating to sequentially higher temperatures, and monitoring composition vs. temperature. We refer

to this as variable temperature annealing. The second consisted of heating to a fixed temperature of 460-480 K and monitoring composition vs. time. We refer to this as fixed temperature annealing. The variable temperature experiments are presented first.

3.2.1 Variable temperature annealing: Compositional evolution from XPS

The pseudo-ten-fold sample was first cleaned by Ar⁺ sputtering for 10 minutes. After XPS, the sample was annealed at 380 K for 2 hours. The sample was then cooled down to room temperature for XPS analysis. This experimental process (sputtering, annealing for two hours, cooling down, and measuring XPS) was repeated again with annealing temperatures of 430 K, 460 K, and 510 K. The final cycle consisted of annealing at 540 K for 10 minutes. Higher temperatures were not used because of the possibility of Zn evaporation. The results are shown in Fig. 6a. The error bars at 300 K represent the range of surface concentrations after five similar sputtering preparations at 300 K. From Fig. 6a, it is clear that Zn concentration began to increase rather abruptly above 400 K, accompanied by decreasing Al and Pd concentrations. The fact that the Zn concentration eventually exceeded its bulk concentration by a significant amount—more than a factor of two—means that Zn segregated to the surface, partially replacing both Al and Pd.

The two-fold sample was treated similarly, except the annealing temperatures were different: 380 K, 430 K, 470 K, and 510 K, all for a constant time of 2 hours. The results are shown in Fig. 6b. The result resembles that for the pseudo-ten-fold surface: Above 400 K, Zn segregated to the surface, displacing both Al and Pd. Note that XPS provides a depth-weighted average composition over the top 5-10 nm of material, or

approximately 25-50 atomic layers. It is possible that Zn covered the entire surface above 400 K, and that Al and Pd XPS signals mainly originated below the Zn layer.

The final compositions of both samples are shown in Table 2, along with the bulk composition for reference.

In both samples, the surface composition reached that of the bulk at about 460-470 K. This observation prompted the following set of experiments, in which the samples were held in that temperature range for extended periods of time in the hope that the quasicrystalline approximant phase could stabilize at the surface.

3.2.2 Constant temperature annealing: Compositional evolution from XPS

The initial pseudo-ten-fold surface was prepared, as before, by sputtering for 10 minutes at 300 K. After XPS, the quasicrystal was annealed at 460 K for 30 minutes, and re-cooled to room temperature for XPS. This cycle (anneal, cool, and measure XPS) was repeated three more times, for a total of two hours of heating at 460 K. The results are shown in Fig. 7a. The treatment of the two-fold sample was the same, except that annealing times were variable, consisting of 60 minutes, 90 minutes, and 120 minutes at constant temperature of 480 K. The results are shown in Fig. 7b. It is clear that Zn segregated under these conditions as well. We conclude that surface segregation of Zn occurs very readily in this material.

The final compositions of both samples are shown in Table 3, along with the bulk composition for reference.

In the constant-temperature and variable-temperature annealing experiments, the pseudo-ten-fold and the two-fold samples yielded similar results. For both, the Zn

surface concentration increased as temperature or time increased, while the Al and Pd surface concentrations decreased. However, there is some discrepancy between the two types of annealing experiments, and this holds true for both the pseudo-ten-fold and two-fold surfaces. For instance, from Fig. 6A, after the pseudo-ten-fold surface was annealed for two hours at 460 K, the concentrations of Al, Pd, and Zn were 53%, 22%, and 26%, respectively. From Fig. 7A, after the same cumulative treatment ($T = 460$ K, two hours) the surface concentrations were 57%, 28%, and 15%. Both of these data sets should match up at this specific temperature and time. The 2f surface shows a similar discrepancy. In Fig. 6B (at $T = 480$ K, $t = 2$ hrs), the surface concentrations of Al, Pd, and Zn were approximately 61%, 22%, and 17%, while in figure 7B, the concentrations were 58%, 14%, and 28% after treatment at the same temperature and time. However, the temperature-time programs were not identical in the two kinds of experiments; the annealing interruptions in the constant-temperature experiment might have affected surface compositions.

3.3 STM

3.3.1 STM image feature

The pseudo-ten-fold sample was annealed at 440 K, 490 K, and 545 K for 15 minutes each. Between heating, it was cooled to room temperature for STM imaging. The micrographs are shown in Fig. 8. The surface was very rough, with no evidence of a terrace-step type structure even after the 545 K treatment. The two-fold sample was treated similarly, except that the annealing temperatures were different (400 K and 520 K) and the annealing time was longer (two hours). Both Side A and Side B were imaged,

and results are shown in Fig. 9. After annealing at 400 K (Fig. 9A-B), the surface was again very rough, but after annealing at 520 K (Fig. 9C-D), some hint of a terrace-step structure emerged. Where they were visible, the maximum width of the terraces was about 10 to 15 nm.

The heights of steps can be a fundamental clue to the surface structure. The step heights are revealed in the line profiles shown in Fig. 10A-F. Step heights were variable, but there seems to be a significant cluster of values in the range 0.23-0.26 nm, and perhaps another cluster in the range 0.35-0.43 nm. It is difficult to judge the significance of these step heights, but 0.23-0.26 nm is consistent with interplanar spacings between close-packed planes of many elemental metals. Considering the metals in the quasicrystal, the spacings between close-packed planes are 0.27 nm for elemental Zn, and 0.23 nm for both Al and Pd. However, the second cluster of step heights falls short of being twice the value of the first, so they could not result from simple step bunching.

It is also interesting to compare the data for equivalent 2f surfaces of other decagonal, Al-rich quasicrystals. Based upon STM studies, these surfaces all have steps with minimum height (d_0) and other steps whose heights (d_1 , d_2 , etc) are related to d_0 by the Golden Mean, $\tau = 1.618\dots$ However, the exact values are rather scattered. For instance, on the equivalent 2f surface of Al-Cu-Co Duguet et al. find $d_0 = 0.47 \pm 0.05$ nm [21]. On Al-Ni-Co, Groening et al. report $d_0 = 0.24$ nm and $d_1 = 0.39$ nm [22], while Park et al. find $d_0 = 0.19$ nm and $d_1 = 0.47$ nm [23]. Of course, one would not expect to find exactly the same values for different alloys, but these values give some idea of what might be expected. The range of values reported here for Al-Pd-Zn is very similar to the values found by Groening et al. for Al-Ni-Co.

3.3.2 Sample roughness from STM

The roughness of these surfaces was evaluated quantitatively after various surface treatments. Figure 11 shows the rms roughness, w , as a function of image area for individual experiments. As expected, it always increases toward an asymptotic value at large image size [24].

Figure 11A shows the roughness of the 10f surface after annealing at three different temperatures for 15 minutes each. Normally, one expects roughness to decrease as temperature increases (for temperatures below the roughening transition), because the rate of surface and near-surface diffusion increases. However, this variation of w with T did not occur. There was no difference in w after annealing at 440 K and 490 K, and at 545 K w actually increased. This increase may be due to incipient evaporation of Zn. (Recall from Sec. 2 that Zn could be detected in the gas phase starting at 600 K.)

Figure 11A also shows data for the two-fold sample, after annealing at 400 K and 520 K for two hours each. These treatments produced no difference in w for a fixed sample location. However, the two regions of the sample did show a difference in roughness of about 1 nm. This might be due to uneven heating across the sample (cf. Fig. 2). But what is interesting in Fig. 11A, is the roughness at 300 K (sputtering, no annealing). It shows the surface to be smoother than when the approximant is annealed at high temperatures. Normally, one expects $w(T)$ to be decreasing function for a surface that is initially prepared by sputtering. In other words, one expects annealing to heal the damage induced by sputtering and smoothen the surface. Figure 11B shows that this expectation is met for three other metallic samples that have been studied in our laboratory: (1) the (110) surface of a crystalline binary alloy, NiAl; (2) a Zr-Ni-Cu-Al

metallic glass; and (3) the two-fold surface of a quasicrystal, decagonal Al-Cu-Co. However, the roughnesses of the two Al-Pd-Zn surfaces behave differently. For them, $w(T)$ starts high and increases strongly.

The limiting values of w in Fig. 11, 2-4 nm, are very large relative to the roughness of other surfaces with which we have worked. For instance, Fig. 11B compares data for the pseudo-ten-fold and two-fold Al-Pd-Zn surfaces with data for a Zr-Ni-Cu-Al metallic glass, 2f Al-Cu-Co, and NiAl(110) [21; 25]. The metallic glass was sputtered with Ar^+ ions for 21 minutes at 1.5 keV energy, with the incident beam normal (90°) to the surface at $T = 300$ K. After both samples were sputtered, it was then held at 520 K for two hours. Both sides of the two-fold Al-Pd-Zn sample were rougher than the glass by at least a factor of two. The glass consisted of metals with relatively low vapor pressures. This suggests that in the approximant, segregation and/or sublimation of Zn substantially enhances surface roughness. This would also explain the fact that the approximants surface roughness does not decrease with increasing temperature, as expected; the contribution from segregation and/or sublimation would increase with increasing temperature. This would also explain why the roughness is less after sputtering, but before annealing, than at high annealing temperatures. STM settings, such as tunneling current and tip bias voltage did not affect w which is shown in Table 4.

4. Surface Oxidation

In this set of experiments, our goal was to determine which elements in the quasicrystal were most prone to oxidation. In other studies of Al-rich quasicrystals and

their approximants, it had been found that Al was usually the only metal to oxidize upon exposure to oxygen or dry air. The Al formed a passivating layer of pure or nearly-pure alumina, accompanied by some segregation of Al even at room temperature.

In the experiments with Al-Pd-Zn, the surface was oxidized under two conditions. The most gentle condition, corresponding to the lowest chemical potential of oxygen, was exposure of the clean surface to a low pressure of oxygen in UHV. The most aggressive condition, corresponding to the highest chemical potential of oxygen, was exposure of the polished surface to air.

4.1 Oxidation in UHV

The 10f sample was first cleaned by Ar⁺ sputtering, then annealed at 440 K for 20 minutes. After the sample had been cooled to room temperature, it was exposed to O₂ in the following sequence: 0.2 L, 1 L, 10 L, 100 L, and 200 L for a total of 300 L. Before and after each exposure, the XP spectrum was recorded. In between the 100 L and 200 L O₂ exposures, the sample was annealed at 430 K for 20 minutes. The XP spectra are shown in Fig. 12, and the surface composition as a function of O₂ exposure is given in Table 5. In order to make sure oxygen was exposed on the surface, a ratio was taken between the O 1s and Pd 3p peak with the pure Pd 3d peak. As expected, the ratio increased from 0.42 at 0 L of O₂ to 0.57 at 300 L of O₂.

Figure 12A shows the progression of the Zn 2p_{3/2} peak. Between the initial spectrum and the one after 300 L exposure, there was no distinguishable change in the position or shape, indicating that Zn did not oxidize. However, the intensity decreased with oxygen adsorption, because Zn was increasingly screened by an upper aluminum

oxide layer (see below). Figure 12B shows the region of the spectrum that encompassed the Pd $3d_{3/2}$ and $3d_{5/2}$ peaks. There was no detectable shift or change in shape of the Pd $3d_{3/2, 5/2}$ peaks. Therefore, the Pd did not oxidize under these conditions. This is not surprising, since oxidation of Al-Pd-Mn quasicrystals has been thoroughly studied, and Pd has never been found to oxidize under *any* conditions in that system.

The oxygen 1s peak has a binding energy of 532 eV, which overlaps the Pd $3p_{3/2}$ at a binding energy of 531 eV. This region of the spectrum is shown in Fig. 12C. In order to see if there was any oxygen on the surface, a clean XPS spectrum was used to find the basis area ratio in the Pd $3p_{3/2}$ peak and the Pd 3d peak. When oxygen was being exposed on the surface, an area ratio was performed by using the overlap of (O 1s and Pd $3p_{3/2}$) and the Pd 3d peaks. The O 1s contribution was then carried out by the difference between the two ratios. The O 1s contribution to (O 1s and Pd $3p_{3/2}$) area is shown in Fig. 13 as a function of O₂ exposure. The O 1s contribution increased, indicating the surface was oxidized. A close-up view from 0 L to 20 L of oxygen exposure is also shown in Fig. 13. The oxygen adsorbed species increased over a period of time until it reached full saturation. This took about 10 L of oxygen exposure. However, this trend was interrupted at 100 L of oxygen exposure since the surface was annealed at 430 K for 20 minutes and was then cooled down to 300 K. Exposing 200 L of oxygen onto the surface did not increase the O 1s contribution. Hence, the surface was already saturated by oxygen.

Figure 12D shows that the Al 2p peak initially had a shoulder at high binding energy, and this shoulder increased in relative intensity as oxygen exposure increased. The clean Al 2p peak had a binding energy of 72.7 eV. After 300 L O₂ had been exposed

on the surface, the Al 2p peak had a binding energy of 72.5 eV. However, a shoulder was seen on the left side of the Al 2p peak. The shoulder had a higher binding energy between 76 eV and 74 eV. This indicates that there was some oxidation of Al. It is likely that a thin skin of aluminum oxide formed, and the XPS peak at lower binding energy originated from metallic Al below this oxide layer. Such a situation has been observed in other Al-rich quasicrystals.

4.2 Air-oxidized sample

Information is also available from the evolution of XPS peaks as the sample was sputtered, after air exposure. These data are shown in Fig. 14, and they correspond to the depth profile shown in Fig. 5.

As the initial surface was sputtered, the Zn 2p_{3/2} peak in Fig. 14A clearly showed a shift from 1023 eV (ZnO) to 1021.5 eV (Zn), for a total binding energy shift of 1.5 eV. The change from ZnO to Zn started after 39 minutes of sputtering. As sputtering proceeded, the peak first broadened and then became narrower. Presumably, the broadening was due to coexistence of the ZnO and Zn peaks at an intermediate stage. According to the handbook of x-ray photoelectron spectroscopy, the ZnO peak is in the range between 1021.8 eV and 1022.5 eV while the Zn 2p peak is in the range between 1021.5 eV and 1021.8 eV [26]. This matched closely with our results. We therefore conclude that Zn oxidized as a result of air exposure, in contrast to exposure in UHV.

Figure 14B shows that the Pd 3d_{3/2, 5/2} peaks are invariant during sputtering (held constant at 336 eV), except for an increase in intensity which can presumably be attributed to removal of a blanketing oxide. The handbook of x-ray photoelectron

spectroscopy showed the Pd 3d peak between 335.1 eV and 335.5 eV and PdO between 336.2 eV and 336.7 eV [26]. This indicates that Pd does not oxidize, even in air.

Figure 14C shows a clear shift in the Al 2p peak position, from 75 eV (Al_2O_3) to 72.5 eV (Al metal), for a total binding energy shift of 2.5 eV. The handbook of x-ray photoelectron spectroscopy had Al 2p between 72.5 eV and 73 eV and Al_2O_3 between 73.5 eV and 74.8 eV [26]. Our results matched perfectly well with the XPS handbook. The shift from Al_2O_3 to Al was detectable after 54 minutes of sputtering. The predominance of the Al_2O_3 peak on the initial surface indicates that the surface was more extensively oxidized (the oxide was thicker) in air, than after 300 L O_2 exposure in UHV (Fig. 12D). Again, this is similar to observations previously reported for other Al-rich quasicrystals [27-29].

Note that ZnO began shifting to Zn earlier than Al oxide began shifting to Al. This suggests that the Zn oxide was thinner than the Al oxide, and in fact the two coexisted at the top of the surface layer. It is probable the oxide was a chemically-mixed (Al, Zn) oxide, rather than consisting of distinct domains of Zn and Al oxides. We suggest that the compositional sequence from the top was: Mixed Zn and Al oxides, then Al oxide plus metallic Zn, then metallic Al, Zn, and Pd.

4.3 Comparison between oxidation conditions

After UHV oxygen exposure, there was partial oxidation of Al, but no detectable oxidation of Zn or Pd. After air exposure, there was oxidation of both Al and Zn, but not Pd. This suggests that the elements are most susceptible to oxidation in the sequence $\text{Al} > \text{Zn} > \text{Pd}$. This hypothesis is consistent with the sequence of enthalpies of formation of

oxides of Al, Zn, and Pd. At room temperature, they are: -1632 kJ/mol for Al_2O_3 , -348 kJ/mol for ZnO, and -85 kJ/mol for PdO [30]. The heat of formation per M-O bond of aluminum oxide, palladium oxide, and zinc oxide are: 5.20 eV, 2.47 eV, and 2.60 eV [31]. These numbers were arrived by taking the bond energy and dividing it by the number of bonds. This was then converted from kJ/mol to eV. Studies of other Al-rich quasicrystals such as Al-Cr-Fe, Al-Cu-Fe, Al-Pd-Mn, and Al-Cu-Fe-Cr all show Al to be the only metal that oxidizes in vacuum.¹²

Table 6A provides the surface compositions of Al-Pd-Zn after oxidation under the two conditions, as well as the compositions of the clean surface and the bulk. For comparison, Table 6B lists the surface compositions of Al-Pd-Mn under the same two conditions. These comparisons show that oxidation of Al-Pd-Zn, both in air and in vacuum, causes stronger enrichment in Al, than does oxidation of Al-Pd-Mn. For instance, after 300 L exposure at room temperature in vacuum, the Al-Pd-Mn sample is +3% enriched in Al relative to the bulk composition, and the Al-Pd-Zn sample is +21% enriched in Al relative to the bulk composition. The reason for this difference in response is not clear.

5. Conclusions

The main goal of this study was to determine whether the Al-Pd-Zn approximant could be prepared with a surface morphology that would lend itself to surface structure determination. Our conclusion is that it cannot. The reason is that Zn strongly segregates to the surface, and evaporates at relatively low temperature (detectable in the gas phase at

600 K). Zn segregation and evaporation occur before the surface and near-surface region can rearrange into the necessary terrace-step morphology. It appears that Zn segregation and/or evaporation exacerbate the surface roughness. This conclusion rests partly upon the fact that the surface did not become smoother as temperature increased above room temperature (and Zn segregation, and eventually Zn evaporation, set in). In fact, in one case the surface became rougher upon annealing. This conclusion is also based upon comparison with the surface roughness of a metallic glass that had been sputtered and annealed similarly—the glass was less than half as rough as the approximant. We can also conclude that Zn is bonded very weakly in the approximant, perhaps as weakly as in elemental Zn. This is based upon several observations. The first is the high vapor pressure of Zn, which we estimate to be about 10^{-4} Torr above the approximant at 600 K. This is the same order-of-magnitude as the vapor pressure above elemental Zn at 600 K. The second is the preferential sputtering of Zn. Preferential sputtering is favored by good mass-match with the incident ion, and weak bonding in the solid. In other Al-rich quasicrystals, Al is always removed preferentially, but in this material it is Zn, even though Zn is a worse mass-match to the Ar^+ ion than Al. Therefore, the preferential sputtering of Zn must be due to its weak bonding in the solid. The third is the fact that Zn segregates to the surface. In general, three factors promote surface segregation of one metal over other constituents in an alloy: Large atomic radius, low surface energy, and low bond energy in the alloy. Zn is actually the smallest of the atoms in Al-Pd-Zn, so size is not responsible. Elemental Zn has the lowest surface energy, but it is only slightly lower than Al (0.99 J/m^2 for the close-packed surface of Zn vs. 1.2 J/m^2 for Al and 1.9

J/m² for Pd) [32]. It is reasonable that low cohesive energy also promotes the segregation of Zn in this system.

Finally, we find that under mild oxidation conditions (10^{-8} - 10^{-7} Torr O₂ at room temperature), Al is the only metal to oxidize. Under harsher conditions (air at room temperature), Al and Zn both form oxides, and the oxide is thicker. Oxidized Zn is more localized at the surface than oxidized Al. Comparing the results from the two types of oxidation experiments, the propensity for oxidation in this material must be Al > Zn > Pd, which is consistent with thermodynamic data for the pure oxides.

Acknowledgements

This work was supported by the Office of Science, Basic Energy Sciences, Materials Sciences and Engineering Division of the US Department of Energy (USDOE). This manuscript has been authorized by Iowa State University of Science and Technology under Contract No. DE-AC02-07CH11358 with the US Department of Energy. We are indebted to Srinivasa Thimmaiah and Gordon Miller for allowing us to collaborate on their newly discovered phase. We thank William Yuhasz, James Anderegg and Srinivasa Thimmaiah for growing and characterizing the bulk samples.

References

- [1] P.A. Thiel, *Progress in Surface Science* 75 (2004) 69-86.
- [2] H.R. Sharma, M. Shimoda, A.P. Tsai, *Advances in Physics* 56 (2007) 403-464.
- [3] K. Chattopadhyay, S. Ranganathan, G.N. Subbanna, N. Thangaraj, *Scripta Metallurgica* 19 (1985) 767-771.
- [4] L. Bendersky, *Physical Review Letters* 55 (1985) 1461-1463.
- [5] V. Fournée, P.A. Thiel, *Journal of Physics D-Applied Physics* 38 (2005) R83-R106.
- [6] V. Fournée, J. Ledieu, P.A. Thiel, *Journal of Physics: Condensed Matter* 20 (2008).
- [7] J.Y. Park, P.A. Thiel, *Journal of Physics-Condensed Matter* 20 (2008) -.
- [8] J.M. Dubois, V. Fournée, P.A. Thiel, E. Belin-Ferre, *Journal of Physics-Condensed Matter* 20 (2008) -.
- [9] D. Rouxel, P. Pigeat, *Progress in Surface Science* 81 (2006) 488-514.
- [10] A.I. Goldman, R.F. Kelton, *Reviews of Modern Physics* 65 (1993) 213-230.
- [11] L. Barbier, D. Gratias, *Progress in Surface Science* 75 (2004) 177-189.
- [12] Z. Papadopolos, G. Kasner, J. Ledieu, E.J. Cox, N.V. Richardson, Q. Chen, R.D. Diehl, T.A. Lograsso, A.R. Ross, R. McGrath, *Physical Review B* 66 (2002) 184207.
- [13] H.R. Sharma, V. Fournée, M. Shimoda, A.R. Ross, T.A. Lograsso, A.P. Tsai, A. Yamamoto, *Physical Review Letters* 93 (2004) 165502.
- [14] T. Cai, V. Fournée, T. Lograsso, A. Ross, P.A. Thiel, *Physical Review B* 65 (2002) 140202.

- [15] H.R. Sharma, M. Shimoda, K. Sagisaka, H. Takakura, J.A. Smerdon, P.J. Nugent, R. McGrath, D. Fujita, S. Ohhashi, A.P. Tsai, *Physical Review B* Submitted (2009).
- [16] Samples were synthesized at the Materials Preparation Center, Ames Laboratory USDOE, Ames, IA, USA.
- [17] G.W. Burns, M.G. Scroger, G.F. Strouse, M.C. Croarkin, W.F. Guthrie, *National Institute of Standards and Technology Monograph* 175 (1993) 630.
- [18] I. Horcas, R. Fernandez, J.M. Gomez-Rodriguez, J. Colchero, J. Gomez-Herrero, A.M. Baro, *Review of Scientific Instruments* 78 (2007) -.
- [19] See www.CasaXPS.com.
- [20] C.J. Jenks, J.W. Burnett, D.W. Delaney, T.A. Lograsso, P.A. Thiel, *Applied Surface Science* 157 (2000) 23-28.
- [21] T. Duguet, et al., *Physical Review B* 80 (2009) 024201.
- [22] O. Groening, R. Widmer, P. Ruffieux, P. Groening, *Philosophical Magazine* 86 (2006) 773.
- [23] J.Y. Park, D.F. Ogletree, M. Salmeron, R.A. Ribeiro, P.C. Canfield, C.J. Jenks, P.A. Thiel, *Physical Review B* 72 (2005) 220201.
- [24] I. Heyvaert, J. Krim, C. Van Haesendonck, Y. Bruynseraede, *PRE* 54 (1996) 349.
- [25] D.P. Jing, B. Unal, F.L. Qin, C. Yuen, J.W. Evans, C.J. Jenks, D.J. Sordelet, P.A. Thiel, *Thin Solid Films* 517 (2009) 6486-6492.
- [26] J.F. Moulder, W.F. Stickle, P.E. Sobol, K.D. Bomben, *Handbook of X-ray Photoelectron Spectroscopy: a reference book of standard spectra for identification and interpretation of XPS data*, Perkin-Elmer Corporation, Physical Electronics Division, Eden Prairie, Minnesota, 1992.

- [27] S.L. Chang, J.W. Andereg, P.A. Thiel, *Journal of Non-Crystalline Solids* 195 (1996) 95-101.
- [28] P.J. Pinhero, J.W. Andereg, D.J. Sordelet, M. Besser, P.A. Thiel, *Philosophical Magazine B* 79 (1999) 91.
- [29] V. Demange, J.W. Andereg, J. Ghanbaja, F. Machizaud, D.J. Sordelet, M. Besser, P.A. Thiel, J.M. Dubois, *Applied Surface Science* 173 (2001) 327-338.
- [30] D.D. Wagman, W.H. Evans, V.B. Parker, R.H. Schumm, I. Halow, S.M. Bailey, K.L. Churney, R.L. Nuttall, *The NBS tables of chemical thermodynamic properties: Selected values for inorganic and C1 and C2 organic substances in SI units*, American Chemical Society and American Institute of Physics, Washington D.C., 1982.
- [31] *CRC Handbook of chemistry and physics*, CRC Press, Boca Raton, Fla., 2002.
- [32] L. Vitos, A.V. Ruban, H.L. Skriver, J. Kollar, *Surface Science* 411 (1998) 186-202.

Figure Captions

Figure 1

A decagonal quasicrystal has three families of high-symmetry axes: a single periodic tenfold (10f) axis and two groups of five aperiodic twofold (2f) axes. (a) is a schematic diagram of a decagonal quasicrystal; (b) Al-Pd-Zn decagonal quasicrystal which was grown by William Yuhasz at the Materials Preparation Center, Ames Laboratory USDOE, Ames, Iowa USA.

Figure 2

A piece of Al-Pd-Zn sample was heated in a tested chamber in order to measure the effective pressure of Zn as a function of sample temperature. At 600 K, the gas-phase of Zn rose above its baseline of 5×10^{-10} Torr.

Figure 3

A schematic diagram of the Al-Pd-Zn samples. (a) a 10f Al-Pd-Zn polygrained sample, where a marked area is a single grain as noted by "S"; (b) a 2f Al-Pd-Zn single grained sample, where a fracture line appeared in the middle, the left region noted as "Side A" and the right "Side B".

Figure 4

XP survey spectra of the 10f and 2f samples. (a) 10f initial survey spectrum after it was introduced from air to UHV; (b) clean 10f final survey spectrum after 204 minutes of sputtering; (c) 2f initial survey spectrum after it was introduced from air to UHV; (d) clean 2f final survey spectrum after 40 minutes of sputtering.

Figure 5

XPS depth profile of Al, Pd, and Zn after the 10f sample was introduced from air to UHV.

Figure 6

Variable temperature annealing: Compositional evolution from XPS. (a) a 10f Al-Pd-Zn sample was annealed at temperatures of 380 K, 430 K, 460 K, and 510 K for 2 hours while the final cycle was annealed at a temperature of 540 K for 10 minutes; (b) a 2f Al-Pd-Zn sample was annealed at temperatures of 380 K, 430 K, 470 K, and 510 K for 2 hours. The error bars in (a) and (b) at 300 K represent the range of surface concentrations after five similar sputtering preparations.

Figure 7

Constant temperature annealing: Compositional evolution from XPS. (a) a 10f Al-Pd-Zn sample was annealed at a constant temperature of 460 K for every 30 minutes; (b) a 2f Al-Pd-Zn sample was annealed at a constant temperature of 480 K at different annealing times of 30 minutes, 60 minutes, 90 minutes, and 120 minutes.

Figure 8

STM images of a 10f Al-Pd-Zn sample that was annealed at given temperatures for 15 minutes and then cooled down to 300 K. All images are 250 x 250 nm. The tunneling conditions are (a) $I = 0.5$ nA and $V\text{-tip} = -1$ V; (b) $I = 0.2$ nA and $V\text{-tip} = -1$ V; and (c) $I = 0.2$ nA and $V\text{-tip} = -1$ V.

Figure 9

STM imaging of a 2f Al-Pd-Zn sample that was annealed at given temperatures for 2 hours and then cooled down to 300 K. Side A (left side of the fracture) are figures (a) and (c) while Side B (right side of the fracture) are figures (b) and (d). All images are 250 nm x 250 nm. The tunneling conditions for all images are $I = 0.5$ nA and $V\text{-tip} = -1$ V.

Figure 10

STM images and line profiles of the 2f sample (a) through (f). The 2f sample was annealed at 520 K for 2 hours and then cooled down to 300 K for STM. STM figure sizes are as follows: (a) 100 nm x 100 nm, (b) 73 nm x 73 nm, (c) 87 nm x 87 nm, (d) 87 nm x 87 nm, (e) 85 nm x 85 nm, and (f) 108 nm x 108 nm. The tunneling conditions for all images are $I = 0.5$ nA and $V\text{-tip} = -1$ V.

Figure 11

Annealing results for the 10f and 2f samples. (a) a 10f Al-Pd-Zn sample was held at the given temperature for 15 minutes, then cooled to 300 K for STM imaging; (b) a 2f Al-Pd-Zn sample was held at the given temperature for 2 hours, then cooled to 300 K for STM imaging; (c) both the 2f Al-Pd-Zn and the Zr-Ni-Cu-Al metallic glass samples were annealed at 520 K for 2 hours, then cooled down to 300 K for STM imaging.

Figure 12

XP spectra for oxidation in UHV. (a) Zn 2p; (b) Pd 3d; (c) O 1s and Pd 3p; (d) Al 2p. Oxygen exposure is indicated by numbers. (1) clean surface; (2) 0.2 L O₂; (3) 1 L O₂; (4) 10 L O₂; (5) 100 L O₂; (6) annealed at 430 K for 20 minutes, then cooled down to 300 K; (7) 300 L O₂.

Figure 13

O 1s contribution to the (O 1s and Pd 3p_{3/2}) area as a function of O₂ exposure. A close up view is shown as well between 0 L to 20 L of O₂ exposure.

Figure 14

XP air-oxidized spectra after the 10f sample was introduced from air to UHV. (a) Zn 2p_{3/2}; (b) Pd 3d; (c) Al 2p.

Tables**Table 1**

Final surface composition of Al, Pd, and Zn for the 10f and 2f samples after several cycles of sputtering. Bulk composition is also shown as reference.

	Al	Pd	Zn
10f (204 minutes)	67%	30%	3%
2f (40 minutes)	62%	32%	6%
Bulk	57%	30%	13%

Table 2

Variable temperature annealing: compositional evolution from XPS. The final compositions for the 10f and 2f samples that was annealed at given temperatures and was then cooled down to 300 K.

	Al	Pd	Zn
10f (540 K)	49%	21%	30%
2f (513 K)	53%	14%	33%
Bulk	57%	30%	13%

Table 3

Constant temperature annealing: compositional evolution from XPS. The final compositions for the 10f and 2f samples that was annealed at given temperatures and was then cooled down to 300 K.

	Al	Pd	Zn
10f (460 K)	52%	22%	26%
2f (478 K)	58%	22%	20%
Bulk	57%	30%	13%

Table 4

RMS surface roughness held constant at different STM settings such as tunneling current and tip bias voltage.

Approximant	Surface Area (nm x nm)	Tunneling Current (nA)	Bias Voltage (V)	RMS surface roughness (nm)
10f	100 x 100	0.5	-2	0.4953
10f	100 x 100	0.5	+2	0.6737
10f	100 x 100	0.5	+1	0.8044
10f	100 x 100	0.5	-1	0.8337
2f	50 x 50	0.5	-1	0.3897
2f	50 x 50	0.5	+1	0.3852
2f	100 x 100	0.5	-1	0.5860
2f	100 x 100	0.5	+1	0.5805
2f	500 x 500	0.5	-1	0.7766
2f	500 x 500	0.5	+1	0.7969
2f	1000 x 1000	0.5	-1	0.847
2f	1000 x 1000	0.5	+1	0.8208

Table 5

Surface composition of Al, Pd, and Zn as a function of O₂ exposure when surface was exposed to oxygen in UHV. Bulk composition is also shown as a reference.

O₂ Exp. (L)	Al (%)	Pd (%)	Zn (%)
0	60	33	7
0.2	64	30	6
1	64	30	6
10	66	29	5
100	66	31	3
100 (Annealed at 430 K for 20 minutes, then cooled down to 300 K)	69	29	2
300	69	30	1
Bulk	57	30	13

Table 6A

Surface composition of Al, Pd, and Zn after oxidation under two conditions, as well as the clean surface and the bulk as reference. The percent changed in Al relative to clean surface and the bulk is also shown.

	% Al	% Pd	% Zn	% Δ Al relative to clean surface	% Δ Al relative to bulk
Bulk Composition	57	30	13	-	-
Clean Surface Composition	60	33	6.8	-	-
After exposure to oxygen in vacuum at 300 K (300 L)	69	30	1.4	+15	+21
After exposure to air at 300 K	85	6.9	8.03	+42	+49

Table 6B

Surface composition of Al, Pd, and Mn after oxidation under two conditions, as well as the clean surface and the bulk as reference. The percent changed in Al relative to clean surface and the bulk is also shown.

	% Al	% Pd	% Mn	% Δ Al relative to clean surface	% Δ Al relative to bulk
Bulk Composition	70	21	9	-	-
Clean Surface Composition	70.5	23.1	6.4	-	-
After exposure to oxygen in vacuum at 300 K (> 80 L)	72.1	21	6.9	+2.3	+3
After exposure to air at 300 K	89.5	8.3	2.2	+27	+28

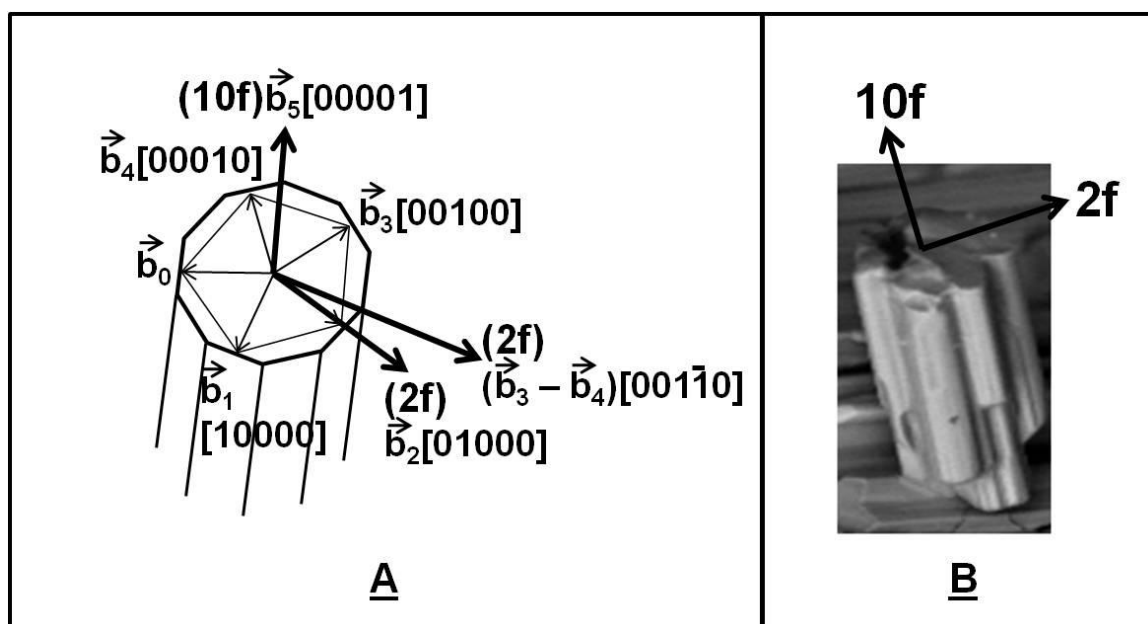


Figure 1

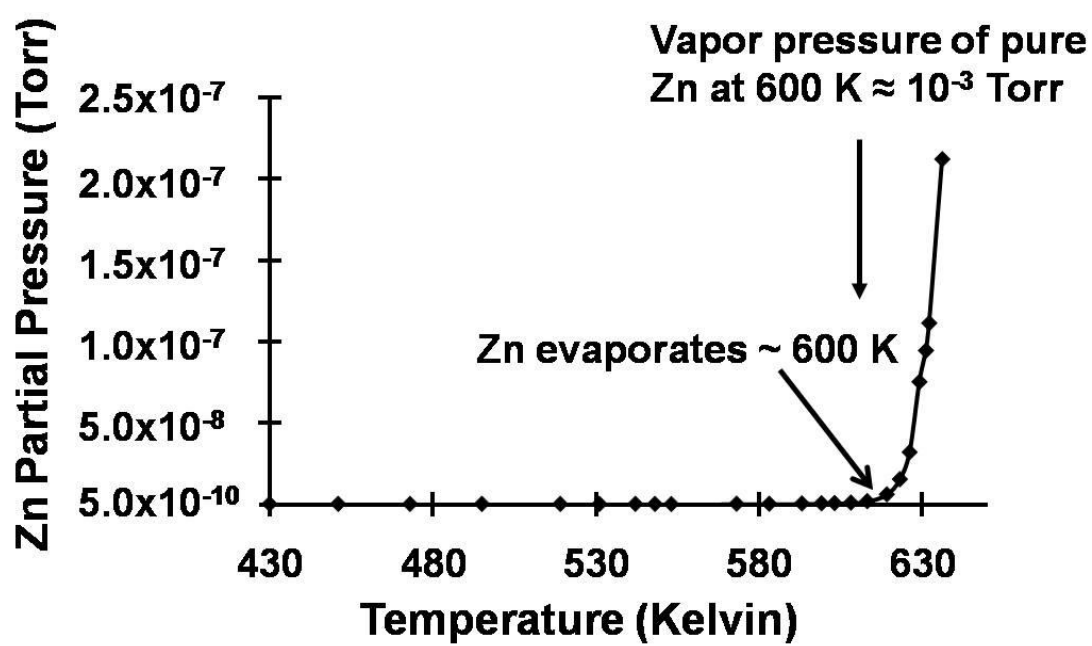


Figure 2

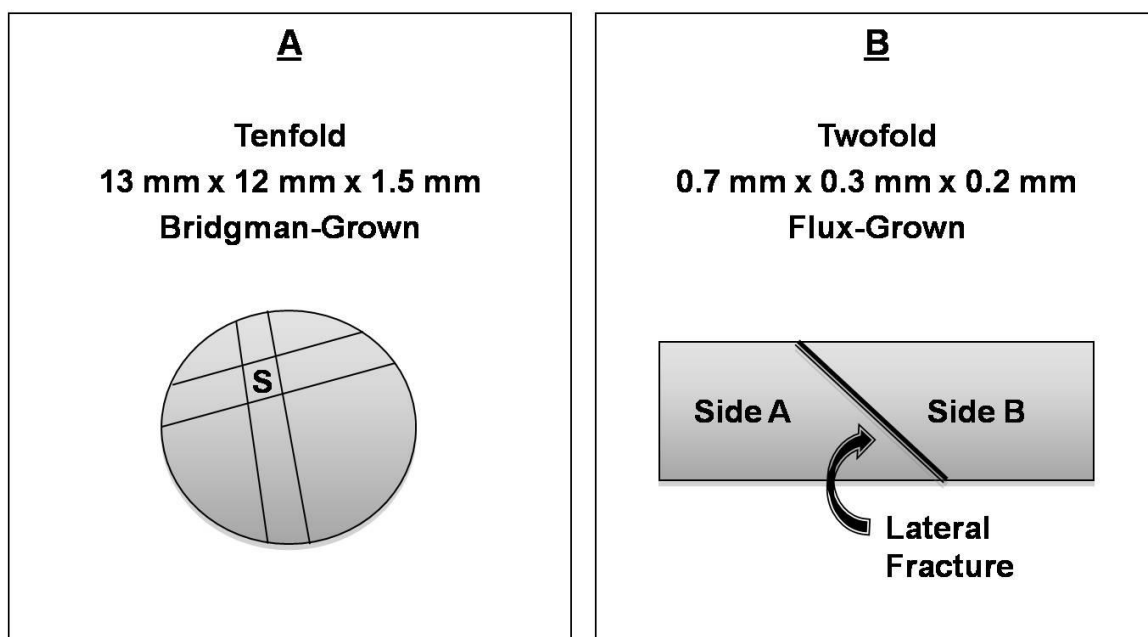


Figure 3

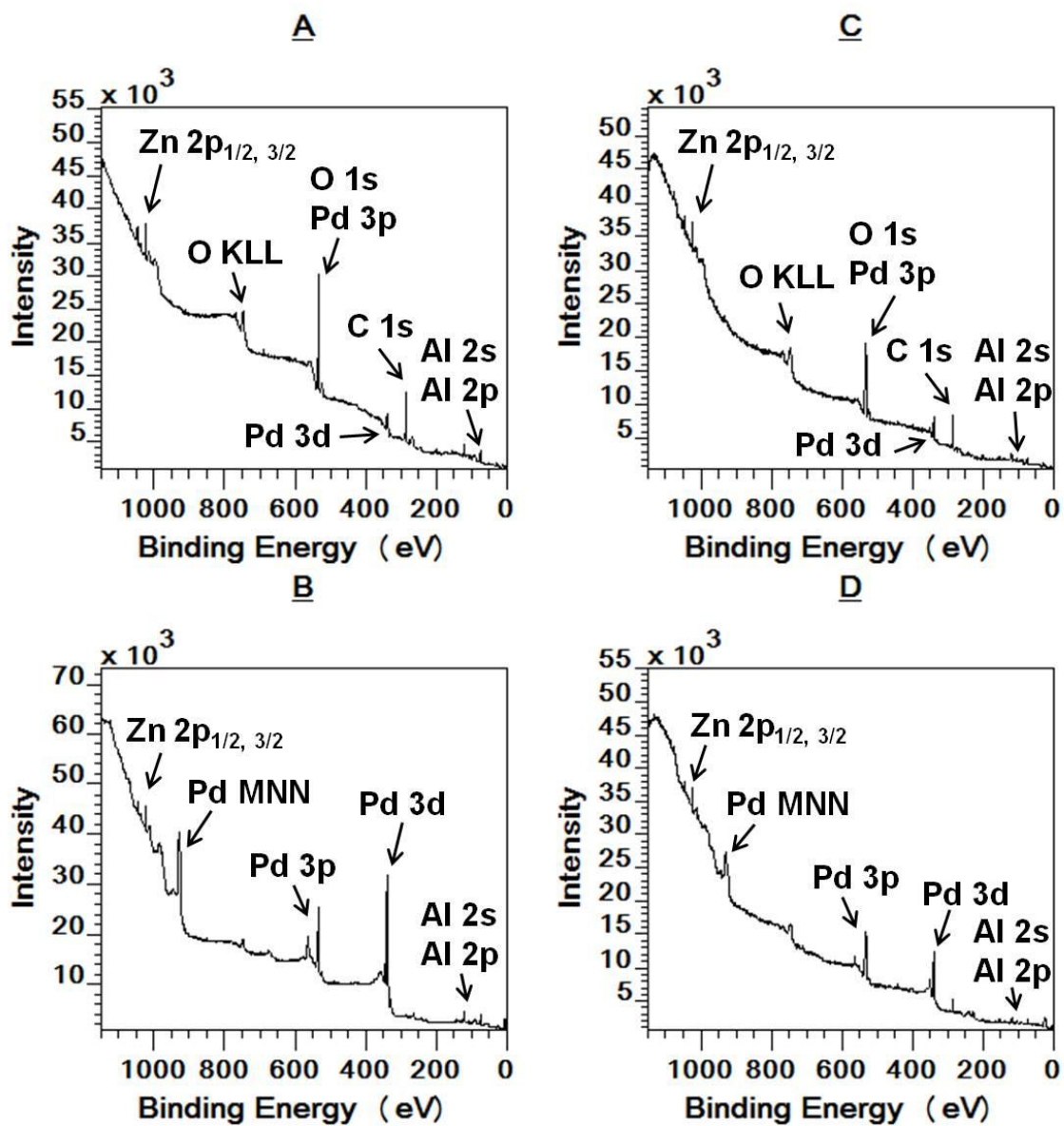


Figure 4

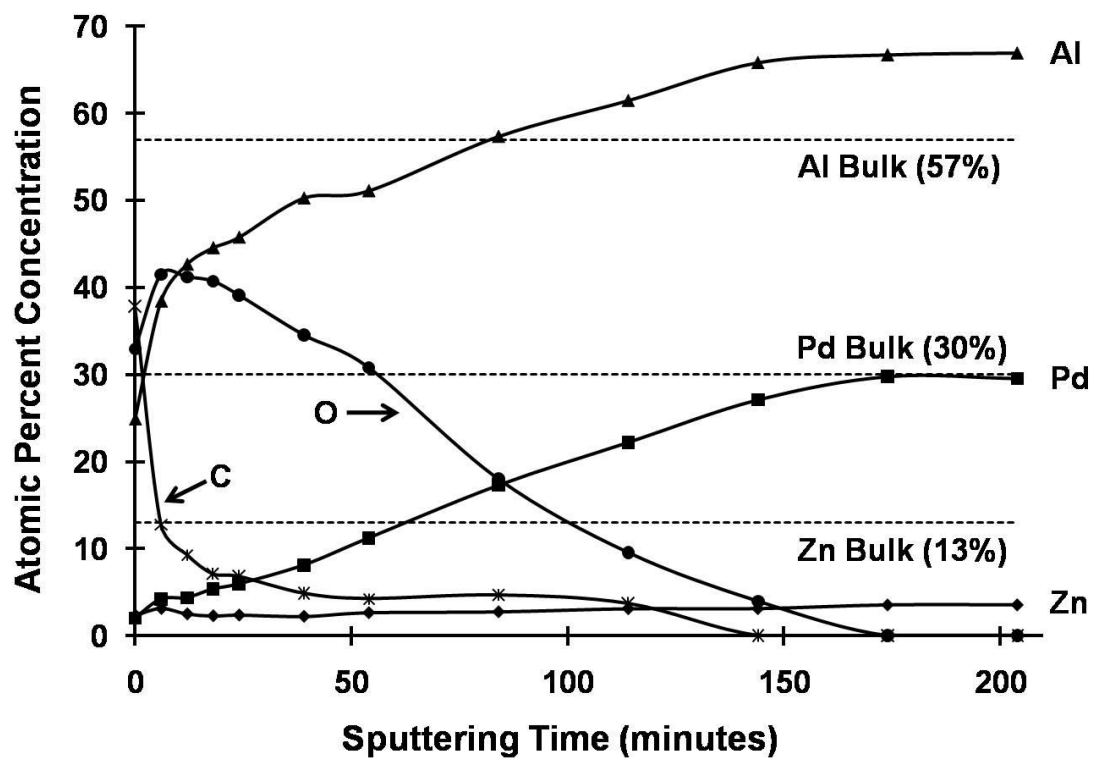


Figure 5

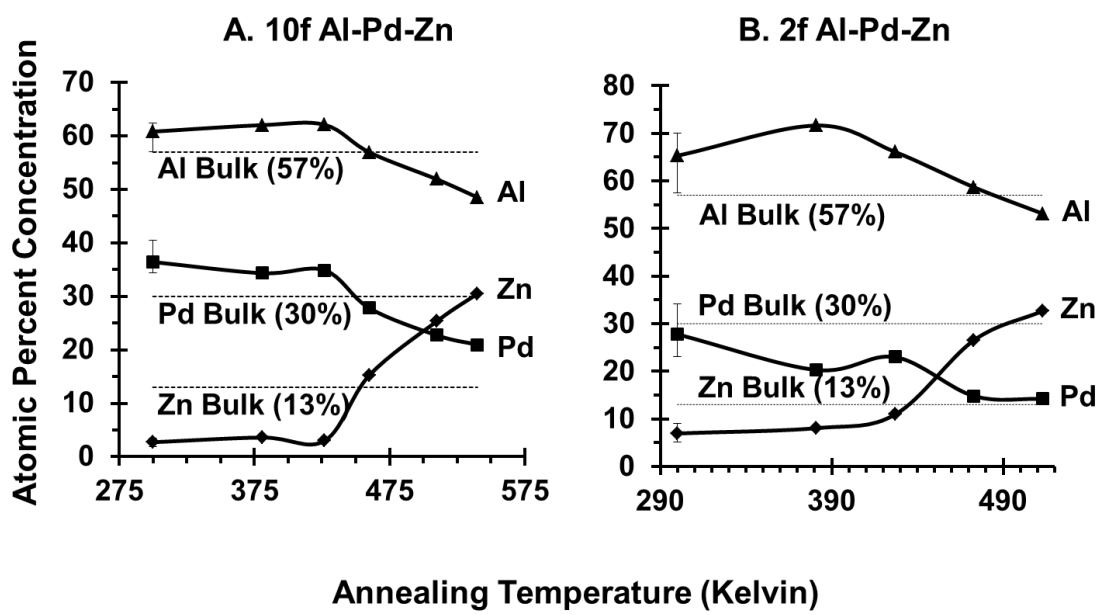


Figure 6

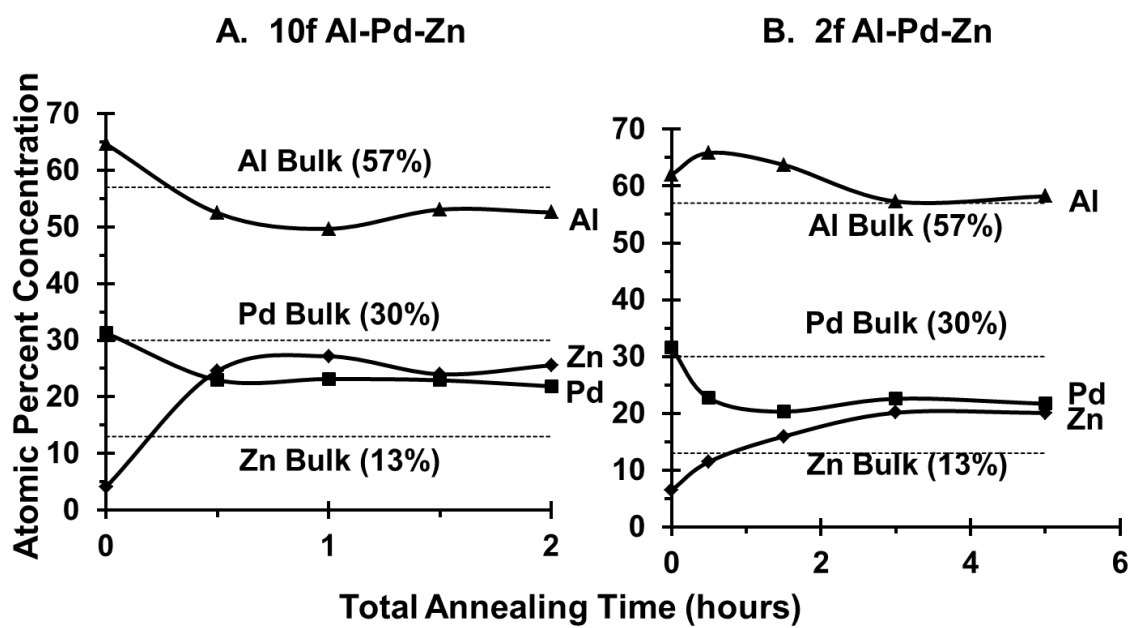


Figure 7

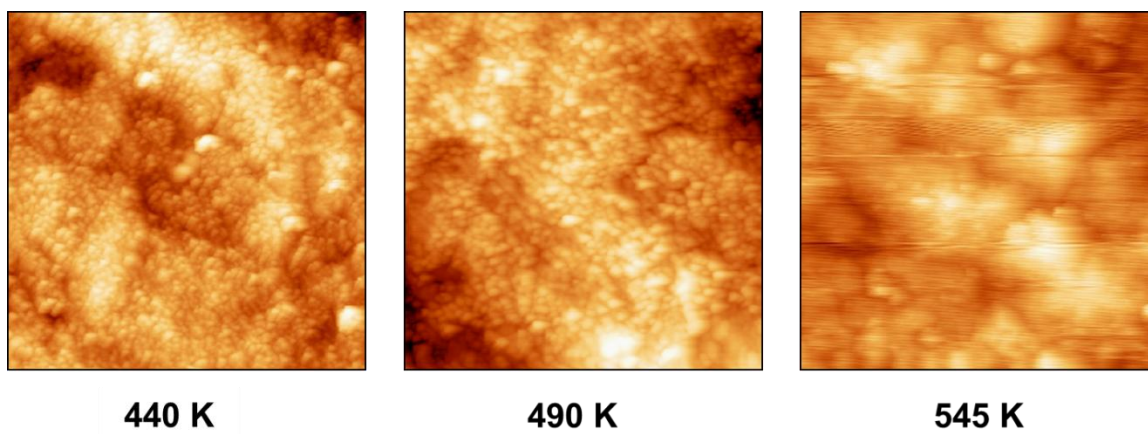


Figure 8

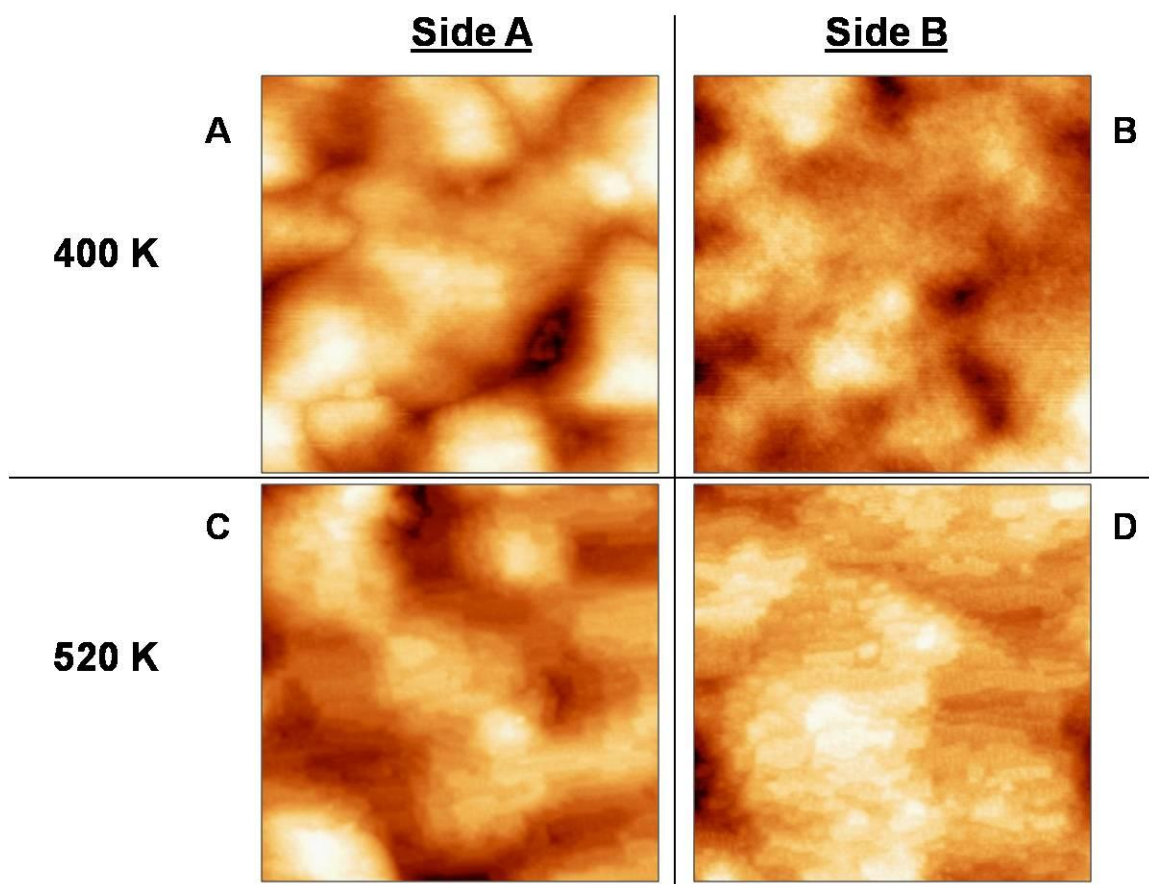


Figure 9

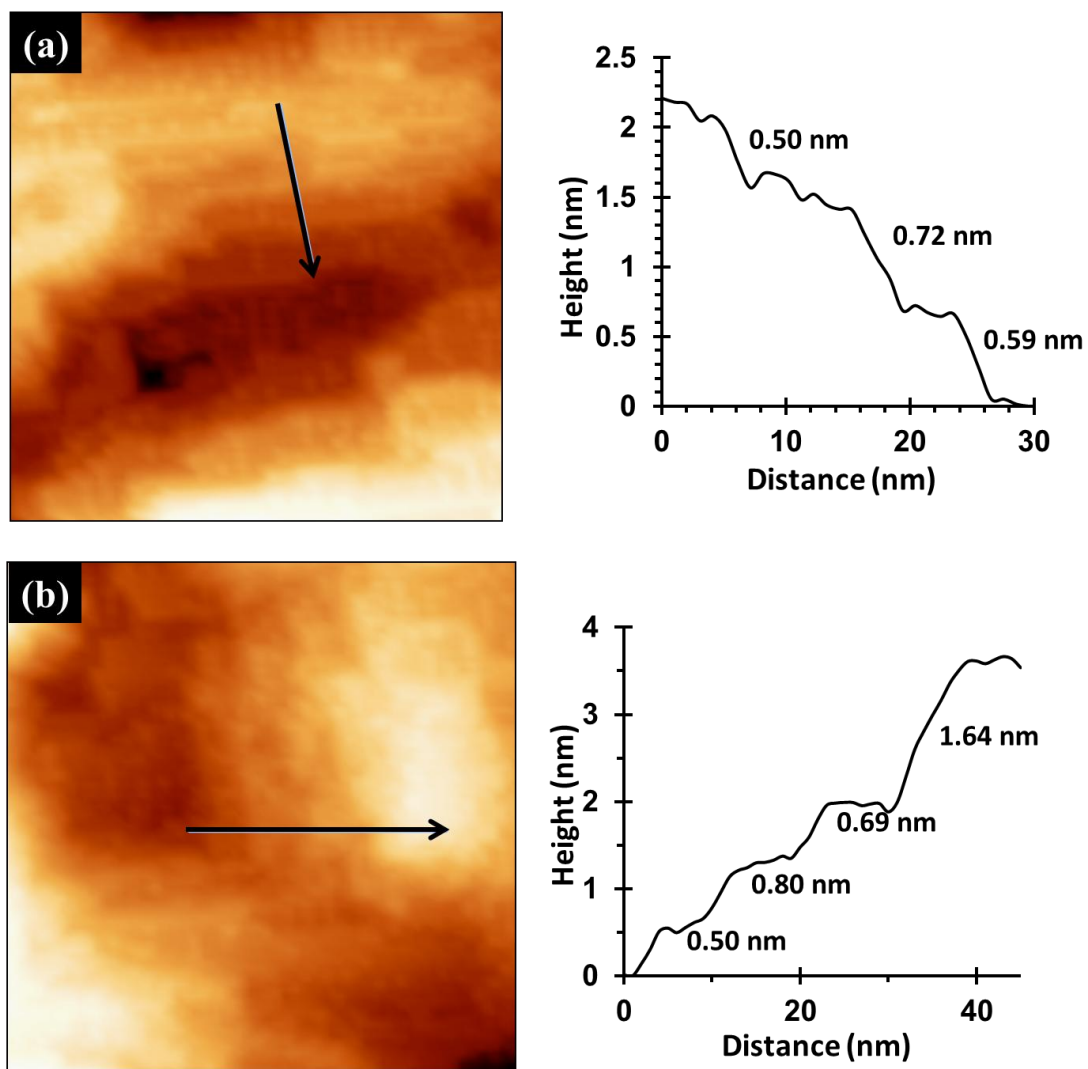


Figure 10

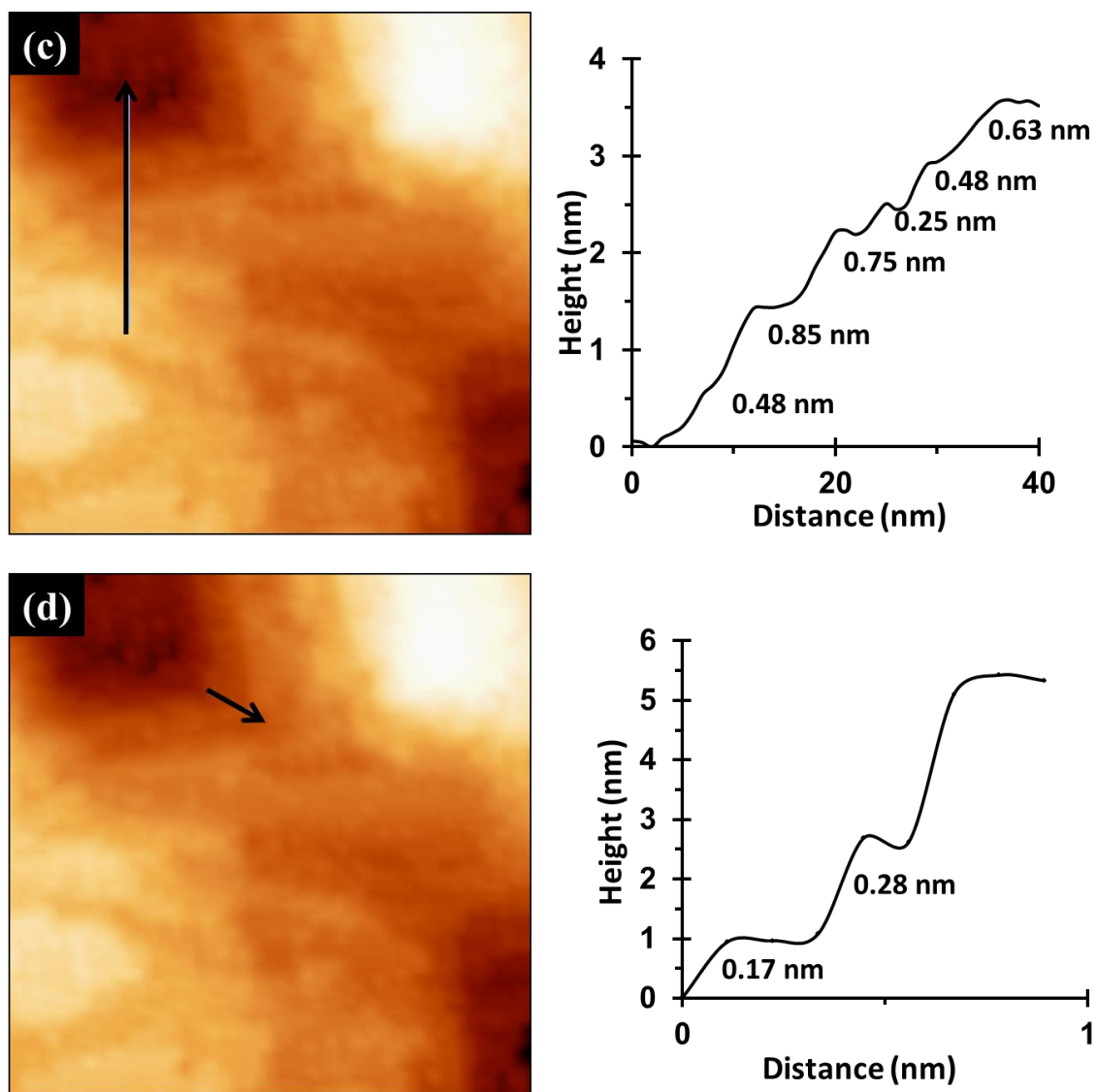


Figure 10 (Continue)

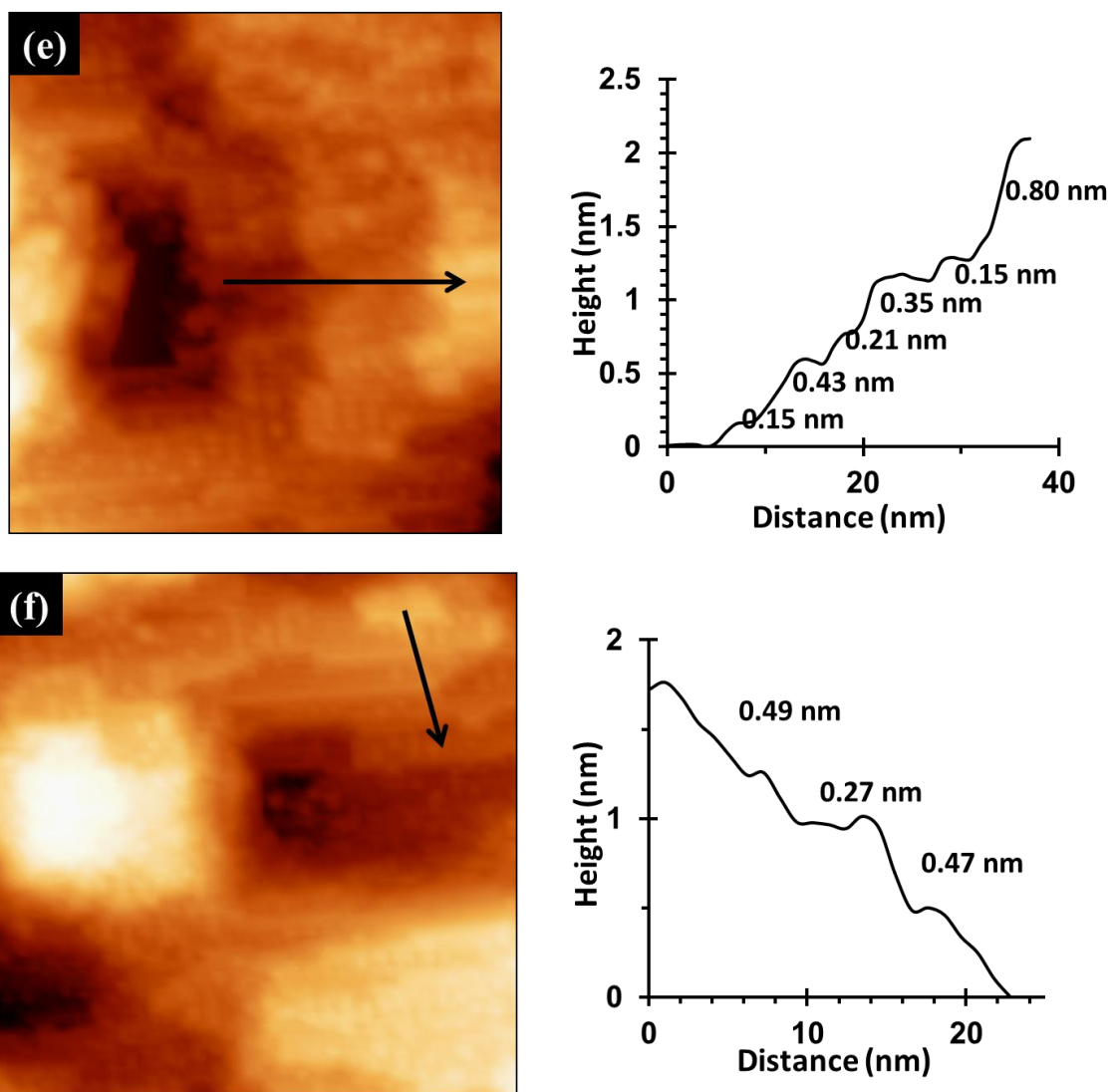


Figure 10 (Continue)

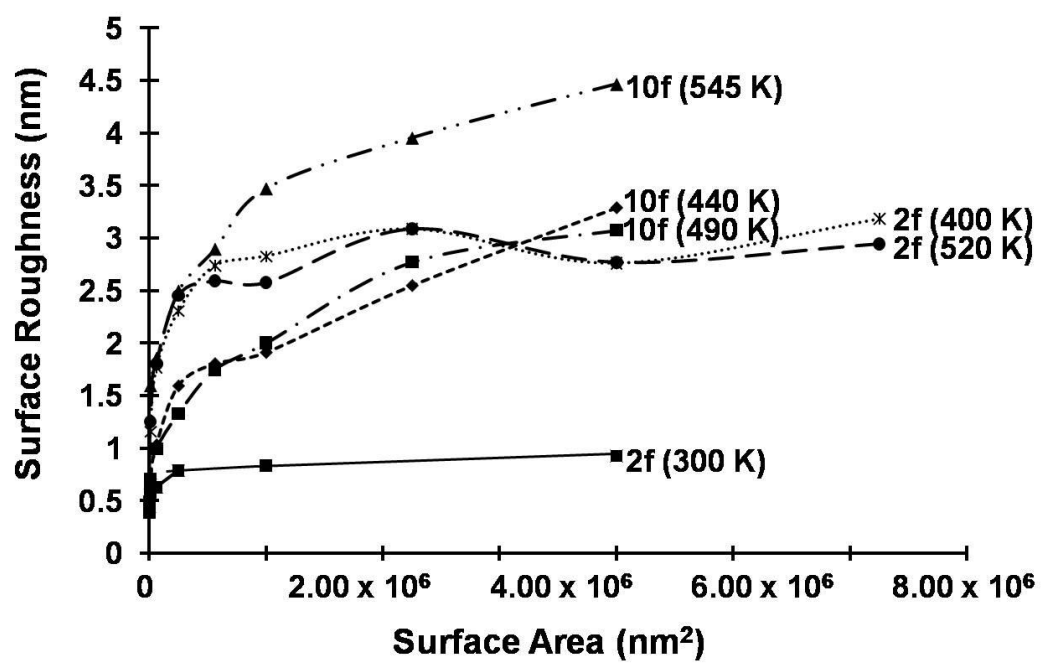


Figure 11A

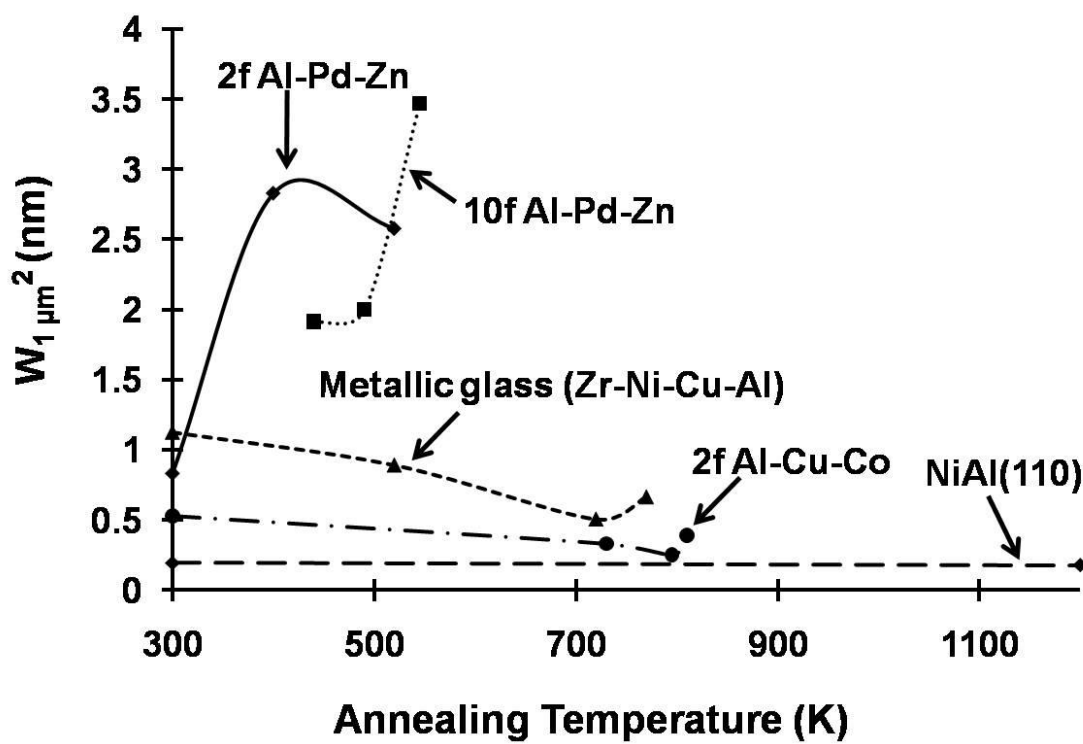


Figure 11B

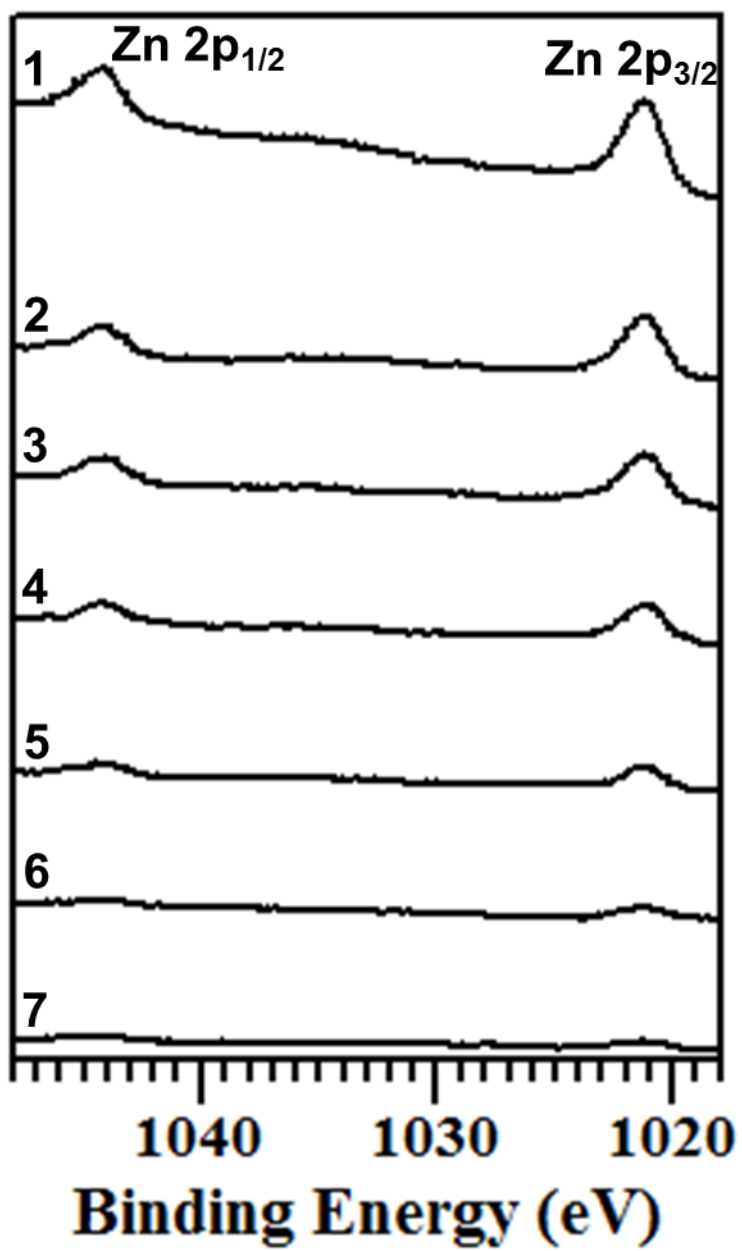


Figure 12A

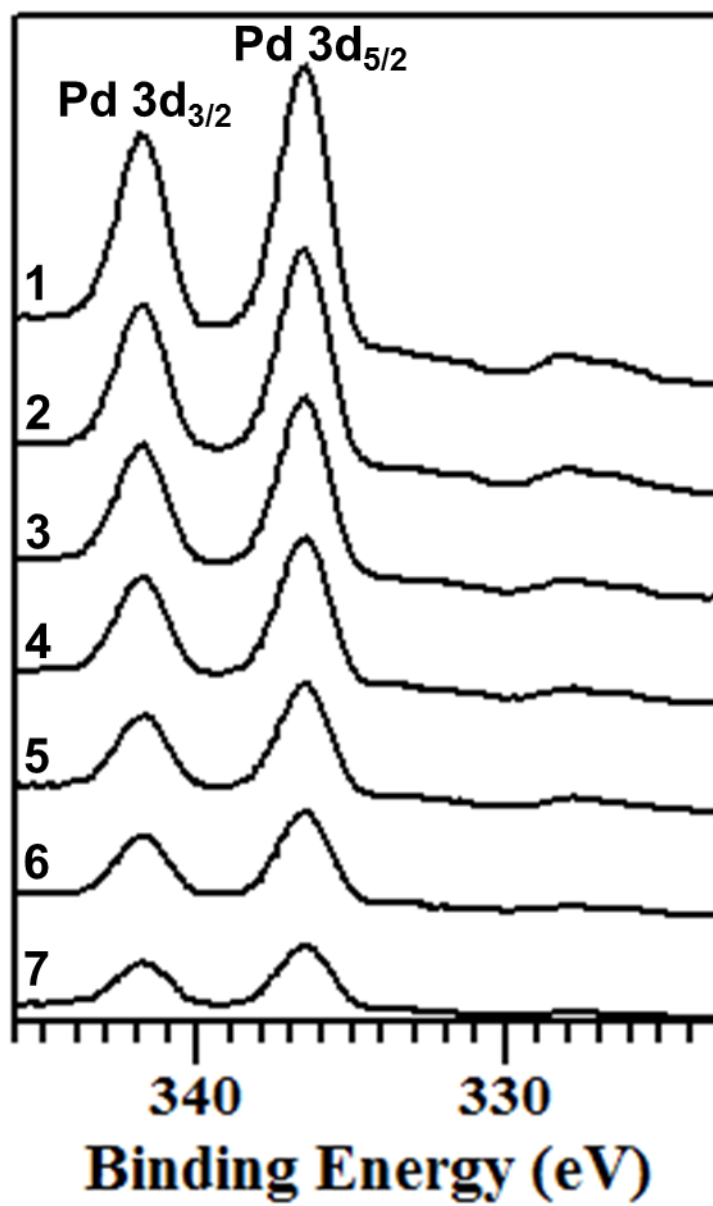


Figure 12B

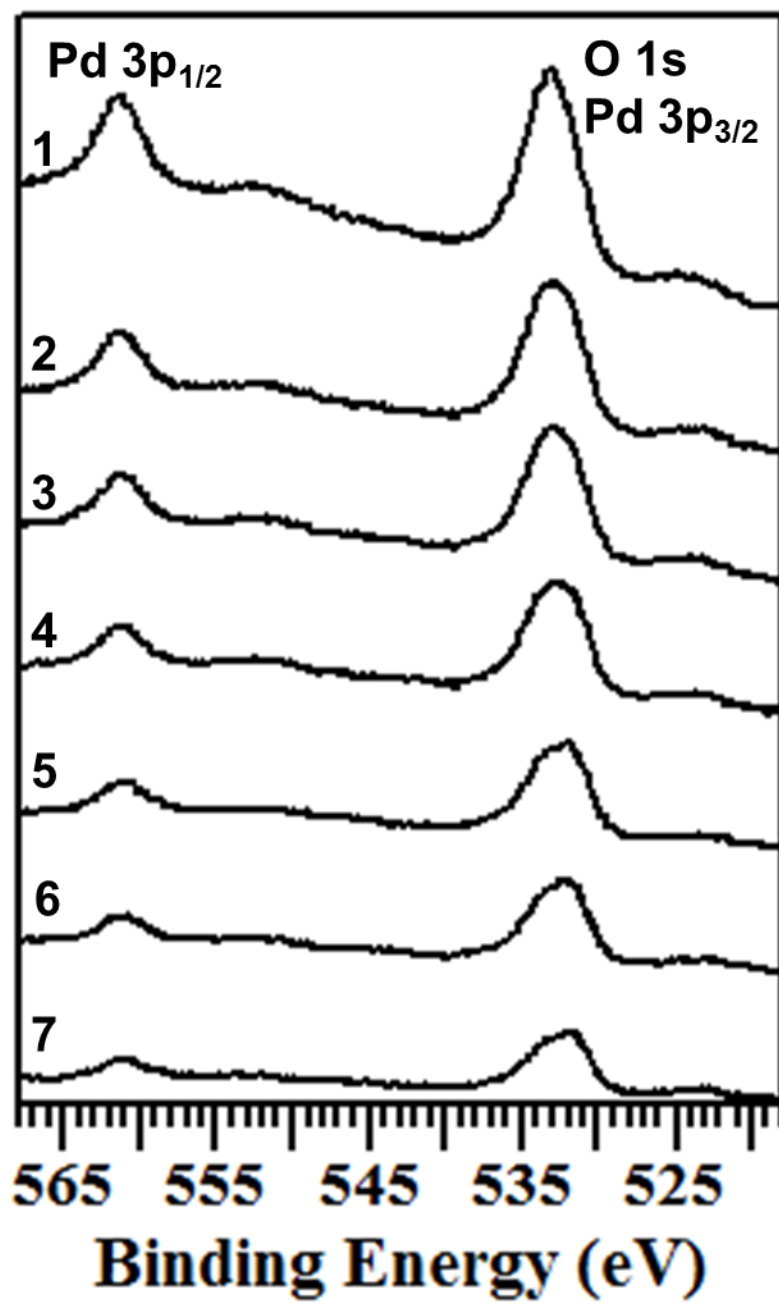


Figure 12C

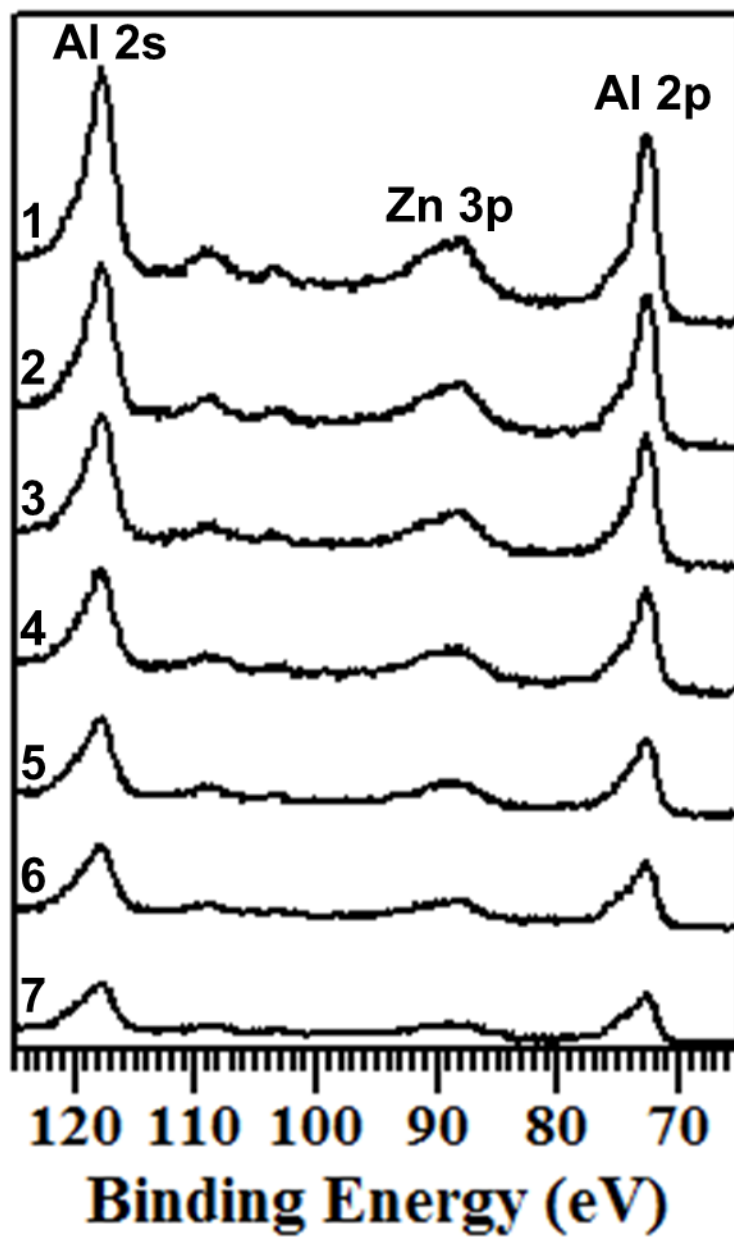


Figure 12D

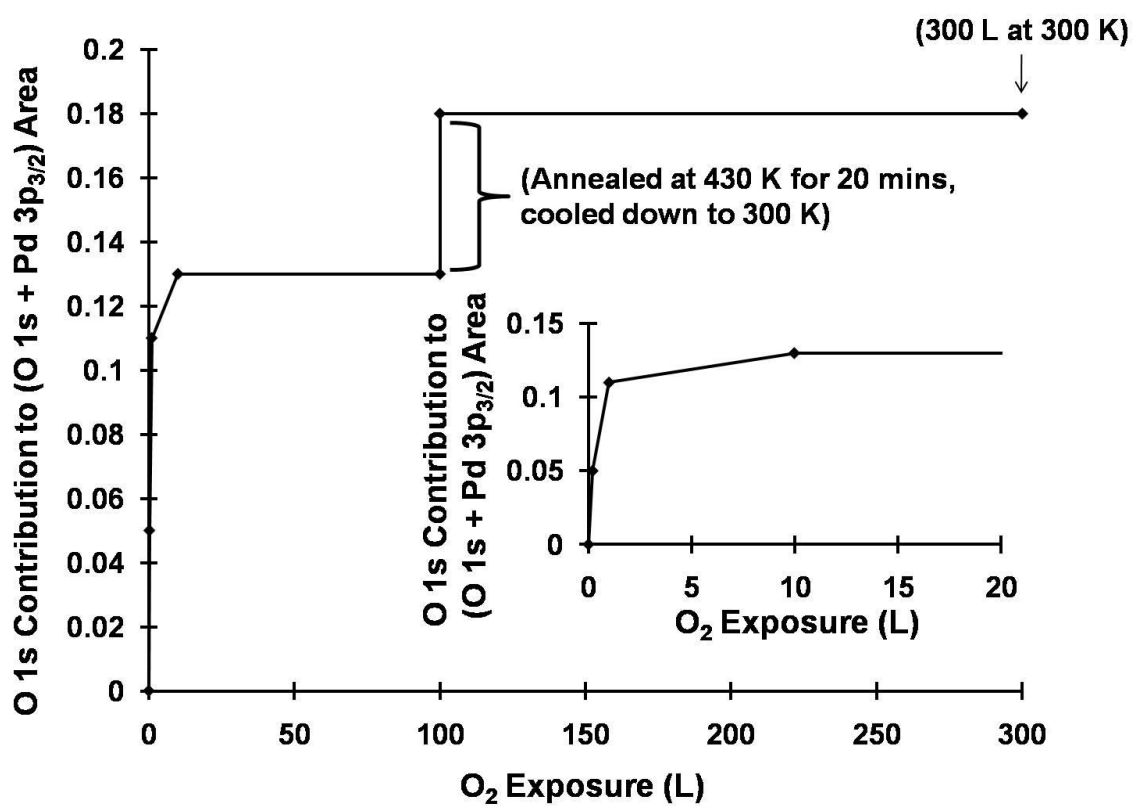


Figure 13

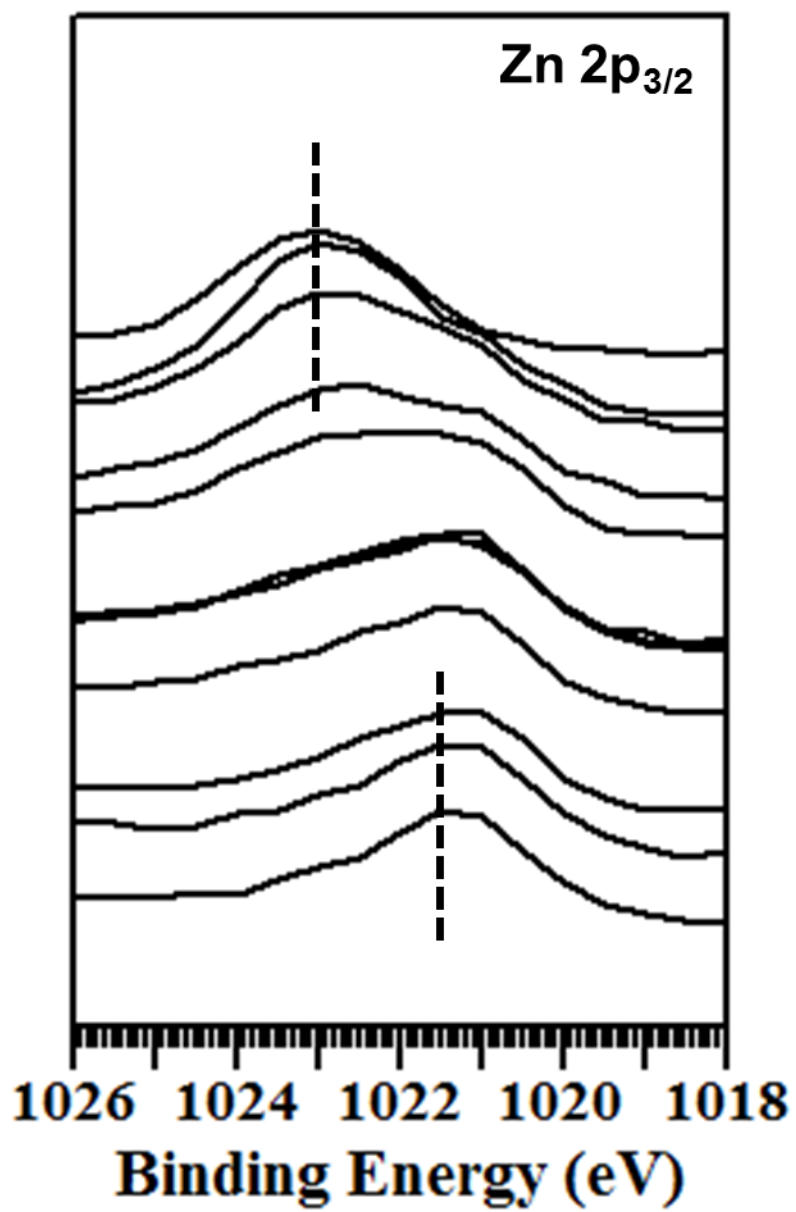


Figure 14A

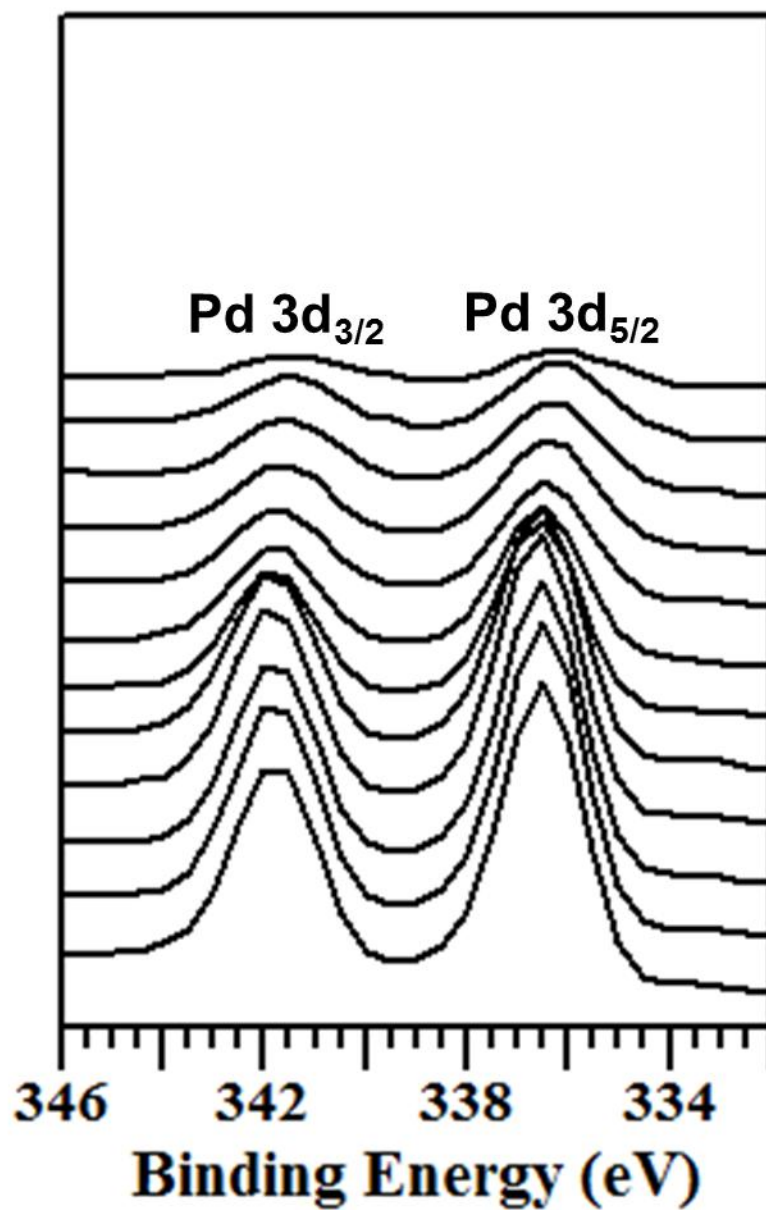


Figure 14B

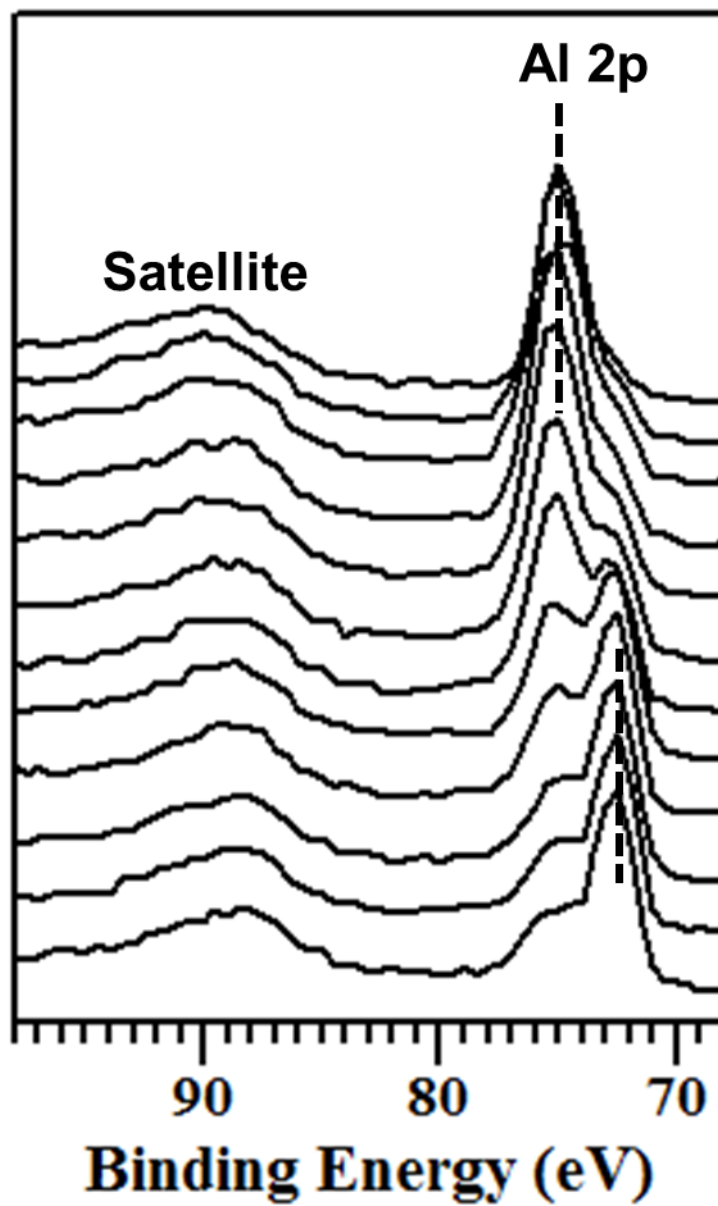


Figure 14C

CHAPTER 3

Structure of the Clean $\text{Gd}_5\text{Ge}_4(010)$ Surface

Chad D. Yuen,^{1,2} Gordon J. Miller,^{1,2} and Patricia A. Thiel^{1,2,3}

¹Ames Laboratory, Iowa State University, Ames, Iowa, 50011

²Department of Chemistry, Iowa State University, Ames, Iowa 50011

³Department of Material Science and Engineering, Iowa State University, Ames, Iowa 50011

Abstract

We have characterized four different samples of the (010) surface of Gd_5Ge_4 . Using X-ray photoelectron spectroscopy, data from samples #1-3 show the surface composition is the same as the bulk composition within ± 5 atomic %, both after sputtering and after annealing at various temperatures. Using scanning tunneling microscopy, data from samples #1-2 show the surface exhibits two main types of terraces, which have much different fine structures. The two types of terraces alternate across the surface. Under some conditions they have comparable areas and the alternation is visually striking. Under other conditions a single type dominates, but the second type is still discernible as part of a step bunch. Step heights between similar terraces correspond well to the separation between equivalent layers along the $\langle 010 \rangle$ direction in the bulk structure, and step heights between dissimilar terraces correspond to the distance between certain dissimilar but dense layers. However, the fine structure on the terraces does not correlate with the bulk structure, and we suggest that there is significant surface

reconstruction. In addition, data from scanning electron microscopy, optical microscopy, Auger electron spectroscopy and Auger electron microscopy reveal small amounts of a Gd_5Ge_3 secondary phase at the surface of sample #4.

1. Introduction

The Gd_5Ge_4 binary alloy and its pseudobinary $\text{Gd}_5(\text{SixGe}_{1-x})_4$ have been extensively investigated for their magnetic and thermomagnetic properties [1-3]. These alloys or compounds are promising materials for magnetic refrigeration near or below room temperature [4; 5]. They were discovered in the 1960s by Smith et al. [6] and Holtzberg et al. [7], separately.

We choose the (010) surface because the closest-packed planes in the bulk are (010)-type, meaning that this is likely to be the most stable surface.

In addition, it is well-established that a small amount of a secondary phase is always present in single-crystal samples of Gd_5Ge_4 and other closely-related compounds. The secondary phase is Gd_5Ge_3 . More details of this secondary phase are discussed later.

The primary goal of the present work is to study the structure and composition of the Gd_5Ge_4 (010) surface, and to compare these features with its bulk characteristics. A secondary goal is to characterize the surfaces of the lines of Gd_5Ge_3 phase within the Gd_5Ge_4 (010) surface.

In Section 2, we describe our experimental procedures. In Section 3, we provide background about the bulk structures of Gd_5Ge_4 and Gd_5Ge_3 . In Section 4, we present the experimental results of our study by using XPS and STM. In Section 5, we compare our

STM results with the bulk structure of Gd_5Ge_4 . In Section 6, we characterize the Gd_5Ge_3 thin plates on the Gd_5Ge_4 surface using SEM, AES, OM, STM, and SAM.

2. Experimental Procedures

A single crystal of Gd_5Ge_4 was synthesized at the Materials Preparation Center (MPC) of the Ames Laboratory [8]. Appropriate quantities of Gd, 99.996% pure (wt. %) and Ge, 99.999% pure, were cleaned and arc melted several times under an argon atmosphere. The arc melted button was then used as the charge material in a tri-arc crystal pulling unit. A tungsten rod was used as the seed material, which resulted in a randomly oriented Gd_5Ge_4 crystal. A detailed description of the tri-arc method is available elsewhere [9].

The as-grown Gd_5Ge_4 crystal was oriented, by back-reflection Laue, to within $\pm 0.25^\circ$ of the (010) direction. The crystallographic direction was verified on the basis of an X-ray diffraction (XRD) two-theta scan of the single crystal face. From the single crystal, four oriented samples were cut by spark erosion. Samples #1 and #2 had dimensions of 10.4 mm x 1.9 mm x 2.9 mm, and 10.0 mm x 2.0 mm x 1.6 mm, respectively. Each rectangular sample was polished on one of its (010) faces using standard metallographic techniques. The final abrasive was $\frac{1}{4}$ micron diamond paste. Once polished, two 0.127 mm thick tantalum foils were spot-welded onto a tantalum plate to hold each sample in place for analysis. In this text, the Gd_5Ge_4 samples are called sample #1 (MPC hmd-1-73) sample #2 (MPC dls-7-68-2), sample #3 (MPC dlw-1-97), and sample #4 (MPC dlw-1-

1). Of these, samples #1, #2, and #4 were taken from the same ingot (MPC Ingot #Ta-2-113) and sample #3 was taken from a different ingot (MPC Ingot #Ta-2-115).

The first three samples were used for experiments in an Omicron ultrahigh vacuum (UHV) chamber with base pressure $\leq 1.0 \times 10^{-10}$ mbar. The chamber was equipped with an ion sputter gun, mass spectrometer, and other basic UHV instrumentation. X-ray photoelectron spectroscopy (XPS) experiments were performed with an Omicron X-ray source (Al K α), Variable Temperature Scanning Tunneling Microscopy (VT-STM), and an Omicron EA 125 hemispherical electron energy analyzer. This chamber will be referred to as the STM/XPS UHV chamber.

Ion bombardment was used to clean each sample. The sample was bombarded with Ar^+ ions at 1.5 KeV energy, with the incident beam at an angle of 45° to the surface plane and the sample held at 300 K. The chamber was back-filled with Ar to a pressure of 2×10^{-6} mbar. Typical sputtering duration was 9 minutes total—3 minutes on each of the 3 different positions of the sample (left and right sides, and middle).

Each cleaning *cycle* consisted of sputtering and heating, where the heating served to heal the surface damage induce by sputtering. A pyrolitic born nitride (PBN) element was mounted on the manipulator, below the sample plate, and could be heated resistively. Annealing was achieved by slowly increasing the heating current at a rate of 0.2-0.3 A every 4 minutes until the desired temperature was reached. Temperature was maintained for 30 and 60 minutes in XPS and STM experiments, respectively. Power supply settings of 38.8 V and 1.7 A were adequate to maintain temperature at 900 K. The sample was then cooled slowly by decreasing the current by 0.2-0.3 A every 4 minutes. With this regimen, it took about 40 minutes to cool from 900 K to almost 300 K, for an average

cooling rate of 15 K/min starting from 900 K. Starting from 1200 K, the average cooling rate was 20 K/min. Typical temperature-power and temperature-time programs are shown during sample cooling, starting from 900 K and from 1200 K, both for sample #1 and sample #2, in Fig. 1.

The sample temperature was measured by several means. The simplest, but least accurate, was a K-type thermocouple spotwelded to the manipulator. The source of error with this method was the fact that the thermocouple was not directly attached to the sample, but rather to the sample plate. Hence, one could expect the temperature at the thermocouple to be lower than at the sample. A more accurate method was optical pyrometry, which was limited to temperatures above 900 K due to emissivity and is somewhat inconvenient. Because of its drawbacks, optical pyrometry was used only occasionally to check temperature. A third method relied simply on the heating power. Previously, a relationship had been established between the sample temperature and heating power for this instrument, by attaching a thermocouple directly to a sample, temporarily[10]. In our experiments, we found that when the Gd-Ge sample temperature from the power reading was 1200 K, the pyrometer read 1190 K (a difference of only 10 K) and the thermocouple read 1055 K (lower—as expected—by 135 K). Temperatures reported in this paper are based on the power calibration.

For sample #2, a temperature gradient existed on the surface during annealing. Optical pyrometry showed that the two sides were hotter than the middle of the sample. Specifically, the pyrometer showed that the middle was coolest, the right side 10 K hotter, and the left side 20 K hotter than the middle, at a nominal temperature of 900 K from the power calibration. There was no measurable temperature gradient on sample #1.

The XPS source was perpendicular to the sample plate, and the take-off angle (the angle between the entrance axis of the analyzer and the sample surface plane) was 45° . The angular acceptance range was $\pm 8^\circ$. The aperture used in the EA 125 analyzer was 6 mm x 12 mm. The most intense photoelectron peaks of Gd and Ge were the Gd $3d_{5/2}$ peak at a binding energy of 1186 eV, and the Ge $2p_{1/2}$ peak at 1248 eV. XP spectra were analyzed with CasaXPS software [11].

STM was used to study the surface morphology of each Gd_5Ge_4 (010) sample. Data processing was performed by WSxM scanning probe microscopy software [12]. A tungsten tip was used, and tip bias voltages ranged from -1 V to +1 V. The tunneling current was set at 0.5 nA. A single STM image could be acquired in ~ 2 minutes. All STM was carried out with the sample at room temperature. If the sample had been annealed, it was allowed to equilibrate for one hour after the heating power supply was turned off completely, before STM began.

Some experiments were performed in another chamber, equipped for scanning electron microscopy (SEM), scanning Auger electron microscopy (SAM), and Auger electron spectroscopy (AES). In this chamber, the base pressure was $\leq 10^{-9}$ mbar. The system was a JEOL Jamp-7830F Field Emission Auger Microprobe. The Gd_5Ge_4 (010) sample was held in a homebuilt Mo sample holder.

3. Background: Bulk Phases

3.1 Gd₅Ge₄

The binary Gd₅Ge₄ alloy is a line compound that contains 55 at. % Gd and 45 at. % Ge. According to the published phase diagram (Fig. 2) [13], peritectic decomposition to Gd₅Ge₃ occurs at ~1970 K, with the liquidus at 2073 K [14]. Thermal analysis was performed on a portion of the MPC-grown Gd₅Ge₄ sample, and results were consistent with the published information. Lattice parameters, space groups, and prototypes of all the Gd-Ge binary alloys are presented in Table 1 as reference [13; 15; 16].

Gd₅Ge₄ is an orthorhombic Sm₅Ge₄-type structure with space group Pnma, Z = 4, and lattice parameters a = 0.769 nm, b = 1.482 nm, and c = 0.778 nm. It contains 36 atoms in the unit cell [17; 18]. The crystal structure is shown in Figure 3(a). The rectangular box in 3(a) represents the unit cell. As shown in Figure 3(a), the orthorhombic structure is built by stacking pseudo-two dimensional slabs along the (010) direction (along the b axis). Each slab contains five planes consisting of Gd, Ge, or a mixture of Gd and Ge atoms. The slabs repeat at separations of 0.741 nm along the b direction, which is half the b lattice constant, 1.482 nm [1; 2; 14; 19].

The top two planes of atoms in the (010) surface are depicted in Fig. 3(b). The large dark blue circles represent the Gd atoms and the small light blue circles represent the Ge atoms. The bulk unit cell, shown by the rectangle, is nearly square, being 0.769 nm and 0.778 nm on the edges.

3.2 Gd_5Ge_3 Thin Plates

In 1999, linear features were first reported on the $Gd_5(Si_xGe_{1-x})_4$ surface by Szade et al [20], on the basis of Scanning Electron Microscopy (SEM) Auger Electron Spectroscopy (AES), and optical microscopy. The authors determined that these linear features were not grain boundaries, nor were they parallel to any crystallographic directions with low indices.

Since then, these linear features have been identified as thin plates of $Gd_5(Si,Ge)_3$ [21-24] which has the hexagonal Mn_5Si_3 -type structure[25; 26]. Analogous features have been found on Gd_5Ge_4 surfaces, as well as on RE_5Si_4 , $RE_5(Si_{1-x}Ge_x)_4$, and RE_5Ge_4 surfaces, where RE is either Gd, Tb, Dy, and Er lanthanides [21]. For Gd_5Ge_3 , the lattice parameters are $a = b = 0.8546$ nm and $c = 0.6410$ nm [13; 15; 23; 27]. This phase is included in Table 1. The Gd_5Ge_3 alloy has a bulk composition of 63 at. % Gd and 37 at. % Ge [28]. The thin plates reportedly intersect at angles of 80° when viewed along the (010) direction [23], cover 1 to 6 % of the surface area [24] and are about 250 nm wide [23]. The reasons for the consistent presence of this second phase are unknown, but it appears to form via a solid-state reaction during cooling [23].

4. Experimental Results

4.1 XPS

4.1.1 XPS: Initial Depth-Profiling after Air Exposure (Sample #1)

Immediately after the Gd_5Ge_4 (010) sample was placed in the STM/XPS UHV chamber, surface compositional analysis with XPS was conducted. Fig. 4 shows the

surface composition as a function of sputter time (the depth profile) during the initial cleaning cycle. At the beginning, carbon and oxygen peaks have high intensity. No other contaminants such as sulfur are detected. In addition, low concentrations of Gd and Ge are detected. This is expected since the surface had been exposed to air, which typically leaves a thick layer of oxygen and carbon contamination. After a total of 118 minutes of sputtering, the oxygen and carbon are undetectable and the surface composition (from XPS) is 56 at. % Gd and 44 at. % Ge, very close to the bulk composition of 55 at. % Gd and 45 at. % Ge.

4.1.2 XPS: Surface Composition as a Function of Annealing Temperature in UHV (Sample #1, #2, and #3)

In these experiments, the Gd_5Ge_4 (010) sample was annealed at temperatures ranging from 400 K to 1200 K for 30 minutes. After annealing, the sample was slowly cooled to room temperature for XPS analysis. At this point, the intensities of the Ge $2p_{1/2}$ and the Gd $3d_{5/2}$ photoelectron peaks were measured.

Figure 5(a) shows the result for sample #1. On this sample, two of the annealing temperature data points—900 K and 1200 K—were measured twice to check reproducibility. This is reflected in the error bars (which are quite large at 1200 K). Note that the error bar on the Ge concentration at 1200 K is shifted laterally, to prevent confusing overlap with the Gd error bar. At all temperatures, the surface composition is within ± 5 at. % of the bulk. The data suggest that there may be a decrease in Gd at high temperatures, but the error bars are so large at high temperature that this conclusion is dubious. For this reason, the experiment was performed again on a different sample.

Figure 5(b) shows the result for sample #2. On this sample, all of the annealing temperatures were replicated. Data from the two runs are very consistent. Between 300 K and 500 K, there are minor variations in concentration, but a stable plateau seems to exist between 500 and 900 K. Above 900 K, minor variations again occur. In addition, the opened squares and diamonds in Figure 5(b) is the result from sample #3. At all temperatures, the surface composition is within ± 5 at. % of the bulk for both sample #2 and sample #3.

4.1.3 XPS: Depth-Profiling after Annealing at Different Temperatures in UHV (Samples #1, #2, and #3)

The procedure described in Section 4.1.2 was followed, except that after initial measurement of the Ge and Gd peak intensities, the surface was subjected to 2-minute intervals of Ar⁺ sputtering. XPS was measured between each interval, until a total sputtering time of 10 minutes had elapsed. Sample #1 was used for all these experiments except for the 900 K annealing treatment. There, sample #2 was used and also, total sputtering time was longer, 28 minutes.

Figure 6(a-b) shows the surface concentration as a function of sputtering time for Gd and Ge. The two curves are complementary, as they must be since the alloy is binary, but both are shown for completeness. The horizontal dotted lines in Figure 6(a-b) show the bulk concentrations of Gd (55 at. %) and Ge (45 at. %), for reference.

Throughout the depth profiles, measured compositions are within ± 5 at. % of the bulk concentration.

The depth profiles show cyclic variations in composition. This is especially obvious in Figure 6(c) and Figure 6(d), where the curves are separated vertically and ordered in sequence of annealing temperature. For Gd, sputtering always causes an initial increase in concentration. If the surface is annealed between 500 and 900 K, maxima at 2 and 6 minutes of sputtering time are consistently produced. Of course, for Ge, the results are complementary. If the surface is annealed below 500 K, the maxima and minima are not so regular, although the initial increase in Gd content is always manifest. The oscillations are self-consistent between 500 and 900 K. They are very small at 900 K, although this may be related to the fact that a different sample (#2) was used for the 900 K experiment than for the others (#1).

Depth-profiling was also done on Sample #3. In this case, the sputtering interval was shortened (from 2 minutes to 30 seconds) in order to obtain a denser set of data points as a function of time. Otherwise, its treatment and treatment history were similar to those of Samples #1 and #2. Depth profiles were measured after annealing at four temperatures: 700 K, 900 K, 1100 K, and 1200 K. Figure 7(a-d) shows the result. The horizontal dotted lines in Figures 7(a-b) show the bulk concentration of Gd (55 at. %) and Ge (45 at. %) for reference, and all experimental data are plotted against the same ordinate. As with Samples #1 and #2, the compositions are always within ± 5 at. % of the bulk concentration. Unlike Samples #1 and #2, the concentrations move steadily closer to the bulk composition as depth profiling proceeds, with the initial concentrations being slightly Gd-depleted and Ge-rich. Another difference with respect to Samples #1 and #2 is that in Sample #3, the Gd concentration always *decreases* during the first one or two sputtering cycles. This effect may be seen more clearly in Figure 7(c-d), where the

experimental curves are displaced vertically for clarity and so do not overlap. Most curves show a maximum in Gd concentration after about 2 minutes, consistent with Fig. 6 where the sputtering intervals were 2 minutes. It is possible that the density of data points in Fig. 6 was not sufficient to reveal the true trends in the data.

However, given the discrepancies between the different depth profiling experiments, further work would be necessary to determine which (if any) of the trends in concentration vs. depth is reproducible and significant. No conclusions about the depth profiles can be drawn at present, except that the concentrations are always within ± 5 at% of the bulk.

4.1.4 Summary and Analysis of XPS Data

Based upon the data from all three types of XPS experiments (Sections 4.1.1-4.1.3), neither preferential sputtering nor preferential segregation occurs, to within ± 5 at%. This is true over a temperature range of 300 K to 1200 K.

Preferential sputtering occurs when an element is removed at a rate that is disproportionately high relative to its bulk composition[29]. Light atomic mass and weak interatomic bonding both favor preferential removal. Gd and Ge have atomic masses of 157 amu and 73 amu, respectively, so the atomic mass difference alone would favor preferential loss of Ge. Since Ge is not removed preferentially, chemical bonding must be influential.

It might be tempting to hypothesize that Gd-rich and Ge-rich planes/layers are alternately exposed as sputtering progresses, leading to the observed oscillations in concentration during depth profiling (Section 4.1.3). However, to our knowledge such a

regular variation in layer termination with ion sputtering has not been observed in any system previously. On the contrary, it is generally thought that sputtering induces such severe damage that planar terminations do not survive, and this is often corroborated by STM images showing very rough surfaces—without terraces—after ion bombardment. As the following section shows, rough surfaces also result from ion sputtering of the Gd_5Ge_4 sample.

4.2 STM

4.2.1 STM: General Comments

In the STM data for both sample #1 and #2, there will be two main types of terraces: those which are relatively smooth, and those which are covered by small bumps, about 0.3-0.4 nm high on average. We will denote terraces *without bumps* as “A,” and those *with bumps* as “B.” The “A” terraces are also distinguished by a fine structure containing parallel lines (always running diagonally through the images), about 0.04 nm high and separated by about 1.0 nm. More details are given in following sections.

In the STM data, it will be useful to consider the quantitative dimensions of certain features that are observed repeatedly. These dimensions are heights of steps between terraces, heights and areas of bumps on B-terraces, and depths of pits. While the features themselves are robust, the conditions under which they are observed will vary—between samples, between regions of a given sample, and between annealing treatments. We find it useful to collect the dimensions of these features in tables, in order to facilitate comparison of values measured under different conditions. Table 2 provides heights of steps between similar terraces, i.e. steps that separate two A-terraces or two B-terraces.

Step heights are always determined in such a way that bumps or pits do not contribute to the value. Table 3 summarizes heights of steps between dissimilar terraces, i.e. steps that separate A- and B-terraces. Tables 4-7 gives various characteristics of the bumps on B-terraces: Their heights, average individual area, fraction surface coverage, and number density. Table 8 provides depths of pits that form at 1200 K on one of the samples. Each Table specifies the sample and the conditions that correspond to a given value.

The experimental sequence was as follows. First, an extensive set of XPS and STM experiments was performed on sample #1. Next, an extensive set of STM experiments was performed on sample #2. The STM data from these two samples will be discussed separately. These two samples were cut from the same ingot, as noted in Section 2.

4.2.2 STM: Sample #1

4.2.2.1 STM Images after Sputtering at Room Temperature (Sample #1)

This sample was introduced into the STM/XPS UHV chamber from air, then subjected to 18 cleaning cycles and 9 depth-profiles (Fig. 6 and Section 4.1.3) prior to STM.

Figure 8 shows typical STM images of this surface after annealing at 900 K, then sputtering at room temperature. The surface is very rough, as shown by the line profiles, where peak-to-peak heights are ≥ 4 nm. Once, a region with small terraces was found, shown in Fig. 9. Figures 9(b) and (d) show a portion of Fig. 9(a) (enclosed by a box) at successively higher magnification. Terraces, about 50-100 nm wide and decorated with protrusions, are visible. The step heights between these small terraces are 0.75 ± 0.16 nm.

These terraces may be remnants of those produced by high-temperature annealing (discussed below), which somehow survived the subsequent ion bombardment process. We emphasize that these terraces are not characteristic of the freshly sputtered surface; the great majority of the surface is rough, with no terraces apparent.

Table 2 shows the step heights on the middle, right, and left sides of this sample after sputtering, followed by annealing to different temperatures. The row labeled “300 K” corresponds to the data in Fig. 8 and Fig. 9. There is only one entry in this row, since terraces were observed in only one location at 300 K.

4.2.2.2 STM Images after Annealing at 900 K (Sample #1)

For STM studies, 900 K was the lowest annealing temperature used. After annealing at 900 K, most of sample #1 was rough. A few terraces were found; examples are shown in Fig. 10. The heights of A-A or B-B are 0.75 ± 0.16 nm (see Table 2). The heights of downgoing B-to-A (height of B-terraces) and A-to-B (height of A-terraces) steps are 0.35 ± 0.07 nm and 0.39 ± 0.07 nm, respectively (see Table 3). Further, small circular bumps are visible on terraces. They can be seen in Fig. 10(c) and Fig. 10(d). Terraces with bumps like this are called B-terraces. The bumps have an average height of 0.38 ± 0.09 nm and the average individual bump area is 2.68 ± 0.80 nm² (see Tables 4-5). The fractional area covered by bumps on B-terraces and the number density by bumps are 16 % and 0.06 nm⁻² (see Tables 6-7).

4.2.2.3 STM Images after Annealing above 900 K (Sample #1)

For this sample, the next annealing temperatures were 1050 K and 1100 K. Figure 11 and Figure 12 show representative STM images after these treatments. The major terraces remain the B-terraces, covered by small bumps.

For this sample, a significant change occurs after annealing at 1200 K. Relative to 1150 K, the A-terraces are broader, and they alternate with the B-terraces. Figure 13 shows representative STM images after the sample had been annealed at 1150 K and Figure 14 shows representative STM images after the sample had been annealed at 1200 K. On the other hand, the areal size of bumps on the B-steps, and their number density, are both significantly higher than at 900 K. This suggests that the bumps change upon annealing to sufficiently high temperatures.

4.2.3 STM: Sample #2

4.2.3.1 STM Images after Annealing to 900 K (Sample #2)

This sample was introduced into the STM/XPS UHV chamber from air, then subjected to 11 cleaning cycles. Each cycle consisted of annealing at 900 K, and a depth profile (900 K curve in Figure 6), prior to STM. A step-terrace morphology was visible over most of this surface after annealing at 900 K. In this respect it was much different than sample #1, which was very rough after the 900 K anneal (Figure 900K1 and Section 4.2.2).

Examples of STM images from this sample are shown in Figure 15. Figure 15(a) and Figure 15(b) are from the coolest part of the sample (the middle), Figure 15(d) and Figure 15(e) are from the intermediate region (right side), and Figure 15(g) and Figure

15(h) are from the hottest part (left side). Figure 15(c), Figure 15(f), and Figure 15(i) are line profiles that correspond to the black horizontal lines in Figure 15(b), Figure 15(e), and Figure 15(h), respectively.

Terraces are almost all A-type in the middle and on the right side of the sample (see Figures 15(a-b) and 15(d-e)). The step heights from the line profiles in those areas (Figure 15(c) and Figure 15(f)) are 0.74 ± 0.09 nm, respectively. Very small regions of another terrace type, presumably B-type, are observed sometimes protruding at the A-terrace step edges. Two cases are encircled in Figure 15(b) and (e).

On the hottest region of the sample, B-type terraces are more prominent than on the cooler regions. This is illustrated by Figure 15(g) and Figure 15(h). Based on the line profile in Figure 15(i), the step heights range from 0.3 nm to 0.5 nm, i.e. significantly less than step heights on the smoother terraces in Figure 15(a-b) and Figure 15(d-e). It is also very interesting that A- and B-terraces alternate in sequence.

The preponderance of A-type steps after 900 K annealing makes this sample different than sample #1, where there were only a few terraces and those were mostly B-type, after 900 K annealing. It is also interesting that the alternating sequence of A- and B-terraces was observed on both samples, but after annealing at different temperatures. For sample #1, the A/B alternation was seen after annealing to 1200 K (Figure 14), whereas for sample #2 it was seen after annealing to only 900 K (Figure 15).

At high magnification, we see the features shown in Figure 16(a) on the A-terraces. The most prominent motifs are parallel, diagonal rows. The diagonal rows are all in one direction, going from the top right corner down to the bottom left corner of the image. In other words, there are no rotational domains. The spacing between the rows is

1.04 ± 0.03 nm and the height of the rows is 0.04 ± 0.01 nm (where the baseline is taken as the minimum between the rows). The angle of the rows is $68^\circ \pm 1^\circ$. This angle is measured relative to the bottom edge of the image.

In addition to the diagonal rows, white bumps (protrusions) and black holes (depressions) appear throughout Figure 16(a). A line profile is given in Figure 16(b). The protrusions are 0.10 ± 0.03 nm high, and the depressions are 0.09 ± 0.02 nm deep (relative to the same baseline, i.e. the minimum between rows). The protrusions cover 12 % of the surface, while the depressions cover 17 %. The heights of these protrusions is significantly lower than the heights of the bumps on the B-steps, meaning that they probably have a different origin.

On the other hand, as shown in Figure 16(c), the fine structure on the B-terraces contains no diagonal motif. Rather, small circular bumps are visible on the surface. The heights of these bumps are 0.40 ± 0.05 nm, which is in good agreement with the height of 0.38 ± 0.09 nm measured for the bumps on B-terraces on Sample #1 after annealing at the same temperature (see Tables 4-7).

Figure 17 shows both types of fine structure on several different terraces. In all cases, the diagonal row or the bump motif is visible, although sometimes not as clearly as in Figure 16. The diagonal rows have parallel orientation on all A-terraces.

4.2.3.2 STM Images after Annealing Above 900 K (Sample #2)

This sample was annealed at 1050 K and 1200 K. After 1050 K, major terraces are all B-type, step edges are rounder, and some small A-terraces are visible. These surface features are shown in Figure 18. Figure 18(a) and Figure 18(b) are taken in the

coolest (middle) part of the sample, while Figure 18(c) and Figure 18(d) are taken from the intermediate (right) part, and Figure 18(e) and Figure 18(f) from the hottest (left) side. The major step heights are 0.74 ± 0.11 nm, as shown in Table 2. Where A-terraces are separable, their step heights are 0.35 ± 0.08 nm (Table 3). The heights of bumps on B-terraces are 0.32 ± 0.09 nm (Table 4).

In addition to these basic surface features, pits are common, which can be seen especially well in the low-magnification images on the left side of Figure 18. The pits are irregular in shape but have a depth of 0.76 ± 0.11 nm. This value is shown in Table 5, which includes depths of pits at different positions and after annealing at different temperatures.

After annealing at 1200 K, the B-terraces are gone. In the cool middle of the sample, Figures 19(a-b), terraces are smooth and the step heights are 0.73 ± 0.07 nm. This is very similar to the step heights at the lower annealing temperatures—see Table 2.

On the warm right side of the sample, an increased number of pits exist. They can be seen in Figures 19(c) and 19(d). The pits have a height of 0.80 ± 0.08 nm—see Table 5. On the hot left side, pits also exist. In addition, features that we will call vacancy-voids have also appeared in the fine structure as well as inside the vacancy-pit. This can be seen in Figures 19(e-h). In the figures, pits are deep holes that have a height of 0.76 ± 0.09 nm (Table 5). On the other hand, the vacancy-voids are shallow, flat regions that have a height of 0.17 ± 0.04 nm on the terrace (fine structure) and 0.12 ± 0.04 nm in the vacancy-pits.

On the terraces, we resolve two different structures. The first is the diagonal row structure characteristic of the A-terraces. The second is a checkerboard pattern that seems

to emanate from down-going step edges. Figure 20 shows the two types of surface structures. Figure 20(a) is a raw image, and Figure 20(b) is the same image after differentiation, which emphasizes boundaries between regions and thus makes the diagonal-row phase more distinguishable from the checkerboard phase. Figure 20(c) is a magnified view of the black box in Figure 20(b), which encompasses both structures.

Figure 20(d) is the profile of the line in Figure 20(c), which also crosses both structures. The checkerboard patches are separated from the diagonal row structure by a ridge, marked by an asterisk (*) in the line profile of Figure 20(d). From the image in Figure 20(c), the ridge has a height of 0.16 ± 0.04 nm. Furthermore, the line profile in Figure 20(d) shows a height difference of 0.04 nm between the two structures.

For the diagonal row structure, the height of the rows is 0.04 ± 0.01 nm (relative to the valley between them), and the separation between rows is 0.90 ± 0.02 nm. Relative to the structure observed at 900 K annealing, the row height is identical and the row separation is slightly smaller (0.90 ± 0.02 nm vs. 1.04 ± 0.03 nm). In addition, the angle is slightly smaller, $61^\circ \pm 1^\circ$ relative to 900 K. A clear difference is that after 1200 K annealing, the diagonal rows show fewer protrusions and depressions. It is not clear whether the differences between the diagonal row structure at 900 K and 1200 K are significant enough to signal two different surface phases.

Figure 20(e) is a higher-magnification view of the checkerboard structure. The angle between the two principle axes is $96 \pm 1^\circ$. The average surface unit cell length is 0.44 ± 0.04 nm along the near-horizontal direction and 0.40 ± 0.03 nm along the near-vertical direction. We conclude that the surface unit cell is square or nearly so.

4.2.4 Summary of STM Data

The progression of surface structures on the two samples is summarized in Table 6. While there are differences between the two sets of data, they have the following features in common.

- 1) There are two main types of terraces, A- and B-type.
 - A-terraces have parallel lines, interspersed with shallow depressions and low protrusions.
 - Characteristics of the fine structure on A-terraces:
 - Parallel lines are 1.04 nm apart and 0.04 nm high.
 - Parallel lines (aka diagonal lines) have same orientation on all A-terraces.
 - Low protrusions are 0.10 nm high and shallow depressions are 0.09 nm deep. Their total areas are comparable, suggesting that they may be related.
 - B-terraces have bumps that are 0.3-0.4 nm high (Table 4).
 - A- and B-terraces alternate. Under some conditions they have about equal areas and the alternation is striking (cf. sample #1 at 1200 K in Figure 1200K1 and sample #2 at 900 K in Figure 15(g-h)). Under other conditions one terrace constitutes the majority, but even then, there are small protrusions at step edges that are probably extensions of the other terrace.
 - Step heights are rather robust:

- Steps that separate A-A or B-B terraces are 0.75 nm high (Table 2).
- Steps that separate A-B terraces are 0.3-0.4 nm high (Table 3).
- In one experiment, a striking checkerboard pattern was adjacent to a A-like structure.
 - Its surface unit cell is square or nearly so.
 - Lateral dimensions are 0.40 nm and 0.44 nm.
 - Angle between basis vectors is 96° .

These features will be used to correlate surface structure with bulk structure in Section 5.

5. Comparison of STM Results (Section 4.2) with Bulk Structure

For purposes of discussion, it is convenient to divide the surface information into two parts:

- 1) Step heights, and lateral arrangement of terraces; and
- 2) Fine structure on the terraces.

Part (1) consists of these specific facts.

- A- and B-terraces alternate.
- Steps that separate A-A or B-B terraces are 0.75 nm high.
- Steps that separate A-B terraces are 0.31-0.39 nm high.

The objective is to see whether the bulk structure can be terminated in a way that is consistent with these observations. Consider the representation of the bulk in Figure 21. This shows that, perpendicular to the $\langle 010 \rangle$ axis, there are three kinds of dense planes. Two are pure Gd, and one is mixed Ge-Gd. The two pure, dense Gd planes are

mirror images. One way to describe their difference is that one has a dilute layer of Ge above, and the other has a dilute layer of Ge below. We will name the three dense planes Gd_{d1} , Gd_{d2} , and $Ge-Gd_d$ as shown in the Figure. There are also two kinds of dilute (sparse) planes of Ge atoms, labeled Ge_{s1} and Ge_{s2} .

First, it is apparent that the measured separation between A-A or B-B planes, 0.75 nm, is half the b-axis, 1.48 nm. This is entirely reasonable, since the bulk unit cell consists of two equivalent slabs that are stacked in the b-direction.

Second, we can rule out the possibility that terraces A and B are dense Gd and Ge-Gd planes (or vice-versa). If that were the case, the A-B step height would be either 0.21 or 0.53 nm based on the bulk structure. Both values are incompatible with our experimental data, for which the average values range from 0.31 to 0.39 nm (Table 3, right two columns). Furthermore, one might well expect that both of the dense Gd planes would serve as terminations, in addition to the Ge-Gd plane, since the dense Gd planes are rather similar to one another. Then there would be three different terminations, not two as observed.

On the other hand, if terraces A and B are Gd_{d1} and Gd_{d2} planes, there is a good match with the data. The A-B step height would be 0.32 and 0.42 nm based on the bulk structure, which is much more compatible with the experimental range of average values, 0.31 to 0.39 nm. Furthermore, there would be only two types of terminations and they would alternate, as observed. We conclude that the A- and B-terminations correspond to Gd_{d1} and Gd_{d2} planes, although we do not know which is which based upon this analysis.

Part (2), the fine structure on the terraces, consists of these facts:

- A-terraces have parallel lines, interspersed with shallow depressions and low protrusions.
 - Parallel lines are 1.04 nm apart and 0.04 nm high.
 - Parallel lines have identical orientation on all A-terraces.
 - Low protrusions are 0.10 nm high and shallow depressions are 0.09 nm deep. Their total areas are comparable, suggesting that they are related.
- B-terraces have bumps that are 0.3-0.4 nm high.
- A checkerboard pattern was found embedded in an A-like terrace.
 - Its lateral dimensions are 0.40 nm and 0.44 nm.
 - The angle between its basis vectors in the surface plane is 96° .

A natural question is, what is relationship between the parallel lines on the A-terraces and the bulk atomic structure? In order to answer this, it is necessary to determine the orientation of the bulk basis vectors \vec{a} and \vec{c} , which are illustrated in Figure 3. We made this determination in two independent ways. One relied on the presence of the Gd_5Ge_3 secondary phase in the Gd_5Ge_4 sample [23]. This phase forms thin plates which, on (010) surface, lie in two different directions that do not intersect at right angles. The bulk basis vector \vec{a} bisects the acute angle, and the vector \vec{c} bisects the obtuse angle. We identified the orientation of the secondary phase plates using optical microscopy, and made the assignment of \vec{a} and \vec{c} in our sample based on this information. The second way was to use X-ray diffraction, which was performed by Dr. Deborah Schlager in the Materials Preparation Center of the Ames Laboratory. (A small portion was cut from

Sample #2 for this purpose.) Both of these approaches were consistent. The resultant vectors \vec{a} and \vec{c} are shown in Figure 16; the accuracy of this determination is believed to be about $\pm 5^\circ$. The parallel lines in the STM image make an angle of about 28° with \vec{c} . This orientation is shown by the straight diagonal line in Figure 3. It appears that there is no simple relationship between the orientation of the parallel lines in the STM images and the bulk-terminated structure. We therefore suggest that the surface of this material deviates from the bulk-terminated structure.

The B-terraces have bumps that are 0.3-0.4 nm high. Their height is the same as the spacing between adjacent dense Gd-pure planes, as shown in Figure 21. Perhaps these bumps are regions where the B-terraces are ‘rebuilding’ into A-terraces. If that is the case, however, the bumps seem unexpectedly stable in the sense that they are observed over a broad range of annealing temperatures.

Finally, the identity of the checkerboard pattern is interesting. Among known phases in the Gd-Ge system, it fits reasonably well with GdGe. This material is orthorhombic with lattice constants $a=0.42$ nm and $c=0.40$ nm. The lateral dimensions of the checkerboard phase measured with STM are 0.44 and 0.40 nm. Only a small depletion of Gd (or enrichment in Ge), relative to Gd_5Ge_4 , would be needed to stabilize this phase.

6. Characterizing Gd₅Ge₃ Thin Plates (Samples #2 and #4)

The goal of this part of the project was to identify the 5:3 plates, to determine whether they undergo any changes after different surface treatments, and to understand their effect on STM.

6.1 Characterizing Gd₅Ge₃ Thin Plates: Optical Microscopy (Sample #4)

Using optical microscopy, we were able to easily find 5:3 thin plates everywhere on the Gd₅Ge₄ (010) surface. An example is shown in Figure 22. Figure 22(a) was taken before any experiments were performed on the surface and Figure 22(b) was taken after SEM, AES, and SAM experiments were performed. These experiments will be discussed in sections that follow. As we can see from Figure 22, the thin plates lie in two different directions at an 83° angle when viewed from the (010) direction. This compares well with the angle of 80° reported in the literature and helps to confirm that we identify these features correctly. The width of the thin plates varies from 0.40 μm to 2 μm. The relative area of the 5:3 thin plates was 2.3 ± 0.2 % before any other experiments were performed (Figure 22(a)) and 2.1 ± 0.6 % after other experiments were performed (Figure 22(b)), i.e. there was no change in the area covered by the plates. In other words, the sputtering and annealing processes described below did not change the relative population of the 5:3 phase in the 5:4 matrix.

6.2 Characterizing Gd₅Ge₃ Thin Plates: SEM, AES and SAM (Sample #4)

In this set of experiments, we explored whether the 5:3 plates change after different surface treatments.

After the sample was placed into the SEM/AES/SAM chamber, the first surface treatment was one full cleaning cycle (10 minutes sputtering and 1 hour annealing at 900 K). The SEM image shown in Figure 23 was then acquired. The 5:3 plates are visible. They lie in two different directions at an 84° angle, consistent with the optical microscopy results (Figure 22). The dotted lines in the figure represent the two different directions of the 5:3 thin plates.

Figure 24(a) is an SEM of a surface region at higher magnification. Note especially the bright line, about $0.3\ \mu\text{m}$ wide, that crosses left to right about halfway down the image. This is a 5:3 thin plate, based upon the SAM images in Figure 24(b-c). Figure 24(b) is a Gd map, showing that the bright line in Figure 24(a) is Gd-rich compared with the surrounding 5:4 matrix, while Figure 24(c) is a Ge map showing that the line is Ge-poor. The other marks in Figure 24(a) are probably scratches from polishing or handling.

Semi-quantitative verification of the phase assignments is available from AES. Figure 25 is an SEM image, showing another bright line on the surface. Auger spectra were acquired at the points labeled 1-6, and the compositions from Auger analysis are given in the table below the image. The first three numbered points (1, 2, and 3) are on the darker matrix and the last three points (4, 5, and 6) are on the bright line. From the table included in the Figure, the surface compositions at points 1, 2, and 3 are consistent with the bulk compositions of Gd and Ge in the Gd_5Ge_4 phase. However, the surface compositions at points 4, 5, and 6 do not match the nominal composition of Gd_5Ge_4 (55 at. % Gd, 45 at. % Ge). In fact, they are closer to the ideal composition of Gd_5Ge_3 (63 at. % Gd, 37 at. % Ge).

The next treatment consisted of several Ar^+ sputtering cycles (without annealing), until AES detected no carbon or oxygen on the surface. The SEM image shown in Figure 26(a) shows the clean surface after this treatment. The dark shadow that crosses left to right, about halfway down the image, is a 5:3 thin plate. This is based upon the Gd map in Figure 26(b), showing Gd-enrichment along the line, and the Ge map in Figure 26(c), showing Ge-depletion along the line. The other linear marks in Figure 26(a) are probably scratches from polishing or handling.

Finally, the sample was subjected to six full cleaning cycles (sputtering plus annealing at 900 K for 30 minutes), and several SEM images were taken after each cycle. Some are shown in Figure 27. Figure 27(a) was taken after the third cleaning cycle, Figure 27(b) after the fourth, Figure 27(c) after the fifth, and Figure 27(d) after the sixth. In these 4 panels, lumps appear, and they increase in density and size with each cleaning cycle. These lumps eventually aggregate along the scratches and also along the 5:3 plates (Figure 27(d)). This assignment rests on Figure 27(f), where the red lines show the features that are probably the 5:3 plates. Many of the marked lines are parallel, and another line makes an angle of 88° with the parallel group, making them all likely 5:3 plates. On the other hand, some of the lines decorated by lumps are simply scratches, since they make angles that are far from the angle of 83° observed in optical microscopy (Section 4.5.1).

AES was performed at five different locations on the Gd_5Ge_4 (010) surface after the sixth cleaning cycle. Results are shown in Figure 28. Locations 3, 4, and 5 are on the lumps, while positions 1 and 2 are on the smoother region. The surface compositions of these five different AES locations are shown in the table in Figure 28. The lumps have a

lower Gd surface composition and correspondingly *higher* Ge concentration than the 5:4 matrix (which is opposite to the 5:3 phase). Their average composition is 47 at. % Gd and 53 at. % Ge. Among the bulk phases listed in Table 1, the closest match in composition is GdGe. Of course, the area analyzed with AES is not necessarily a single phase. It is interesting, however, that GdGe is the same phase that is the most likely candidate for the checkerboard pattern in STM, seen after annealing Sample #2 to 1200 K (see Section 5.)

After annealing at a higher annealing temperature, 1150 K for 30 minutes, more lumps are seen in SEM. This is shown in Fig. 29. AES was performed at four different locations (four different lumps) on the Gd_5Ge_4 (010) surface. These points are shown in Fig. 29(c). The surface compositions of the lumps are shown in the table in Fig. 29. The lumps have a lower Gd surface composition and a higher Ge concentration than at the lower annealing temperature of 900 K. Their average composition is now 39 at. % Gd and 59 at. % Ge,. This composition has the closest match to Gd_3Ge_5 when comparing it to the bulk phases listed in Table 1. Regardless of whether the lumps correspond to a single phase, one can conclude that their formation, on this sample, is associated with loss of Gd at the surface at high temperature. As we will see in the following section, however, this phenomenon is not universal among the samples.

6.3 Characterizing Gd_5Ge_3 Thin Plates: SEM (Sample #2)

The results described in Section 6.2 suggest that sputter-annealing cycles may cause large changes in surface morphology—specifically, lumps, which form preferentially at surface scratches and at the Gd_5Ge_3 phase inclusions. We therefore checked whether lumps were also present on the surface of a sample after it had been

annealed and used for STM experiments, Sample #2. Sample #2 was used for the STM experiments described in Section 4.3.2. It was extensively sputter-annealed, and its treatments included annealing at 1200 K. It was then transferred to the SEM/SAM/AES chamber. SEM images of the sample's surface are shown in Fig. 30. In Fig. 30(a), we begin to see the usual 5:3 thin plates. The black dotted lines in the figure represent the two different directions, as expected. High magnification SEM images are shown in Figs. 30(b) and 30(c). There are no lumps on this surface. Thus, the lumps do not complicate the interpretation of the STM data in Section 4. The reasons why lumps formed on Sample #4 but not on Sample #2, under comparable conditions, is not known. One difference is that the base pressure in the SAM/AES chamber, where Sample #4 was sputtered and annealed, was at least an order of magnitude higher than the base pressure in the STM/XPS chamber, where Sample #2 was sputtered and annealed. Conceivably, some reaction with background gas or impurity in the sputtering gas triggered growth of the lumps on Sample #4 but not on Sample #2.

6.4 Characterizing Gd_5Ge_3 Thin Plates: STM (Sample #2)

With STM, we would expect to see two different phases: the Gd_5Ge_4 matrix and areas of embedded Gd_5Ge_3 . However, in STM (as presented in Section 4.2), we did not find two distinct phases. Generally, features were very similar all over the sample, except for differences due to thermal gradients with sample #2. This might be due to the fact that the Gd_5Ge_3 thin plates comprise only 2% of the surface area (as shown in Section 6.1), so it is statistically unlikely that the STM tip will happen to land on a thin plate. Therefore,

we looked for evidence of the thin plates with STM over much larger areas, i.e. at lower magnification.

Figure 31 shows different surface areas ranging from $2\ \mu\text{m} \times 2\ \mu\text{m}$ to $4\ \mu\text{m} \times 4\ \mu\text{m}$, after annealing to 900 K. Large-scale linear features are present. These may be plates or scratches. In Figure 31(a), two parallel lines are shown going across the surface. The lines are $0.9\ \mu\text{m}$ apart. If they are boundaries of a thin plate, then its width is $0.9\ \mu\text{m}$, which is a plausible value. However, it may also represent a polishing mark or other type of scratch. The same is true of the diagonal lines shown in Figures 31(b-d).

Figure 32(a) shows another region on the terrace where there is a $1.19\ \mu\text{m}$ -wide linear stripe that cuts roughly horizontally through the figure. This again is a candidate for a thin plate. Figure 32(b) shows a closer view that includes the region above the stripe, and an upper part of the stripe. The terraces inside and outside the stripe are visibly different. In Figure 32(a), several vacancy-pits are present above and below the stripe, while within the stripe, there are no visible pits on terraces. This suggests that the regions may represent two different phases. In addition, bumps and elongated islands appear above and below the stripe, but not within the stripe. Figure 32(c) shows a closer view of part of the upper area and Figure 32(d) shows terraces within the stripe. In Figure 32(c), the elongated islands are aligned along two different directions, making an angle of about 70° . These elongated islands are not typical of the surface.

7. Conclusions

We have characterized the (010) surface of Gd_5Ge_4 using STM and XPS. XPS reveals the surface compositions to be within ± 5 at. % with its bulk composition, both after sputtering and annealing at various temperatures. With STM, the surface exhibits two main types of terraces which alternate across the surface. Step heights between similar terraces correspond well to the separation between equivalent layers along the $\langle 010 \rangle$ direction in the bulk structure, and step heights between dissimilar terraces correspond to the distance between certain dissimilar but dense layers. In addition, two fine structure types appeared on terraces at various annealing temperatures. (1) Diagonal lines after the sample had been annealed to 900 K and (2) checkerboard pattern after the sample had been annealed to 1200 K. These fine structures do not correlate with the bulk structure, and therefore, we suggest that there is significant surface reconstruction.

In addition, we also characterized the Gd_5Ge_3 secondary phase on the (010) surface of Gd_5Ge_4 using OM, SEM, AES, SAM, and STM. As expected, thin plates were seen using OM and SEM on the Gd_5Ge_4 surface. These thin plates were identified as the Gd_5Ge_3 secondary phase based on their compositions from AES and SAM. In STM images at low magnification, long stripes can be found on the surface, with widths between $0.9 \mu\text{m}$ and $1.19 \mu\text{m}$. These may be thin plates, or polishing scratches.

Acknowledgments

This research was supported by the U.S. Department of Energy, Office of Basic Energy Sciences, Division of Materials Sciences and Engineering, under Contract No. DE-AC02-07CH11358. James W. Andereg, Mark Wallingford, and Holly Walen

assisted with some of the experiments. D. L. Schlager expertly grew, oriented, and polished the samples, and performed optical microscopy. Shalabh Gupta and Srinivasa Thimmaiah gave insights into the bulk structure, and assisted in its representation. We thank them all.

References

- [1] D. Paudyal, V.K. Pecharsky, K.A. Gschneidner, B.N. Harmon, *Physical Review B* 75 (2007) 094427.
- [2] D. Paudyal, V.K. Pecharsky, K.A. Gschneidner, *Journal of Physics-Condensed Matter* 20 (2008) 235235.
- [3] J.D. Moore, G.K. Perkins, Y. Bugoslavsky, M.K. Chattopadhyay, S.B. Roy, P. Chaddah, V.K. Pecharsky, K.A. Gschneidner, L.F. Cohen, *Applied Physics Letters* 88 (2006) 072501.
- [4] V.K. Pecharsky, J.K.A. Gschneidner, *Physical Review Letters* 78 (1997) 4494-4497.
- [5] E. Bruck, O. Tegus, D.T.C. Thanh, K.H.J. Buschow, *Journal of Magnetism and Magnetic Materials* 310 (2007) 2793-2799.
- [6] G.S. Smith, A.G. Tharp, W. Johnson, *Acta Crystallographica* 22 (1967) 940-943.
- [7] F. Holtzberg, R.J. Gambino, T.R. McGuire, *Journal of Physics and Chemistry of Solids* 28 (1967) 2283-2289.
- [8] Samples were synthesized at the Materials Preparation Center, Ames Laboratory USDOE, Ames, IA, USA.

- [9] D.L. Schlagel, T.A. Lograsso, A.O. Pecharsky, J.A. Sampaio, *Light Metals* 2005 (2005) 1177-1180
1236.
- [10] T. Cai, *Scanning Tunneling Microscopy Studies of Surface Structures of Icosahedral Al-Cu-Fe Quasicrystals*, Iowa State University, Ames, 2001.
- [11] See www.CasaXPS.com.
- [12] I. Horcas, R. Fernandez, J.M. Gomez-Rodriguez, J. Colchero, J. Gomez-Herrero, A.M. Baro, *Review of Scientific Instruments* 78 (2007) -.
- [13] T.B. Massalski, H. Okamoto, P.R. Subramanian, L. Kacprzak (Eds.), *Binary Alloy Phase Diagrams*, ASM International, Materials Park, Ohio, 1990.
- [14] V.K. Pecharsky, K.A. Gschneidner, *Journal of Alloys and Compounds* 260 (1997) 98-106.
- [15] P. Eckerlin, H. Kandler, *GaVO - GeLaS*, SpringerMaterials - The Landolt-Bornstein Database.
- [16] P.H. Tobash, D. Lins, S. Bobev, N. Hur, J.D. Thompson, J.L. Sarrao, *Inorganic Chemistry* 45 (2006) 7286-7294.
- [17] H.F. Yang, G.H. Rao, G.Y. Liu, Z.W. Ouyang, W.F. Liu, X.M. Feng, W.G. Chu, J.K. Liang, *Journal of Alloys and Compounds* 361 (2003) 113-117.
- [18] G.S. Smith, Q. Johnson, A.G. Tharp, *Acta Crystallographica* 22 (1967) 269-272.
- [19] A.O. Pecharsky, K.A. Gschneidner, V.K. Pecharsky, C.E. Schindler, *Journal of Alloys and Compounds* 338 (2002) 126-135.
- [20] J. Szade, G. Skorek, A. Winiarski, *Journal of Crystal Growth* 205 (1999) 289-293.

- [21] O. Ugurlu, L.S. Chumbley, D.L. Schlagel, T.A. Lograsso, A.O. Tsokol, *Scripta Materialia* 53 (2005) 373-377.
- [22] J.S. Meyers, L.S. Chumbley, F. Laabs, A.O. Pecharsky, *Scripta Materialia* 47 (2002) 509-514.
- [23] O. Ugurlu, L.S. Chumbley, D.L. Schlagel, T.A. Lograsso, *Acta Materialia* 53 (2005) 3525-3533.
- [24] L.S. Chumbley, O. Ugurlu, R.W. McCallum, K.W. Dennis, Y. Mudryk, K.A. Gschneidner Jr, V.K. Pecharsky, *Acta Materialia* 56 (2008) 527-536.
- [25] E.I. Gladyshevskii, *Journal of Structural Chemistry* 5 (1965) 852-853.
- [26] N.C. Baenziger, J.J. Hegenbarth, *Acta Crystallographica* 17 (1964) 620-621.
- [27] O. Ugurlu, L.S. Chumbley, D.L. Schlagel, T.A. Lograsso, *Acta Materialia* 54 (2006) 1211-1219.
- [28] Q. Cao, L.S. Chumbley, Z. Qian, *Intermetallics* 18 1021-1026.
- [29] C.J. Jenks, J.W. Burnett, D.W. Delaney, T.A. Lograsso, P.A. Thiel, *Applied Surface Science* 157 (2000) 23-28.

Figure Captions

Figure 1

Typical temperature-power and temperature-time cooling rate after the Gd₅Ge₄ (010) had been annealed to (a-b) 900 K and (c-d) 1200 K. Sample #1 and Sample #2. NOTE: Temperature readings are based on power calibration.

Figure 2

Phase diagram on the Gd-Ge binary alloys. Reprinted with permission of ASM International. All rights reserved. www.asminternational.org.

Figure 3

Bulk unit cell structure of the Gd₅Ge₄ binary alloy, (a) side view and (b) top view. Dimensions are taken from Yang et al. J. Alloys and Comps. 361 (2003), 113. The rectangular box (a) and square box (b) represents the unit cell.

Figure 4

XPS depth profile of Gd and Ge after the (010) sample was introduced from air to UHV at 300 K. Bulk compositions are shown for reference by the horizontal dash lines. Sample #1.

Figure 5

Surface composition as a function of annealing temperature on two photoelectron peaks, Gd 3d_{5/2} and Ge 2p_{1/2}. (a) Sample #1. (b) Sample #2. Error bars represent the standard deviation. The error bar on the Ge concentration at 1200 K in (a) is shifted laterally, to prevent confusing overlap with the Gd error bar. The opened squares and diamonds in (b) are Sample #3.

Figure 6

XPS depth-profiles after annealing at different temperatures. The surface concentration is shown in at. % as a function of sputtering time based on two photoelectron peaks. (a) Gd 3d_{5/2}, (b) Ge 2p_{1/2}. In (c) and (d) the curves are displaced vertically so they can be shown without overlap. The surface was sputtered for two minute intervals, for ten minutes in total, except for the cure that follows annealing at 900 K. There the interval was the same but the total duration was 28 minutes. Dotted lines represent the bulk concentrations. All curves represent Sample #1 except for the 900 K data, which represent Sample #2.

Figure 7

XPS depth-profiles after annealing at different temperatures. The surface concentration is shown in at. % as a function of sputtering time based on two photoelectron peaks. (a) Gd

$3d_{5/2}$, (b) Ge $2p_{1/2}$. In (c) and (d) the curves are displaced vertically so they can be shown without overlap. The surface was sputtered for 30 second intervals, for ten minutes in total. Dotted lines represent the bulk concentrations. All curves represent Sample #3.

Figure 8

STM images of the Gd_5Ge_4 (010) rough surface after annealing at 900 K and sputtering at room temperature, (a) 500 nm x 500 nm, $I = 0.5$ nA, $V\text{-tip} = -1$ V, (b) line profile taken from the black arrowhead in (a), (c) 500 nm x 500 nm, $I = 0.5$ nA, $V\text{-tip} = -1$ V, (d) line profile taken from the black arrowhead in (c), (e) 500 nm x 500 nm, $I = 0.5$ nA, $V\text{-tip} = -1$ V, and (f) line profile taken from the black arrowhead in (e). Sample #1.

Figure 9

STM images of the Gd_5Ge_4 (010) surface after annealing at 900 K and sputtering at room temperature, (a) 250 nm x 250 nm, $I = 0.5$ nA, $V\text{-tip} = -1$ V, (b) 100 nm x 100 nm, $I = 0.5$ nA, $V\text{-tip} = +1$ V, (c) line profile corresponding to arrow in panel (b), and (d) 50 nm x 50 nm, $I = 0.5$ nA, $V\text{-tip} = -1$ V. Each frame is a magnification of part of the previous image, outlined in the box. Sample #1.

Figure 10

STM images of the Gd_5Ge_4 (010) surface after annealing at 900 K. (a) 100 nm x 100 nm, $I = 0.5$ nA, $V\text{-tip} = +1$ V, (b) 250 nm x 250 nm, $I = 0.5$ nA, $V\text{-tip} = +1$ V, (c) 100 nm x 100 nm, $I = 0.5$ nA, $V\text{-tip} = +1$ V, and (d) 250 nm x 250 nm, $I = 0.5$ nA, $V\text{-tip} = +1$ V. Sample #1.

Figure 11

STM images at room temperature after the sample were annealed to 1050 K for 15 minutes. Surface features show (a) bumps on B-terraces and the emergence of A-terraces, (b) the emergence of A-terraces. All STM images are 100 nm x 100 nm and tunneling conditions are (a) $I = 0.5$ nA, $V\text{-tip} = +1$ V and (b) $I = 0.5$ nA, $V\text{-tip} = -1$ V. Sample #1.

Figure 12

STM images at room temperature after the sample was annealed to 1100 K for 15 minutes. Surface features show (a) bumps on B-terraces and the emergence of A-terraces; (b) bumps on B-terraces the emergence of A-terraces. STM images and tunneling conditions are (a) 250 nm x 250 nm, $I = 0.5$ nA, $V\text{-tip} = -1$ V, and (b) 100 nm x 100 nm, $I = 0.5$ nA, $V\text{-tip} = -1$ V. Sample #1.

Figure 13

STM images at room temperature after the sample were annealed to 1150 K for 15 minutes. Surface features show (a) bumps on B-terraces and the emergence of A-terraces; (b-c) close-up view of the bumps; (d) bumps on B-terraces and the emergence of A-terraces. STM image sizes are as follows: (a) 100 nm x 100 nm, $I = 0.5$ nA, $V\text{-tip} = +1$ V; (b) 50 nm x 50 nm, $I = 0.5$ nA, $V\text{-tip} = +1$ V; (c) 50 nm x 50 nm, $I = 0.5$ nA, $V\text{-tip} = -1$ V; (d) 100 nm x 100 nm, $I = 0.5$ nA, $V\text{-tip} = +0.5$ V. Sample #1.

Figure 14

STM images on the Gd_5Ge_4 (010) surface after it had been annealed to 1200 K, (a) 250 nm x 250 nm, $I = 0.5$ nA, $V\text{-tip} = +1$ V (middle), (b) 100 nm x 100 nm, $I = 0.5$ nA, $V\text{-tip} = +1$ V (middle), and (c) 100 nm x 100 nm, $I = 0.5$ nA, $V\text{-tip} = +1$ V (middle). Sample #1.

Figure 15

STM images on the Gd_5Ge_4 (010) surface after it had been annealed to 900 K, (a) 500 nm x 500 nm, $I = 0.5$ nA, $V\text{-tip} = +1$ V (middle sample), (b) 250 nm x 250 nm, $I = 0.5$ nA, $V\text{-tip} = +1$ V (middle sample), (c) line profile taken from the black arrowhead in (b), (d) 1000 nm x 1000 nm, $I = 0.5$ nA, $V\text{-tip} = +1$ V (right side sample), (e) 500 nm x 500 nm, $I = 0.5$ nA, $V\text{-tip} = +1$ V (right side sample), (f) line profile taken from the black arrowhead in (e), (g) 250 nm x 250 nm, $I = 0.5$ nA, $V\text{-tip} = +1$ V (left side sample), (h), 100 nm x 100 nm, $I = 0.5$ nA, $V\text{-tip} = +1$ V (left side sample), and (i) line profile taken from the black arrowhead in (h). Circles in (b) and (e) show B-terraces near A-terrace step edges. Sample #2.

Figure 16

High magnification STM images of the Gd_5Ge_4 (010) surface after it had been annealed at 900 K for 1 hour which was then slowly cooled down to room temperature, (a) A-terrace fine structure showing diagonal rows, 33 nm x 31 nm, $I = 0.5$ nA, $V\text{-tip} = +1$ V, (b) line profile taken from the black arrowhead in (a). Sample #2. (c) B-terrace fine structure show bumps, 34 nm x 27 nm, $I = 0.5$ nA, $V\text{-tip} = +1$ V, (d) line profile taken from black arrowhead in (c). The parallel lines in the STM image (a) make an angle of about 28° with \vec{c} . Sample # 2.

Figure 17

STM images on the Gd_5Ge_4 (010) surface after it had been annealed to 900 K, (a-f) show the fine structures of A- and B-terraces, where the diagonal rows are on A-terraces and bumps on B-terraces. Rectangular boxes are zoomed-in images. The tunneling conditions are (a) $I = 0.5$ nA, $V\text{-tip} = +1$ V, (b) $I = 0.5$ nA, $V\text{-tip} = +1$ V, (c) $I = 0.5$ nA, $V\text{-tip} = +1$

V, (d) $I = 0.5$ nA, V-tip = +1 V, (e) $I = 0.5$ nA, V-tip = +1 V, and (f) $I = 0.5$ nA, V-tip = +1 V. Sample #2.

Figure 18

STM images on the Gd_5Ge_4 (010) surface after it had been annealed to 1050 K, (a) 1000 nm x 1000 nm, $I = 0.5$ nA, V-tip = -1 V (middle side), (b) 250 nm x 250 nm, $I = 0.5$ nA, V-tip = +1 V (middle sample), (c) 1000 nm x 1000 nm, $I = 0.5$ nA, V-tip = +1 V (right side sample), (d) 100 nm x 100 nm, $I = 0.5$ nA, V-tip = +1 V (right side sample), (e) 1000 nm x 1000 nm, $I = 0.5$ nA, V-tip = +1 V (left side sample), and (f) 250 nm x 250 nm, $I = 0.5$ nA, V-tip = +1 V (left side sample). Sample #2.

Figure 19

STM images on the Gd_5Ge_4 (010) surface after it had been annealed to 1200 K, (a) 500 nm x 500 nm, $I = 0.5$ nA, V-tip = -1 V (middle), (b) 250 nm x 250 nm, $I = 0.5$ nA, V-tip = -1 V (middle), (c) 1000 nm x 1000 nm, $I = 0.5$ nA, V-tip = +1 V (right side), (d) 500 nm x 500 nm, $I = 0.5$ nA, V-tip = +1 V (right side), (e) 500 nm x 500 nm, $I = 0.5$ nA, V-tip = -1 V (left side), (f) 250 nm x 250 nm (left side), $I = 0.5$ nA, V-tip = +1 V, (g) contour image showing the vacancy voids on surface in (f), and (h) contour image showing the vacancy voids on surface, 100 nm x 100 nm, $I = 0.5$ nA, V-tip = -1 V (left side). Sample #2.

Figure 20

High magnification STM images of the Gd_5Ge_4 (010) surface after it had been annealed at 1200 K for 15 minutes which was then slowly cooled down to room temperature, (a) 250 nm x 250 nm, $I = 0.5$ nA, V-tip = -1 V, (b) differentiated image from (a), (c) 30 nm x 16 nm, $I = 0.5$ nA, V-tip = -1 V, (d) line profile from the black arrowhead in (c), and (e) 11.5 nm x 7 nm, $I = 0.5$ nA, V-tip = -1 V. The checkerboard patches are separated from the diagonal row structure by a ridge, marked by an asterisk (*) in (c) and (d).

Figure 21

Showing dense planes on the bulk unit cell structure of the Gd_5Ge_4 binary alloy. Dimensions are taken from Yang et al. J. Alloys and Comps. 361 (2003), 113.

Figure 22

Images using optical microscopy (OM) showing 5:3 thin plates on the binary Gd_5Ge_4 alloy sample, (a) was taken before any experiments were performed and (b) was taken after. The black dotted lines behind the OM image are shown visually seeing the 5:3 thin plates. Sample #4.

Figure 23

SEM image of the binary Gd_5Ge_4 alloy sample that shows 5:3 thin plates after the sample had been annealed to 900 K for 30 minutes. The black dotted lines behind the SEM image are shown visually seeing the 5:3 thin plates. The 5:3 thin plates lie in two different directions at an 84° angle. The red marker bar shows a length of 100 μm . Sample #4.

Figure 24

Images of the binary Gd_5Ge_4 alloy sample that shows (a) the SEM image, and SAM images of (b) the Gd concentration and (c) the Ge concentration after first cleaning cycle. The red marker bar in (b) is 1 μm long, and the scale is the same for all 3 panels. Sample #4.

Figure 25

SEM image of the binary Gd_5Ge_4 alloy sample. AES was taken on six different locations in the SEM image after the first cleaning cycle. The table shows the surface concentration of Gd and Ge at the six different locations. The first three locations are on the 5:4 matrix and the last three locations are on the 5:3 thin plates. Red bar is 1 μm long. Sample #4.

Figure 26

Images of the Gd_5Ge_4 (010). (a) SEM image, (b) SAM image of the Gd concentration, and (c) SAM image of the Ge concentration after one cleaning cycle and several sputtering treatments without annealing. Red bar is 2 μm long. Sample #4.

Figure 27

SEM image of the binary Gd_5Ge_4 alloy sample after (a) the third cleaning cycle, (b) the fourth cleaning cycle, (c) the fifth cleaning cycle, (d)-(f) the sixth cleaning cycle. A cleaning cycle represents Ar^+ sputtering and annealing to 900 K for 30 minutes. The black dotted lines in (f) serve to visually highlight the 5:3 thin plates. Sample #4.

Figure 28

An SEM image of the binary Gd_5Ge_4 alloy sample after the sixth cleaning cycle. AES was taken at five different locations in the image. The table shows the surface concentration of Gd and Ge at the five different locations. A cleaning cycle represents Ar^+ sputtering and annealing to 900 K for 30 minutes. The red bar is 1 μm long. Sample #4.

Figure 29

SEM images of the Gd_5Ge_4 (010) surface after annealing to 1150 K for 30 minutes. AES was taken at four different locations in (c). The table shows the surface concentration of Gd and Ge at the four different locations (four different lump locations). Sample #4.

Figure 30

SEM images on the Gd_5Ge_4 (010) surface showed no lumps on Sample #2 after it had been annealed and used for STM experiments. The black dotted lines in (a) serve to visually highlight the 5:3 thin plates.

Figure 31

STM images of a binary Gd_5Ge_4 (010) alloy sample that was annealed to 900 K for one hour and then cooled down to 300 K. The STM images were taken at (a) 3000 nm x 3000 nm, $I = 0.5$ nA, $V\text{-tip} = +1$ V (b) 2000 nm x 2000 nm, $I = 0.5$ nA, $V\text{-tip} = +1$ V (c) 4000 nm x 4000 nm, $I = 0.5$ nA, $V\text{-tip} = +1$ V, and (d) 3000 nm x 3000 nm, $I = 0.5$ nA, $V\text{-tip} = +0.5$ V. Sample #2.

Figure 32

STM images of a binary Gd_5Ge_4 (010) alloy sample that was annealed to 900 K for one hour and then cooled down to 300 K. The STM images were taken at (a) 3000 nm x 3000 nm, $I = 0.5$ nA, $V\text{-tip} = +0.5$ V, (b) 2000 nm x 2000 nm, $I = 0.5$ nA, $V\text{-tip} = +0.5$ V, (c) 500 nm x 500 nm, $I = 0.5$ nA, $V\text{-tip} = +0.5$ V, and (d) 500 nm x 500 nm, $I = 0.5$ nA, $V\text{-tip} = +1$ V. Sample #2.

Table 1

Structural data for Gd-Ge binary alloys.

Phase	Space Group	Lattice Parameters	Prototype
[13; 15]Gd ₅ Ge ₃	Pnma	a = b = 0.8546 nm c = 0.6410 nm	Mn ₅ Si ₃ - hexagonal
[13; 15]Gd ₅ Ge ₄	Pnma	a = 0.769 nm b = 1.475 nm c = 0.776 nm	Sm ₅ Ge ₄ – orthorhombic
[13; 15]GdGe	Cmcm	a = 0.4175 nm b = 1.061 nm c = 0.3960 nm	CrB - orthorhombic
[13; 15]Gd ₂ Ge ₃	P6/mmm	a = b = 0.4077 nm c = 1.373 nm	AlB ₂ - hexagonal
[13; 16]α-Gd ₃ Ge ₅	I4 ₁ /amd	a = 0.58281 nm b = 1.7355 nm c = 1.3785 nm	αSi ₂ Th - orthorhombic
[13; 16]β-Gd ₃ Ge ₅	Imma	a = 0.58281 nm b = 1.7355 nm c = 1.3785 nm	αSi ₂ Th - orthorhombic
[13; 15]GdGe ₂	I4 ₁ /amd	a = b = 0.412 nm c = 1.372 nm	αSi ₂ Th - hexagonal

Table 2

Heights of steps between A-A- or B-B-terraces on the Gd_5Ge_4 (010) surface after annealing at different temperatures. Values are derived from line profiles of steps in STM images. A total of 835 step heights were analyzed. Numbers in the column headers refer to samples #1 and #2. The number of steps analyzed to obtain the values are shown in parentheses.

Temperature (K)	Step Height (nm)						
	Left		Middle		Right		Average (number analyzed)
	#1	#2	#1	#2	#1	#2	
300	—	—	0.75 ± 0.16 (39)	—	—	—	0.75 ± 0.16 (39)
900	0.71 ± 0.09 (54)	0.75 ± 0.09 (74)	0.73 ± 0.10 (51)	0.75 ± 0.07 (94)	—	0.77 ± 0.08 (83)	0.75 ± 0.09 (356)
1050	0.76 ± 0.05 (83)	0.71 ± 0.09 (26)	0.76 ± 0.16 (22)	0.78 ± 0.07 (18)	0.79 ± 0.08 (14)	0.77 ± 0.09 (17)	0.76 ± 0.09 (180)
1100	0.75 ± 0.08 (21)	—	0.79 ± 0.12 (47)	—	0.74 ± 0.08 (21)	—	0.77 ± 0.10 (89)
1150	0.75 ± 0.04 (19)	—	0.72 ± 0.07 (18)	—	0.74 ± 0.02 (14)	—	0.74 ± 0.05 (51)
1200	—	0.77 ± 0.09 (38)	0.74 ± 0.05 (6)	0.76 ± 0.07 (36)	—	0.76 ± 0.09 (40)	0.76 ± 0.08 (120)

Table 3

Heights of steps between A- and B-terraces on the Gd₅Ge₄ (010) surface after annealing at different temperatures. Values are derived from line profiles of steps in STM images. A total of 782 step heights were analyzed.

Temperature (K) *Sample 1 †Sample 2	Step Height (nm)							
	Left		Middle		Right		Average (number analyzed)	
	Terrace A	Terrace B	Terrace A	Terrace B	Terrace A	Terrace B	Terrace A	Terrace B
900	†0.36 ± 0.08	†0.37 ± 0.07	†0.40 ± 0.06	†0.35 ± 0.07	†0.40 ± 0.05	†0.34 ± 0.07	0.39 ± 0.07 (183)	0.35 ± 0.07 (183)
1050	*0.38 ± 0.05 †0.33 ± 0.07	*0.30 ± 0.07 †0.44 ± 0.06	*0.31 ± 0.13 †0.41 ± 0.06	*0.46 ± 0.12 †0.37 ± 0.05	*0.26 ± 0.04 †0.36 ± 0.04	*0.44 ± 0.06 †0.39 ± 0.05	0.35 ± 0.08 (83)	0.40 ± 0.09 (83)
1100	*0.39 ± 0.07	*0.31 ± 0.05	*0.28 ± 0.08	*0.43 ± 0.10	*0.34 ± 0.07	*0.29 ± 0.06	0.32 ± 0.09 (34)	0.36 ± 0.10 (34)
1150	*0.35 ± 0.07	*0.33 ± 0.06	*0.29 ± 0.09	*0.39 ± 0.08	*0.36 ± 0.06	*0.29 ± 0.07	0.33 ± 0.08 (48)	0.34 ± 0.08 (48)
1200	—	—	*0.37 ± 0.13 †0.36 ± 0.03	*0.25 ± 0.06 †0.32 ± 0.06	— †0.37 ± 0.09	— †0.33 ± 0.08	0.37 ± 0.09 (43)	0.31 ± 0.08 (43)

Table 4

Bump heights on B terraces on the Gd_5Ge_4 (010) surface after annealing at annealing temperatures. Heights were measured from STM line profiles. A total of 317 bump heights were analyzed.

Temperature (K)	Bump Heights (nm)		
	Sample 1	Sample 2	Average Height (nm) (number analyzed)
900 K	0.38 ± 0.09 (middle)	0.40 ± 0.05 (left)	0.39 ± 0.07 (58)
1050 K	0.29 ± 0.05 (middle) 0.29 ± 0.04 (left)	0.36 ± 0.05 (middle) 0.36 ± 0.13 (right) 0.25 ± 0.05 (left)	0.32 ± 0.09 (78)
1100 K	0.27 ± 0.04 (middle) 0.38 ± 0.07 (right) 0.39 ± 0.06 (left)	—	0.35 ± 0.08 (48)
1150 K	0.32 ± 0.05 (middle) 0.33 ± 0.08 (right) 0.33 ± 0.07 (left)	—	0.33 ± 0.07 (88)
1200 K	0.35 ± 0.05 (middle) 0.28 ± 0.08 (right) 0.29 ± 0.04 (left)	—	0.31 ± 0.07 (45)

Table 5

Average individual bump area on B-terraces on the Gd₅Ge₄ (010) surface after annealing at different temperatures. The number of bumps analyzed for each value is given in parentheses. The values were determined by zooming in and flooding the image, which typically contained several bumps. Values of areas obtained by flooding can be sensitive to the flooding level chosen. The entire range of values of bump areas is shown in square brackets.

Temperature (K)	Average Individual Bump Area (nm ²)		
	Sample #1	Sample #2	Average
900 K	1.84 ± 0.59 (17)	1.69 ± 0.52 (14)	1.78 ± 0.56 (31) [0.32-3.25]
1050 K	1.81 ± 0.90 (17)	2.18 ± 1.52 (17)	1.99 ± 1.24 (34) [0.72-5.59]
1100 K	2.28 ± 0.71 (13)	—	2.28 ± 0.71 (13) [1.02-3.50]
1150 K	4.84 ± 2.41 (33)	—	4.84 ± 2.41 (33) [1.04-12.00]
1200 K	2.26 ± 0.72 (18)	—	2.26 ± 0.72 (18) [1.04-3.96]

Table 6

Fractional area covered by bumps on B-terraces on the Gd_5Ge_4 (010) surface after annealing at different temperatures. The total area analyzed is given in parentheses, in units of nm^2 . This number was determined by flooding STM images. Values derived from such an approach can be sensitive to the flooding level that is chosen.

Temperature (K)	Fractional Bump Area		
	Sample #1	Sample #2	Average
900 K	0.08 (11451.18)	0.22 (47786.1)	0.15 (59237.28)
1050 K	0.05 (69914.93)	0.15 (23111.76)	0.10 (93026.69)
1100 K	0.08 (148712.08)	—	0.08 (148712.08)
1150 K	0.16 (28025.84)	—	0.16 (28025.84)
1200 K	0.22 (28350.39)	—	0.22 (28350.39)

Table 7

Bump density (N) on B-terraces on the Gd₅Ge₄ (010) surface after annealing at different temperatures. NOTE: N is the number of bumps divided by the total image area. The total area analyzed, summed over all images, is shown in parentheses, in units of nm².

Temperature (K)	Bump Density (nm ⁻²)		
	Sample #1	Sample #2	Average
900 K	0.04 (31346.81)	0.10 (8628.39)	0.08 (39975.2)
1050 K	0.02 (55825.35)	0.07 (8594.4)	0.05 (64419.75)
1100 K	0.01 (37312.98)	—	0.01 (37312.98)
1150 K	0.04 (32614.44)	—	0.04 (32614.44)
1200 K	0.06 (28021.31)	—	0.06 (28021.31)

Table 8

Vacancy pit depths on the Gd₅Ge₄ (010) surface after annealing at different temperatures. Values are derived from line profiles from STM images. A total of 136 pit heights were analyzed.

Temperature (K)	Pit Depths (nm)		
	Sample 1	Sample 2	Average (number analyzed)
900 K	—	0.73 ± 0.05 (right) 0.79 ± 0.06 (left)	0.77 ± 0.06 (33)
1050 K	0.73 ± 0.03 (left)	0.74 ± 0.09 (middle) 0.80 ± 0.06 (right) 0.74 ± 0.15 (left)	0.76 ± 0.11 (57)
1150 K	0.77 ± 0.06 (right) 0.82 ± 0.06 (left)	—	0.81 ± 0.06 (12)
1200 K	—	0.80 ± 0.08 (right) 0.76 ± 0.09 (left)	0.79 ± 0.09 (34)

Table 9

Progression of surface features observed with STM on samples #1 and #2, as a function of annealing temperature.

History	Sample #1	Sample #2
Thermal gradient?	None detected	20 K between coolest (middle) and hottest (left side) at 900 K
Surface after 900 K annealing	Mostly rough, with a few regions of B-terraces.	Mainly terrace-step morphology. Cool regions are mainly A-terraces. Hot side has A + B mixture, alternating.
1050 K	Mostly B-terraces.	Mostly B-terraces.
1100 K	Mostly B-terraces.	n/a
1150 K	Mostly B-terraces.	n/a
1200 K	A + B mixture, alternating	Checkerboard on coolest region. Pits on hottest region.
Summary, 900 K \rightarrow 1200 K	Rough \rightarrow B \rightarrow A+B	A \rightarrow A+B \rightarrow B \rightarrow A + checkerboard + pits.

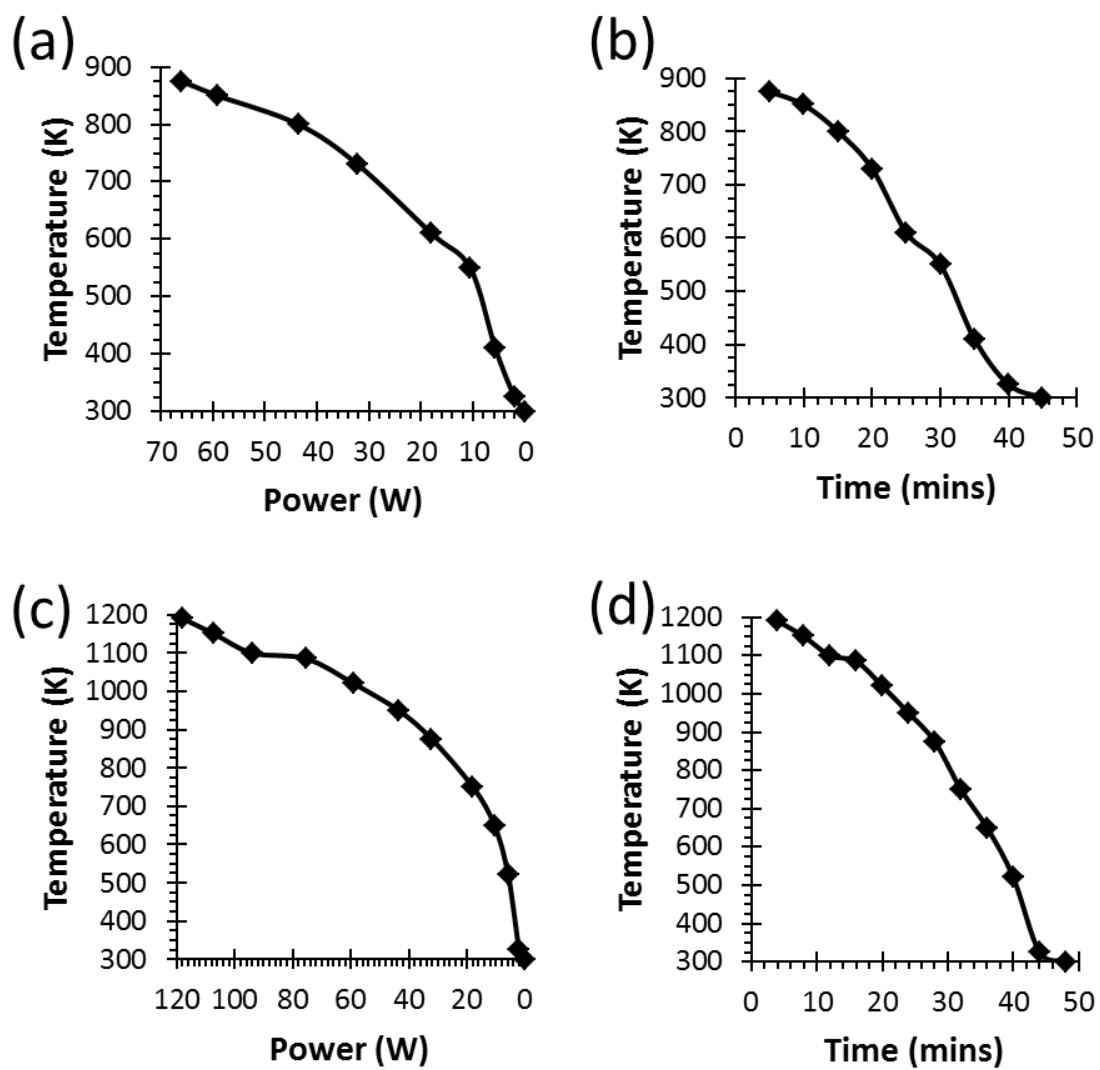


Figure 1

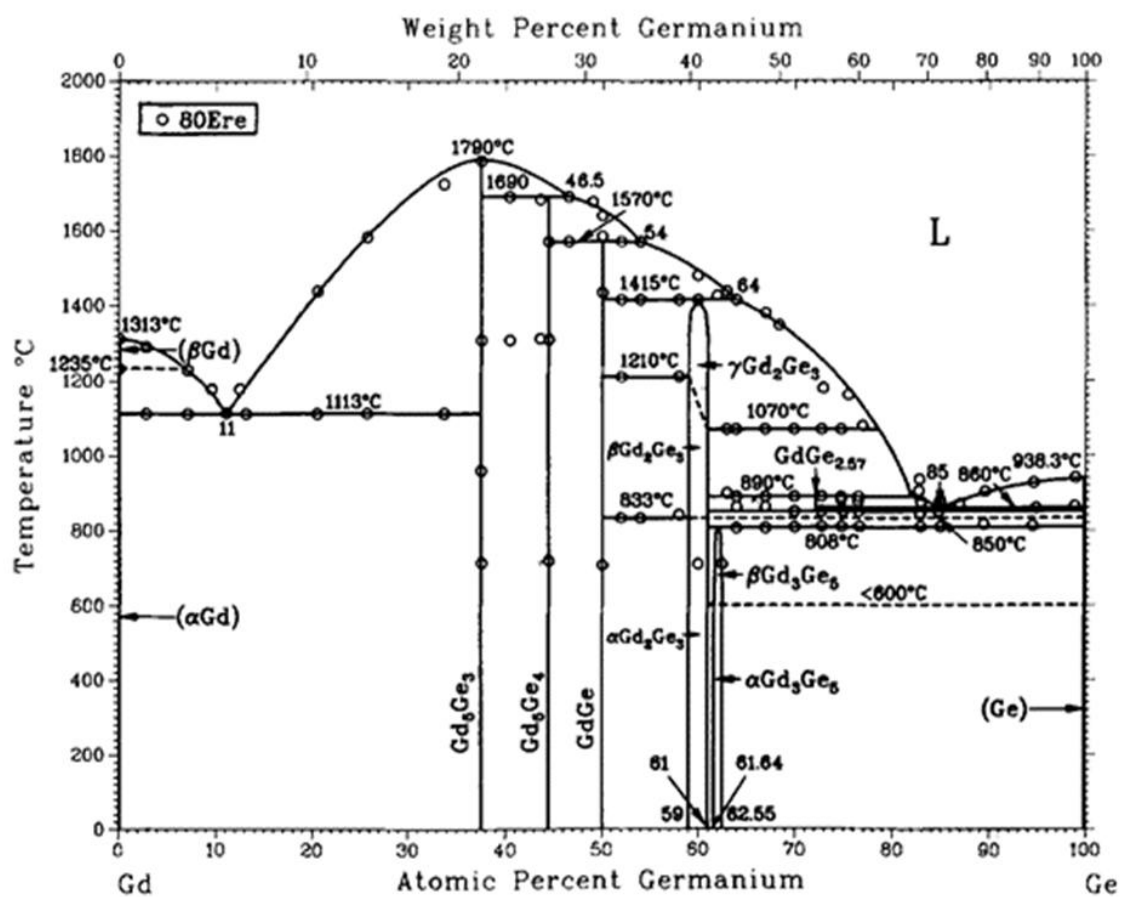


Figure 2

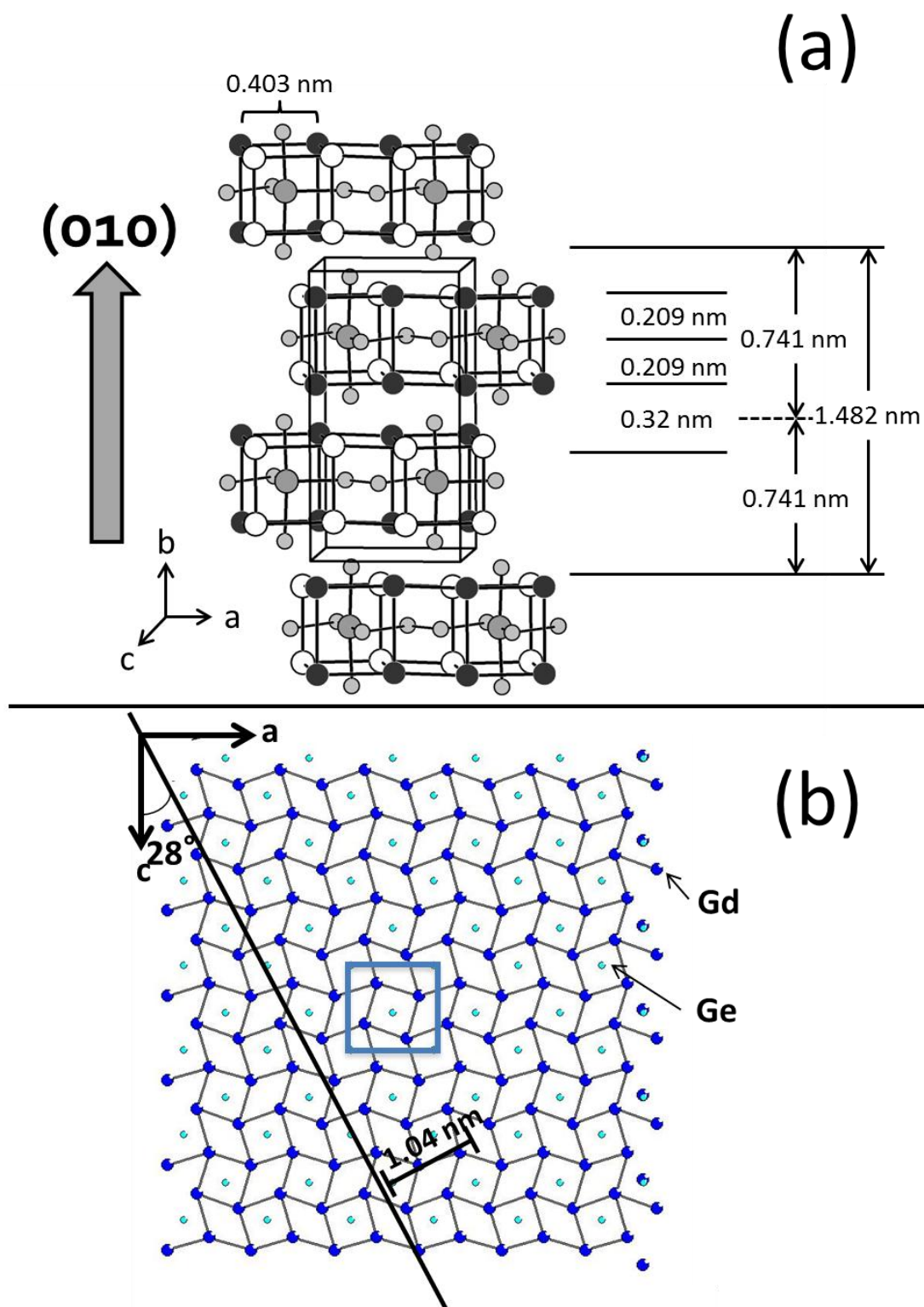


Figure 3

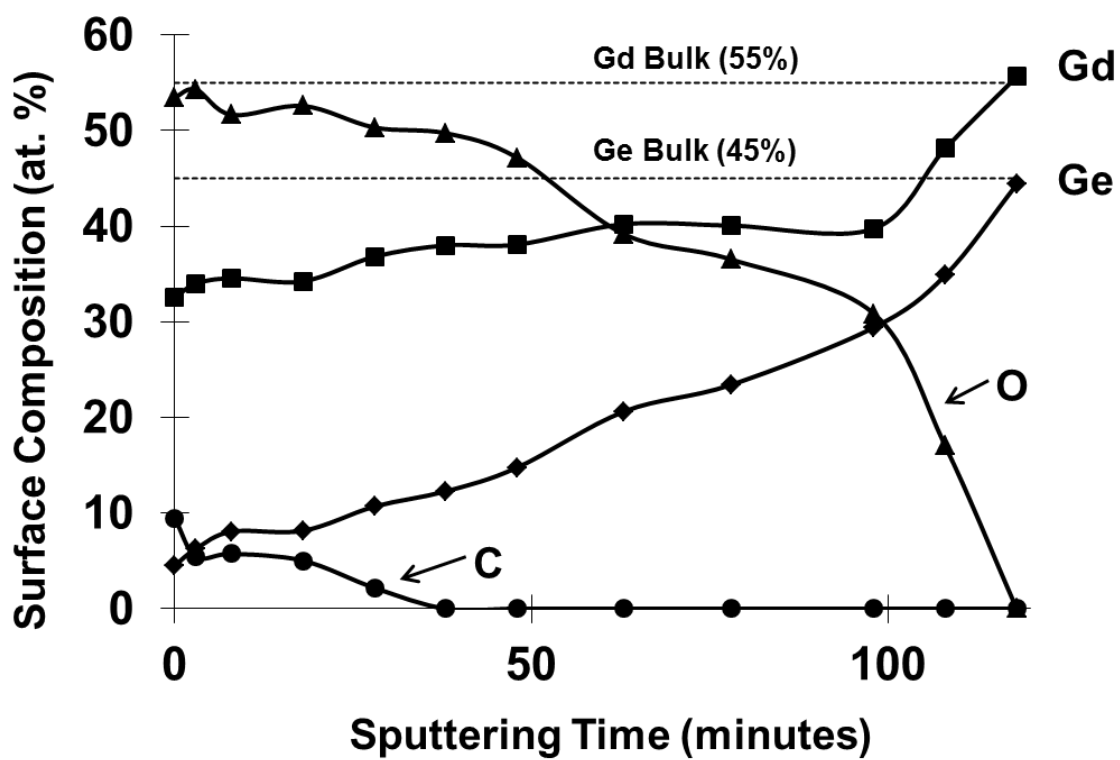


Figure 4

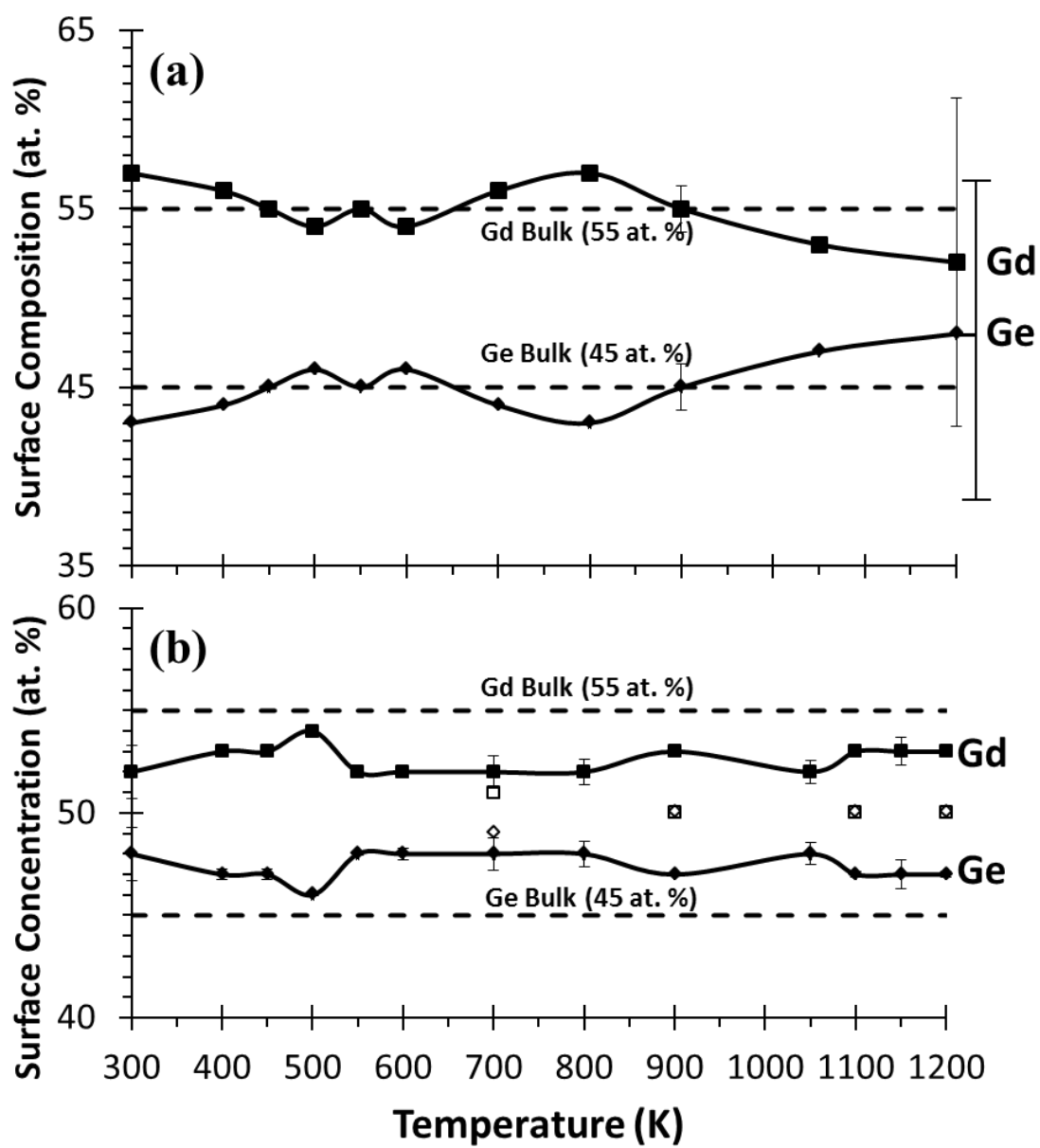


Figure 5

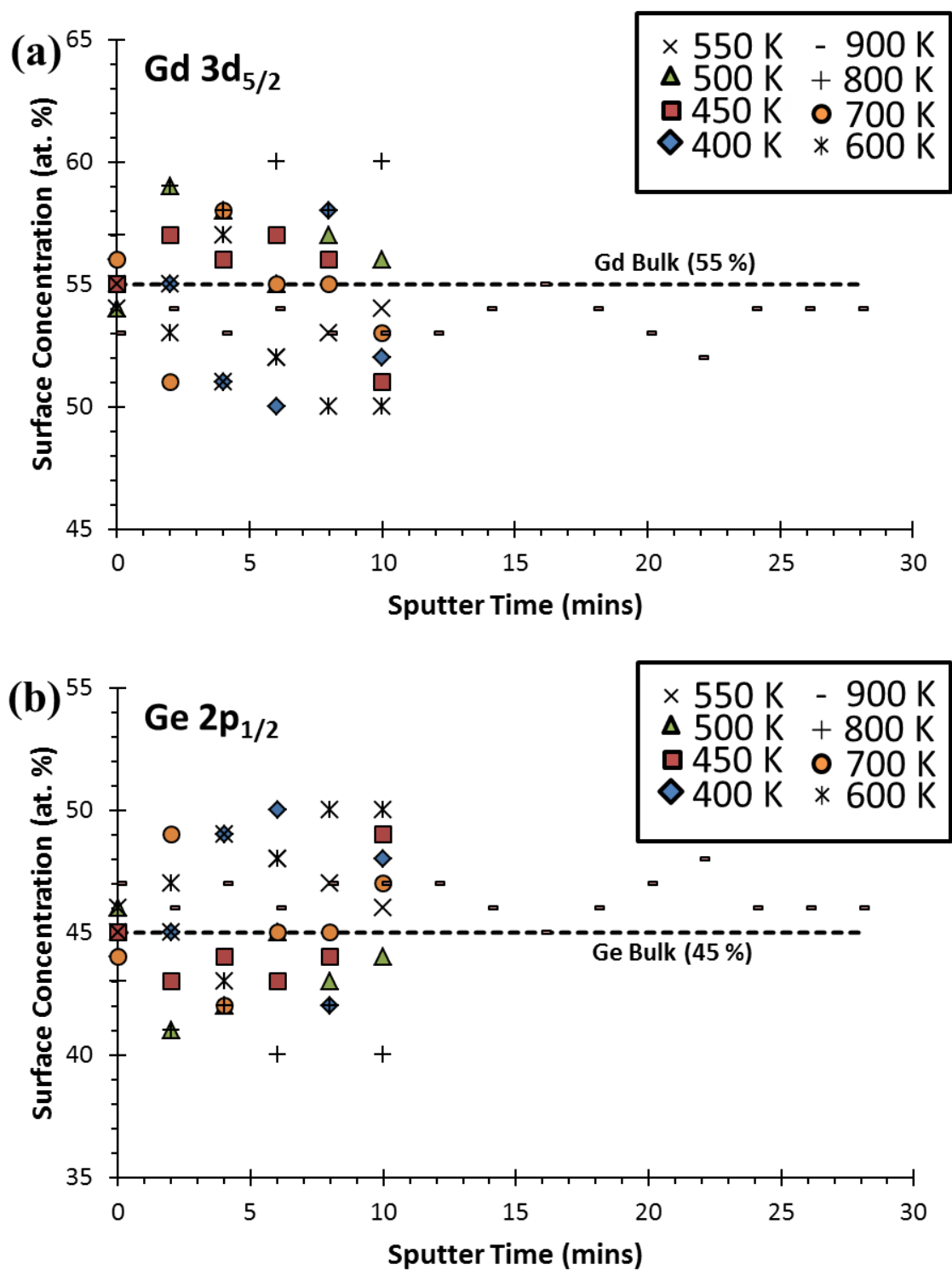


Figure 6

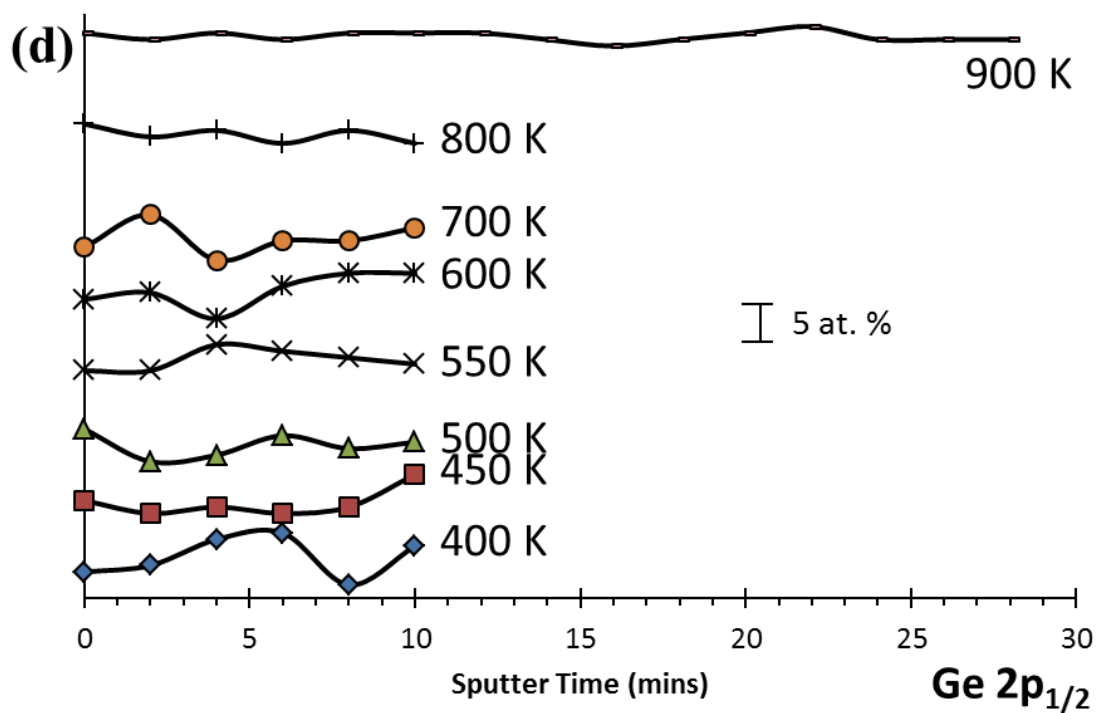
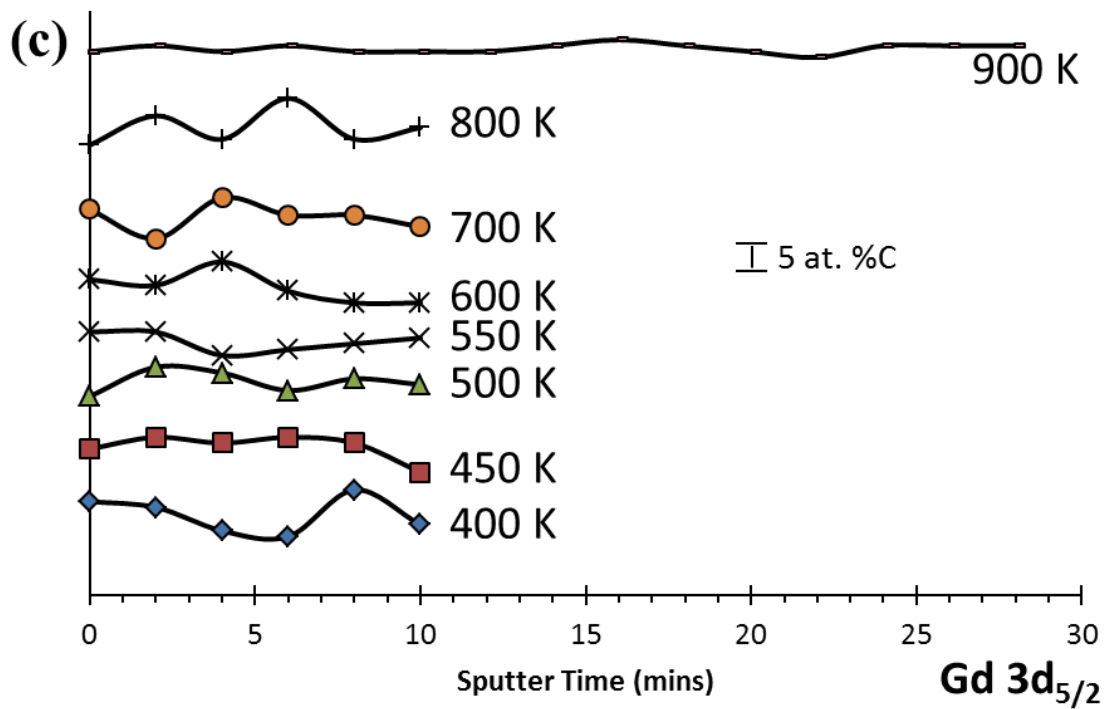


Figure 6 (Continue)

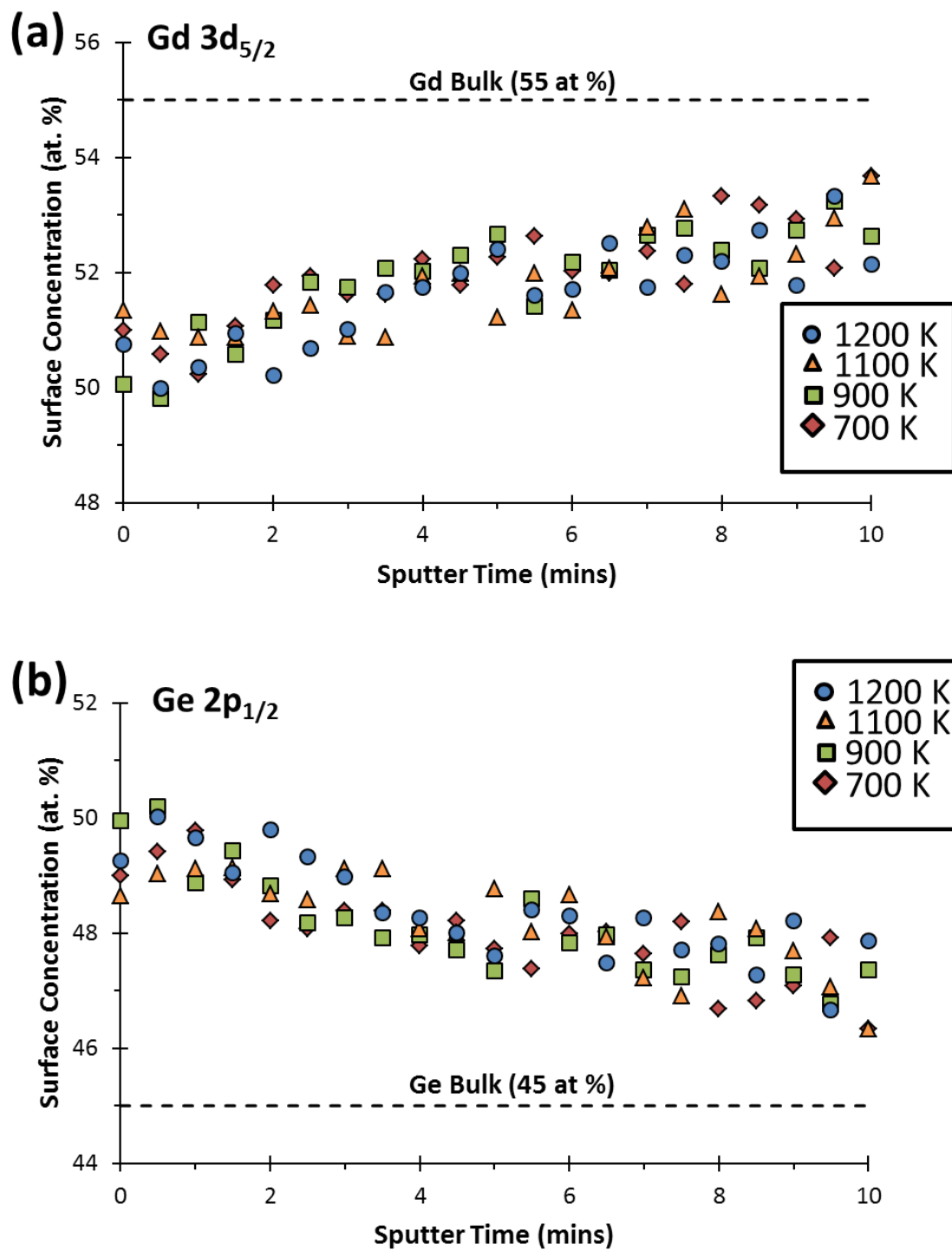
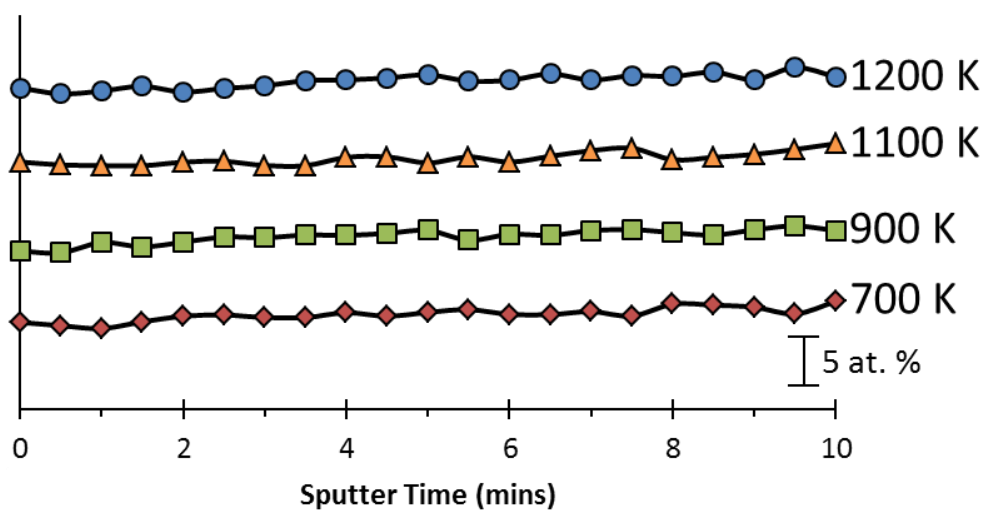


Figure 7

(c)



(d)

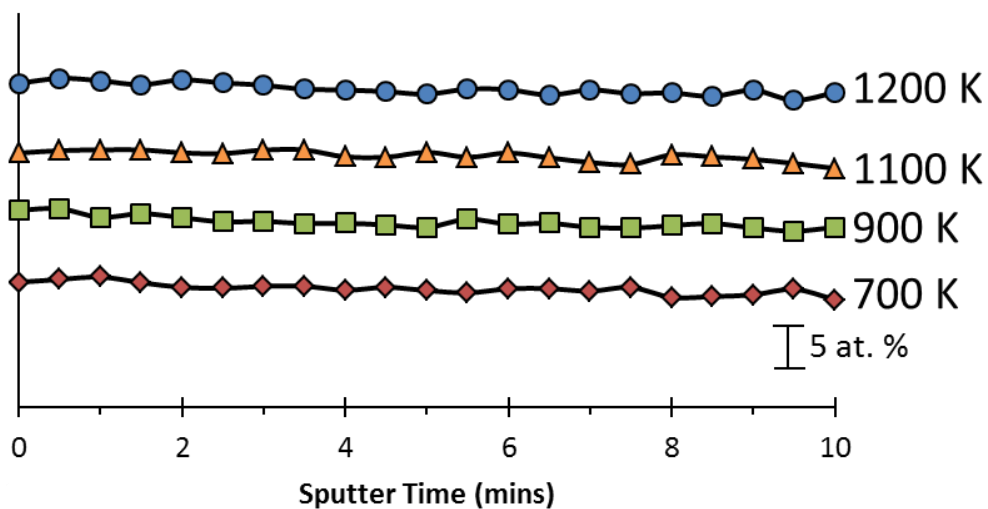


Figure 7 (Continue)

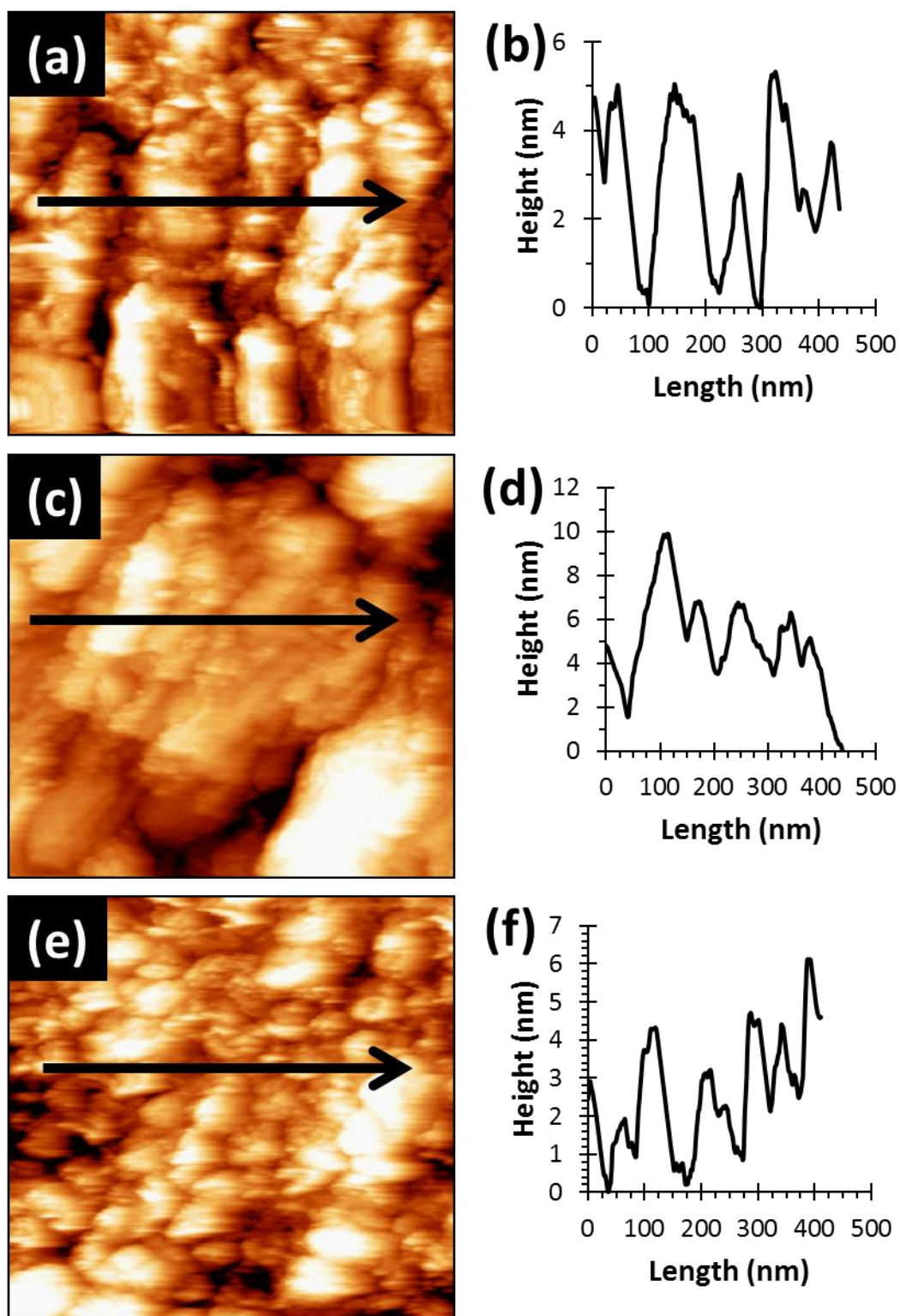


Figure 8

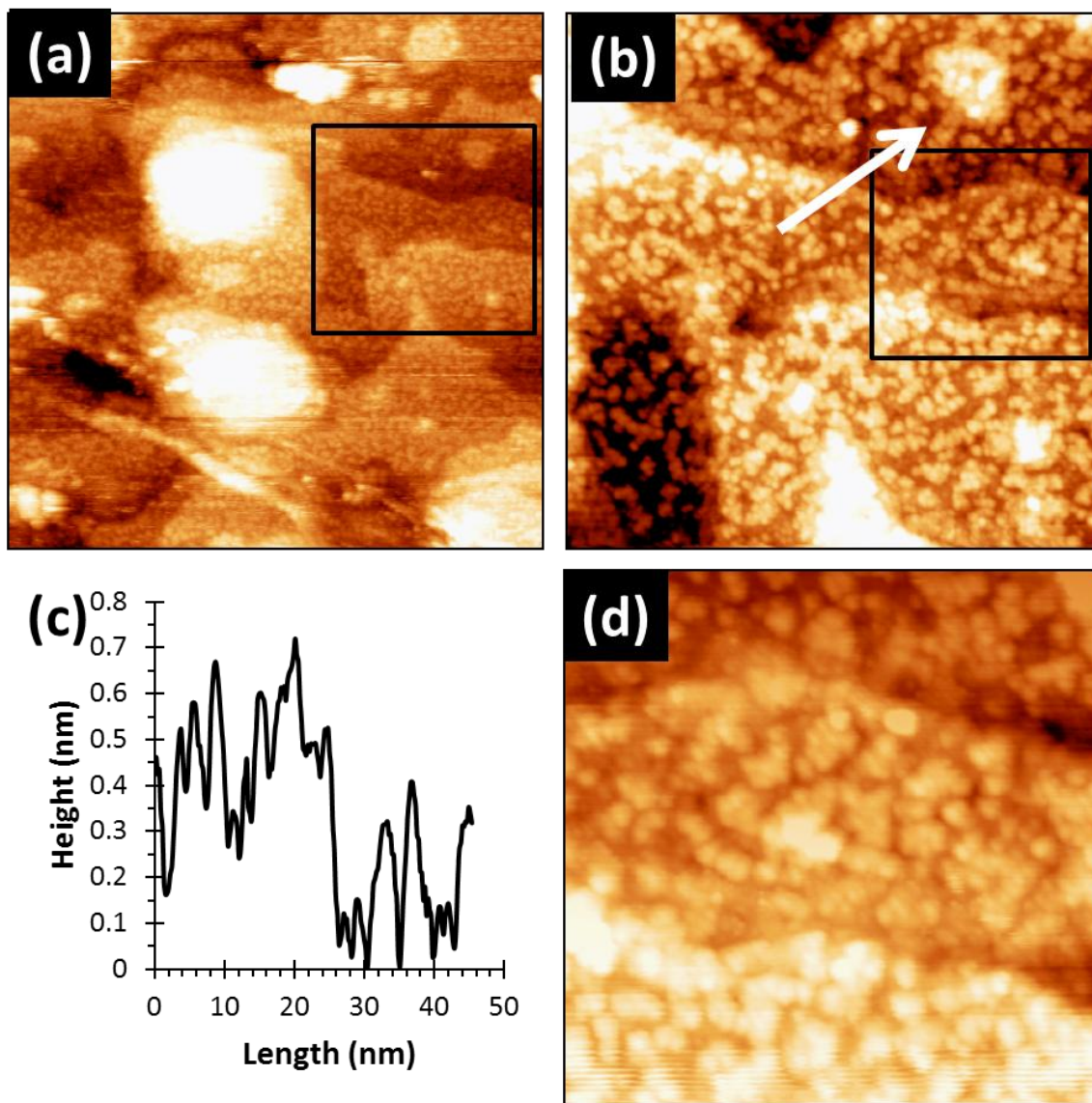


Figure 9

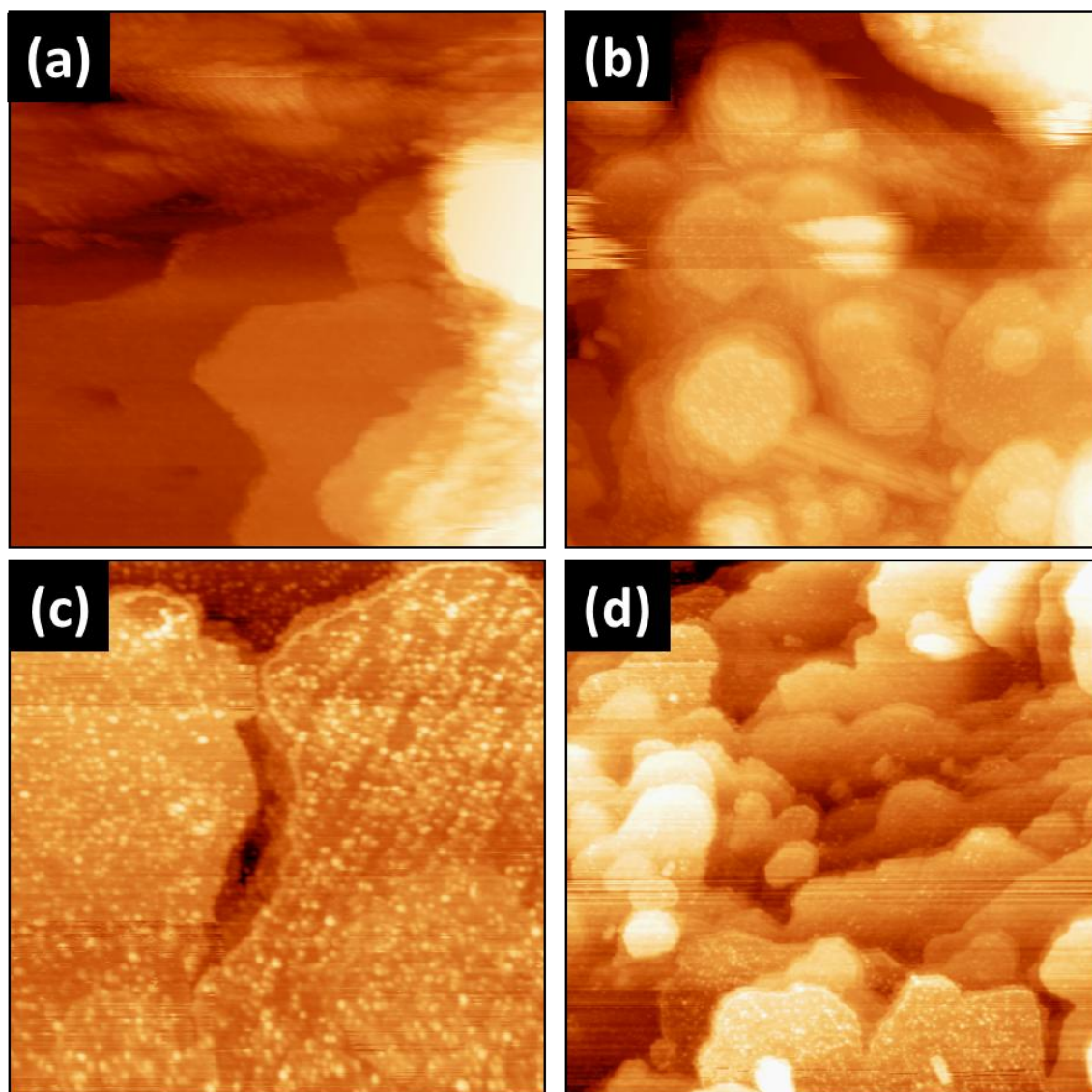


Figure 10

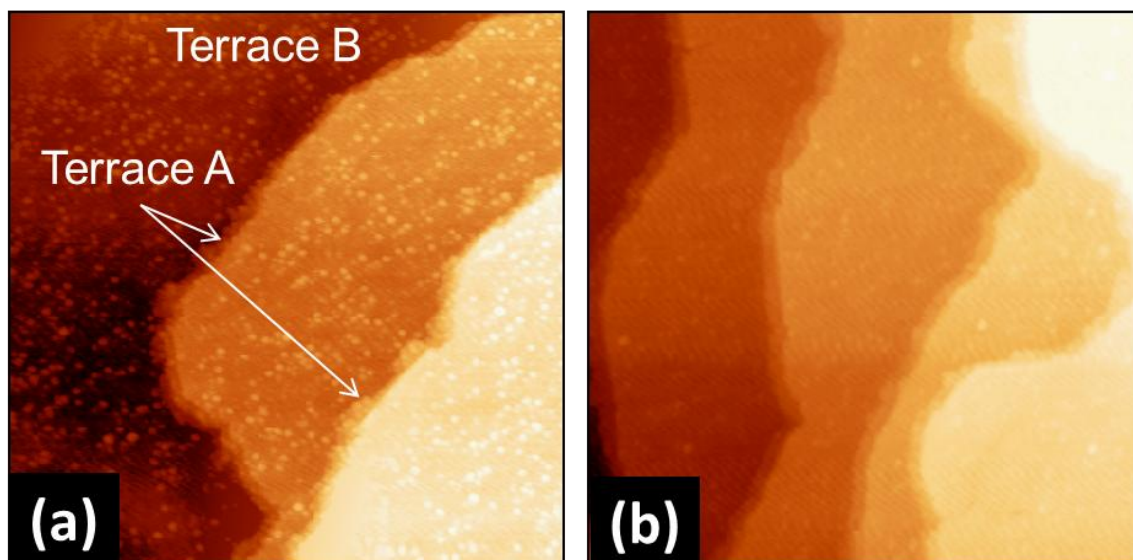


Figure 11

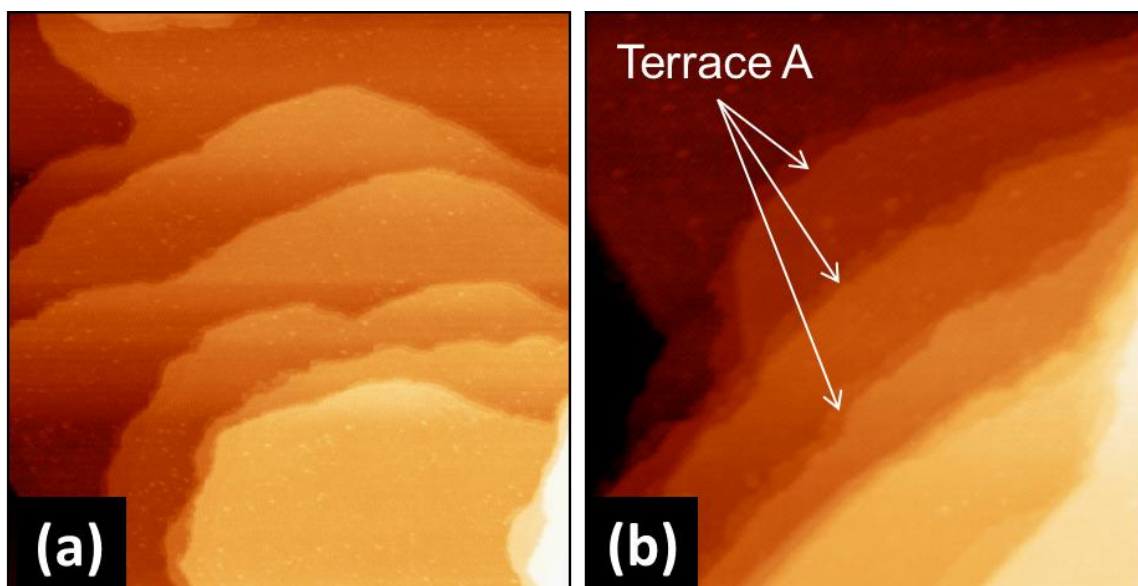


Figure 12

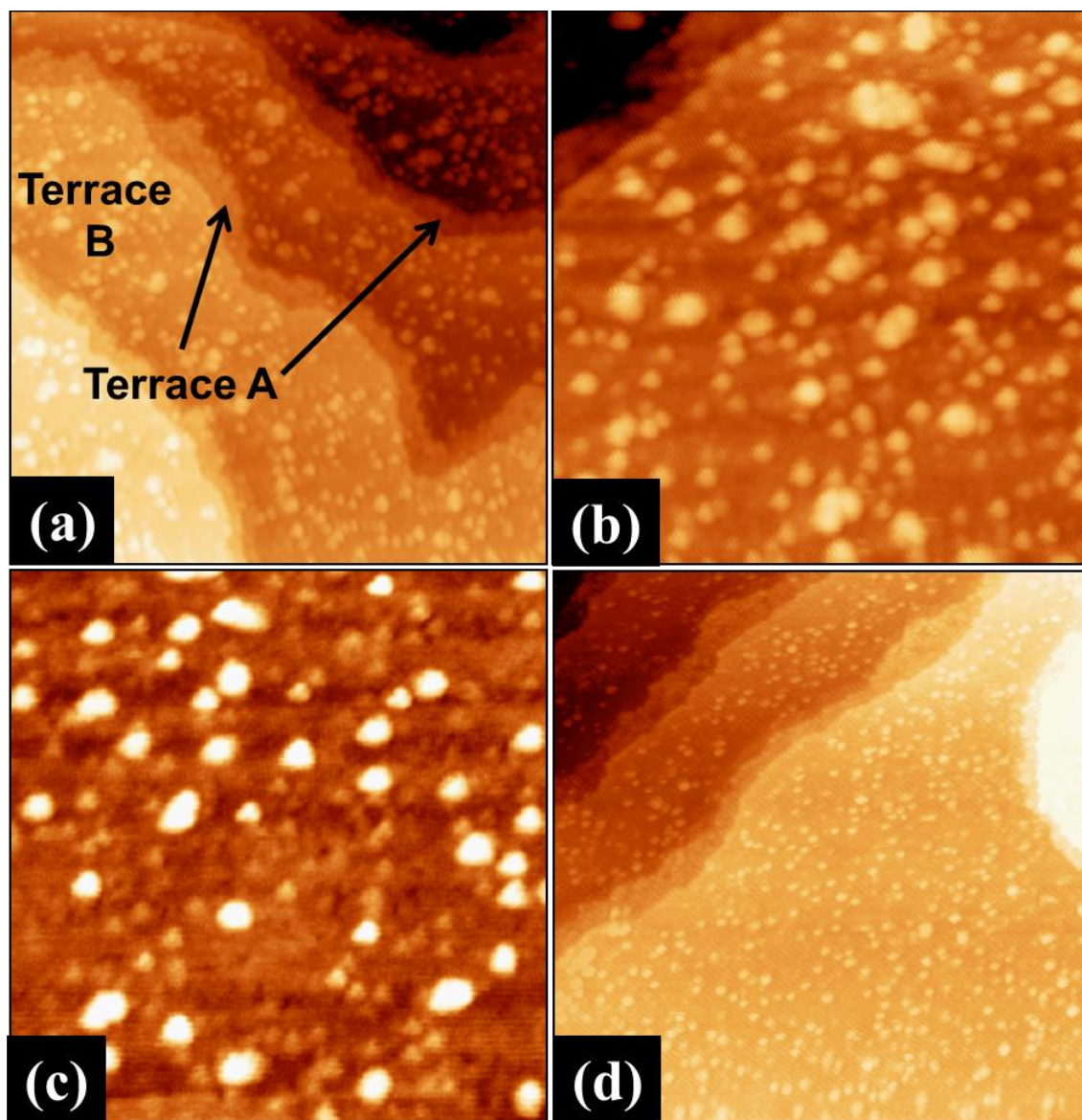


Figure 13

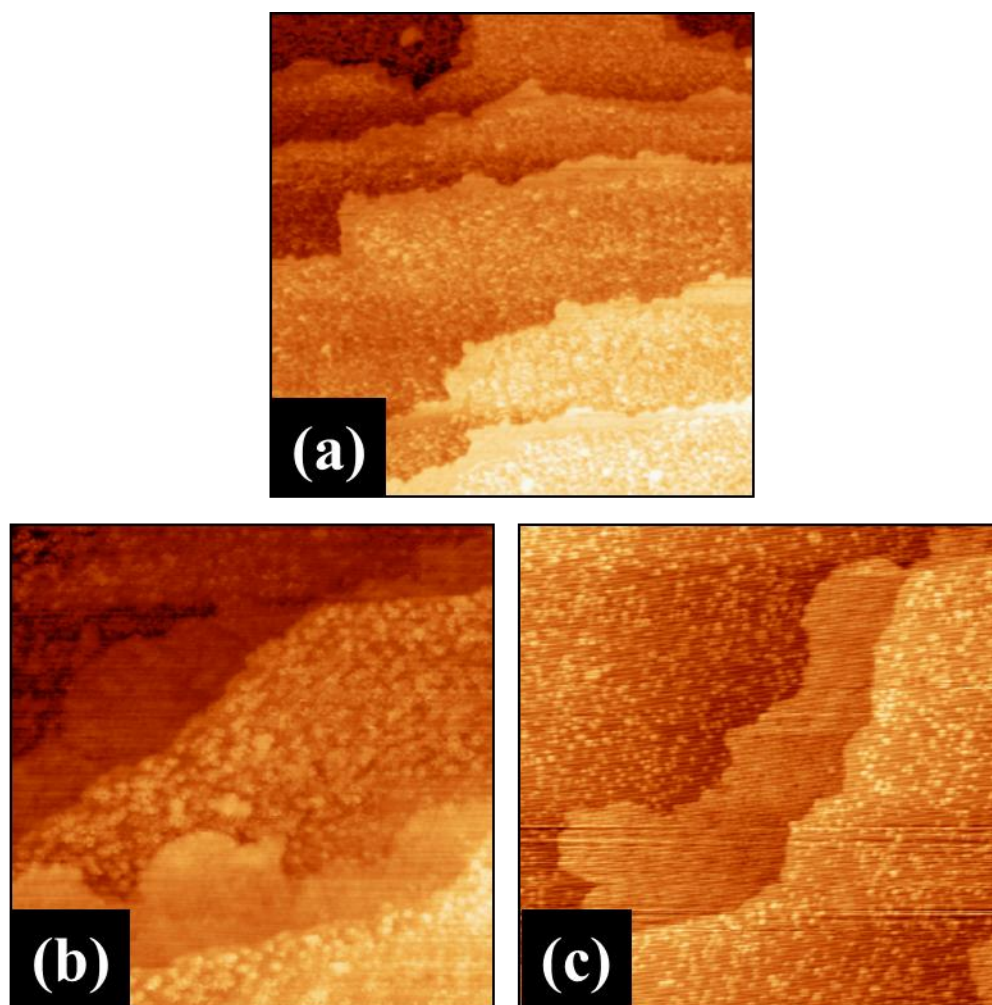


Figure 14

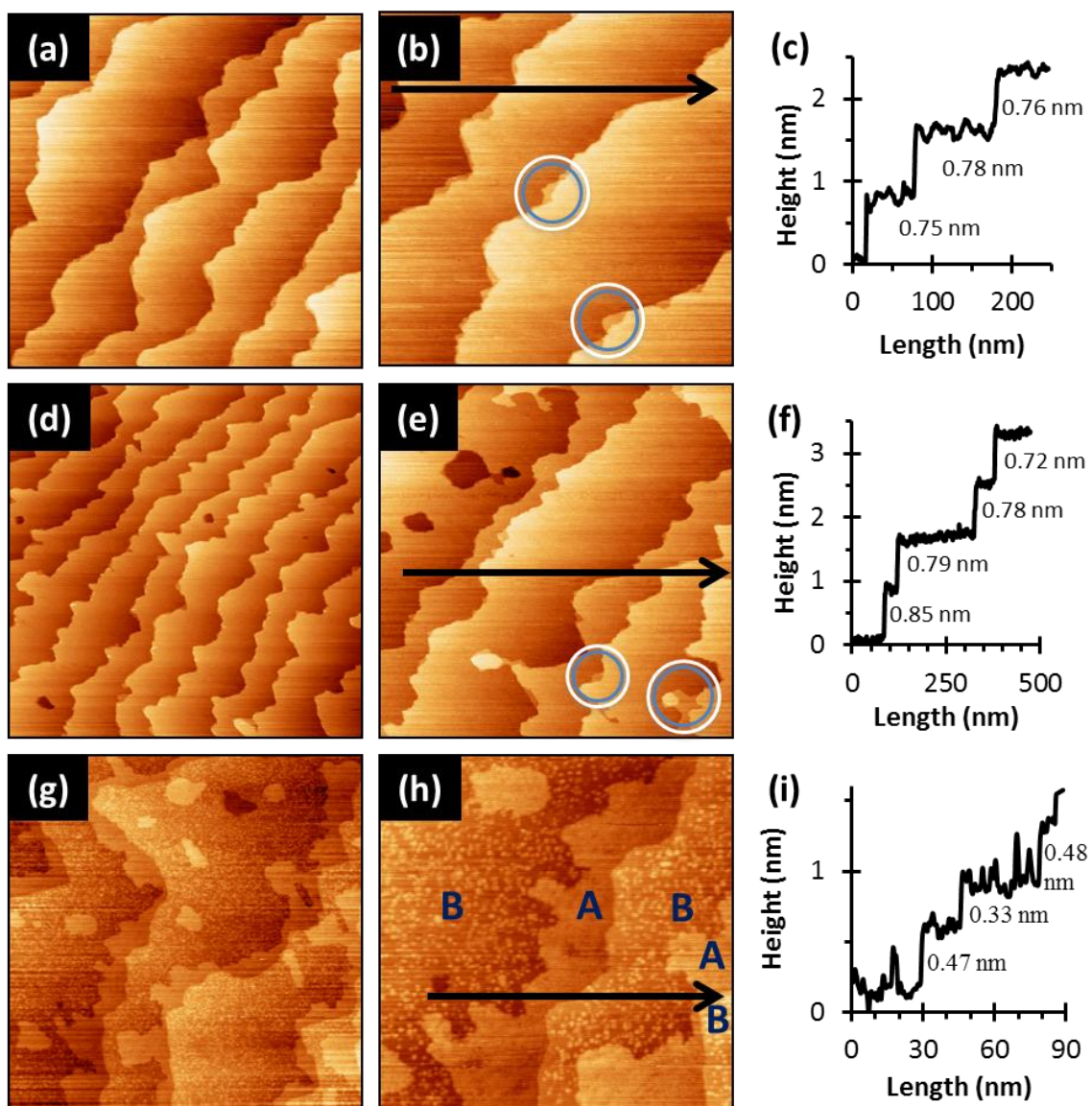


Figure 15

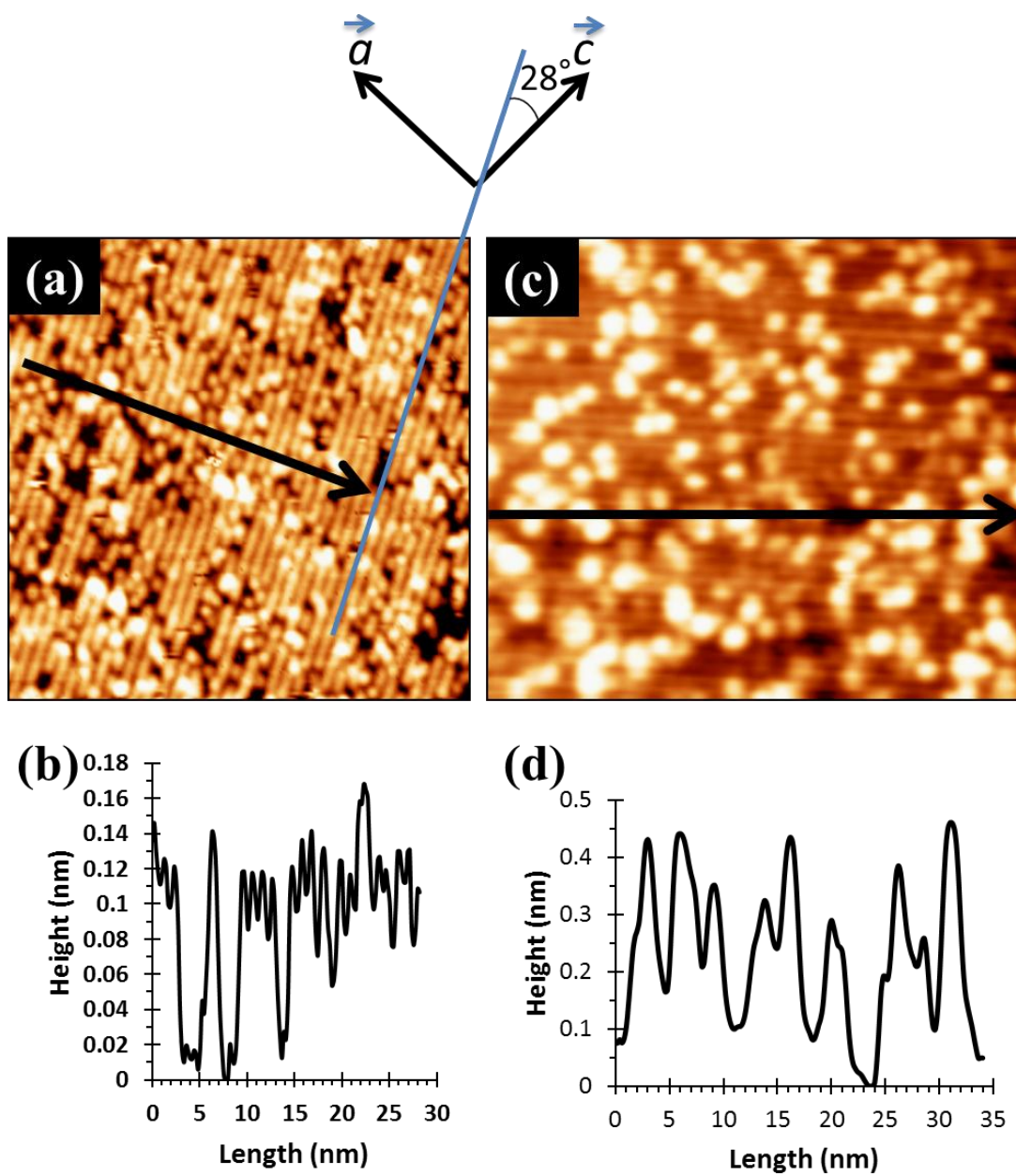
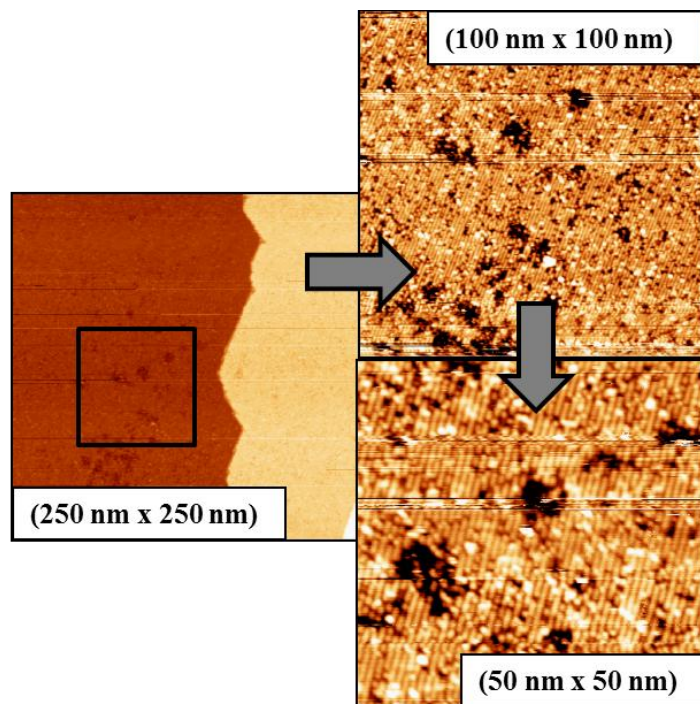
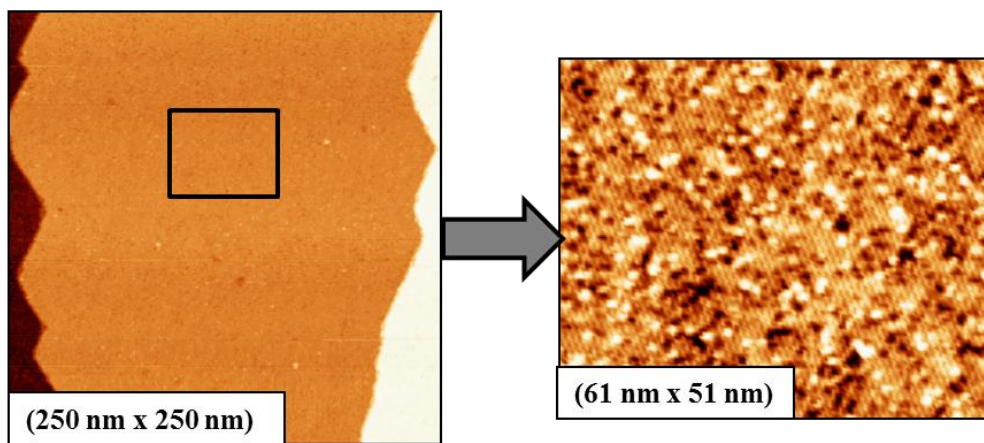


Figure 16



(a)



(b)

Figure 17

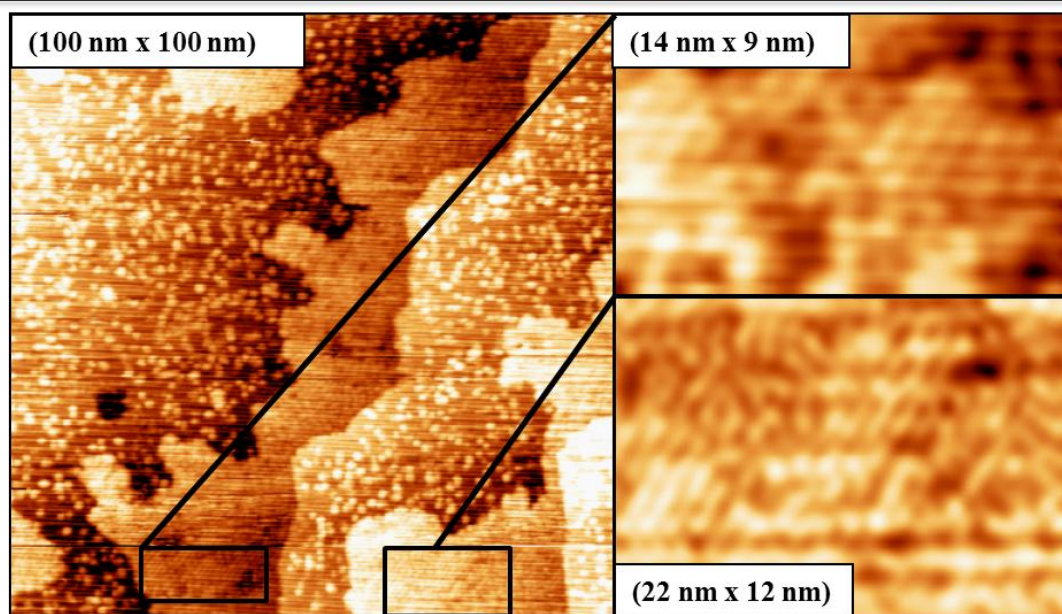
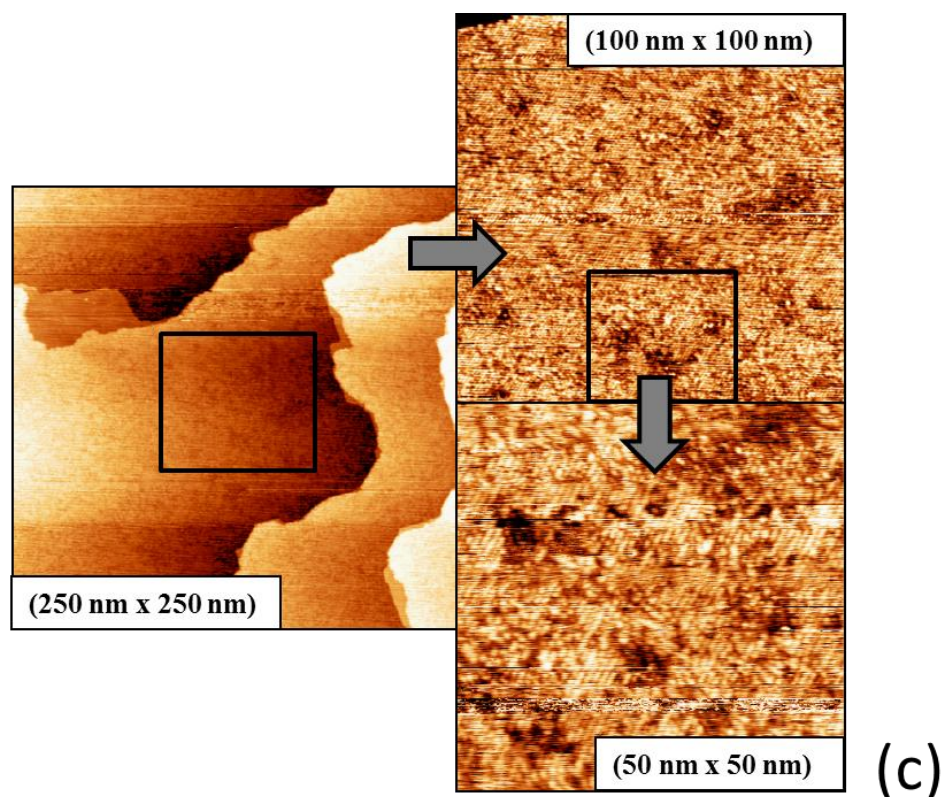


Figure 17 (Continue)

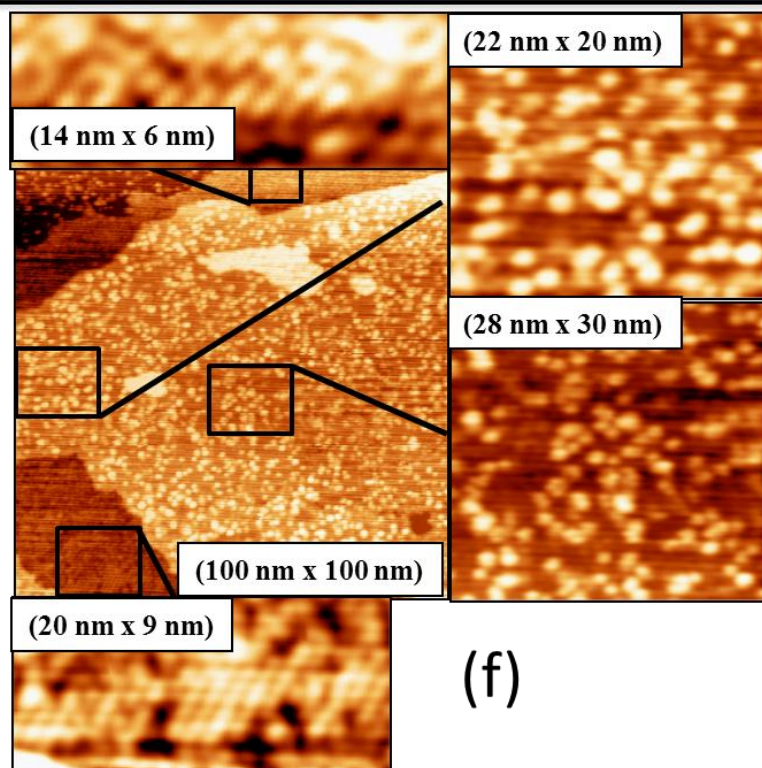
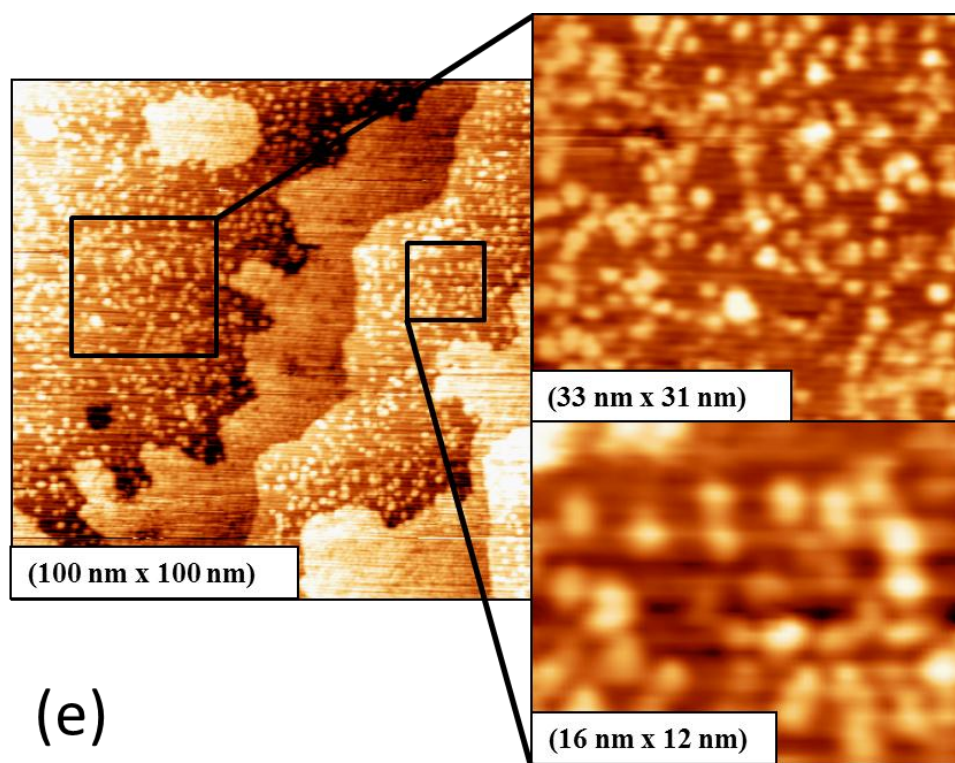


Figure 17 (Continue)

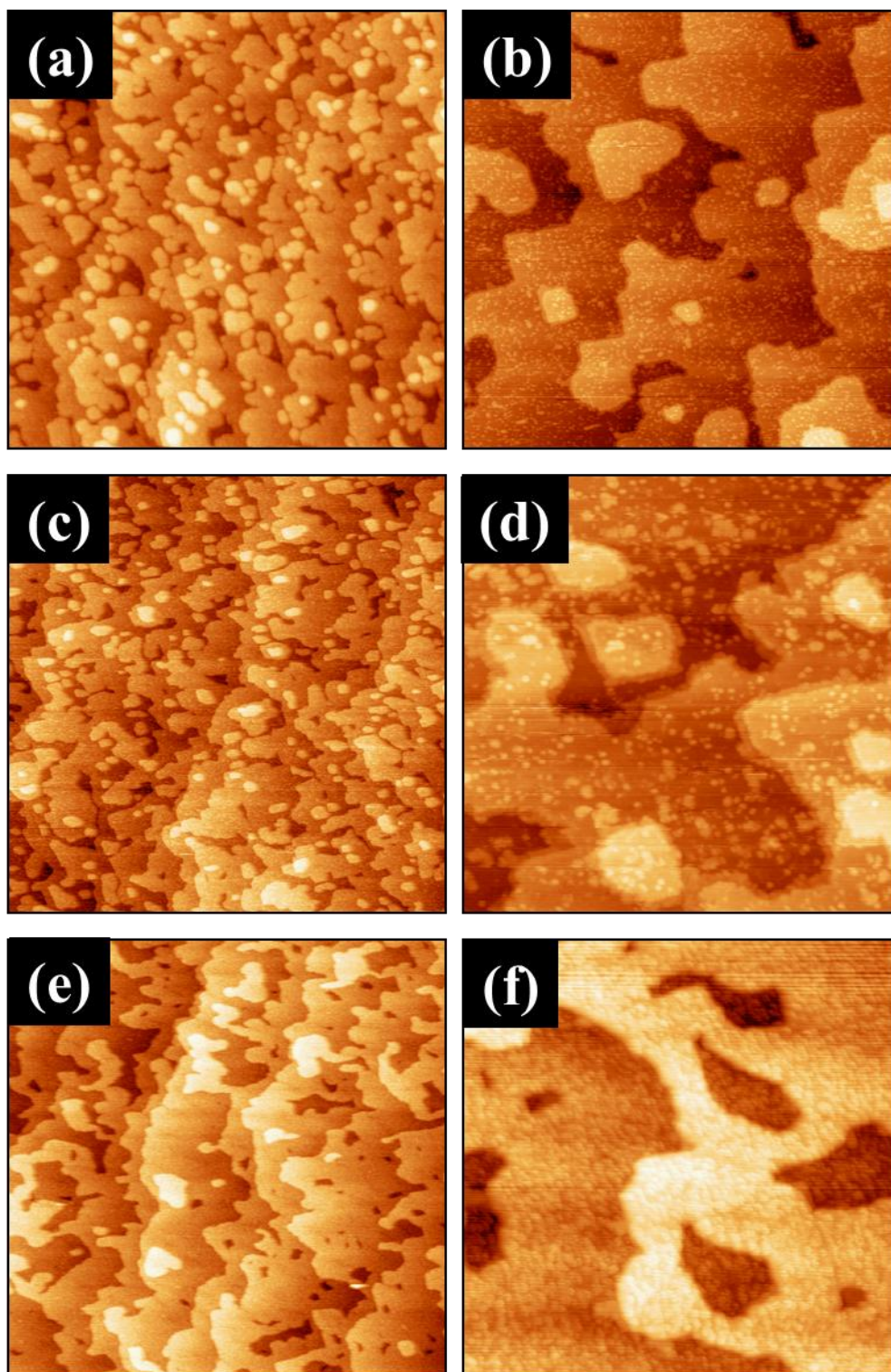


Figure 18

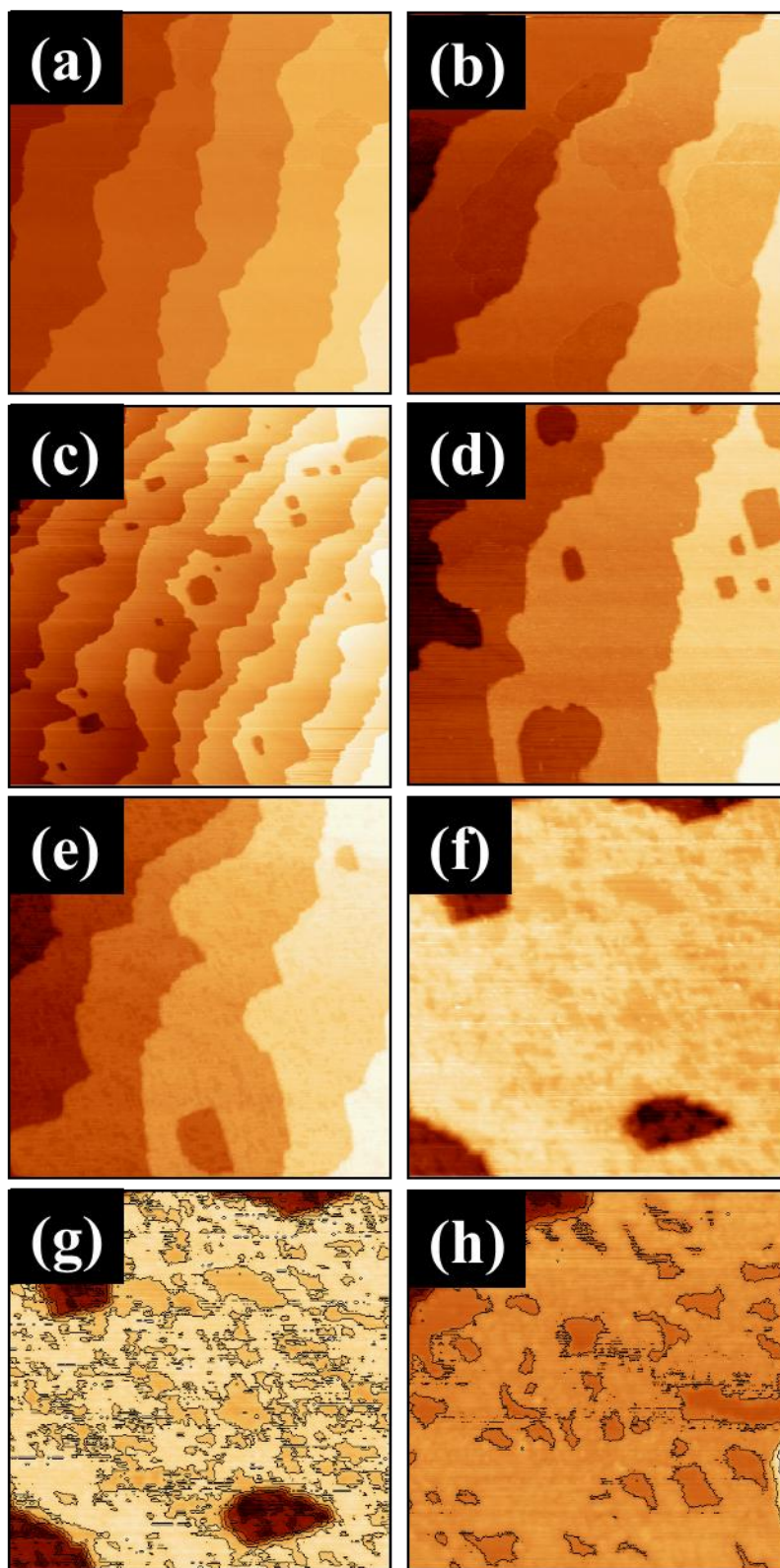


Figure 19

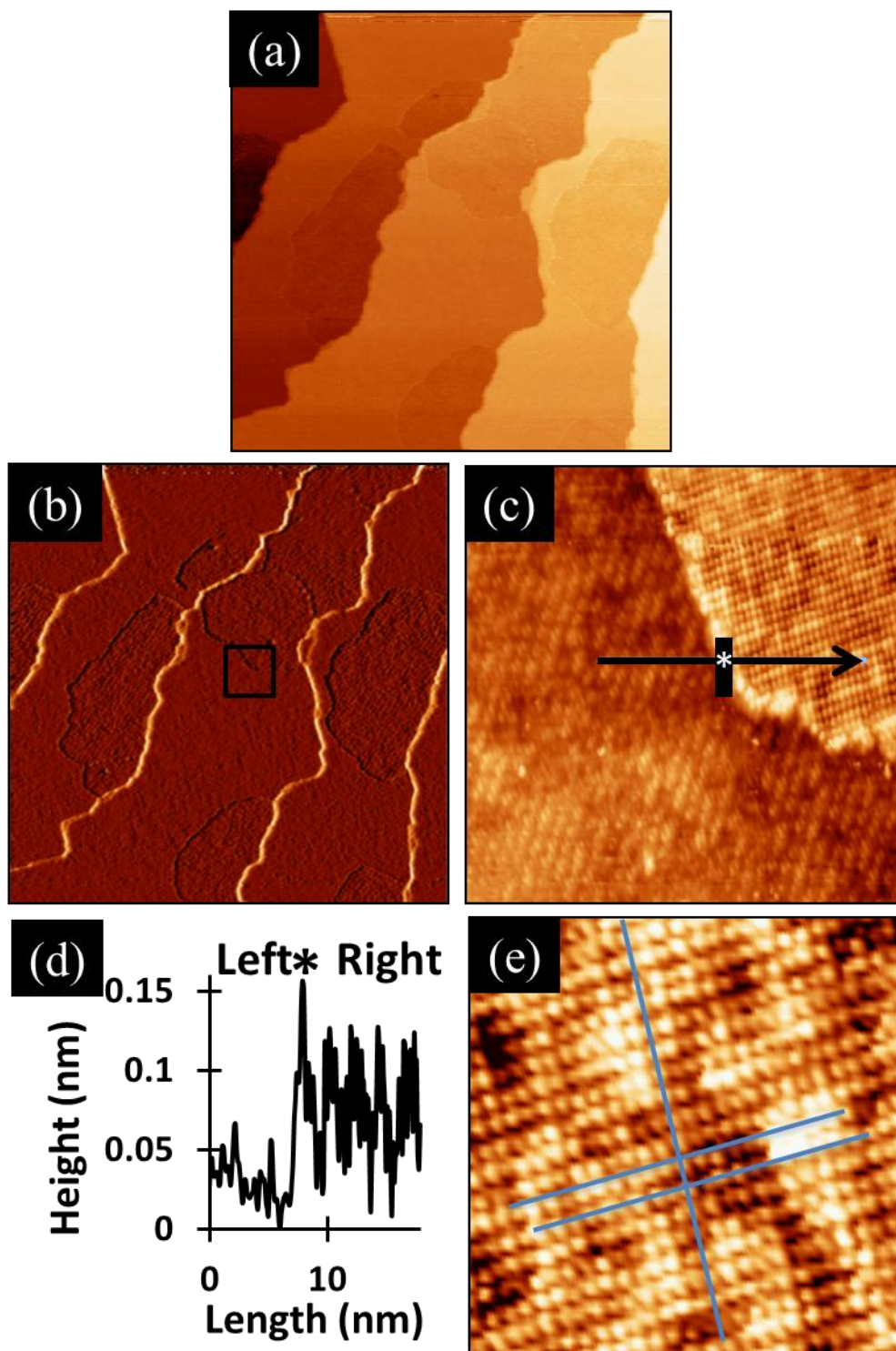


Figure 20

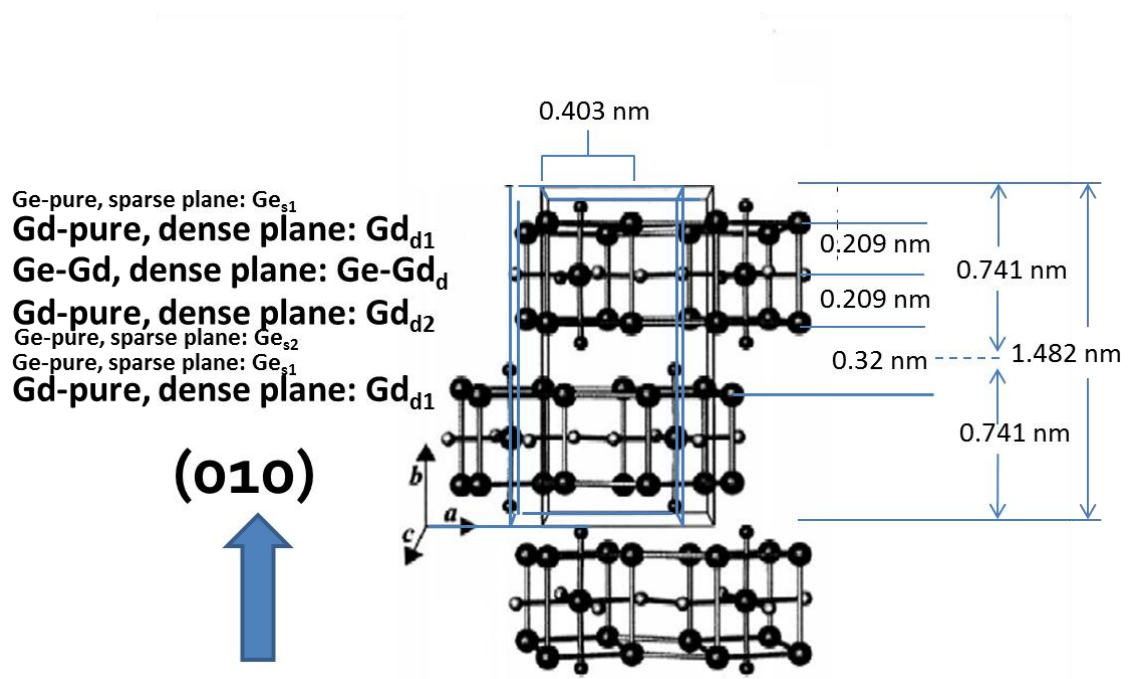


Figure 21

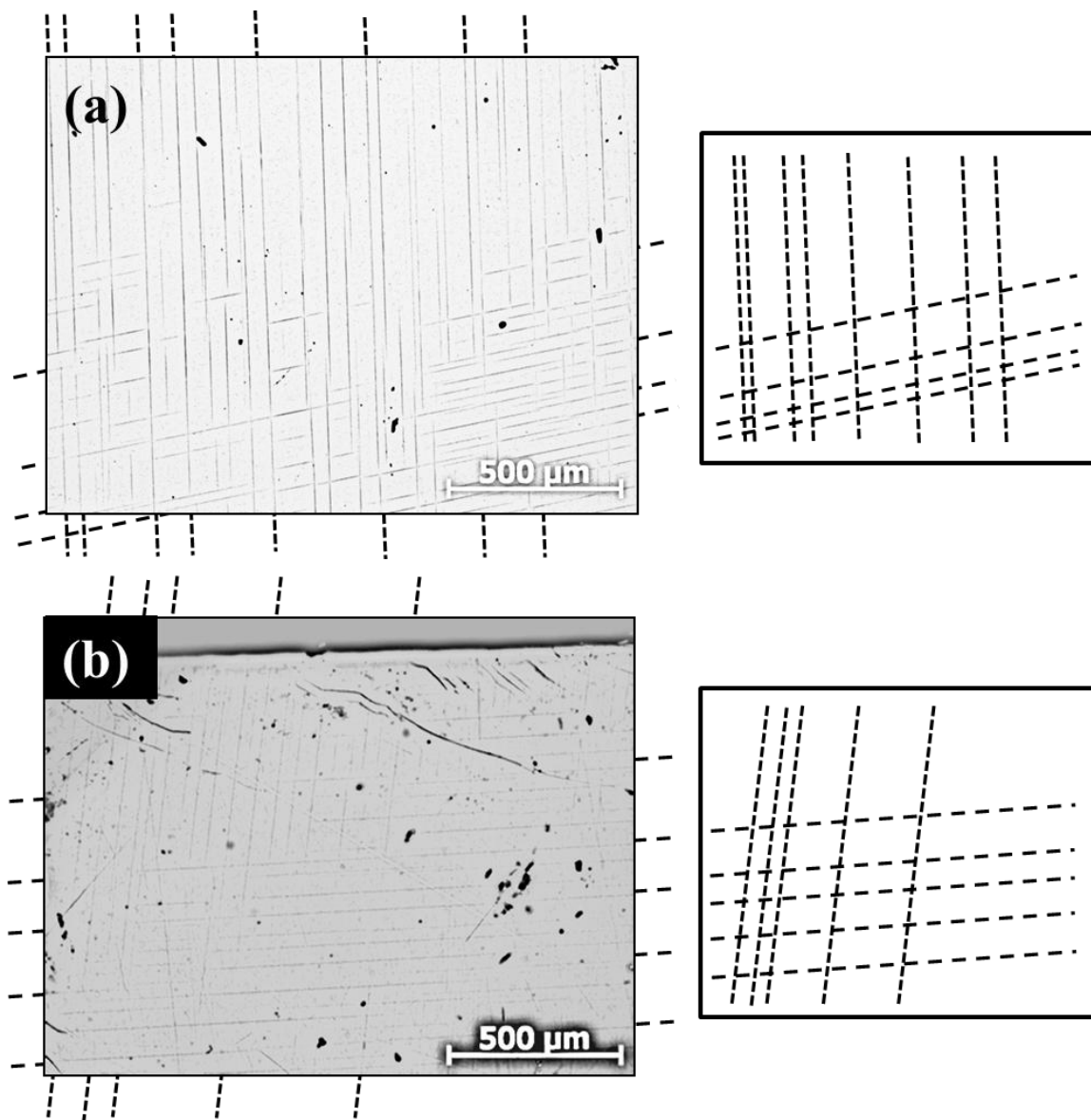


Figure 22

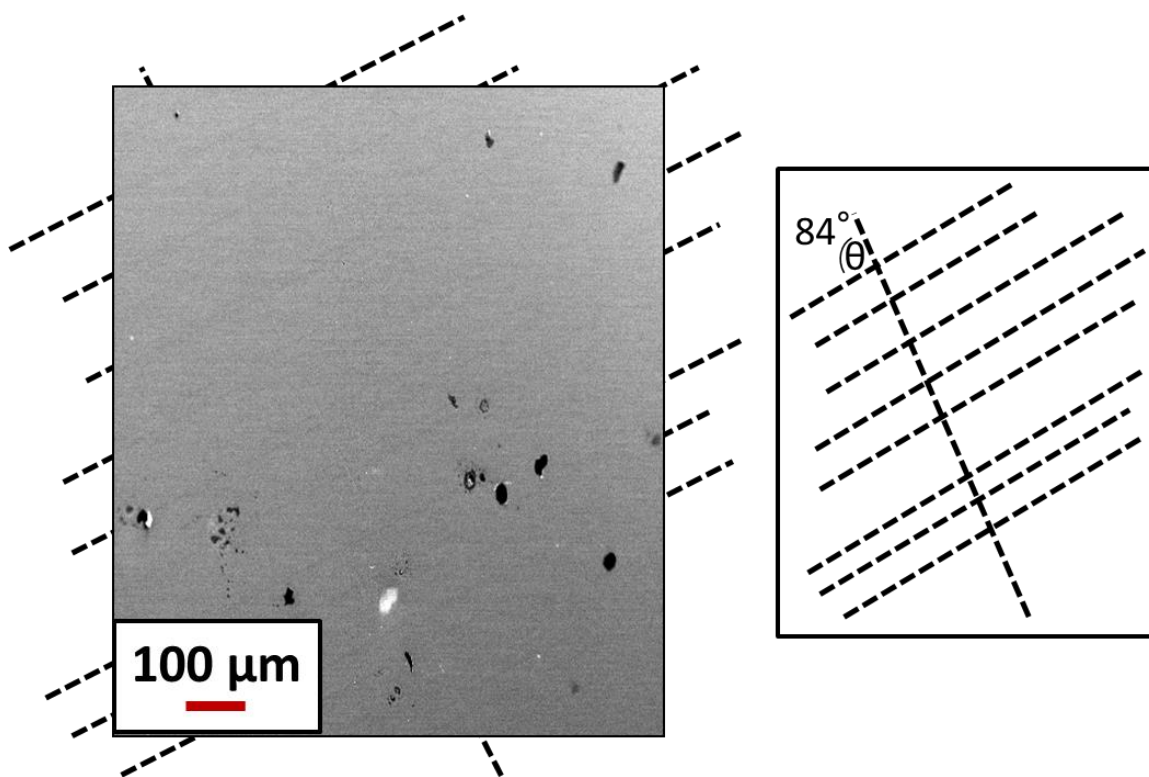


Figure 23

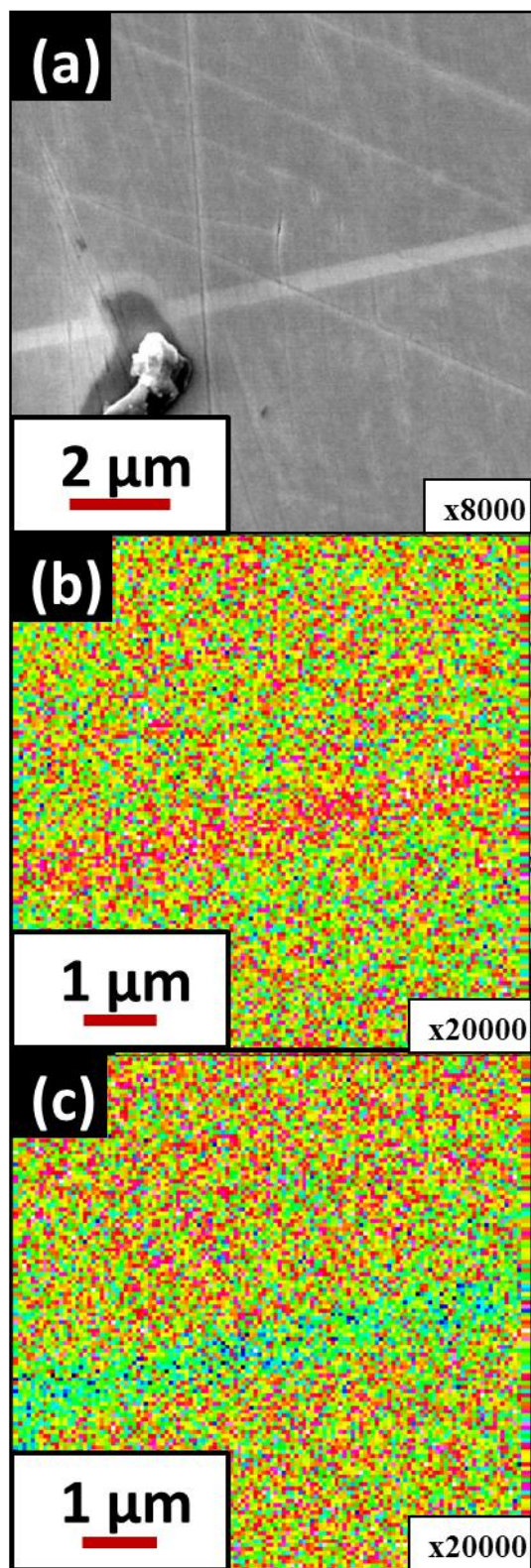
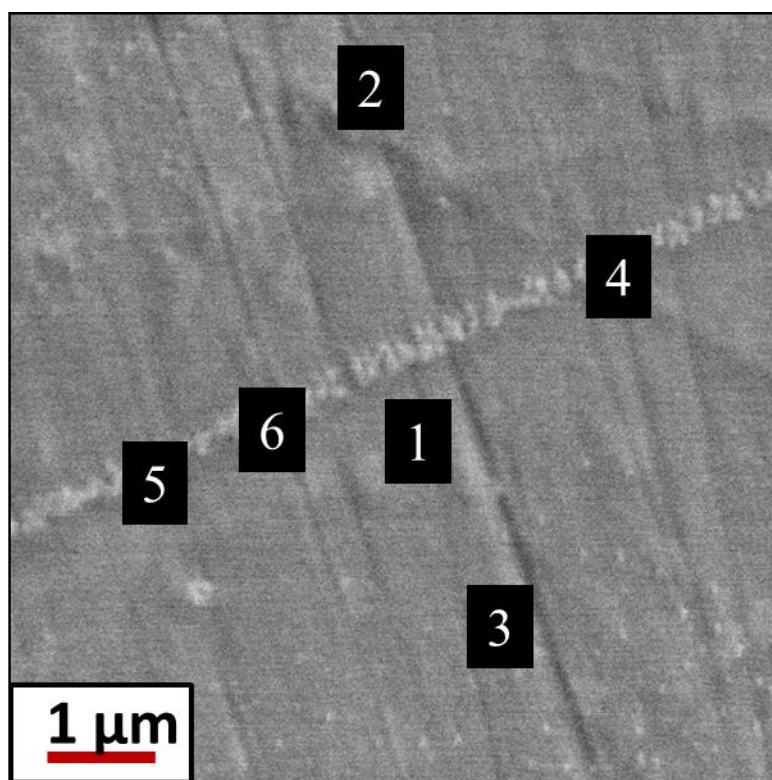


Figure 24



	Gd	Ge
1	53 %	47 %
2	52 %	48 %
3	50 %	50 %
4	64 %	36 %
5	67 %	33 %
6	66 %	34 %
Gd_5Ge_4	55 %	45 %
Gd_5Ge_3	63 %	37 %

Figure 25

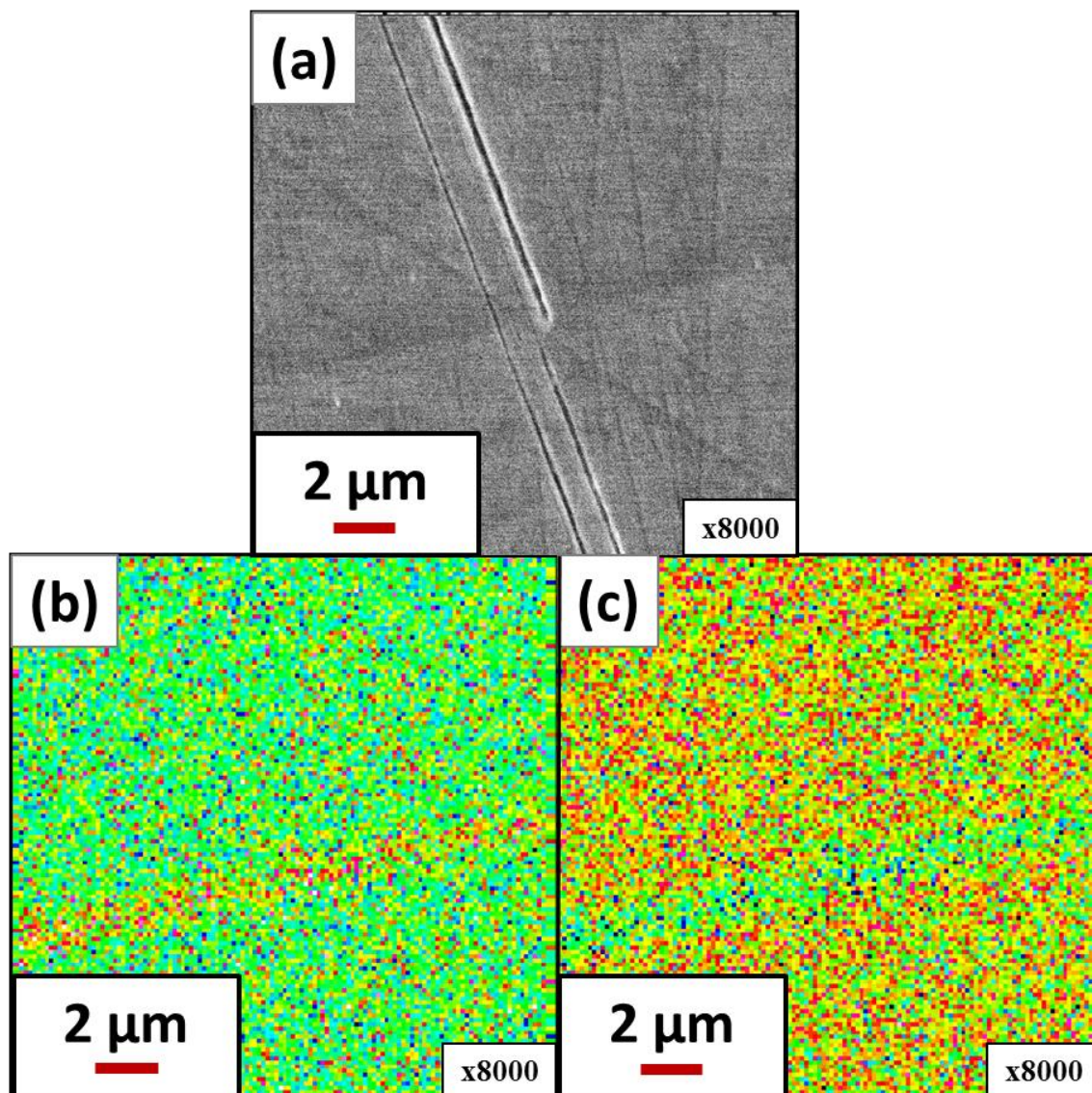


Figure 26

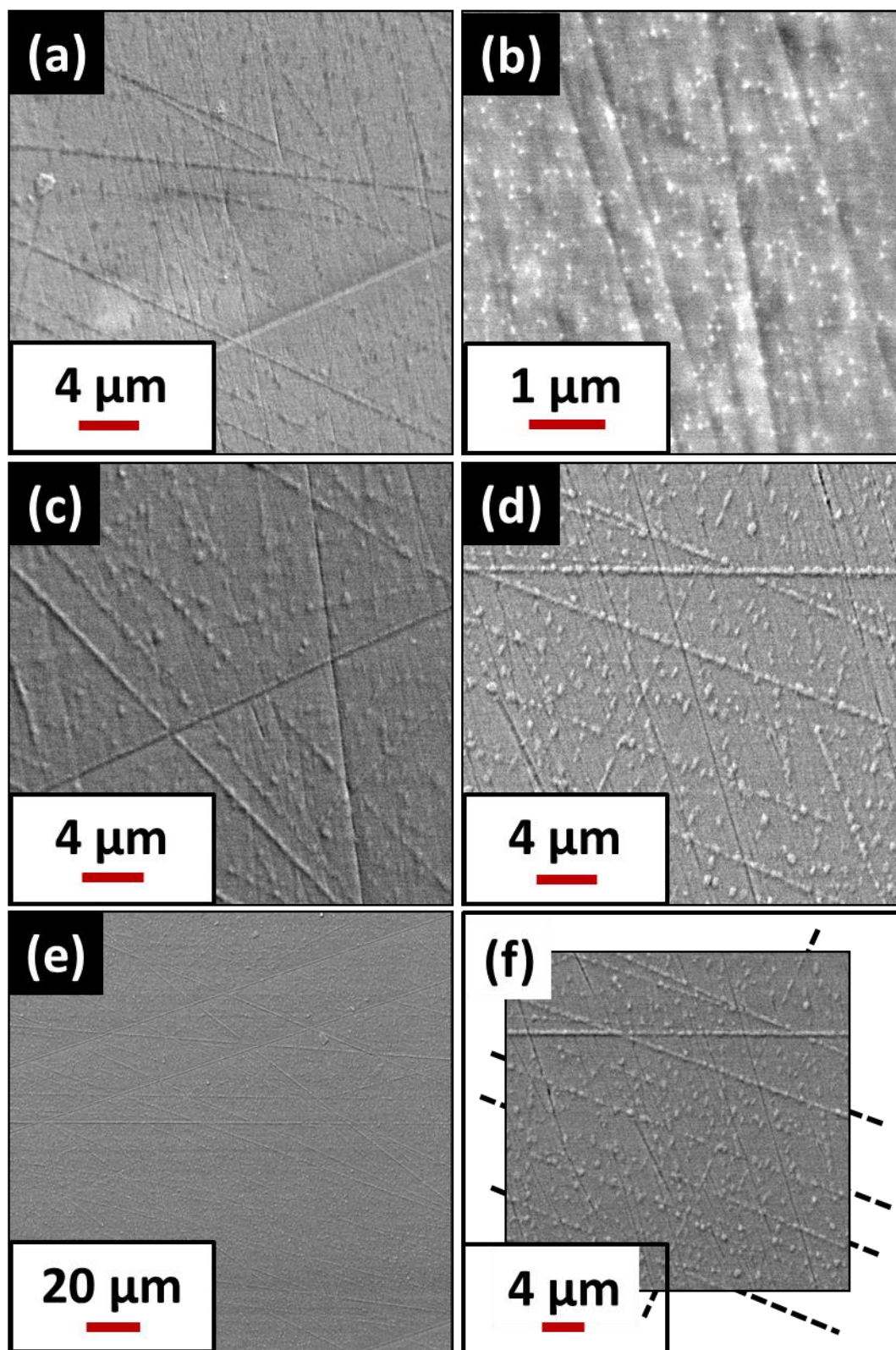
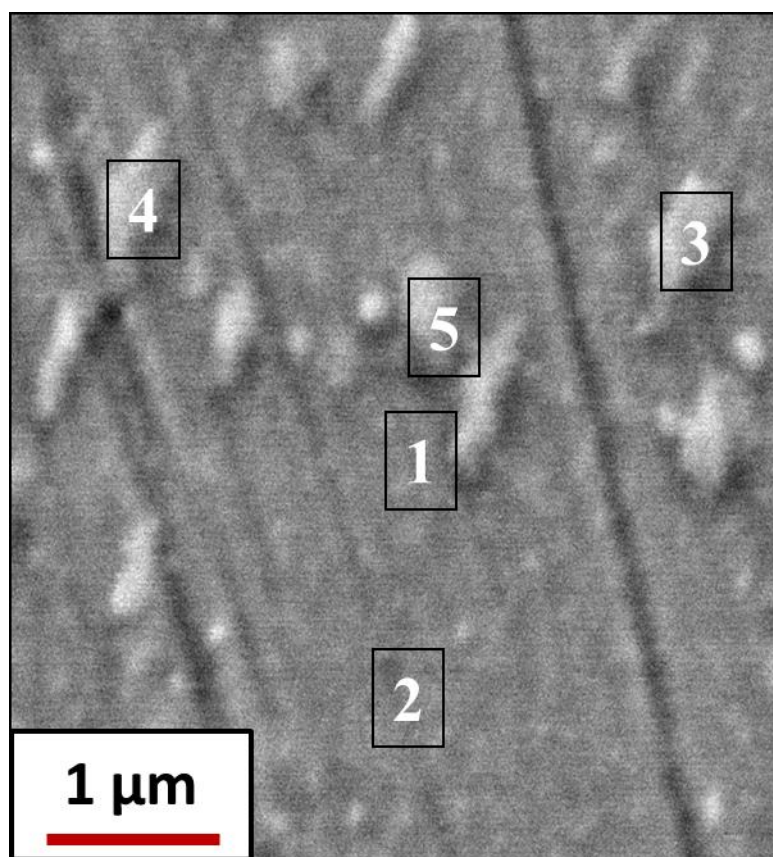
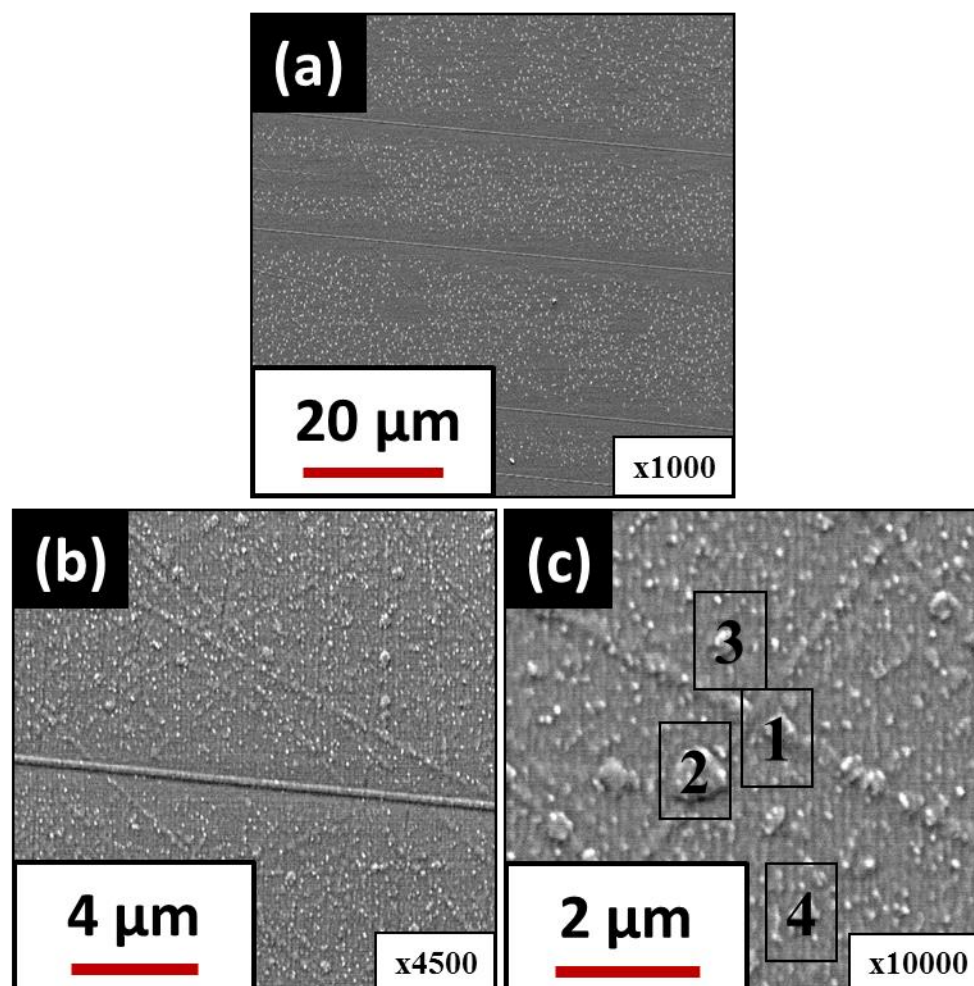


Figure 27



	Gd	Ge
1	53 %	47 %
2	53 %	47 %
3	46 %	54 %
4	46 %	54 %
5	49 %	51 %

Figure 28



	Gd	Ge
1	41 %	59 %
2	34 %	66 %
3	45 %	55 %
4	36 %	54 %

Figure 29

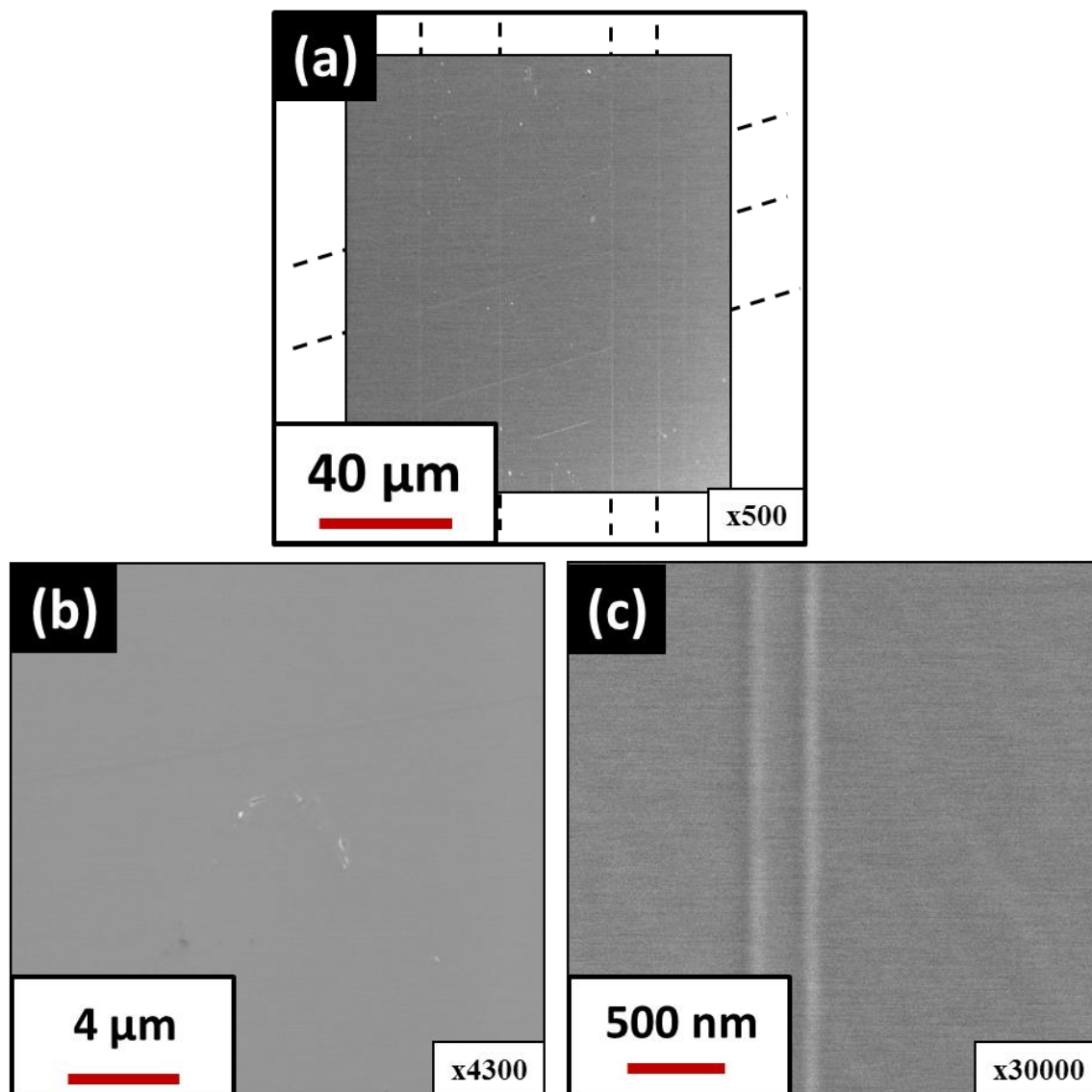


Figure 30

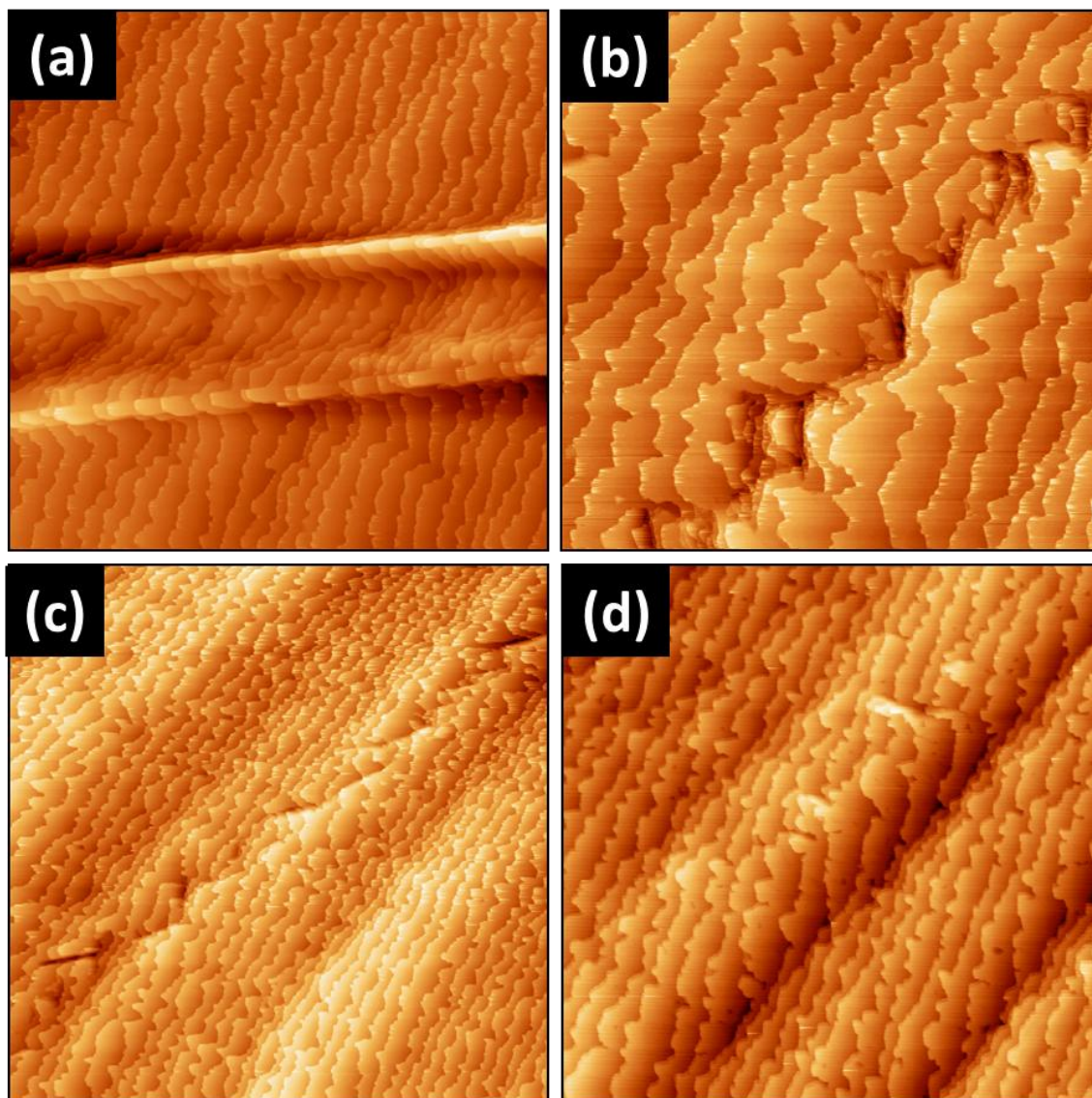


Figure 31

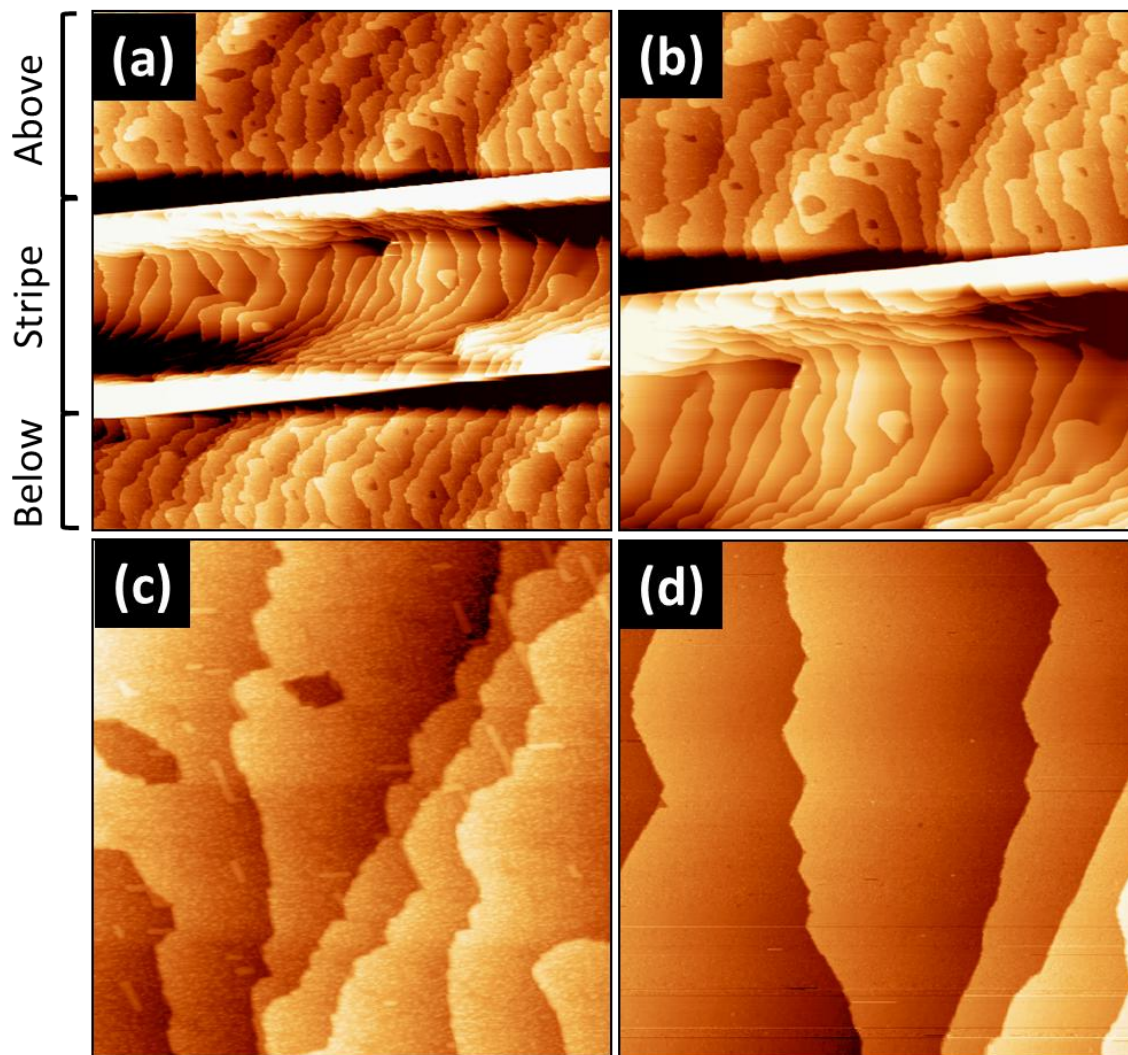


Figure 32

Appendix

Vapor Pressure of Elemental Gd and Ge

Vapor pressures of elemental Gd and Ge are shown in Fig. A1 and A2, from five different sources [1-5].

Vapor pressures of the elements are relevant to the study of Gd_5Ge_4 for at least two reasons. First, surface energy often scales with the heat of vaporization, and in turn, the heat of vaporization is proportional to the logarithm of the vapor pressure. Hence, determining relative vapor pressures may give an indication of the relative surface energies of Gd and Ge. In turn, this could provide an indication of whether one would expect a pure Gd termination to be more favorable than a mixed Gd-Ge termination. Second, the vapor pressures of the elements may help to predict which element is most likely to evaporate selectively from Gd_5Ge_4 at high temperature. Of course, both of these exercises assume that it is valid to extrapolate from the elements to the intermetallic, which may not be valid. Specifically, chemical potentials of Gd and Ge may be much different in Gd_5Ge_4 than in elemental Gd or Ge. However, if the differences between the elements are very large, one might expect the trends to appear also in the intermetallic.

We found five different sources of vapor pressure data that included both Gd and Ge. Of these, two indicated that the vapor pressure of Ge is higher than that of Gd, and the others showed the opposite trend. We concluded that the vapor pressures of Gd and Ge are probably close.

Bumps on B-Terraces

The bumps on the B-terraces are positioned randomly. This conclusion was based on the work illustrated in Fig. A3 and A4. There, images A3a and A4a show large regions of B-terraces with bumps. Images A3b and A4b show the same regions after filtering to isolate the bumps. Images A3c and A4c show the fast Fourier Transforms of the filtered images. Images A3d and A4d show the auto correlation of the filtered images. The lack of distinct spots indicates that the bumps are not arranged periodically.

References

- [1] D. Stull (Ed.) American Institute of Physics Handbook, McGraw Hill, New York, 1972.
- [2] K.J. Lesker, Deposition Techniques: Material names G-L, Kurt J. Lesker Company.
- [3] D.R. Lide (Ed.) CRC Handbook of Chemistry and Physics, CRC Press, Boca Raton, Florida, 2003.
- [4] R.E. Honig, RCA Review 23 (1962) 567.
- [5] L.I. Maissel, R. Glang (Eds.), Handbook of Thin Film Technology, McGraw Hill, Texas, 1970.

Figure Captions

Figure A1

Vapor pressure of elemental Gd and Ge from five different sources. The abbreviations are as follow: (AIP) American Institute of Physics Handbook; (KJL) Kurt J. Lesker; (TFT) Handbook of Thin Film Technology, (CRC) Chemical Rubber Company Handbook of Chemistry and Physics; and (RCA) RCA Review.

Figure A2

Vapor pressure of elemental Gd and Ge from five different sources (zoomed in). The abbreviations are as follow: (AIP) American Institute of Physics Handbook; (KJL) Kurt J. Lesker; (TFT) Handbook of Thin Film Technology, (CRC) Chemical Rubber Company Handbook of Chemistry and Physics; and (RCA) RCA Review.

Figure A3

STM images of the bumps on B-terraces on the Gd_5Ge_4 (010) surface, (a) raw image, (b) filtered image, (c) fast Fourier Transform, and (d) auto correlation after the sample had been annealed to 1150 K. The filter was set to a minimum height of 0.23 nm. The image area and tunneling conditions are 50 nm x 50 nm, $I = 0.5$ nA, $V\text{-tip} = -1$ V. Sample #1, right side.

Figure A4

STM images of the bumps on B-terraces on the Gd_5Ge_4 (010) surface, (a) raw image, (b) filtered image, (c) fast Fourier Transform, and (d) auto correlation after the sample had been annealed to 900 K. The filter was set to a minimum height of 0.23 nm. The image area and tunneling conditions are 50 nm x 50 nm, $I = 0.5$ nA, $V\text{-tip} = +1$ V. Sample #2, left side.

Table 1

Vapor pressure of elemental Gd and Ge from five different sources. The abbreviations are as follow: (AIP) American Institute of Physics Handbook; (KJL) Kurt J. Lesker; (TFT) Handbook of Thin Film Technology, (CRC) Chemical Rubber Company Handbook of Chemistry and Physics; and (RCA) RCA Review.

P (Torr)	Gd (AIP)	Ge (AIP)	P (Torr)	Gd (TFT)	Ge (TFT)	P(Torr)	Gd (CRC.c)	Ge (CRC.b)	P (Torr)	Gd (RCA)
7.60E-08	987	851	1.00E-10	607	667	7.50E-03	1563	1371	1.00E-10	627
7.60E-07	1070	926	1.00E-09	657	707	7.50E-02	1755	1541	6.00E-09	700
7.60E-06	1165	1013	1.00E-08	707	757	7.50E-01	1994	1750	1.00E-08	727
7.60E-05	1270	1114	1.00E-07	762	812	1.50E+00			4.50E-07	800
7.60E-04	1406	1232	1.00E-06	827	877	7.50E+00	2300	2014	1.00E-05	900
7.60E-03	1564	1372	1.00E-05	897	947	1.50E+01			1.00E-02	1227
7.60E-02	1757	1542	1.00E-04	977	1037	3.75E+01			P (Torr)	Ge (RCA)
7.60E-01	1996	1751	1.00E-03	1077	1137	7.50E+01	2703	2360	1.00E-10	705
7.60E+00	2302	2016	1.00E-02	1192	1257	1.50E+02			5.00E-10	700
7.60E+01	2706	2362	1.00E-01	1327	1397	3.75E+02			2.00E-09	727
7.60E+02	3266	2834	1.00E+00	1487	1557	7.50E+02	3262	2831	6.00E-08	800
P (Torr)	Gd (KJL)	Ge (KJL)	1.00E+01	1682	1777	7.60E+02			1.00E-06	900
1.00E-07	760	812	1.00E+02	1947	2047				2.00E-05	1000
1.00E-05	900	957	1.00E+03	2307	2407				6.00E-03	1227
1.00E-03	1175	1167	1.00E+04	2827	2907					

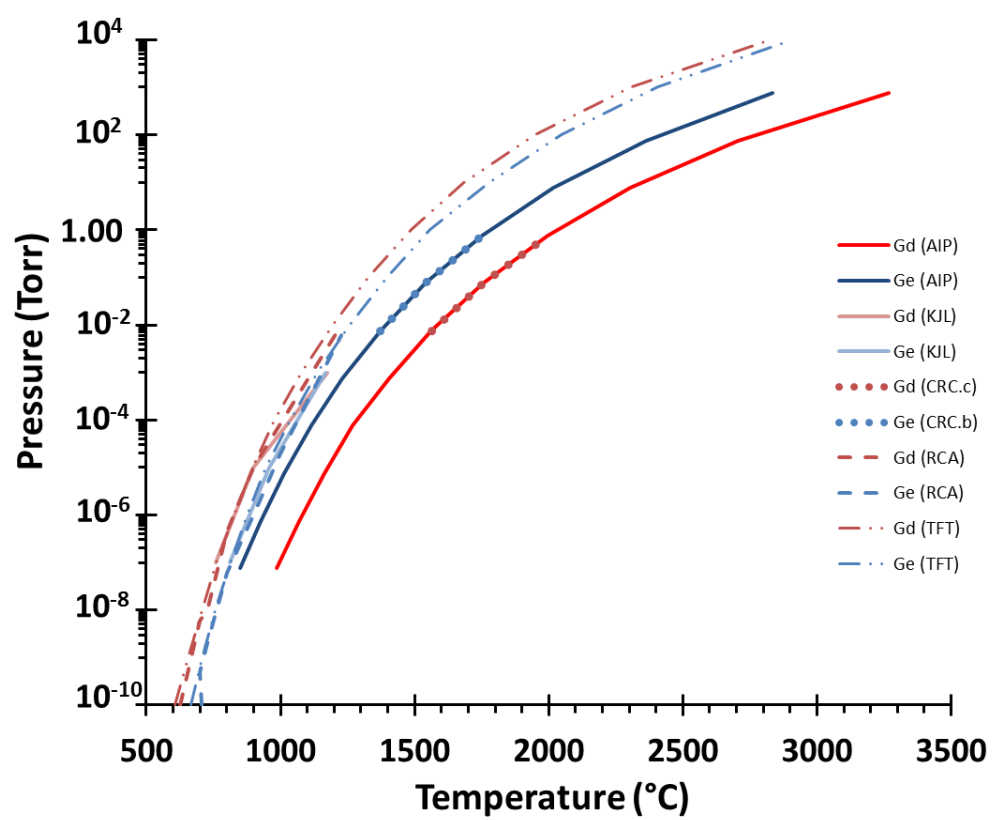


Figure A1

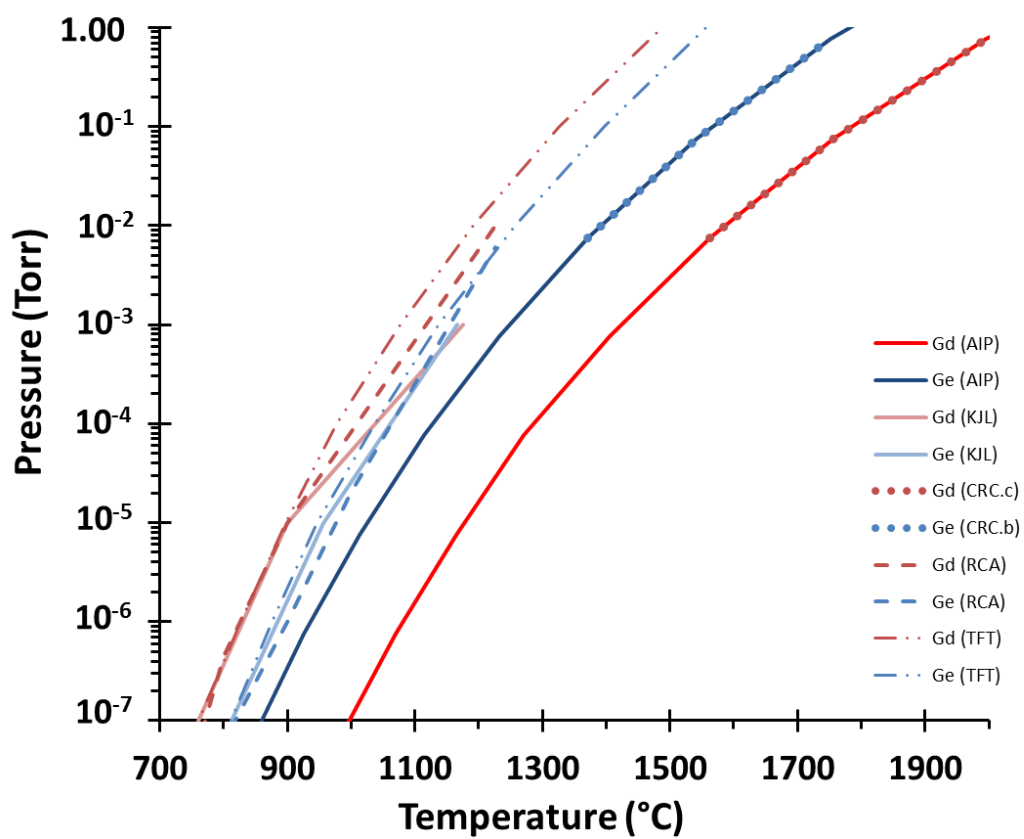


Figure A2

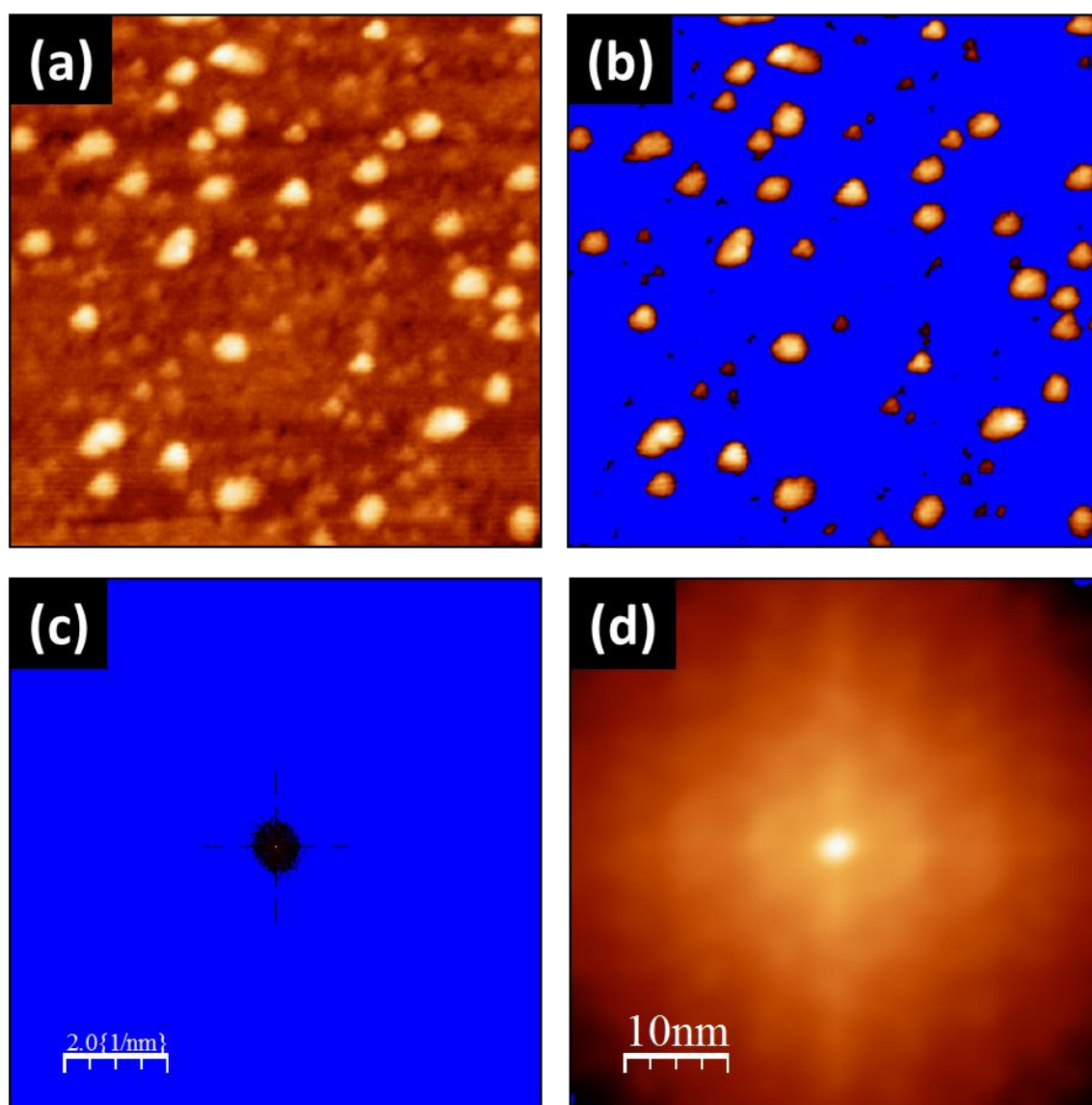


Figure A3

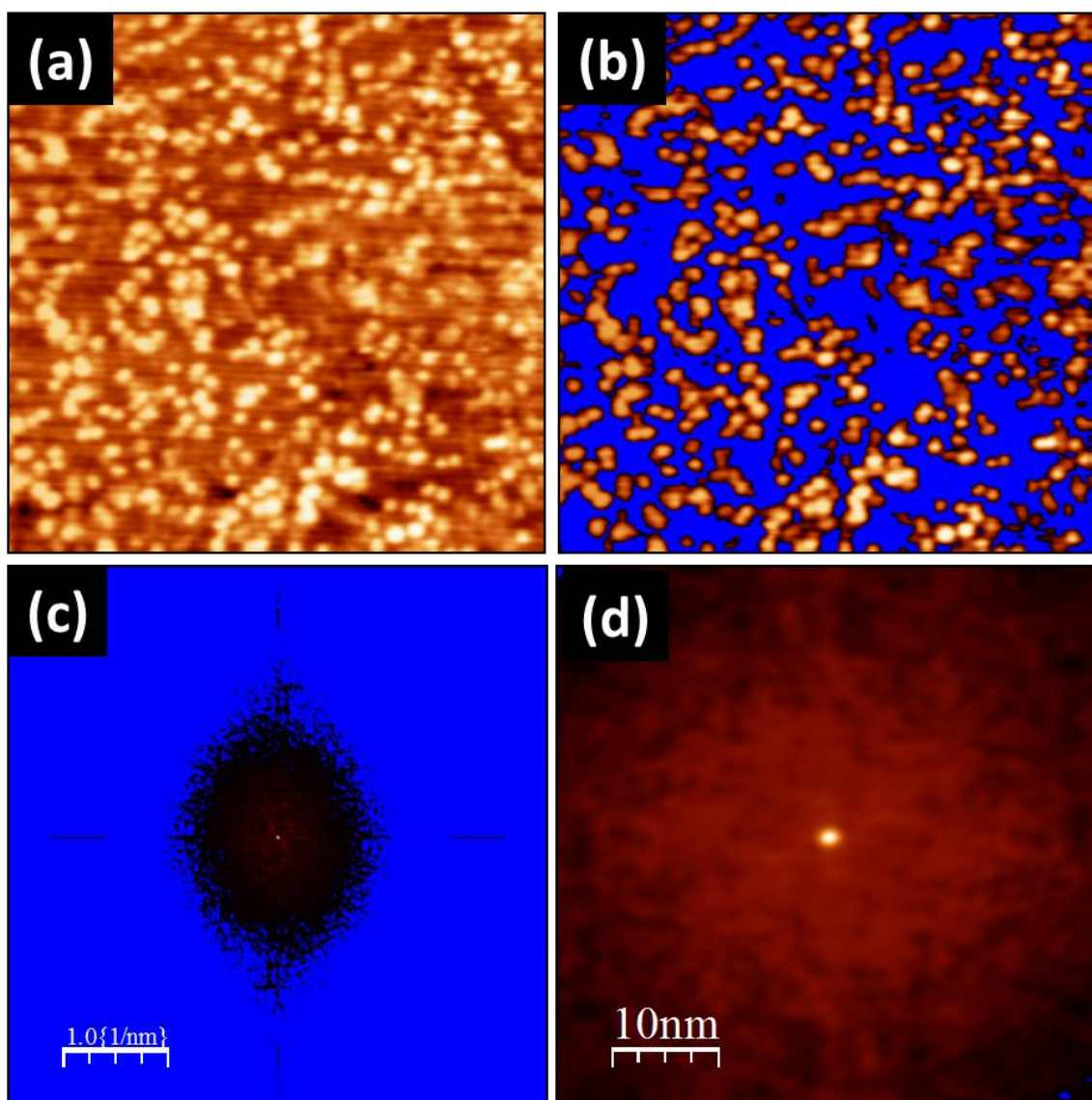


Figure A4

CHAPTER 4

Preferential Surface Oxidation of Gd in Gd_5Ge_4 *

Chad D. Yuen,^{a,b} Gordon J. Miller,^{a,b} and Patricia A. Thiel^{a,b,c}

^aAmes Laboratory, Iowa State University, Ames, Iowa, 50011

^bDepartment of Chemistry, Iowa State University, Ames, Iowa 50011

^cDepartment of Material Science and Engineering, Iowa State University, Ames, Iowa 50011

*Parts of this chapter was published in “Applied Surface Science, 2012”

Abstract

Gd oxidizes preferentially at the (010) surface of Gd_5Ge_4 . This is consistent with thermodynamic data for the bulk oxides. Upon oxidation in vacuum, the gadolinium oxide displaces or covers the Ge. Oxidation is more extensive at 600 K than at 300 K, because more oxygen is incorporated into the surface and the shift of the Gd binding energy is larger.

1. Introduction

The Gd_5Si_4 and Gd_5Ge_4 binary systems [1], plus the pseudobinary $Gd_5(Si_xGe_{1-x})_4$ [2], were discovered in the 1960s by Smith et al. and Holtzberg et al., respectively. These systems are of interest because of their magnetic and thermomagnetic properties [3-5]. Giant magnetocaloric effects were discovered in these systems in 1997 by

Pecharsky and Gschneidner [6]. This and other properties such as giant magnetoresistance [7], spontaneous generation of voltage [8], metastability [9], and phase separation [10] may lead to new refrigeration and other energy conversion technologies.

Previous work has suggested that small amounts of interstitial oxygen can affect the coupled structural and magnetic phase transition in $\text{Gd}_5\text{Si}_2\text{Ge}_2$ [11]. Presumably, oxygen locks in the relative positions of loosely-coupled, slab-like structural units in this type of compound. It has been postulated that oxygen has this effect because it occupies interstitial sites between the slabs. If this is correct, then oxygen would affect magnetic transition temperature, and would reduce the magnetocaloric effect by eliminating the structural transition that often increases the total entropy change during the coupled magnetostructural transitions. Hence, it is important to understand the effect of oxygen in these systems.

Our primary focus here is on surface oxidation of the Gd_5Ge_4 phase. We choose the (010) surface because it is the closest-packed, meaning that it is likely to be the most stable surface. We will show that Gd oxidizes preferentially at this surface and that the oxide covers or displaces Ge.

2. Materials and methods

We used a single crystal of Gd_5Ge_4 , synthesized at the Materials Preparation Center of the Ames Laboratory [12], and cut to expose the (010) surface. X-ray photoelectron spectroscopy (XPS) experiments were performed with an Omicron X-ray source (Al K α), and an Omicron EA 125 hemispherical electron energy analyzer. The

XPS source was perpendicular to the sample plate, and the take-off angle (the angle between the entrance axis of the analyzer and the sample surface plane) was 45° . The angular acceptance range was $\pm 8^\circ$. The aperture used in the EA 125 analyzer was 6 mm x 12 mm. The Gd $3d_{5/2}$ peak, with a binding energy of 1186 eV, was chosen for analysis because it was most intense. The Ge $2p_{1/2}$ peak, at 1248 eV, was chosen because it was the most intense peak that did not overlap with a Gd peak. (The Ge $2p_{3/2}$, which is more commonly used for surface analysis, overlapped with the Gd $3d_{3/2}$ peak.) XP spectra were analyzed with CasaXPS software [13]. The accuracy in determining binding energies, both for Gd and Ge was ± 0.2 eV.

3. Results

After the Gd_5Ge_4 sample was initially placed in UHV, its composition was checked with XPS. This revealed carbon and oxygen contaminants. It was then sputtered at 300 K for several minutes. This process was repeated several times until there was no carbon detectable by XPS, and a small, invariant O 1s peak remained. (The source of the oxygen will be discussed below.) Figure 1a shows the evolution of the Gd $3d_{5/2}$ peak, and Fig. 1b shows that of the Ge $2p_{1/2}$ peak, while the air-exposed sample was sputtered. The curves at the top are the contaminated surface, and those at the bottom are the clean surface. First, we consider intensities. The intensity of the Gd peak decreases, and that of the Ge peak increases, as material is removed. Next, we consider the peak positions (binding energies). The vertical dotted lines in Fig. 1 represent the initial (top) and final (bottom) positions of the Gd and Ge peaks. Initially, the Gd and Ge peaks are at binding

energies of 1187.3 eV and 1247.5 eV. After 118 minutes of Ar⁺ sputtering, they shift down to 1186.1 eV and 1247.1 eV, a change of -1.2 eV and -0.4 eV, respectively. The downward shift in binding energies can be explained by a transition from a more highly oxidized to a less oxidized surface. Key binding energies are summarized in Table 1.

In a separate set of experiments, the surface was annealed at 900 K to restore the surface atomic structure after ion bombardment. This did not change the intensity of the small residual oxygen peak at 531.1 ± 0.4 eV, which was present also after ion bombardment without annealing. It is apparent in the top curve of Fig. 2a. Its intensity corresponds to a concentration of 1.4 ± 0.7 at %. The constant presence and level of this residual oxygen, independent of sample treatment, suggests that a low level of oxygen is a bulk constituent.

After annealing, the sample was exposed to oxygen by backfilling the UHV chamber with O₂ at a pressure of 10^{-7} Torr for 1000 s. This equals an exposure of 100 Langmuir (L).

The sample was held at two temperatures, 300 K and 600 K, during oxygen exposure. The results for 300 K are shown in Fig. 2, and for 600 K in Fig. 3. In both figures, top curves represent the initial surface, and bottom curves represent the surface after oxygen exposure. Upon exposure to oxygen, the O 1s peak increases strongly and its binding energy shifts downward, to 529.8-530.0 eV, as shown in Fig. 2a and Fig. 3a. This indicates that oxygen adsorbs in both cases, i.e. the adsorption probability is substantial.

4. Discussion

With regard to the Gd and Ge peak intensities, the oxygen adsorption experiments in Fig. 2-3 show the reverse of the trends during cleaning the air-oxidized surface as in Fig. 1. Adsorption of oxygen causes the Gd intensity to increase (slightly), and the Ge intensity to decrease. In fact, the Ge peak almost disappears after exposure to 100 L oxygen. It seems that Ge is displaced from the surface, or perhaps preferentially covered by oxygen, as a result of Gd oxidation.

Second, consider the shift in position of the Gd peak. The peak moves up in binding energy by 0.8 eV at 300 K—from 1186.2 eV to 1187.0 eV. Its binding energy also shifts upward, but by a larger amount (1.3 eV) at 600 K—from 1186.2 eV to 1187.5 eV. An upward shift in binding energy is typical for a metal when it oxidizes. The larger shift in the binding energy at 600 K than at 300 K supports the hypothesis that surface oxidation is enhanced at the higher temperature, correlating with a larger oxygen uptake.

To put the extent of oxidation on a more quantitative basis, we have deconvoluted the Gd $3d_{5/2}$ peak into a peak representative of the clean surface, and a peak representative of the oxidized state of Gd. This is shown in Fig. 4, where Fig. 4a shows the spectrum of the clean surface, Fig. 4b the oxidized surface at 300 K, and Fig. 4c the oxidized surface at 600 K. The position and width of the peak in Fig. 4a are used to fix the low-binding-energy component in the fitted spectra of Fig. 4b and 4c, at 1186.2 eV. The spectra in Fig. 4b and 4c are fit well by addition of a second component at higher binding energy, 1189.1 eV. Its relative intensity is higher after 600 K oxidation than after 300 K oxidation, confirming that oxidation is more extensive at higher temperature.

It is also informative to compare the absolute XPS peak positions with published values. The stable form of gadolinium oxide is Gd_2O_3 [14]. For this oxide, the Gd $3d_{5/2}$ binding energy is in the range 1187.0-1189.5 eV, according to the literature [15]. Our value for oxidized Gd is at 1189.1 eV, based upon peak-fitting. This is compatible. The energy range for clean elemental Gd is 1186.0-1186.9 eV [15; 16]. Based upon peak-fitting, our value is 1186.2 eV, which is also compatible.

For Ge, the stable form of the bulk oxide is GeO_2 [14]. For this oxide, the Ge $2p_{1/2}$ binding energy is in the range 1250.6-1251.0 eV [15; 17]. In the air-exposed sample, we find the Ge $2p_{1/2}$ peak at 1247.5 eV. This lies 3.1 eV outside the range expected for GeO_2 . The measured value of the air-oxidized sample does, however, fall within the range for pure Ge, which is 1247.0-1248.2 eV [15]. After oxidation in vacuum, the Ge $2p_{1/2}$ peak is very small and its position is difficult to determine accurately, but it is still not compatible with GeO_2 . Taken together, these observations indicate that Gd oxidizes but Ge does not.

Preferential oxidation of Gd in Gd_5Ge_4 is consistent with the hierarchy of enthalpies of formation of the bulk oxides of Gd and Ge. At room temperature, they are -1819.6 kJ/mol for Gd_2O_3 , and -551.0 kJ/mol for GeO_2 [14]. Thus, preferential oxidation of Gd is thermodynamically-driven.

A similar effect occurs at surfaces of another rare earth alloy, LaNi_5 [18]. In this case, as here, the rare earth oxidizes preferentially and the other component is effectively displaced from the surface. This phenomenon is driven by the well-known stability of the rare earth oxides.

5. Conclusions

We have found that Gd undergoes preferential oxidation at the (010) surface of Gd_5Ge_4 . This is consistent with thermodynamic data for the bulk oxides. Upon oxidation in vacuum, the gadolinium oxide displaces or covers the Ge. Oxidation in vacuum is more extensive at 600 K than at 300 K, based upon the observation that more oxygen is incorporated into the surface and the shift of the Gd binding energy is larger. A small amount of oxygen (about 1.4 at. %) is a bulk constituent in this sample.

Acknowledgments

This work was supported by the Office of Science, Basic Energy Sciences, Materials Sciences and Engineering Division of the U.S. Department of Energy (USDOE). This manuscript has been authorized by Iowa State University of Science and Technology under Contract No. DE-AC02-07CH11358 with the U.S. Department of Energy. We thank Vitalij Pecharsky for a careful reading and useful suggestions.

References

- [1] G.S. Smith, A.G. Tharp, W. Johnson, *Acta Crystallographica* 22 (1967) 940-943.
- [2] F. Holtzberg, R.J. Gambino, T.R. McGuire, *Journal of Physics and Chemistry of Solids* 28 (1967) 2283-2289.
- [3] D. Paudyal, V.K. Pecharsky, K.A. Gschneidner, B.N. Harmon, *Physical Review B* 75 (2007) 094427.

- [4] D. Paudyal, V.K. Pecharsky, K.A. Gschneidner, *Journal of Physics-Condensed Matter* 20 (2008) 235235.
- [5] J.D. Moore, G.K. Perkins, Y. Bugoslavsky, M.K. Chattopadhyay, S.B. Roy, P. Chaddah, V.K. Pecharsky, K.A. Gschneidner, L.F. Cohen, *Applied Physics Letters* 88 (2006) 072501.
- [6] V.K. Pecharsky, J.K.A. Gschneidner, *Physical Review Letters* 78 (1997) 4494-4497.
- [7] L. Morellon, J. Stankiewicz, B. Garcia-Landa, P.A. Algarabel, M.R. Ibarra, *Applied Physics Letters* 73 (1998) 3462-3464.
- [8] E.M. Levin, V.K. Pecharsky, K.A. Gschneidner, *Physical Review B* 63 (2001) 174110.
- [9] M.K. Chattopadhyay, et al., *Physical Review B* 70 (2004) 214421.
- [10] V.K. Pecharsky, A.P. Holm, K.A. Gschneidner, R. Rink, *Physical Review Letters* 91 (2003) 197204.
- [11] Y. Mozharivskyj, A.O. Pecharsky, V.K. Pecharsky, G.J. Miller, *Journal of the American Chemical Society* 127 (2005) 317-324.
- [12] Samples were synthesized at the Materials Preparation Center, Ames Laboratory USDOE, Ames, IA, USA.
- [13] See www.CasaXPS.com.
- [14] D.D. Wagman, W.H. Evans, V.B. Parker, R.H. Schumm, I. Halow, S.M. Bailey, K.L. Churney, R.L. Nuttall, *The NBS tables of chemical thermodynamic properties: Selected values for inorganic and C1 and C2 organic substances in SI units*, American Chemical Society and American Institute of Physics, Washington D.C., 1982.

- [15] J.F. Moulder, W.F. Stickle, P.E. Sobol, K.D. Bomben, Handbook of X-ray Photoelectron Spectroscopy: a reference book of standard spectra for identification and interpretation of XPS data, Perkin-Elmer Corporation, Physical Electronics Division, Eden Prairie, Minnesota, 1992.
- [16] C.J. Powell, A. Jablonski, NIST Electron Effective-Absorption-Length Database - Version 1.3, National Institute of Standards and Technology, Gaithersburg, Maryland, 2011.
- [17] I. Lucy, J. Beynon, B. Orton, Journal of Materials Science Letters 16 (1997) 1477-1479.
- [18] H.C. Siegmann, L. Schlapbach, C.R. Brundle, Physical Review Letters 40 (1978) 972.

Figure Captions

Figure 1

X-ray photoelectron spectra showing (a) Gd 3d_{5/2} and (b) Ge 2p_{1/2} peaks after exposure to air at 300 K. The top curves represent the air-exposed surface, and bottom curves the clean surface. The dashed lines mark the initial and final peak positions. Curves are displaced vertically to avoid overlap.

Figure 2

X-ray photoelectron spectra showing (a) O 1s, (b) Gd 3d_{5/2}, and (c) Ge 2p_{1/2} peaks after 100 L of O₂ exposure within the UHV chamber at 300 K. Curves are displaced vertically to avoid overlap. The intensity scale is the same for all frames.

Figure 3

X-ray photoelectron spectra showing (a) O 1s, (b) Gd 3d_{5/2}, and (c) Ge 2p_{1/2} peaks after 100 L O₂ within the UHV chamber at 600 K. Curves are displaced vertically to avoid overlap. The intensity scale is the same for all frames.

Figure 4

Deconvoluted X-ray photoelectron spectra of Gd 3d_{5/2} peak showing the surface (a) after cleaning by ion bombardment and then annealing to 900 K, (b) after 100 L O₂ exposure at 300 K, and (c) after 100 L O₂ exposure at 600 K. The vertical intensity scale is the same for all frames.

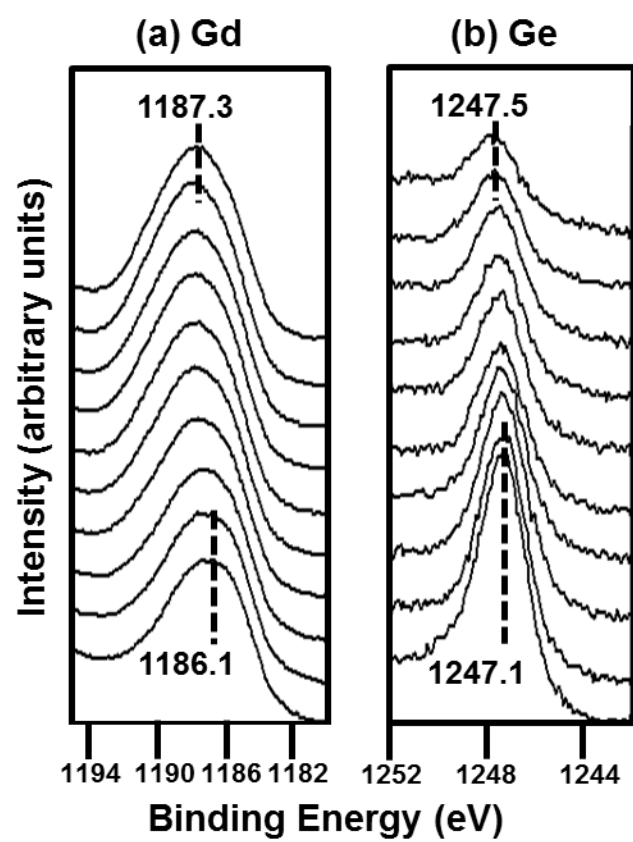


Figure 1

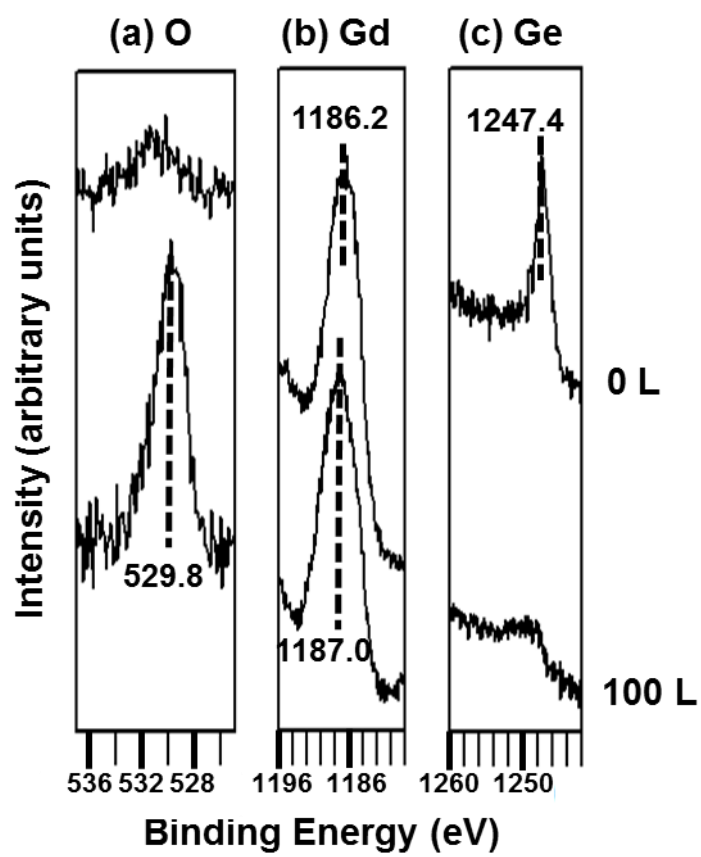


Figure 2

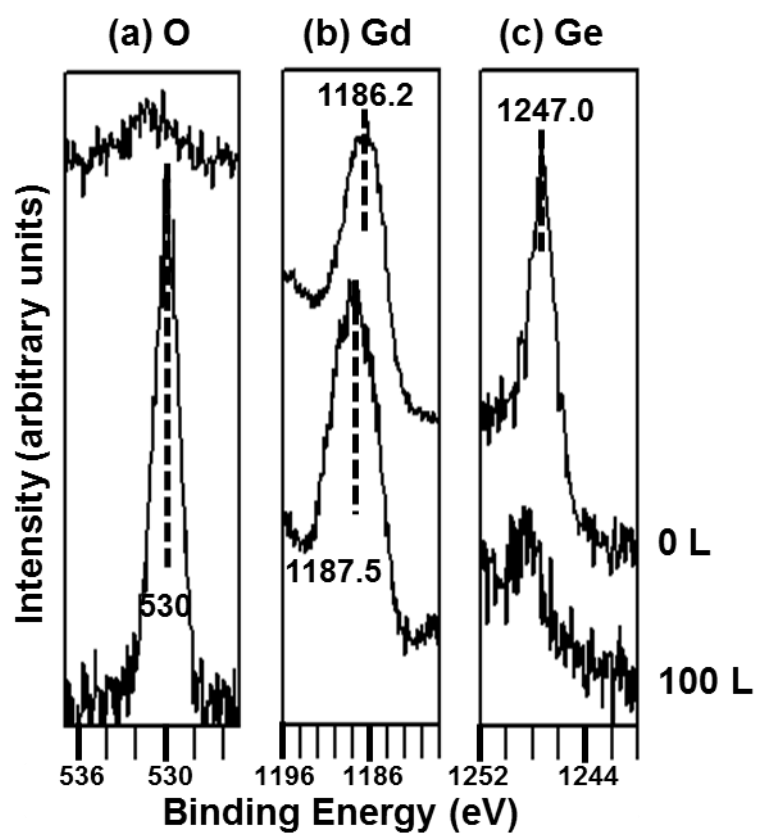


Figure 3

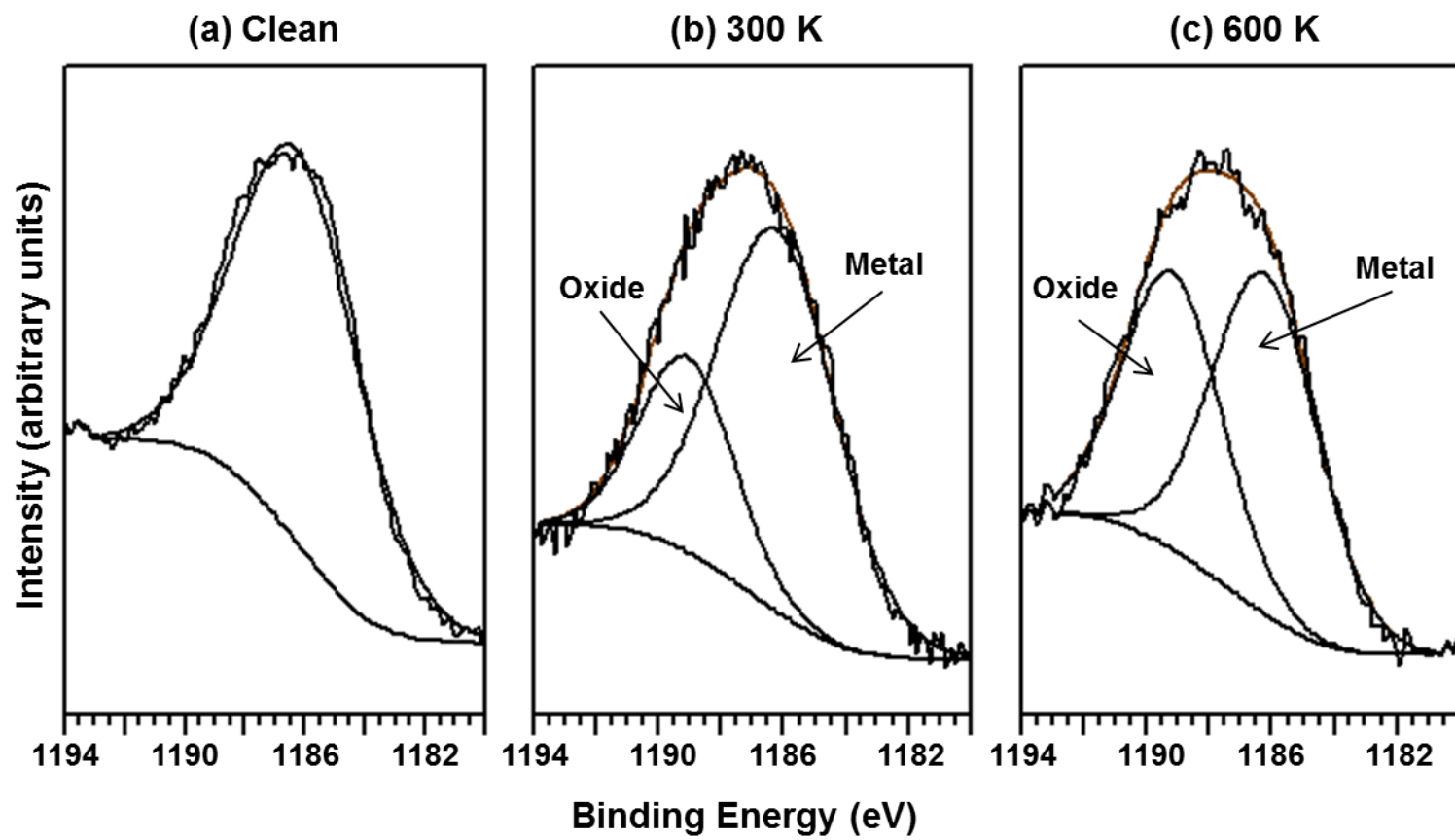


Figure 4

Appendix

Data represented in this chapter thus far, have shown that Gd oxidizes preferentially at the (010) of the Gd_5Ge_4 surface. We begin to represent more data to show that Gd oxidizes. Figure A1, shows the deconvolution of the Gd $3d_{5/2}$ peak of the pure clean metal and the air oxidized Gd.

A sequence of pure oxygen exposures was experimented on the Gd_5Ge_4 (010) surface, starting with 0.5 L, followed by 2 L, 10 L, and 100 L at 300 K. XPS was taken in between each oxygen exposure. XP spectra of Ge $2p_{1/2}$ peak, Gd $3d_{5/2}$ peak, and O 1s peak is shown in Fig. A2a, A2b, and A2c, respectively. We see similar trends such as the Ge peak decreases, almost vanishes after 10 L of oxygen had been exposed onto the surface. This was consistent when the surface was exposed to straight 100 L of oxygen at 300 K and 600 K as shown in Figs. 2 and 3. However, there are some strange results, such that the intensities of the Gd and O peaks, Figs. A2b-c, decrease as more oxygen has been exposed on the Gd_5Ge_4 surface. We would expect an increase in intensities of both peaks as a result of Gd oxidation, similar to Fig. 2-3. This result was due to a broken channeltron in the electron analyzer. Over a period of time, the intensity levels slowly decrease, which leads to error in the results. Thus, Fig. A2 was not used for publication.

With the sequence of pure oxygen exposures on the Gd_5Ge_4 surface, a graph of intensities as a function of oxygen exposure of the Gd $3d_{5/2}$ peak is shown in Fig. A3. In Fig. A3a, shows the trend in intensity levels of the oxide and metal up to 100 L of oxygen whereas Fig A3b, shows the trend up to 2 L of oxygen, a close-up view of Fig. A3a. As oxygen was exposed, the Gd oxide intensity increases while the Gd metal intensity

decreases up to 2 L of oxygen. Afterwards, both the intensity levels of the oxide and the metal decrease, which resulted from the broken channeltron. We would expect to see the oxide intensity increase up until it reaches saturation while the metal intensity decreases.

Figure Captions

Figure A1

Deconvoluted X-ray photoelectron spectra of Gd 3d_{5/2} peak showing the surface after cleaning by ion bombardment and then annealing to 900 K, and after air exposure. The vertical intensity scale is the same for all frames.

Figure A2

X-ray photoelectron spectra showing (a) Ge 2p_{1/2}, (b) Gd 3d_{5/2}, and (c) O 1s peaks after a sequence of O₂ exposure, starting with 0.5 L, followed by 2 L, 10 L, and 100 L within the UHV chamber at 300 K. XPS was taken in between each O₂ exposure. The dashed lines mark the initial and final peak positions. Curves are displaced vertically to avoid overlap.

Figure A3

Graph of intensities as a function of O₂ exposure of the Gd 3d_{5/2} peak. A sequence of O₂ exposure, starting with 0.5 L, followed by 2 L, 10 L, and 100 L within the UHV chamber at 300 K. (a) shows the whole sequence, and (b) shows 2 L of O₂, zoomed in from (a).

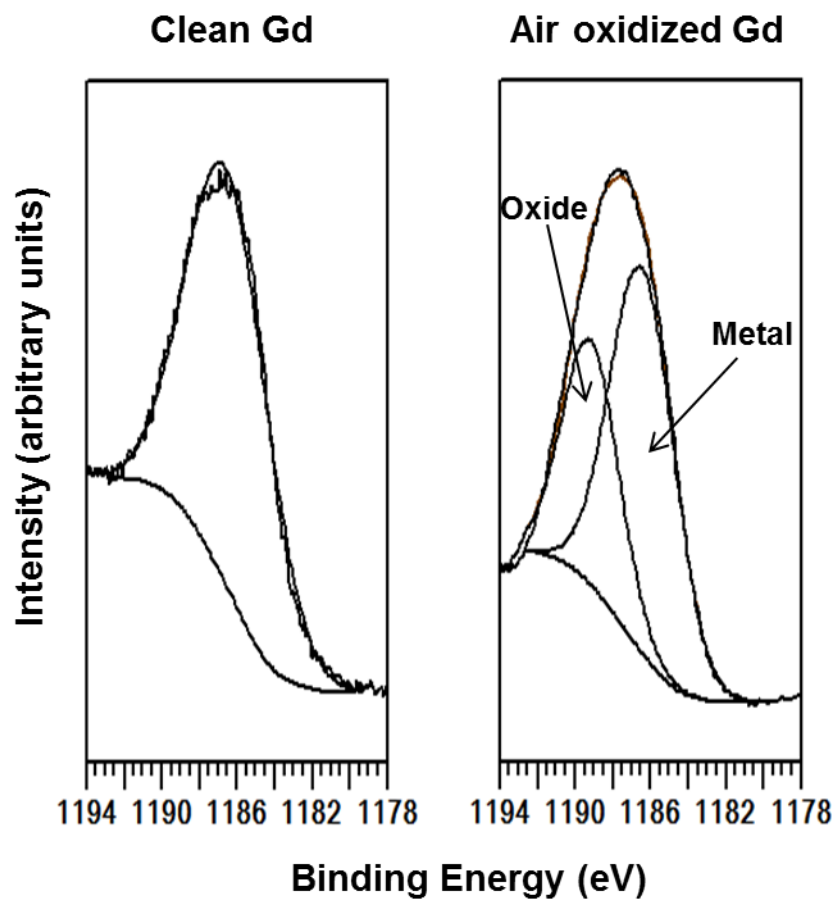


Figure A1

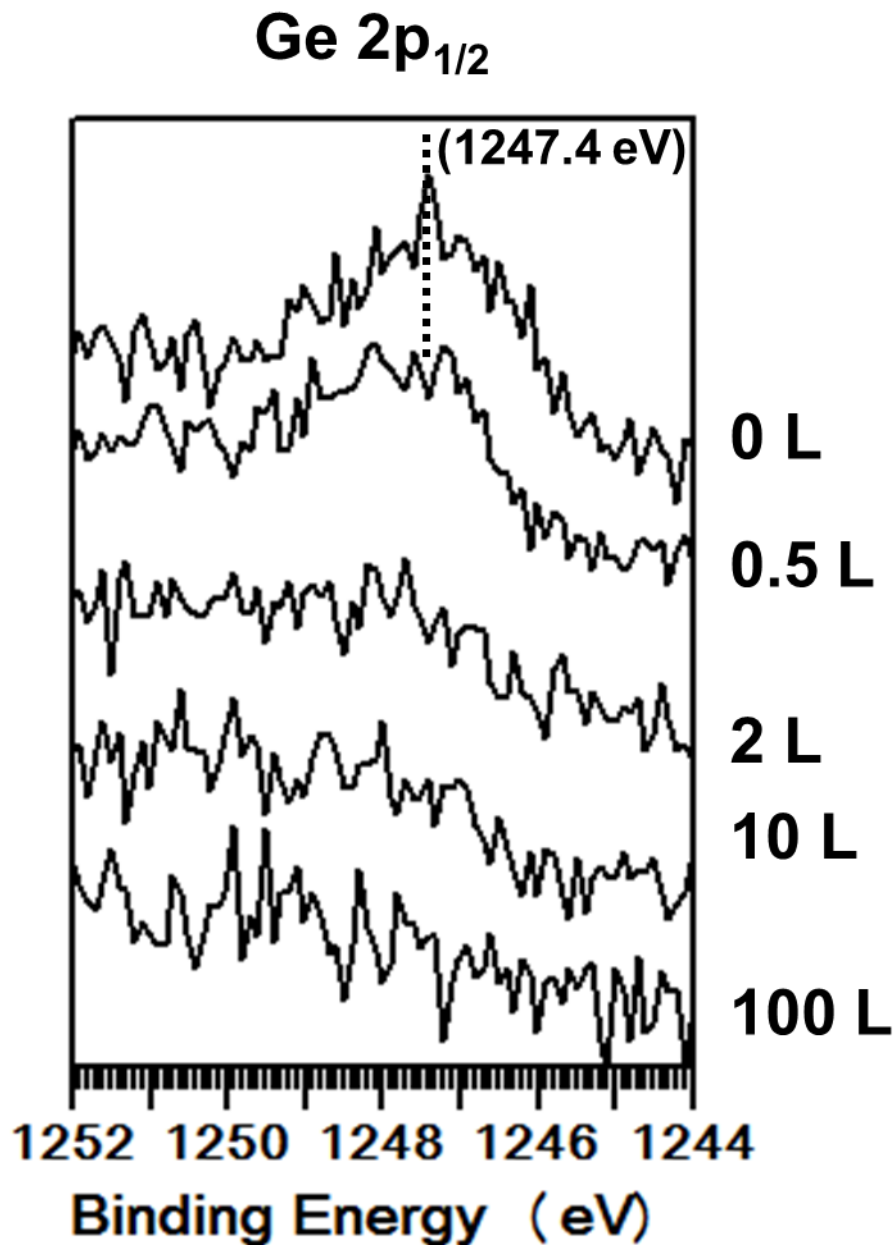


Figure A2a

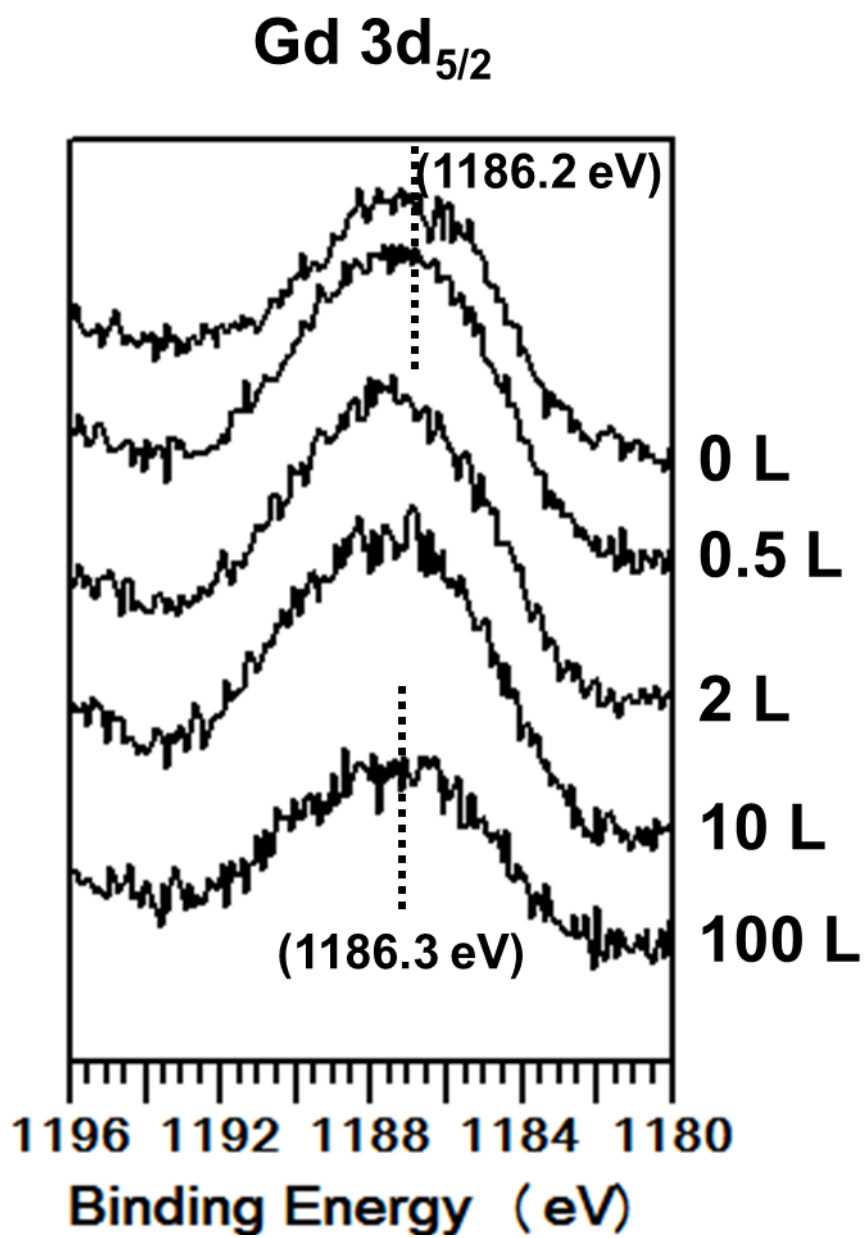


Figure A2b

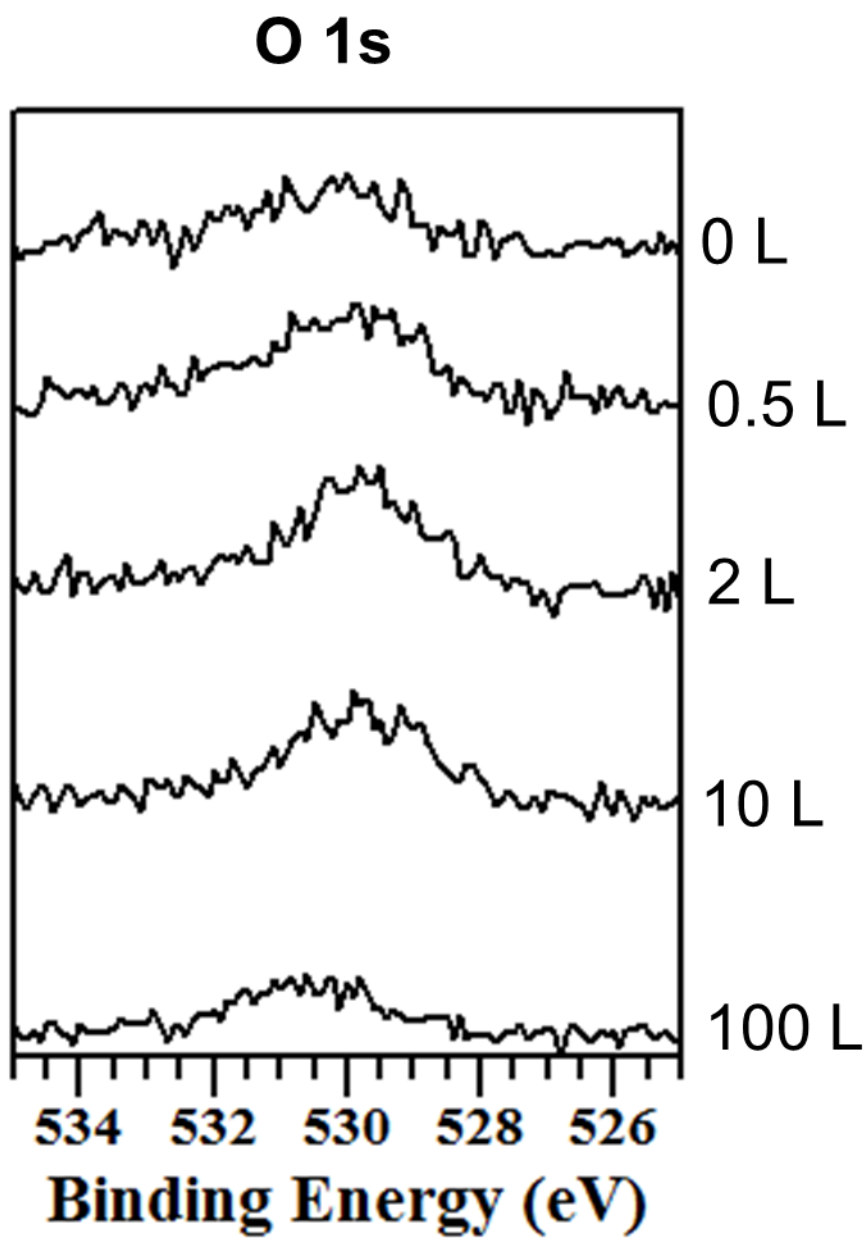


Figure A2c

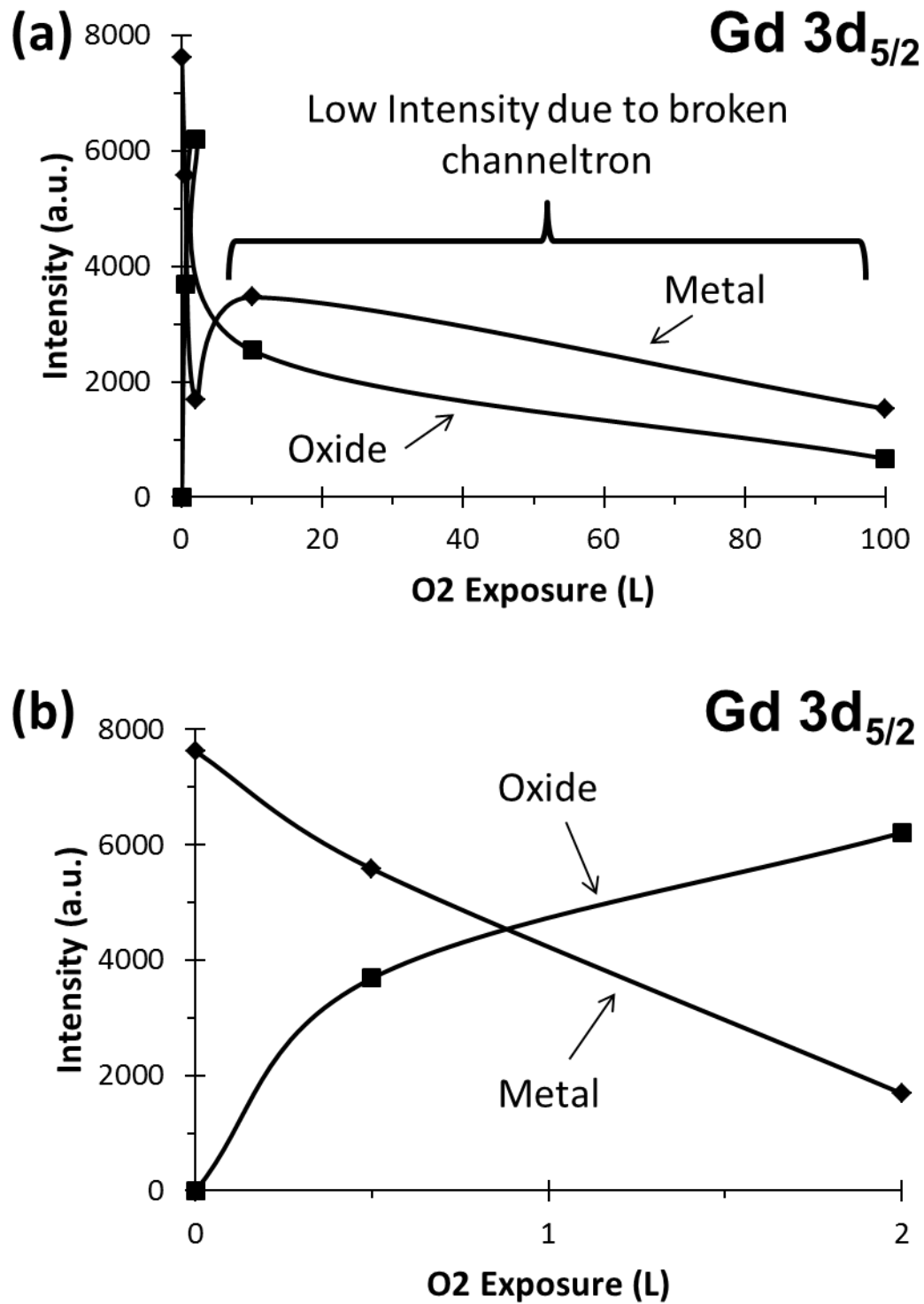


Figure A3

CHAPTER 5

Interaction of Au with the NiAl(110) Surface

Chad D. Yuen,^{1,2} Thomas Duguet,^{1,4} and Patricia A. Thiel^{1,2,3}

¹Ames Laboratory, Iowa State University, Ames, Iowa 50011

²Department of Chemistry, Iowa State University, Ames, Iowa 50011

³Department of Material Science and Engineering, Iowa State University, Ames, Iowa 50011

⁴Present address: CNRS – Centre national de la recherche scientifique, Toulouse area, France

1. Introduction

Surfaces of the binary intermetallic alloy NiAl have been studied extensively, for several reasons. First, NiAl is a prototype within a family of aluminides known as superalloys. These materials find use in the aerospace and power industries because of their low density (relative to steel), strength, creep resistance, and oxidation resistance at high temperatures [1; 2]. Second, NiAl and Ni₃Al serve as excellent substrates for growth of thin, epitaxial aluminum oxide overlayers [3]. In turn, these oxide overlayers can be used as model catalyst supports [3], and as templates for ordered arrays of metal particles [4; 5]. Finally, nickel is often a major component of ternary (or higher) aluminides with useful properties. One example is Al-Ni-Co, which forms the basis for some permanent magnets [6].

NiAl adopts a bcc-like, CsCl structure [7]. Its clean (110) surface, depicted in Fig. 1, has been studied thoroughly, probably because it can be prepared (with relative ease) in a state that is nearly bulk-terminated. The real surface is slightly rippled, with Al atoms displaced outward by 0.02 nm relative to the plane of Ni atoms [8-13]. Defects also are observed on this surface, including a substitutional defect in which a surface Al atom is replaced by Ni [14; 15].

Previously, our group studied the interaction of Ag with this surface [13; 15-18]. We found that Ag grows as islands with a height that corresponds to two atomic layers of fcc(110) Ag. At room temperature, these islands are highly elongated, adopting a needle-like appearance. Our group extensively modeled the growth and evolution of these interesting structures, finding that the two-layer height is stabilized by a quantum size effect, and that the anisotropic shape is a kinetic effect which can be related to the structure of the presumed fcc(110) structure of the epitaxial Ag. Nucleation of the islands is influenced by the NiAl defects, an effect which becomes more pronounced with increasing deposition temperature between 130 and 300 K. Our goal here is to compare the characteristics of Au islands that form on the same NiAl surface. As an interesting aside, it has been reported recently that traces of Au alloyed with NiAl can have a positive effect on the mechanical properties [19].

Like Ag, Au is a noble fcc metal, and its bulk lattice constant nearly equals that of Ag (Au is smaller by only 0.25%). However, one might expect differences between Ag and Au films on NiAl, since many differences exist between the isolated elements. For instance, the Au low-index surfaces reconstruct, whereas those of Ag do not [20; 21]. This difference between Ag and Au has been attributed to relativistic effects in Au, at

least for the (100) surfaces [22]. Another difference, particularly relevant to the present study, is that alloys and intermetallics containing substantial fractions of Au are generally more common than those containing Ag [23].

Previously, our group reported briefly that islands of Au on NiAl(110) are only a single layer high and are less elongated than Ag islands, at 300 K [18]. In this paper, we report a more detailed study of the interaction of Au with the NiAl(110) surface, at temperatures of 200 K to 350 K. We find evidence that Au intermixes with the NiAl substrate at temperatures slightly above 300 K, based both upon x-ray photoelectron spectroscopy (XPS) and scanning tunneling microscopy (STM).

2. Experimental Procedures

A NiAl(110) single crystal was polished using standard metallographic techniques, with the final abrasive being 0.25 μm diamond paste. The sample was then sonicated with acetone and methanol, in sequence. The polished sample was mounted on an Omicron variable-temperature sample plate. The sample was then transferred to an UHV chamber that was equipped with a sputter gun, Omicron X-ray source (Mg K α), Omicron EA 125 hemispherical electron energy analyzer, and an Omicron variable-temperature STM. The base pressure of the chamber was below 1×10^{-10} mbar. The sample was cleaned by repeated cycles of Ar^+ sputtering (30 mins, 2 keV, and $T = 300$ K) followed by annealing to 1150 K for a variety of annealing times from 1.5 hours to 3 hours, until the surface was judged clean by XPS, which detected no contaminants such as oxygen and carbon.

STM images of the clean surface of NiAl(110), as shown in Fig 2(a), revealed that this sample preparation procedure could yield terraces at least 200 nm wide. Steps were pinned by impurities that were undetected with XPS.

STM images were processed using WSxM scanning probe microscopy software [24]. A tungsten tip that was electrochemically etched was used to scan the images with a bias range from -1.5 V to +1.5 V (increments of 0.5 V). The tunneling current was set at 0.1 nA and 0.5 nA. A single STM image took 2 minutes to acquire.

XPS data were analyzed using CasaXPS software [25]. The XPS source was perpendicular to the sample holder, and the take-off angle (defined as the angle between the entrance axis of the analyzer and the sample surface) was 45°. Spectra were acquired in two ways: an overview or survey energy range from 1000 eV to -5 eV; and over smaller energy ranges. The smaller energy ranges showed the Ni 2p_{3/2} binding energy from 880 eV to 830 eV, the Al 2s binding energy from 130 eV to 100 eV, the Au 4f binding energy from 100 eV to 75 eV, and the Ni 3p and Al 2p binding energies from 80 eV to 60 eV. The following settings in our XPS were used: analysis size was less than 1.5 mm in diameter, angular acceptance angle was ± 8°, and the aperture size in the EA 125 analyzer was 6 mm x 12 mm.

Au was deposited on NiAl(110) from a Mantis Quad-EV-C mini e-beam evaporator. The base pressure during Au deposition was below 3×10^{-10} mbar. Au coverage (expressed in units of monolayers, ML) was determined by measuring the fractional surface area of the Au islands, i.e. by flooding the STM image. (If multilayer islands were present, flooding was done in multiple steps and areas were added to obtain total coverage.) From this, the flux was calibrated by taking the ratio of the coverage to

the Au deposition time at 300 K. This gave a flux of $0.034 \text{ ML min}^{-1}$. The filament settings were 1.6 A and 22 W.

Coverage vs. deposition time at 300 K is shown in Fig 3. For each data point, the error bar represents the standard deviation of all the images acquired in that experiment. The linearity of the data indicates that the flux was constant over deposition times of a few minutes up to a few tens of minutes. Further, the data shown in Fig. 3 were acquired over a period of 3 weeks and 2 different experimental runs, indicating that the Au flux was constant in different experiments.

In some cases, the sample was heated slightly above room temperature. In one case, XPS data were acquired, and in the other case, STM data were acquired. The detailed thermal treatment in each case was as follows. For XPS, the sample was first heated to 325 K and held at that temperature for 30 minutes. XP spectra were then measured while the sample was held at 325 K, and the measurement itself lasted 48 minutes. The sample was next heated to 350 K, and held at that temperature for 30 minutes. XP spectra were then measured with the sample held at 350 K, and the measurement again lasted 48 minutes. For STM, the sample was slowly heated from 300 K to 325 K over a period of 1 hour and 25 minutes. After it reached temperature, STM was performed for a period of 1 hour 6 minutes at 325 K. Next, the sample was slowly heated from 325 K to 350 K over a period of 53 minutes, and then STM was performed for a period of 2 hours at 350 K.

3. Experimental Results and Discussion

3.1 Growth at 200 K and 300 K

An STM image following Au deposition at room temperature is shown in Fig 2(b), and it can be compared with the clean surface in Fig. 2(a). Two-dimensional islands exist on terraces and also along step edges. The islands on the terraces are irregular and elongated. Islands on the step edges grow outward from the step.

Figure 4 shows how the islands develop as a function of coverage at 300 K. In this experiment, Au is deposited sequentially, i.e. the surface is not cleaned between successive Au depositions. Between 0.1 and 0.5 ML, terrace islands are flat and irregular, and they grow laterally with increasing coverage. At 0.54 ML, a second layer starts to form, even though the first is far from completion (first-layer islands are clearly separated). The second-layer islands seem more compact and rectangular in shape than the first-layer islands. Their shape changes, however, between 0.8 and 1.3 ML. This can be seen by comparing Fig. 4(f) and Fig. 4(g). In that interval, the first layer coalesces and the second-layer islands grow into irregular shapes that resemble the first-layer islands below 0.5 ML.

Island number density is given in Table 1 as a function of coverage through 0.24 ML. Island density is a slowly increasing function of coverage. At 0.24 ML, it reaches 0.0013 nm^{-2} . This is about a factor of 25 higher than the island density of Ag on this same surface,[16] indicating that the nucleation kinetics are significantly different than for Ag. The island size distribution is shown in Fig. 5(a).

The island heights of the first and second layer islands are shown in Table 1. These island heights are determined from pixel height histograms of the STM images. Two examples are shown in Fig. 6, at coverages of 0.24 ML and 0.60 ML. In the histograms, the large peak on the left is the NiAl substrate, and the small peaks on the right are the Au islands. From the histograms, the first-layer height is constant at about 0.25 nm. An exception occurs at the coverage of 0.54 ML, where the first-layer height from the histograms is 0.37 nm. It is not clear whether this single unusual value is real, or an artifact. For comparison, Fig. 7 shows representative island profiles from this experiment. It can be seen that the profiles are consistent with the histograms.

To test for electronic effects in the measured island morphology, a range of tip bias voltages are employed, from -1.5 V to +1.5 V (in increments of 0.5 V). Fig. 8 shows representative STM images at 0.24 ML and 300 K. There are no apparent differences between island morphologies at different voltages. Corresponding values of island heights are shown in Table 2 for deposition at 300 K, and these values also are independent of bias voltage.

At high magnification and at relatively high coverage (large islands), STM shows a fine structure of stripes on the island tops after Au deposition at 300 K. These stripes are illustrated in Fig. 9 and Fig. 10 (0.60 ML), and Fig. 11 (1.3 ML). There are two domains of stripes, rotated by $\sim 113^\circ \pm 5^\circ$ from one another. The spacing between the stripes is 1.23 ± 0.08 nm, based on the line profiles in Fig. 10 and other STM images. Fig. 11 shows that the stripes occur in both the first and second layer islands, but they do not have the same orientation in the second layer as in the first. In the second layer, the stripe

spacing is 1.16 ± 0.06 nm, which is the same as the spacing in the first layer within experimental uncertainty.

A single coverage of Au, 0.25 ML, was also deposited at lower temperature, 200 K. The resultant island heights are about 0.24 nm, effectively identical to the height of 0.25 nm at 300 K. This value is shown in Table 1. In addition, the bias conditions do not affect the island heights on the surface. This is shown by the STM images of Fig 12, acquired at different bias conditions. Resultant island heights are shown in Table 2. The Au islands are elongated, but they seem less irregular in shape than at 300 K. The island density is about an order of magnitude higher, 0.019 nm^{-2} , than at 300 K. The island size distribution is shown in Fig. 5(b); it is somewhat narrower than at 300 K. No stripes are discernible on these islands, but that could be due to the fact that at this temperature the islands are relatively small. At 300 K, the stripes were not visible until the islands were much larger.

3.2 Thermal Treatments above 300 K

XPS data indicate that the surface changes when the sample is heated above room temperature. Figures 13-16 show the Ni $2p_{3/2}$, Al 2s, Au $4f_{7/2, 5/2}$, Ni 3p, and Al 2p peaks after the sample is prepared by deposition of 0.21 ML at 300 K, then heated to 325 K and 350 K. (The exact thermal program is described in Section 2.) In all cases, the peaks shift to higher binding energies between 300 and 325 K, by increments of 0.5 to 0.8 eV. Changes are smaller (0.0 to 0.3 eV) and not systematic between 325 and 350 K. The peak positions, together with binding energy ranges for the elemental metals [26], are given in Table 3.

One explanation for the peak shifts between 300 and 325 K is surface alloying or exchange. This interpretation is supported by an analysis of the relative peak areas. Peak areas are proportional to the depth-weighted density of atoms of a given element. We calculated ratios of Ni/Au intensities, as well as ratios of Al/Au intensities, and the results are shown in Table 4. Heating causes these ratios to increase by small amounts, ranging from 2% to 10%. Within the scatter, the effect seems to be about the same for Ni and for Al. Since Au is presumably the topmost scatterer after deposition at 300 K, alloying at higher temperature would cause these ratios to increase. As Table 4 shows, an increase is indeed observed with increasing temperature, indicating that both Ni and Al probably exchange with Au at the surface.

STM data also suggest that the surface changes when it is heated above room temperature. In one experiment, 0.21 ML of Au was deposited at 300 K, after which the surface was heated to slightly higher temperatures. Images were then acquired at the elevated temperature. (The exact thermal treatment is described in Section 2.) Fig. 17 shows the resultant STM images at 325 K. In this case, it turns out that the experimental parameter of tip bias is crucial. When the bias magnitude is low, 0.5 eV, all the Au islands are similar. As the bias magnitude increases to 1.0 V and then 1.5 V, some Au islands become brighter than others, indicating different effective heights. The brighter islands are effectively ~ 0.1 nm higher than the dark islands. This is illustrated by the height histograms and line profiles in Fig. 18 and Fig. 19, which show two distinct peaks corresponding to the Au islands. We interpret this to mean that at 325 K, some islands—perhaps the bright ones—are more affected than others by exchange with the NiAl(110) substrate.

As the surface is heated to 350 K, the islands return to a single effective height that falls in the range 0.25 nm - 0.27 nm, independent of bias conditions (see Table 2). This is shown by the STM images in Fig 20, and by the histograms and line profiles in Fig. 21 and Fig. 22, where there is only a single peak corresponding to Au islands. We interpret this to mean that the alloying or exchange process is completed at 350 K. In addition to their heights, the shapes of these ‘alloyed’ islands are very similar to the original ones at 300 K. Compare, for instance, Fig. 20 with Fig. 8. Finally, the island coverage is invariant during the alloying process, remaining constant at 0.21 ML between 300 and 350 K. Hence, the exchange process disrupts neither the island shape nor the island area, in this temperature range. It changes the island heights, but only temporarily.

Stripes like those shown in Fig. 9 through Fig. 11 cannot be discerned after heating to 325 or 350 K, but it is not clear whether the stripes actually disappear or whether the resolution is simply poorer (or noise higher) in the STM images above 300 K.

4. Discussion

4.1 Growth at 200 K and 300 K

Island Heights. Growth of Au islands at 200 K and 300 K produces islands with heights of 0.24-0.25 nm, and this height is bias-independent in both cases. The value of the height indicates that islands are one atom thick. (For instance, [111] and [110] interplanar spacings in bulk Au are 0.236 nm and 0.289 nm, respectively.) By comparison, Ag/NiAl(110) formed first-layer islands that were 0.32 nm high, compatible

with a bilayer of fcc(110) metal. The difference in island heights is one indication that growth is much different for Au than for Ag.

Island Densities. For a fixed coverage of 0.24-0.25 ML and fixed flux of 0.034 ML/min (as presented in Sec. 2), the Au islands are much smaller and denser at 200 K than at 300 K. The island densities are 0.019 and 0.0013, respectively. This trend is in agreement with expectation for homogeneous nucleation, where lower temperature suppresses atomic diffusion and enhances the probability for nucleation of new islands, relative to the probability for attachment to existing islands.

Comparison with Ag/NiAl(110) is interesting here as well. At 300 K, the island density for Au/NiAl(110) is much higher than it is for Ag/NiAl(110). The island density in the latter case was thought to be suppressed strongly by preferential Ag adsorption at defect sites in the NiAl(110) substrate, specifically, at sites where a Ni replaced an Al atom [15]. Density functional theory (DFT) showed that Ag atoms bond more strongly at such sites, by 0.21 eV, relative to the next-most-favorable adsorption sites on the surface [15]. These defect sites thus serve as points of preferential nucleation, and they lead to lower island density than would be obtained with pure homogeneous nucleation. The effect was thought to increase with increasing temperature because diffusion lengths increased, making the defect sites more accessible to Ag atoms. The fact that the island density is about an order of magnitude higher for Au/NiAl(110) under comparable conditions suggests that the defect sites are less important for Au. It would be interesting to test this with DFT.

Island Shapes. At 300 K, first-layer islands have rather irregular shapes. Second-layer islands, which appear at 0.54 ML, are more rectangular and compact. As coverage

increases they become quite elongated. This is particularly evident at 0.8 ML [see Fig. 4(g)]. However, at higher coverage they return to a rather irregular shape, as shown in Fig. 4(h). The reasons for these transitions in shape are not clear. The elongated, compact shape shown by the second-layer islands between 0.6 and 0.8 ML is what one might expect naturally for an fcc(110) island, since it reflects the anisotropy of the fcc(110) structure. (Almond-shaped islands have been predicted and observed for Au on Au(110), but this shape is due to the missing-row reconstruction [27]). Further studies are needed to clarify the origin of the island shapes for Au/NiAl(110).

Fine Structure. At 300 K and at coverages of 0.6 ML or above, the islands show a chevron-like arrangement of stripes that are separated by about 1.2 nm. Domains of stripes are rotated by about $113^{\circ} \pm 5^{\circ}$ within the first layer. Domains of stripes also appear in second-layer islands, but these are not parallel to first-layer stripes.

Similar stripes were observed for Ag/NiAl(110), where they were attributed to a rumpling of the Ag layer that provided strain relief [13]. Only one domain was observed, presumably because the islands were highly anisotropic and served to orient the ripples. One can speculate that the cause of the stripes for Au/NiAl(110) may be similar.

4.2 Thermal effects above 300 K

Ours is the first study of the stability of Au deposited on a NiAl surface at or near room temperature. We propose that surface exchange occurs slightly above room temperature. This stands in contrast to the bulk system. The solubility of Au in bulk NiAl is very low, only 0.3 at. % [19]. At higher concentrations, Au reacts to form AuAl₂, but this occurs well above room temperature [19].

On the other hand, at surfaces, Au intermixes readily with Al or Ni alone. Examples include Al/Au(111) [28], Au/Ni(110) [29], Au/Ni(111) [30], Ni/Au(110) [31], and Ni/Au(111) [32]. In each case, surface intermixing occurs even at 300 K. It should be noted that Au and Ni are bulk-immiscible, illustrating the principle that a surface alloy can form even when a bulk alloy cannot. We propose that this principle applies in the present situation, since Au is nearly-insoluble in bulk NiAl.

To our knowledge, the only prior study of Au deposited on a substrate containing both Al and Ni was that of Shimoda et al. [33], who studied submonolayer Au coverages on the decagonal Al-Ni-Co quasicrystal, using XPS and reflection-high energy electron diffraction. They found that, upon deposition at 300 K, Au mixed preferentially with Al to form an Al-Au alloy. When annealed to 350-400 K, this alloy became more well-defined, both structurally and chemically, and could be identified as AuAl₂.

Our data do not serve to identify the exact nature of the exchange or alloying reaction of Au on NiAl(110) at 325-350 K. The signatures of the change are shifts in the XPS peaks, and (transient) changes in the effective island heights. The XPS area ratios suggest that the reaction affects and involves both Ni and Al, which is not compatible with exclusive formation of AuAl₂. It is somewhat surprising that the change occurs without significantly perturbing the island areas or shapes.

Our data show that this reaction certainly proceeds above 300 K. We cannot rule out the possibility that it occurs partially already at lower temperatures and, indeed, one might expect that this would be the case. On the other hand, the island heights and bias-dependences at 200 K and 300 K are similar and thus provide no evidence of thermally-activated changes in this temperature interval. More extensive investigations of the

temperature-dependence would be necessary to determine the exact thermal evolution of this system, particularly the conditions under which surface exchange or alloying begins.

5. Conclusions

When Au is deposited on the NiAl(110) surface, islands form that are one atom high. After deposition of 0.24 ML at 200 K, islands are small and their number density is about an order of magnitude higher than after deposition at 300 K. At 300 K, first-layer islands adopt larger, more irregular shapes. As coverage increases, second-layer islands appear and over a limited coverage range, they show compact rectangular shapes. At or above 0.6 ML and at 300 K, all island tops exhibit domains of stripes. Upon heating slightly above room temperature, there is evidence of intermixing, from both XPS and STM. More extensive studies are needed to understand these observations.

Acknowledgements

This work was supported by the Office of Science, Basic Energy Sciences, Materials Sciences and Engineering Division of the US Department of Energy (USDOE). This manuscript has been authorized by Iowa State University of Science and Technology under Contract No. DE-AC02-07CH11358 with the US Department of Energy.

References

- [1] S.C. Deevi, V.K. Sikka, *Intermetallics* 4 (1996) 357-375.
- [2] C.T. Liu, J. Stringer, J.N. Mundy, L.L. Horton, P. Angelini, *Intermetallics* 5 (1997) 579-596.
- [3] N. Nilius, A. Cörper, G. Bozdech, N. Ernst, H.-J. Freund, *Prog. Surf. Sci.* 67 (2001) 99-121.
- [4] S. Degen, C. Becker, K. Wandelt, *Far. Disc.* 125 (2004) 343-356.
- [5] S. Gritschneider, C. Becker, K. Wandelt, M. Reichling, *J. Am. Chem. Soc.* (2007) 4925-4928.
- [6] J.E. Gould, *Proc. IEE* 125 (1978) 1137-1150.
- [7] S.C. Lui, J.W. Davenport, E.W. Plummer, D.M. Zehner, G.W. Fernando, *Physical Review B* 42 (1990) 1582-1597.
- [8] M.H. Kang, E.J. Mele, *Physical Review B* 36 (1987) 7371-7377.
- [9] H.L. Davis, J.R. Noonan, *Phys. Rev. Lett.* 54 (1985) 566-569.
- [10] S.M. Yalisove, W.R. Graham, *Surf. Sci.* 183 (1987) 556-564.
- [11] X. Torrelles, F. Wendler, O. Bikondoa, H. Isern, W. Moritz, G.R. Castro, *Surf. Sci.* 487 (2001) 97-106.
- [12] J. Hong, *Phy. Rev. B* 73 (2006) 092413.
- [13] B. Ünal, F. Qin, Y. Han, D.J. Liu, D. Jing, A.R. Layson, C. Jenks, J.W. Evans, P.A. Thiel, *Phys. Rev B* 76 (2007) 195410.
- [14] Z. Song, J.I. Pascual, H. Conrad, K. Horn, H.-P. Rust, *Appl. Phys. A: Mat. Sci. Processing* 72 (2001) S159-S162.

- [15] Y. Han, B. Ünal, D. Jing, F. Qin, C.J. Jenks, D.-J. Liu, P.A. Thiel, J.W. Evans, *Phys. Rev B* 81 (2010) 115462.
- [16] Y. Han, B. Ünal, F. Qin, D. Jing, C. Jenks, D.-J. Liu, P.A. Thiel, J.W. Evans, *Phys. Rev. Lett* 100 (2008) 116105.
- [17] J.W. Evans, Y. Han, B. Ünal, M. Li, K.J. Caspersen, D. Jing, A.R. Layson, C.R. Stoldt, T. Duguet, P.A. Thiel, *AIP Conference Proceedings* 1270 (2010) 26-44.
- [18] T. Duguet, Y. Han, C. Yuen, D. Jing, B. Ünal, J.W. Evans, P.A. Thiel, *Proc. Nat. Acad. Sci.* 108 (2011) 989-994.
- [19] L. Sheng, W. Zhang, J. Guo, F. Yang, Y. Liang, H. Ye, *Intermetallics* 18 (2010) 740-744.
- [20] G.A. Somorjai, Y. Li, *Introduction to Surface Chemistry and Catalysis*, John Wiley & Sons, Inc., Hoboken, NJ, 2010.
- [21] P.A. Thiel, P.J. Estrup, in: A.T. Hubbard (Ed.), *The Handbook of Surface Imaging and Visualization*, CRC Press, Boca Raton, Florida, 1995, p. 407.
- [22] N. Takeuchi, C.T. Chan, K.M. Ho, *Phys. Rev. Lett.* 63 (1989) 1273-1276.
- [23] T.B. Massalski, H. Okamoto, P.R. Subramanian, L. Kacprzak (Eds.), *Binary Alloy Phase Diagrams*, ASM International, 1990.
- [24] I. Horcas, R. Fernandez, J.M. Gomez-Rodriguez, J. Colchero, J. Gomez-Herrero, A.M. Baro, *Review of Scientific Instruments* 78 (2007) -.
- [25] See www.CasaXPS.com.
- [26] J.F. Moulder, W.F. Stickle, P.E. Sobol, K.D. Bomben, *Handbook of X-ray Photoelectron Spectroscopy*, Perkin-Elmer Corporation, Physical Electronics Division, Eden Prairie, Minnesota, 1992.

- [27] M.J. Rost, R. van Gastel, J.W.M. Frenken, *Phys. Rev. Lett* 84 (2000) 1966-1969.
- [28] B. Fischer, J.V. Barth, A. Fricke, L. Nedelmann, K. Kern, *Surface Science* 389 (1997) 366-374.
- [29] L.P. Nielsen, F. Besenbacher, I. Stensgaard, E. Laegsgaard, C. Engdahl, P. Stoltze, K.W. Jacobsen, J.K. Norskov, *Physical Review Letters* 71 (1993) 754-757.
- [30] J. Jacobsen, L. Pleth Nielsen, F. Besenbacher, I. Stensgaard, E. Lægsgaard, T. Rasmussen, K.W. Jacobsen, J.K. Nørskov, *Physical Review Letters* 75 (1995) 489.
- [31] M.B. Hugenschmidt, A. Hitzke, R.J. Behm, *Physical Review Letters* 76 (1996) 2535.
- [32] W.G. Cullen, P.N. First, *Surf. Sci.* 420 (1999) 53-64.
- [33] M. Shimoda, T.J. Sato, A.P. Tsai, J.Q. Guo, *Phys. Rev. B: Condens. Matter Mater. Phys.* 62 (2000) 11288-11291.
- [34] N. Ohtsu, A. Nomura, T. Shishido, *Surf. Sci. Spectra* 17 (2010) 68-75.

Figure Caption

Figure 1

Bulk structure of NiAl (110), (a) top view and (b) side view. The black rectangle box in (a) represents the unit cell.

Figure 2

STM images. (a) clean surface of NiAl(110), taken at 250 nm x 250 nm, $I = 0.5$ nA, V-tip = -1 V; (b) 0.24 ML deposition of Au on NiAl(110) at 300 K, taken at 500 nm x 500 nm, $I = 0.5$ nA, V-tip = -1 V.

Figure 3

All the data points represent experiments in which Au was deposited at 300 K, without heating, except for the point labeled “Fig. 7”, in which Au was deposited at 200 K. Each point is labeled with the name of a figure that represents this experiment. The point itself and its error bars are usually based upon more images than just the figure (not all images are shown as figures in this paper). The straight line is a linear least-squares fit, for which the regression parameter is 0.935. The least-squares fit for a line is shown in the figure and has been taken into account for the uncertainty in the measurement.

Figure 4

STM images of given Au deposition times on NiAl(110) with a coverage of (a) 0.10 ML, (b) 0.16 ML, (c) 0.24 ML, (d) 0.54 ML, (e) 0.54 ML, (f) 0.60 ML, (g) 0.83 ML, and (h) 1.3 ML. STM image size and tunneling conditions are (a) 250 nm x 250 nm, $I = 0.5$ nA, V-tip = -1 V; (b) 250 nm x 250 nm, $I = 0.5$ nA, V-tip = -1 V; (c) 250 nm x 250 nm, $I = 0.5$ nA, V-tip = +1 V; (d) 250 nm x 250 nm, $I = 0.5$ nA, V-tip = -1 V; (e) 100 nm x 100 nm, $I = 0.5$ nA, V-tip = -1 V; (f) 200 nm x 200 nm, $I = 0.5$ nA, V-tip = -1 V; (g) 150 nm x 150 nm, $I = 0.1$ nA, V-tip = +1 V; and (h) 100 nm x 80 nm, $I = 0.1$ nA, V-tip = +1 V.

Figure 5

Island size distribution at 0.24 ML coverage where S = island size and $\langle S \rangle$ = mean island size, (a) 300 K and (b) 200 K.

Figure 6

STM images and height histograms at different Au coverages, (a) 100 nm x 100 nm, $I = 0.5$ nA, V-tip = -1 V, with a coverage of 0.24 ML of Au; (b) height histogram of (a); (c) 100 nm x 100 nm, $I = 0.1$ nA, V-tip = +1 V with a coverage of 0.60 ML of Au; (d) height histogram of (c).

Figure 7

STM images and line profiles at different Au coverages at 300 K. Tunneling conditions at coverages from 0.1 ML to 0.60 ML are $I = 0.50$ nA and V-tip = -1 V and coverages from 0.83 ML to 1.3 ML are $I = 0.1$ nA and V-tip = +1 V.

Figure 8

Au/NiAl(110) at 300 K with different bias conditions. Coverage of 0.24 ML of Au was deposited at 300 K. All of these STM images are $I = 0.5$ nA and 100 nm x 100 nm with a V-tip of (a) -0.5 V, (b) -1.0 V, (c) -1.5 V, (d) +0.5 V, (e) +1.0 V, and (f) +1.5 V.

Figure 9

STM image of Au on NiAl(110) at 300 K at a coverage of 0.60 ML. STM images are (a) 100 nm x 100 nm, (b) 22 nm x 22 nm, (c) 22 nm x 22 nm, (d) 30 nm x 30 nm, (e) 22 nm x 22 nm, and (f) 100 nm x 100 nm. The tunneling conditions are $I = 0.5$ nA and V-tip = -1 V.

Figure 10

Stripes in the Au island on NiAl(110) at 300 K, (a) STM image by 11 nm x 6 nm, (b) line profile from (a) taken by the black arrowhead, (c) STM image by 7 nm x 5 nm, (d) line profile from (c) taken by the black arrowhead, (e) derivative STM image by 11 nm x 11 nm, (f) line profile from (e) taken by the white arrowhead, (g) derivative STM image by 10 nm x 8 nm, and (h) line profile from (g) taken by the black arrowhead. Coverage of 0.60 ML of Au.

Figure 11

STM image of 1.3 ML Au coverage on NiAl(110) at 300 K with dimensions of, (a) is 100 nm x 81 nm, (b) 11 nm x 12 nm (1st layer), (c) 15 nm x 13 nm (1st layer), (d) 11 nm x 16 nm (2nd layer), (e) 22 nm x 17 nm (1st and 2nd layers), and (f) 15 nm x 11 nm (1st layer).

Figure 12

Au/NiAl(110) at 200 K with different bias conditions. Coverage of 0.25 ML of Au was deposited at 200 K. All of these STM images are $I = 0.5$ nA and 100 nm x 100 nm with a V-tip of (a) -0.5 V, (b) -1.0 V, (c) -1.5 V, (d) +0.5 V, (e) +1.0 V, and (f) +1.5 V.

Figure 13

XPS Ni 2p_{3/2} binding energy range from 880 to 830 eV at given temperatures. Deposited Au at 300 K and then annealed to 325 K and 350 K.

Figure 14

XPS Al 2s binding energy range from 130 to 100 eV at given temperatures. Deposited Au at 300 K and then annealed to 325 K and 350 K.

Figure 15

XPS Au 4f_{7/2, 5/2} binding energy range from 100 to 75 eV at given temperatures. Deposited Au at 300 K and then annealed to 325 K and 350 K.

Figure 16

XPS Ni 3p and Al 2p binding energy range from 80 to 60 eV at given temperatures. Deposited Au at 300 K and then annealed to 325 K and 350 K.

Figure 17

Au/NiAl(110) at 325 K with different bias conditions. Coverage of 0.24 ML of Au was deposited at 300 K and was then annealed at 325 K. Different island height is shown at high biases as indicated by dark and light contrast. All of these STM images are $I = 0.5$ nA and are zoomed-in (250 nm x 140 nm) from 250 nm x 250 nm with a V-tip of (a) -0.5 V, (b) +0.5 V, (c) -1.0 V, (d) +1.0 V, (e) -1.5 V, and (f) +1.5 V.

Figure 18

Height histograms which were taken from the STM images in Fig. 8 at 325 K. The tunneling conditions are $I = 0.5$ nA and a V-tip of (a) -0.5 V, (b) +0.5 V, (c) -1.0 V, (d) +1.0 V, (e) -1.5 V, and (f) +1.5 V.

Figure 19

STM images with corresponding line profiles of Au on NiAl (110) at 325 K. The tunneling conditions are $I = 0.5$ nA and V-tip = -1 V.

Figure 20

Au/NiAl(110) at 350 K with different bias conditions. Coverage of 0.24 ML of Au was deposited at 300 K and was then annealed at 350 K. All of these STM images are $I = 0.5$ nA and are 100 nm x 100 nm with a V-tip of (a) -0.5 V, (b) +0.5 V, (c) -1.0 V, (d) +1.0 V, (e) -1.5 V and (f) +1.5 V.

Figure 21

Height histograms which were taken from the STM images in Fig. 10 at 350 K. The tunneling conditions are $I = 0.5$ nA and a V-tip of (a) -0.5 V, (b) +0.5 V, (c) -1.0 V, (d) +1.0 V, (e) -1.5 V, and (f) +1.5 V.

Figure 22

STM images with corresponding line profiles of Au on NiAl (110) at 350 K. The tunneling conditions are $I = 0.500$ nA and V-tip = -1 V.

Table 1

Island heights and island densities after deposition of various coverages of Au at 300 K. Au was deposited on NiAl(110) at 300 K. The tunneling conditions were 0.1 nA and 0.5 nA with a bias voltage between -1.5 V and +1.5 V.

Au Coverage (ML)	Au Deposition Time (min)	1st Layer Height (nm)	2nd Layer Height (nm)	Island Density (nm⁻²)
0.10	2	0.25 ± 0.01	—	0.0006
0.16	4	0.25 ± 0.01	—	0.0008
0.24	8	0.24 ± 0.02	—	0.0013
0.54	16	0.37 ± 0.02	0.25 ± 0.01	
0.60	16.5	0.26 ± 0.02	0.21 ± 0.02	
0.83	24.5	0.27 ± 0.01	0.24 ± 0.01	
1.3	40.5	0.25 ± 0.03	0.24 ± 0.01	

Table 2

Island heights, determined from pixel height histograms, at different bias voltages and different temperatures. The Au coverage is constant at 0.24 ML. The temperatures of 200 K and 300 K are deposition temperatures, while 325 K and 350 K are annealing temperatures. Details of the thermal program are given in Section 2.

Temp (K)	Island Height (nm)					
	-1.5 V	-1.0 V	-0.5 V	+0.5 V	+1.0 V	+1.5 V
200	0.25	0.23	0.25	0.24	0.25	0.25
300	0.23	0.23	0.23	0.23	0.24	0.25
325	0.26	0.27	0.37	0.43	0.29	0.23
	0.33	0.33			0.40	0.39
350	0.25	0.25	0.25	0.26	0.25	0.27

Table 3

Peak positions in XPS after different thermal treatments. The sample was initially prepared by depositing 0.24 ML Au at 300 K. After XPS at 300 K, it was heated to the higher temperatures as indicated. Details of the thermal program are given in Section 2. Peak positions of references are given in the bottom 3 rows.

Temp (K)	Experimental Peak position (eV)					
	Ni 2p _{3/2}	Al 2s	Au 4f _{7/2}	Au 4f _{5/2}	Ni 3p	Al 2p
300	852.6	117.1	83.3	87.3	66.3	72.0
325	853.3	117.9	84.1	87.9	66.8	72.8
350	853.3	117.6	84.1	88.0	66.8	72.5
Clean NiAl(110) – this work	—	—	—	—	66.5	72.0
Fractured, polycrystalline NiAl [34]	853.2	—	—	—	—	72.8
Elemental metals [26]	852.5- 852.9	117.1- 118.0	82.8- 83.9	86.3- 87.7	66.1- 66.9	72.5- 73.0

Table 4

Integrated intensity ratios in XPS after different thermal treatments. In cases where Au was present, the coverage was 0.24 ML and it was deposited at 300 K. After XPS at 300 K, it was heated to the higher temperatures. Details of the thermal program are given in Section 2. The clean NiAl(110) spectrum was measured in a different run, one day before the Au deposition experiments.

Surface	Intensity Ratios					
	(Ni 2p _{3/2}) : (Au 4f _{5/2+7/2})	(Ni 3p) : (Au 4f _{5/2+7/2})	(Al 2s) : (Au 4f _{5/2+7/2})	(Al 2p) : (Au 4f _{5/2+7/2})	(Ni 2p _{3/2}) : (Al 2s)	(Ni 3p) : (Al 2p)
Clean NiAl(110)	—	—	—	—	—	2.24
With Au, 300 K	2.94	0.274	0.172	0.098	17.04	2.81
With Au, 325 K	3.09	0.289	0.174	0.107	17.78	2.70
With Au, 350 K	3.23	0.282	0.176	0.103	18.38	2.73
Relative Change between 300 K and 350 K with Au	+10%	+3%	+2%	+5%	+8%	-3%

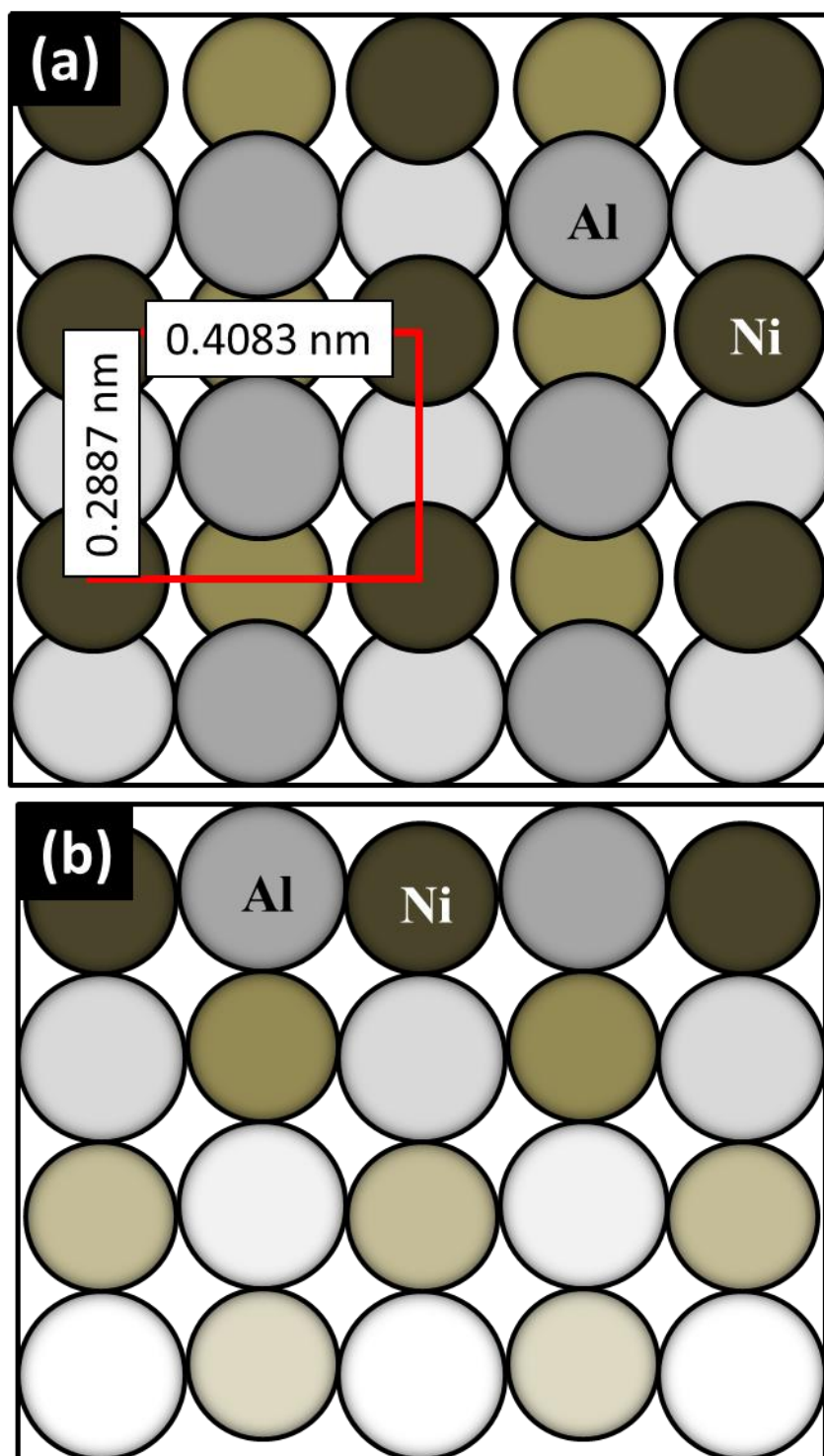


Figure 1

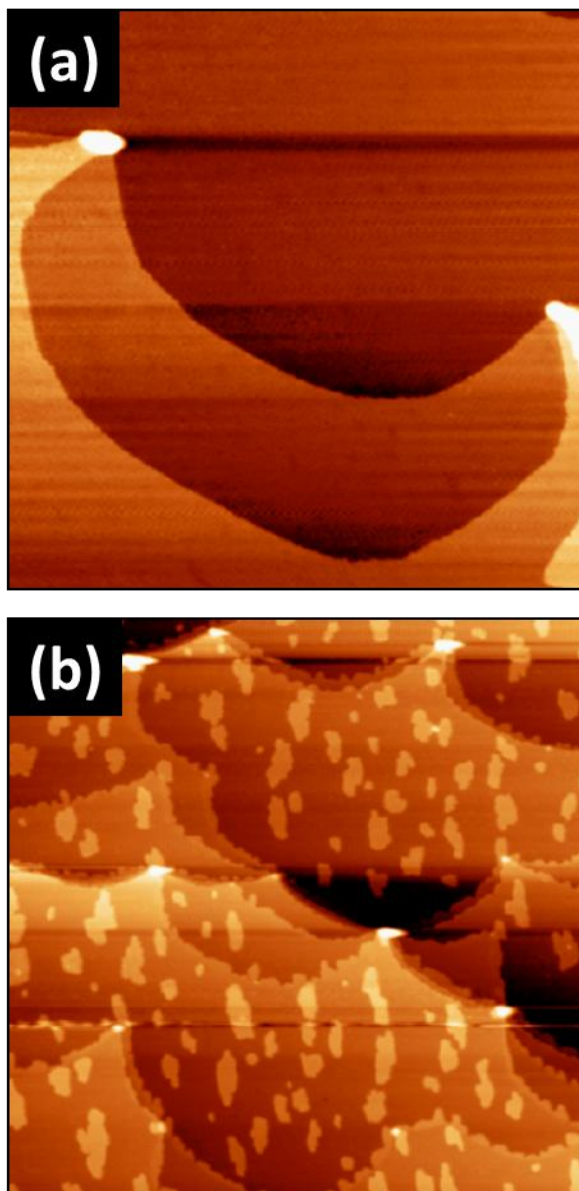


Figure 2

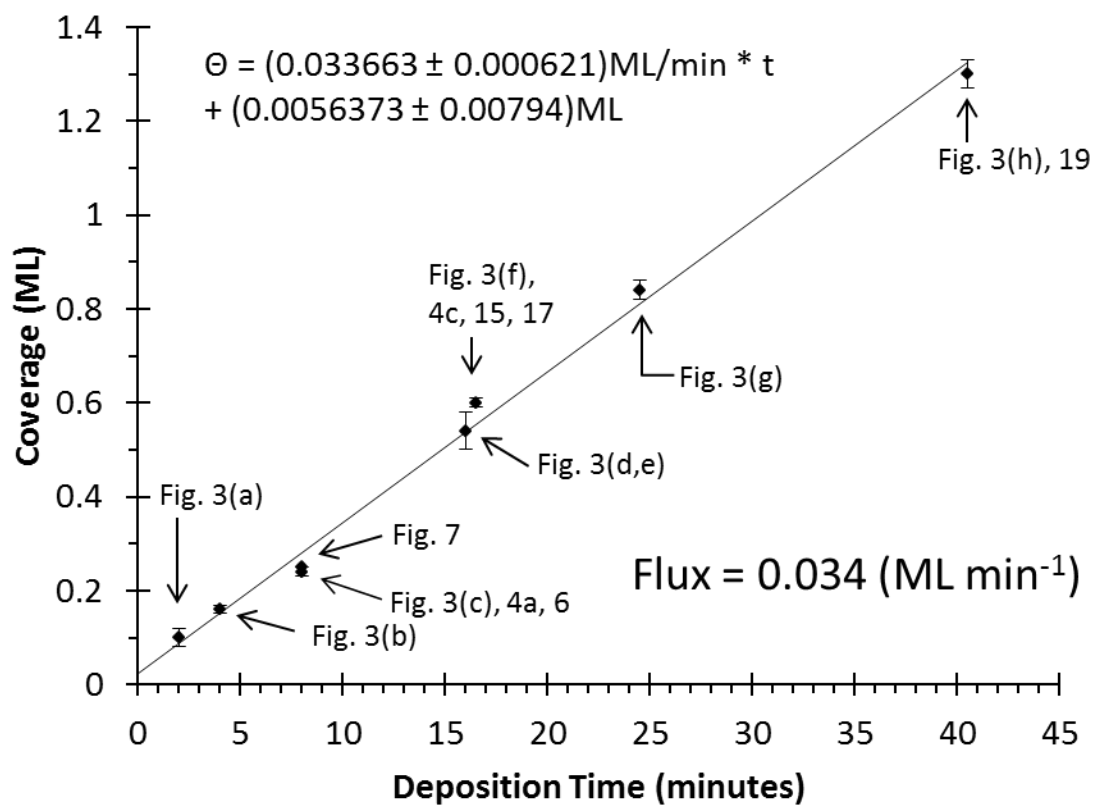


Figure 3

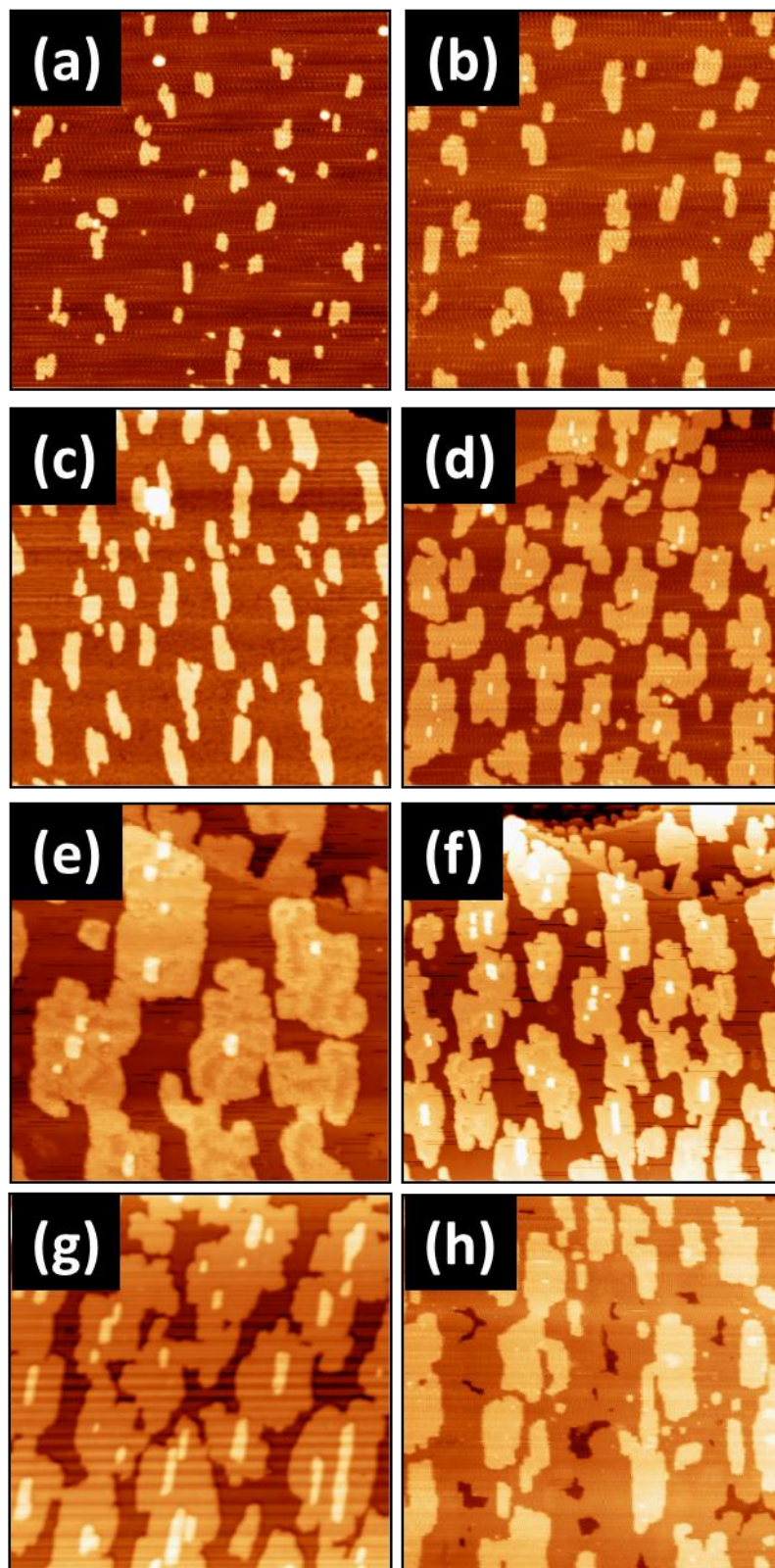


Figure 4

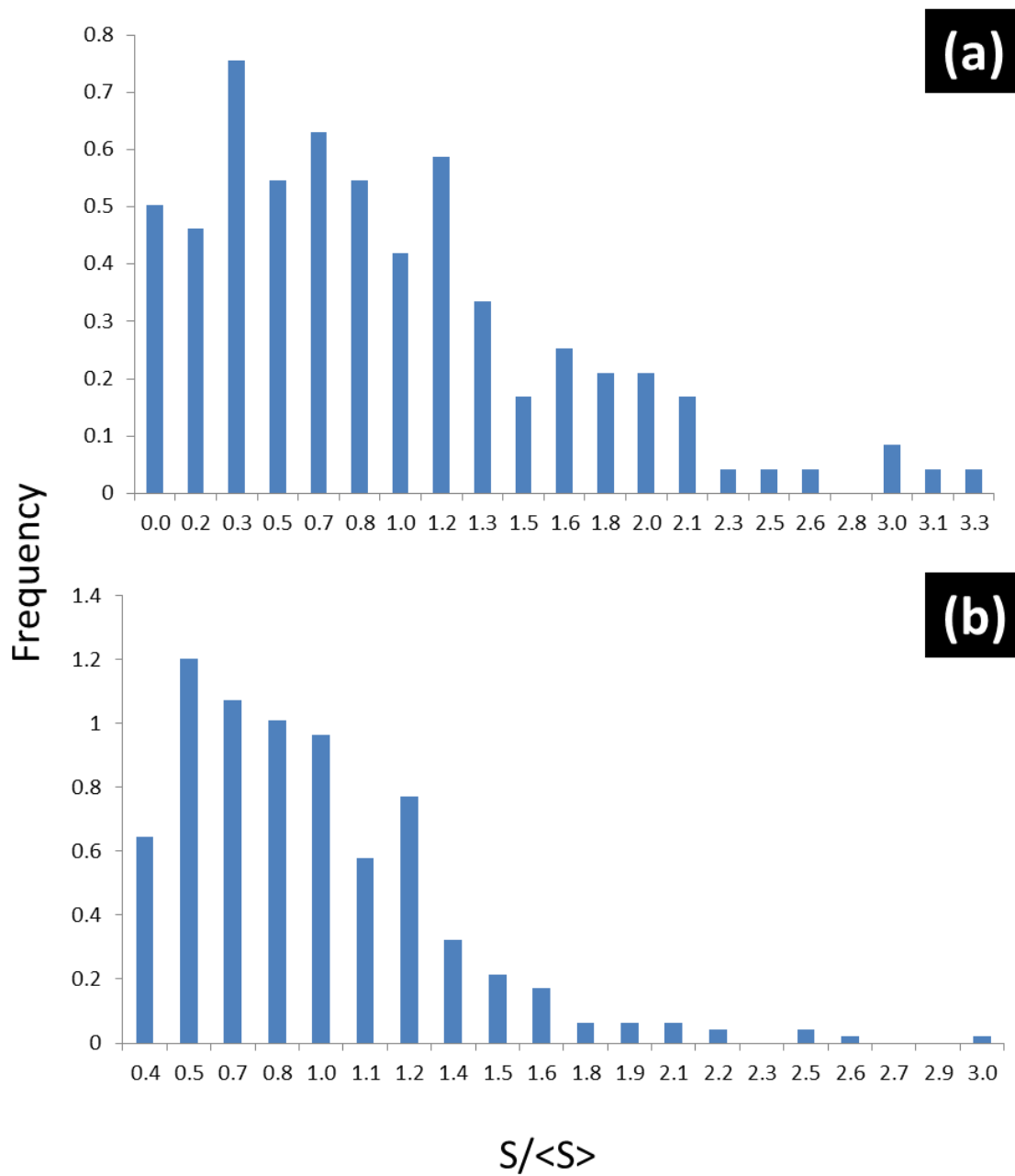


Figure 5

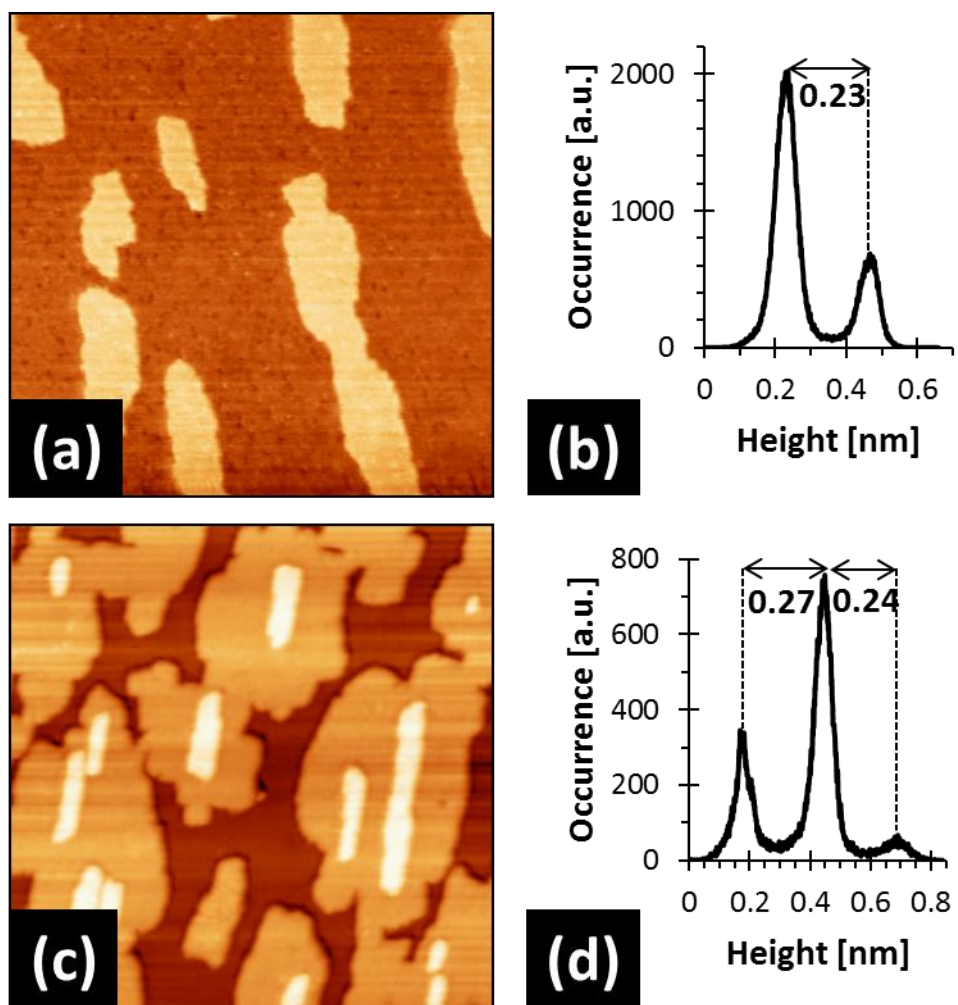


Figure 6

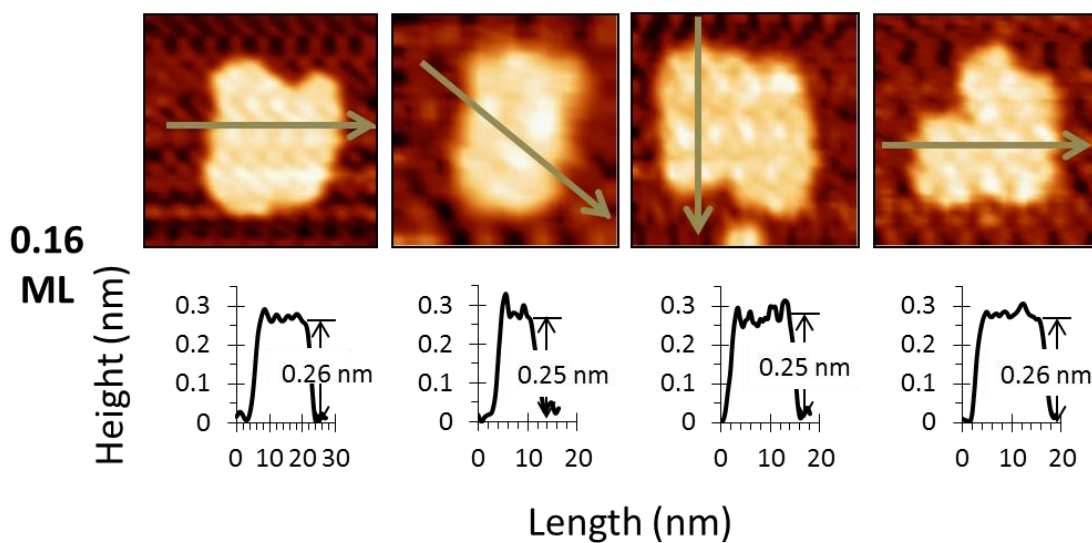
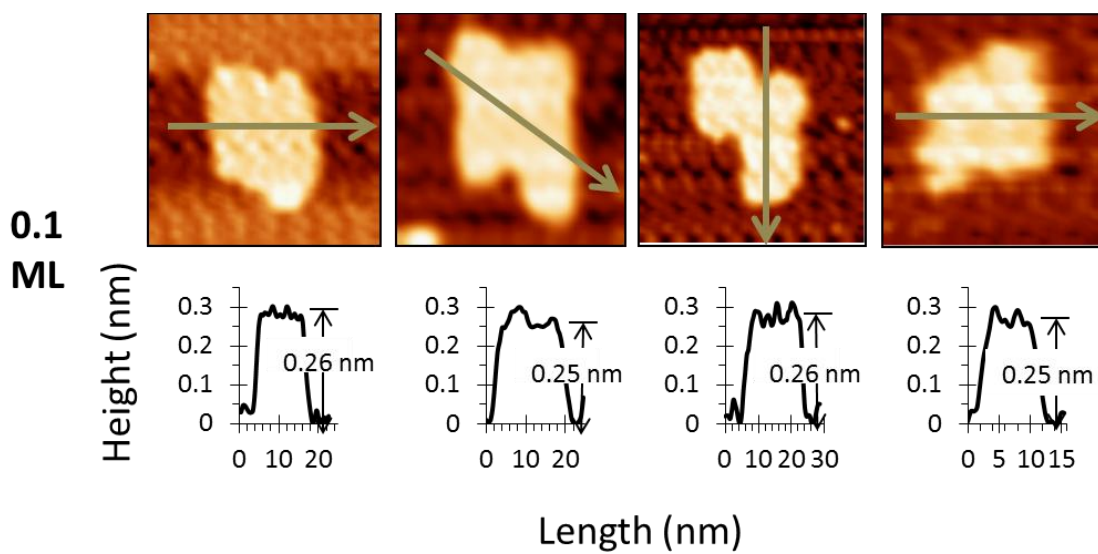


Figure 7

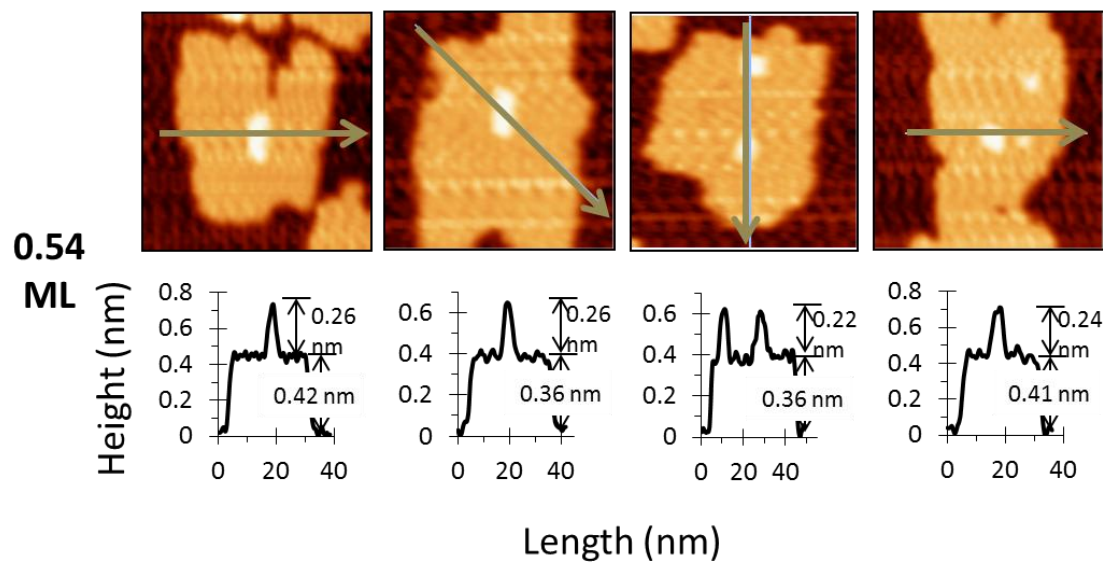
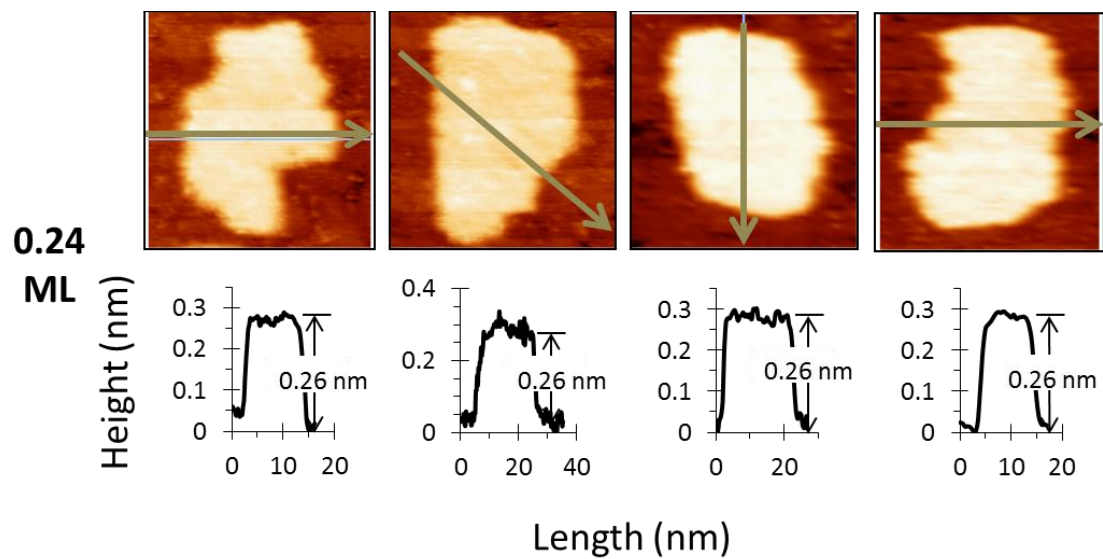


Figure 7 (Continue)

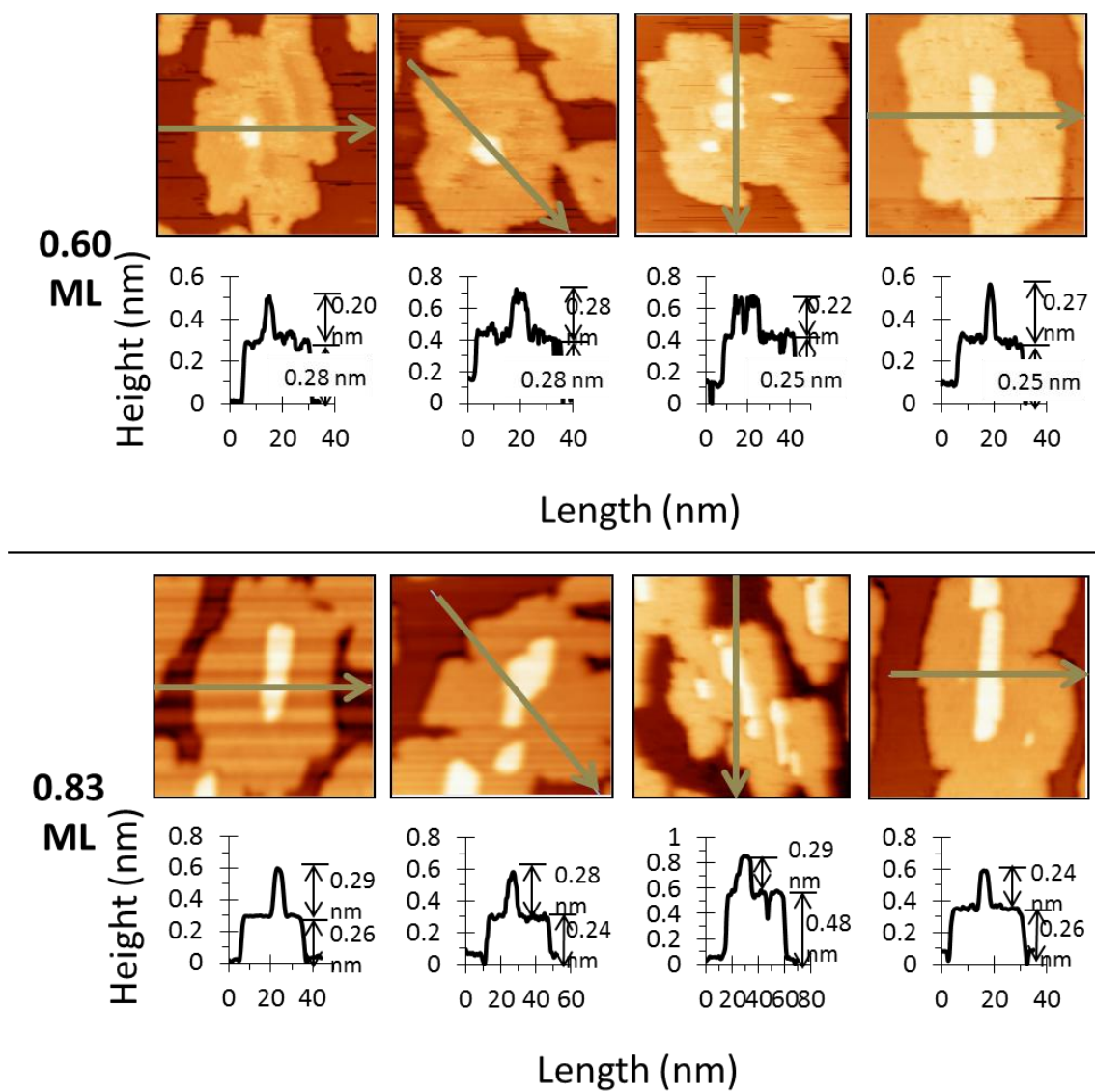


Figure 7 (Continue)

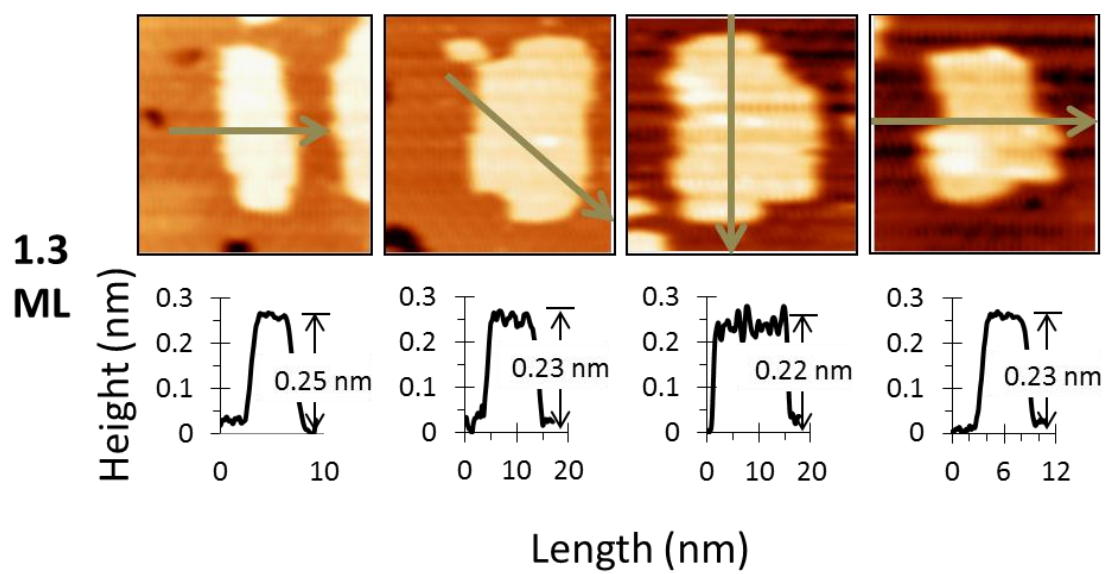


Figure 7 (Continue)

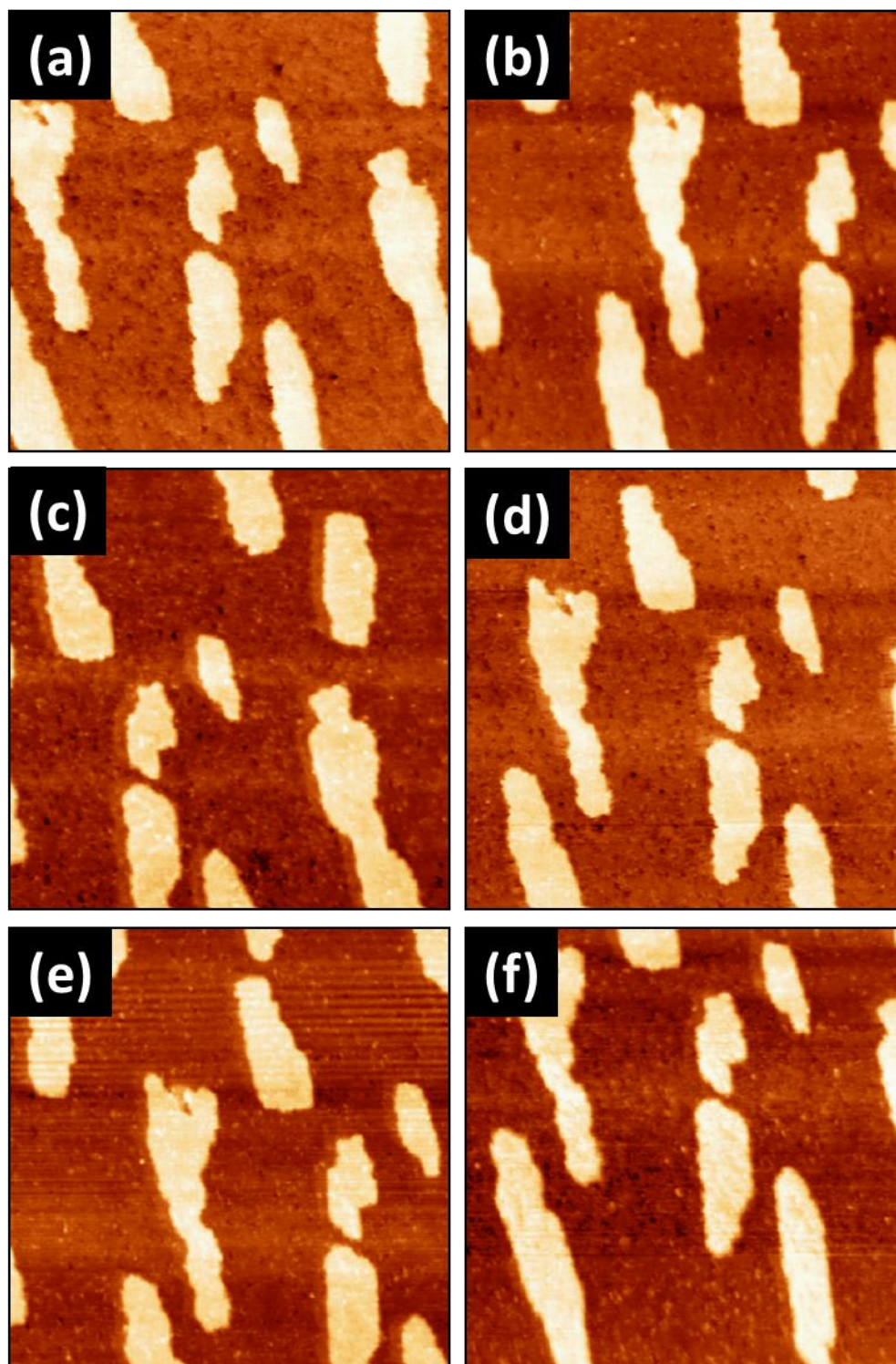


Figure 8

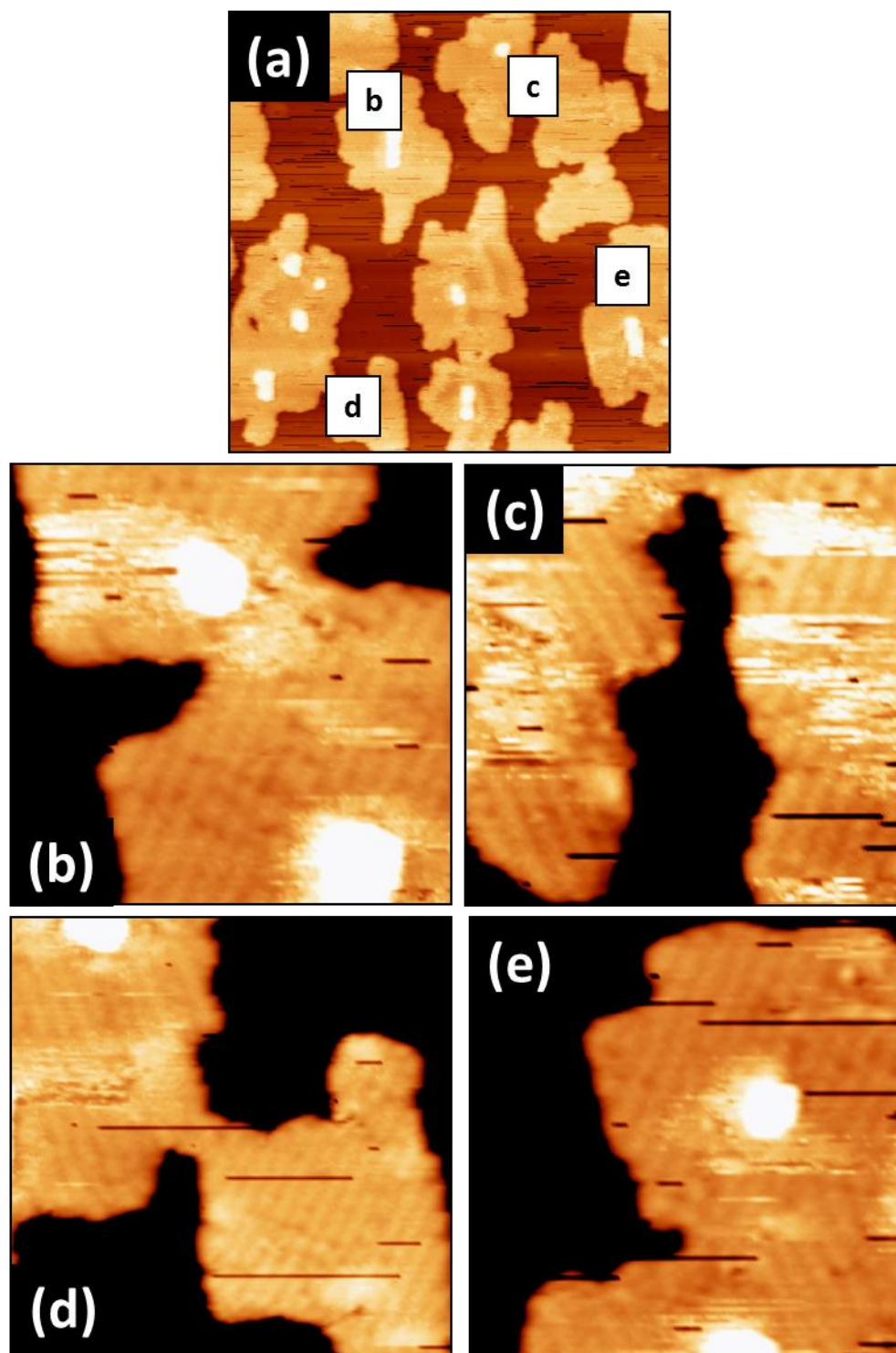


Figure 9

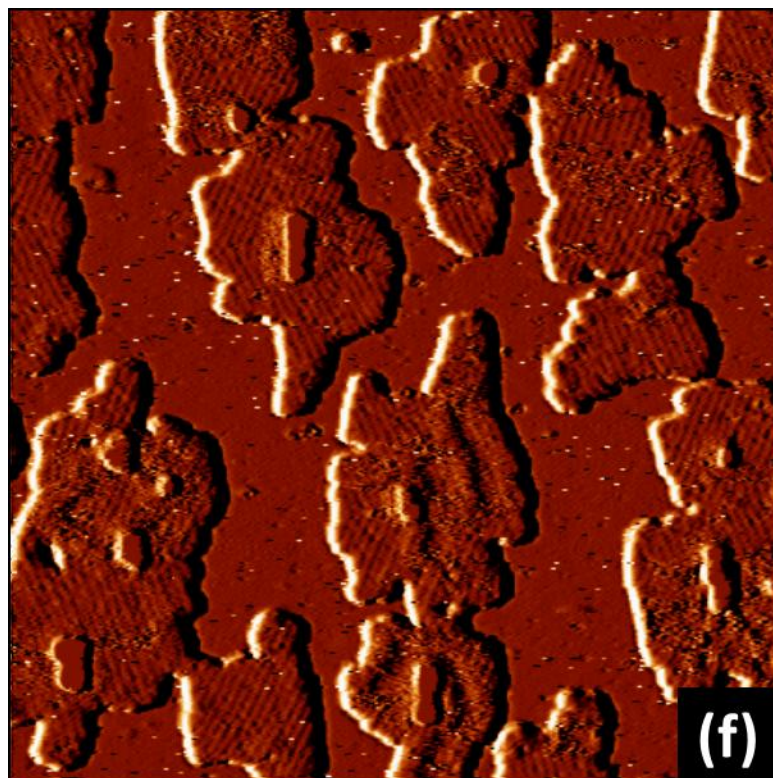


Figure 9 (Continue)

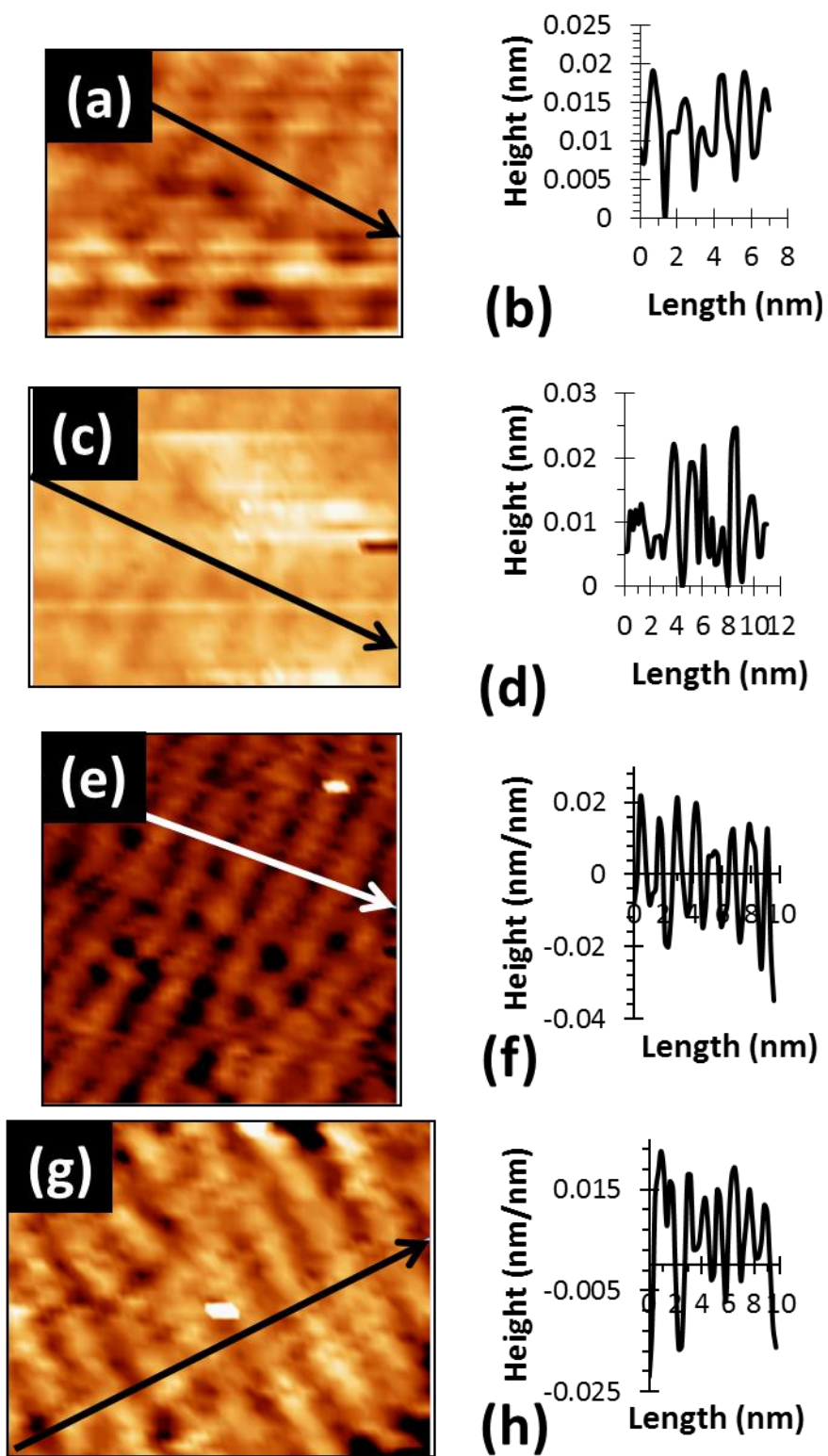


Figure 10

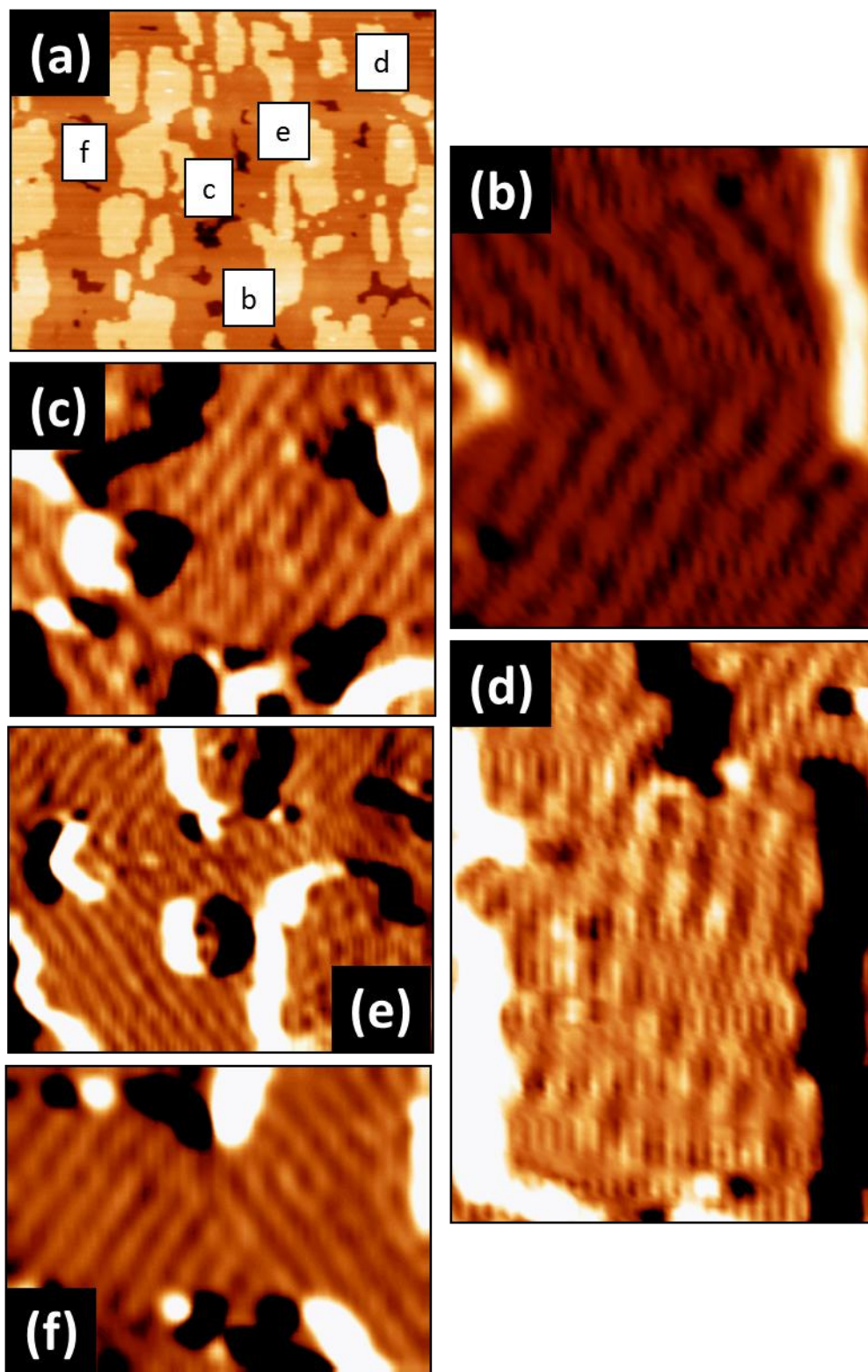


Figure 11

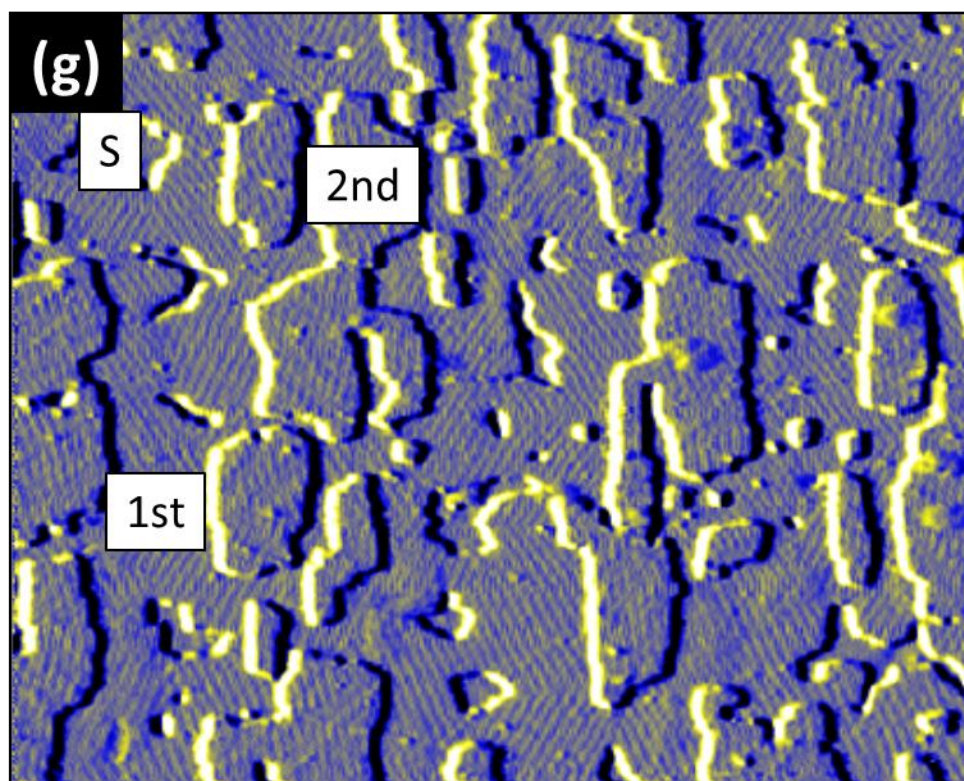


Figure 11 (Continue)

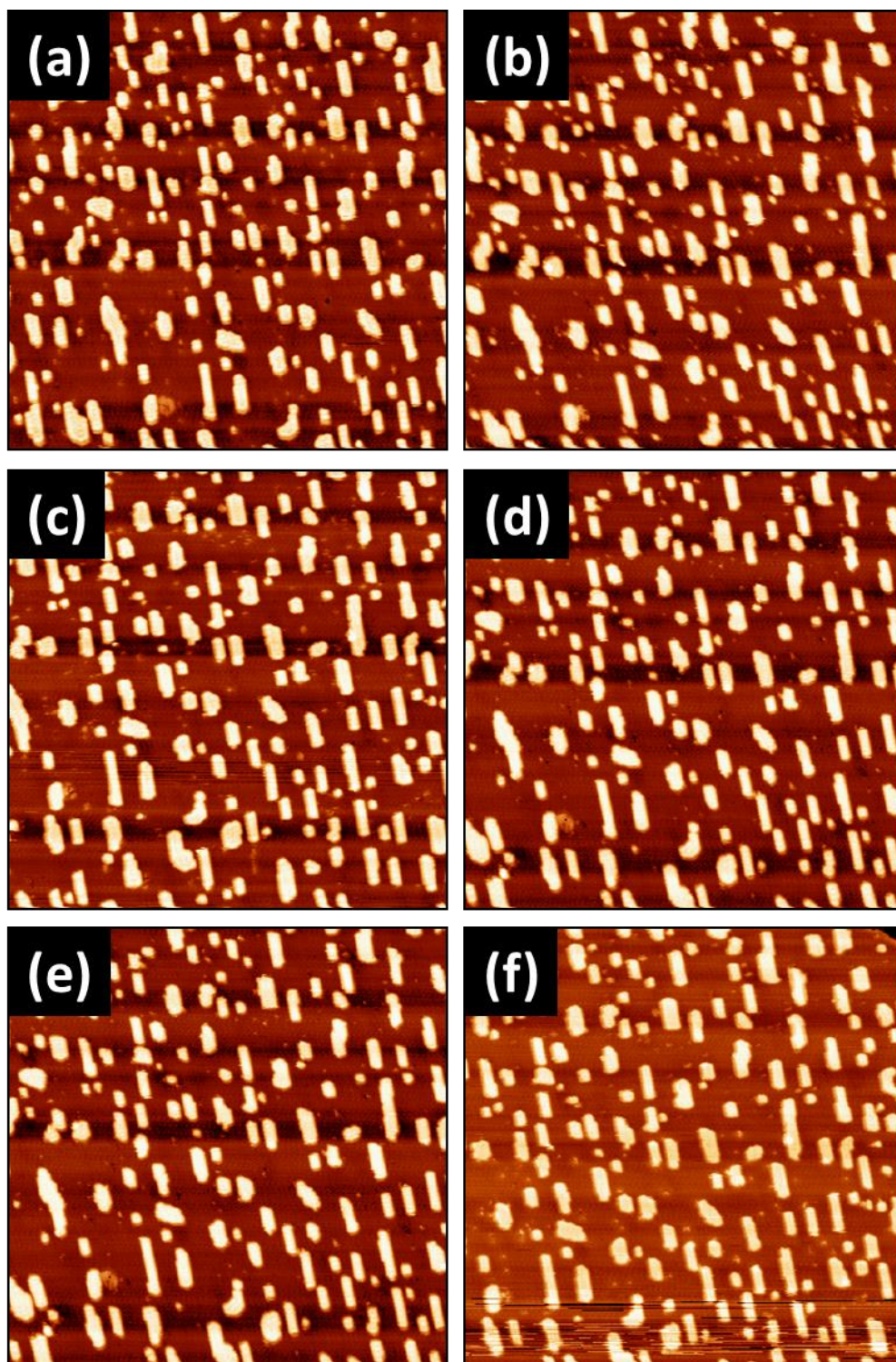


Figure 12

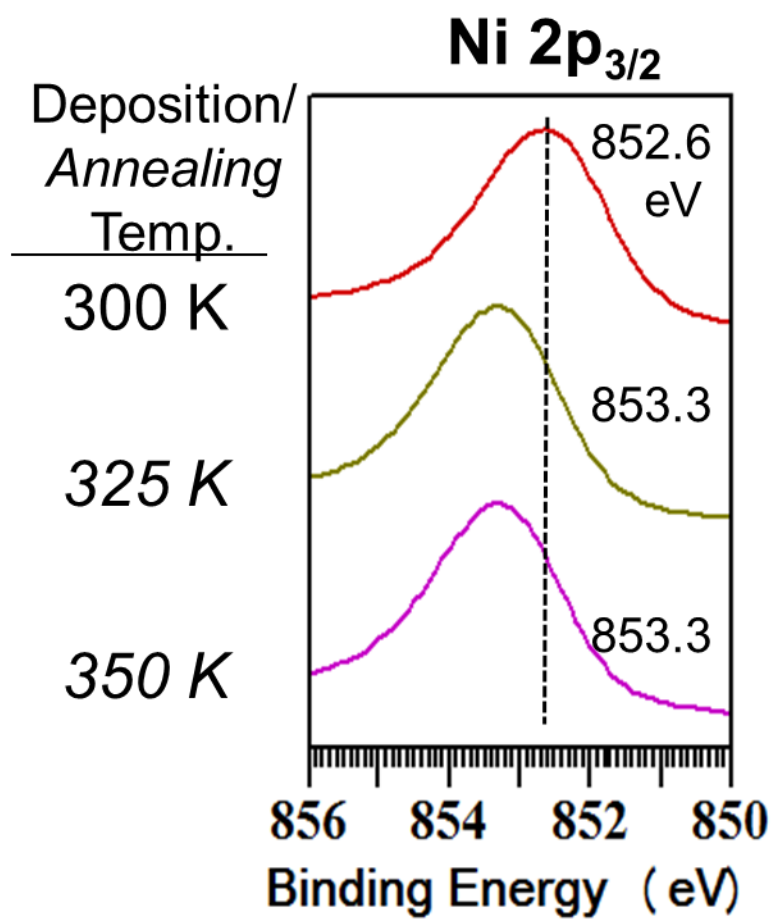


Figure 13

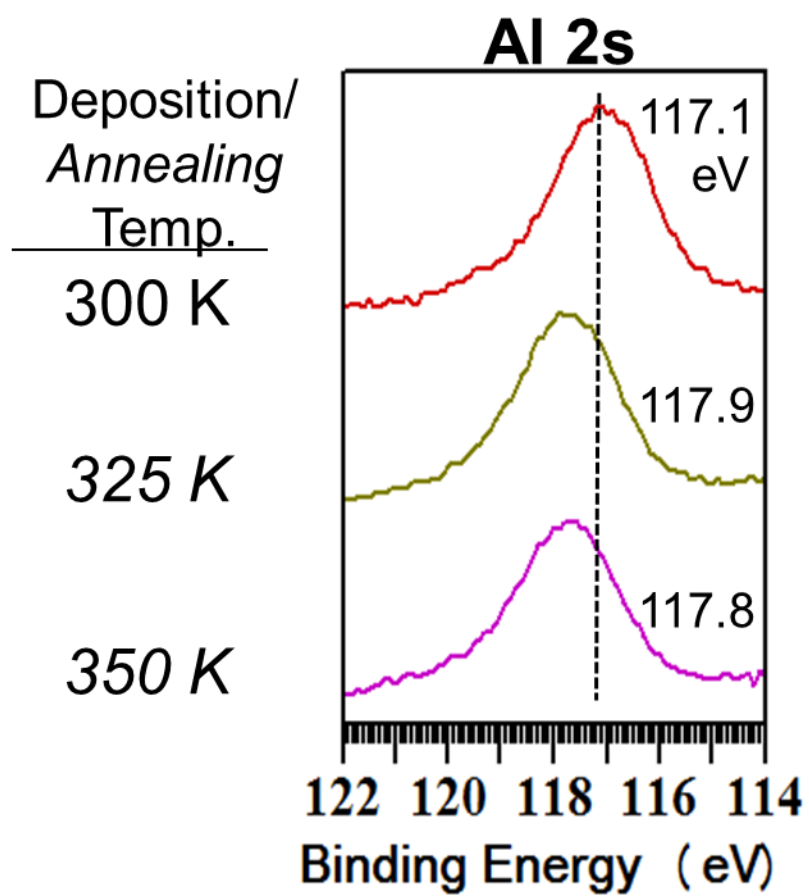


Figure 14

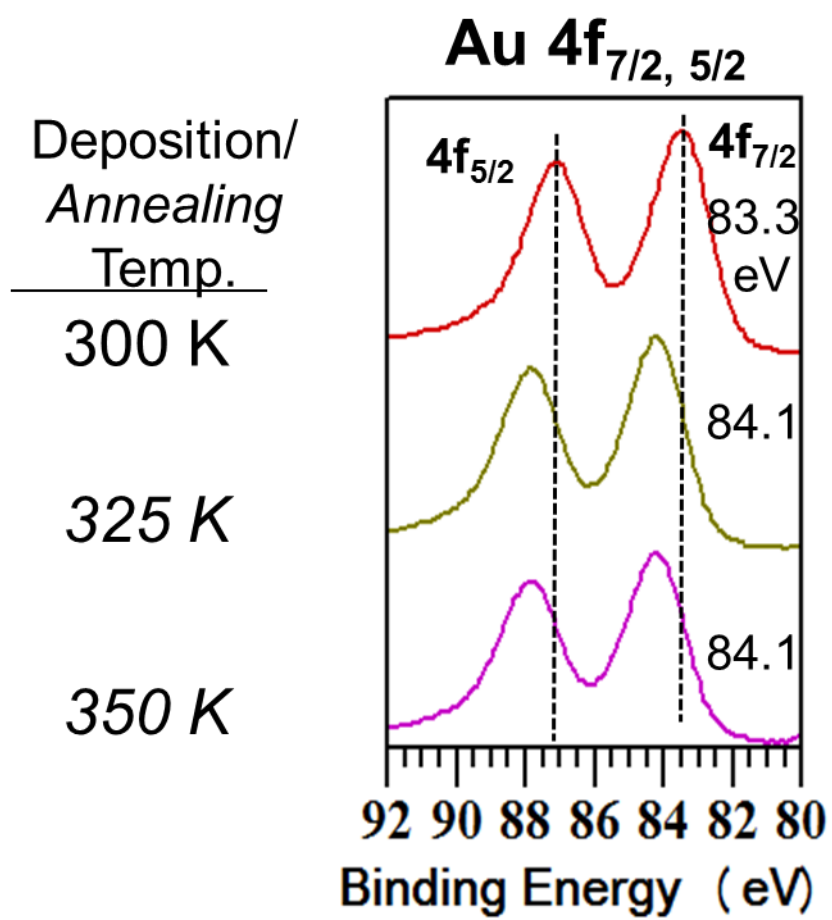


Figure 15

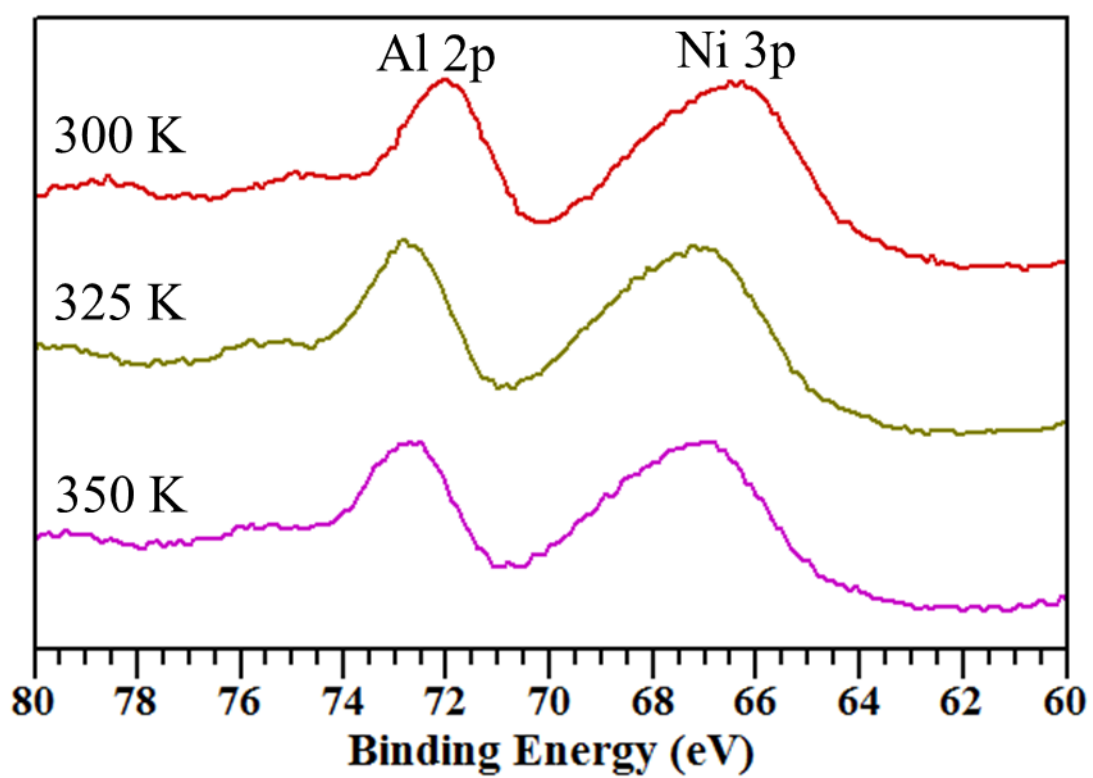


Figure 16

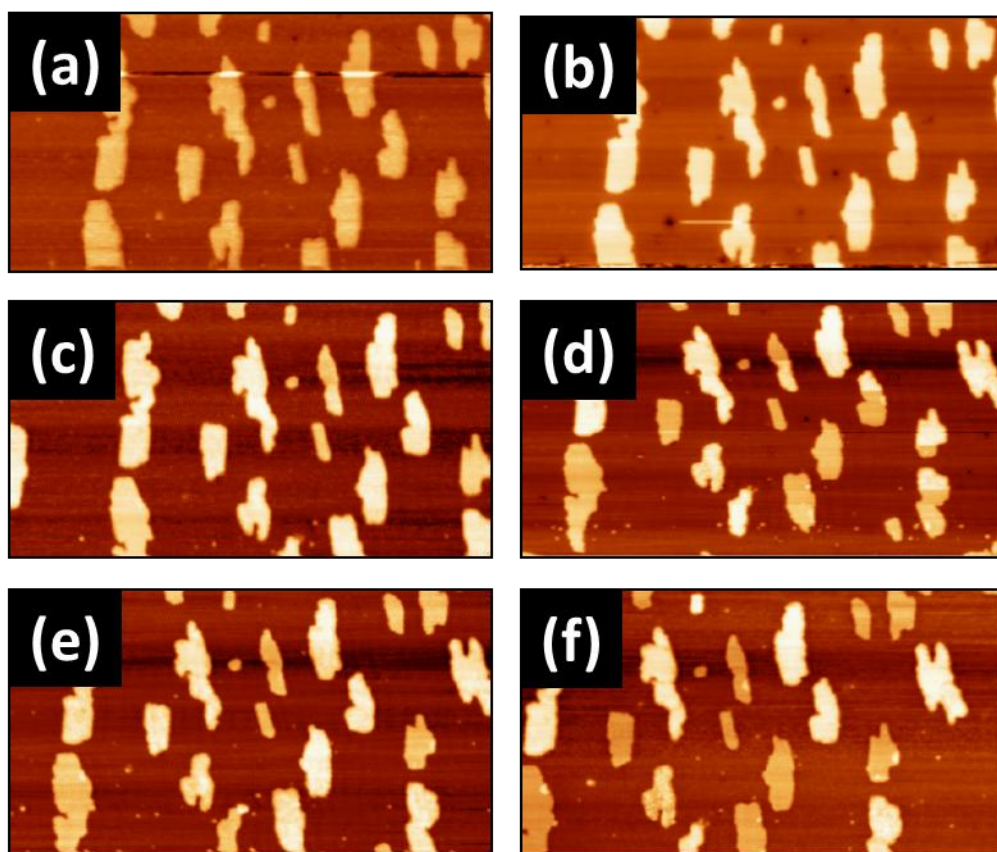


Figure 17

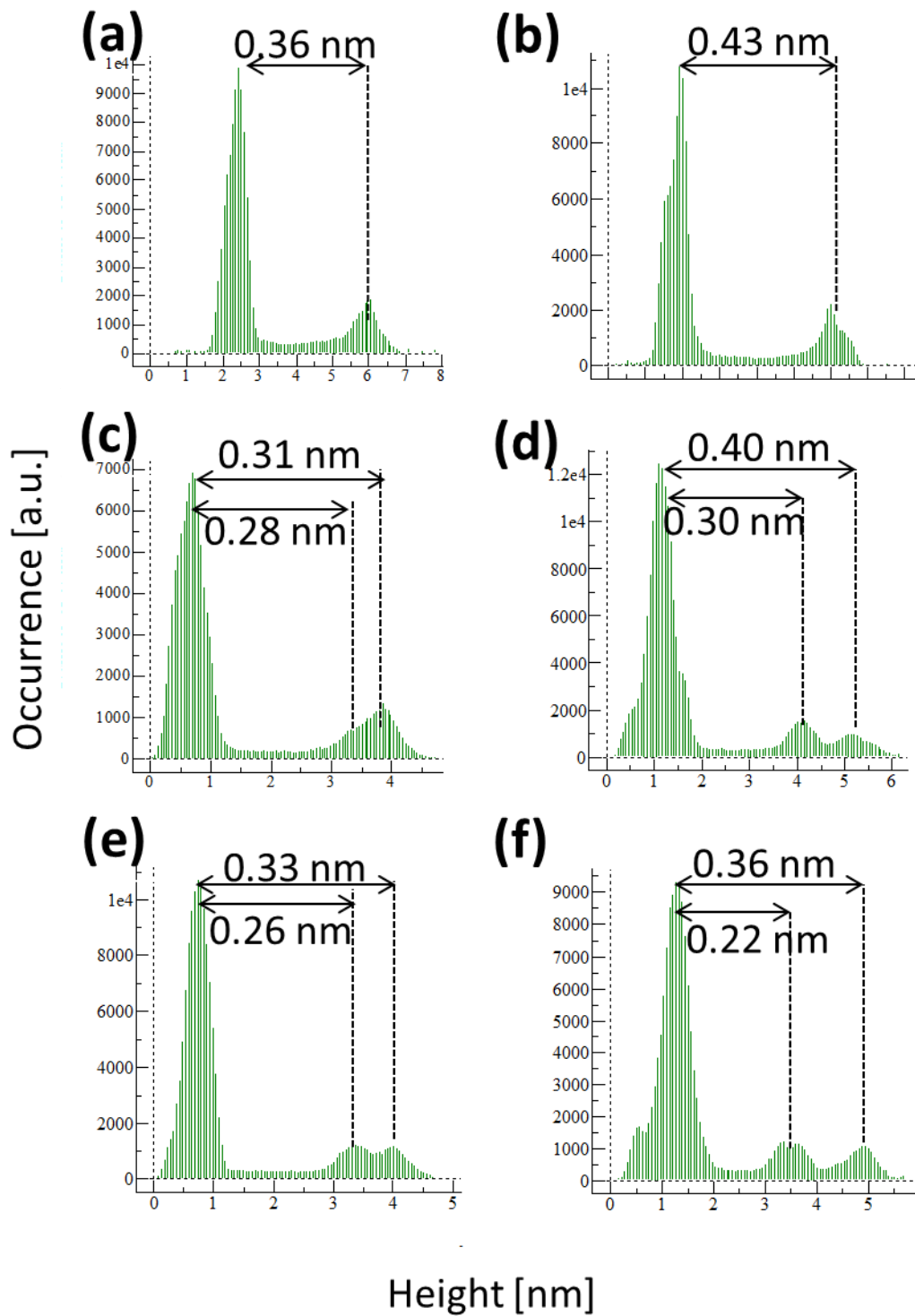


Figure 18

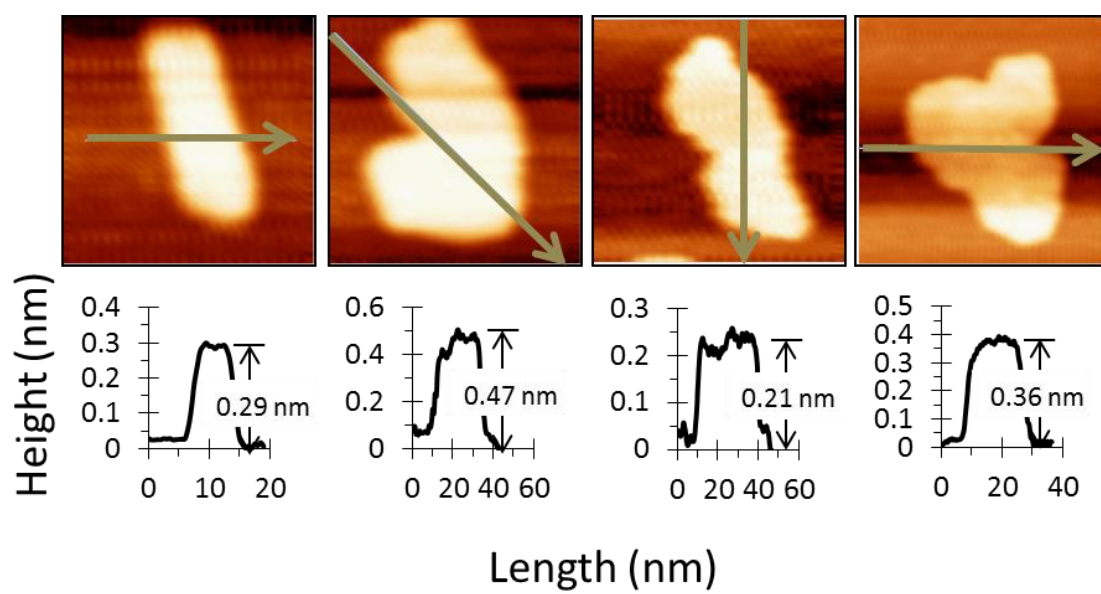


Figure 19

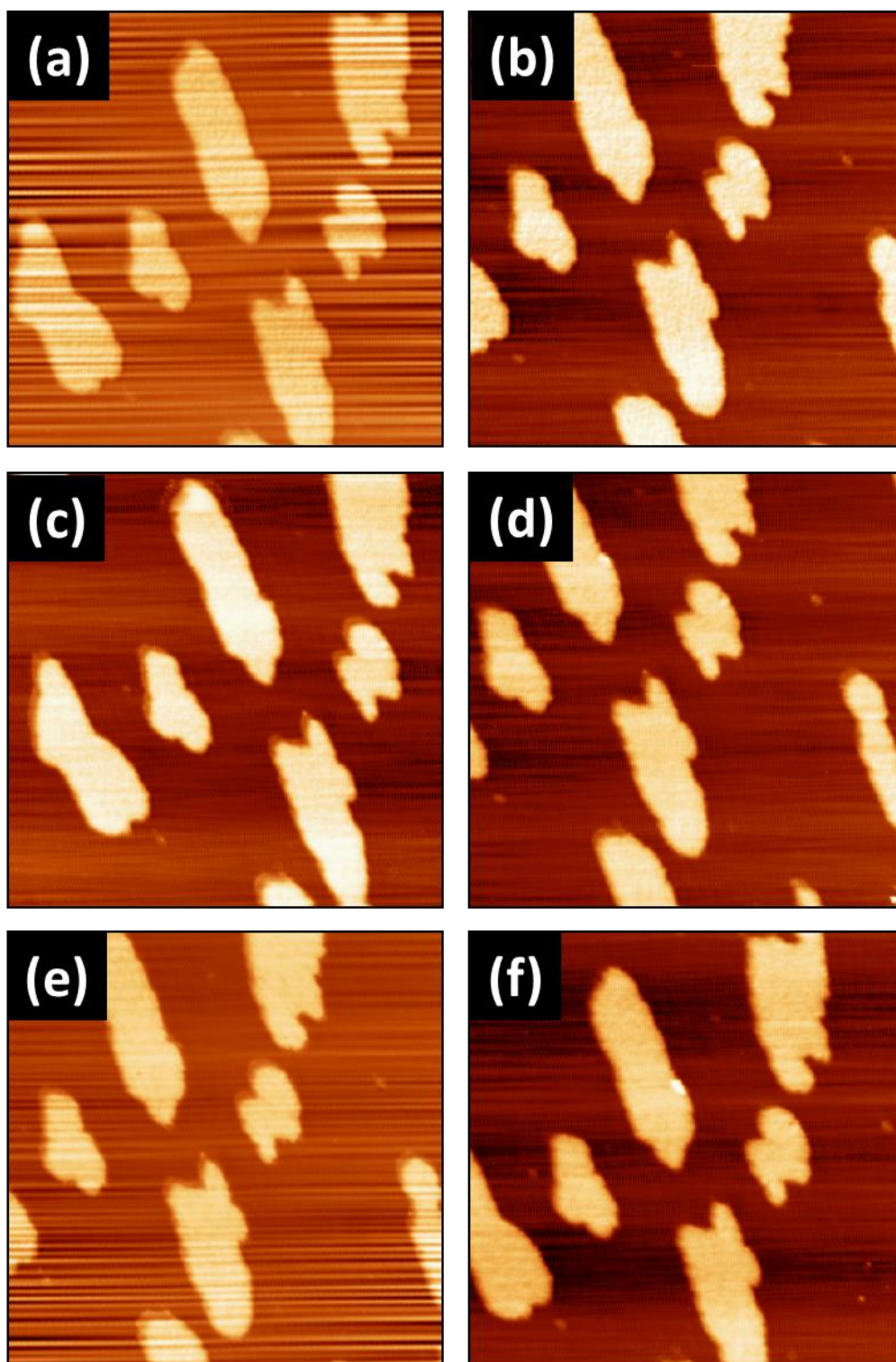


Figure 20

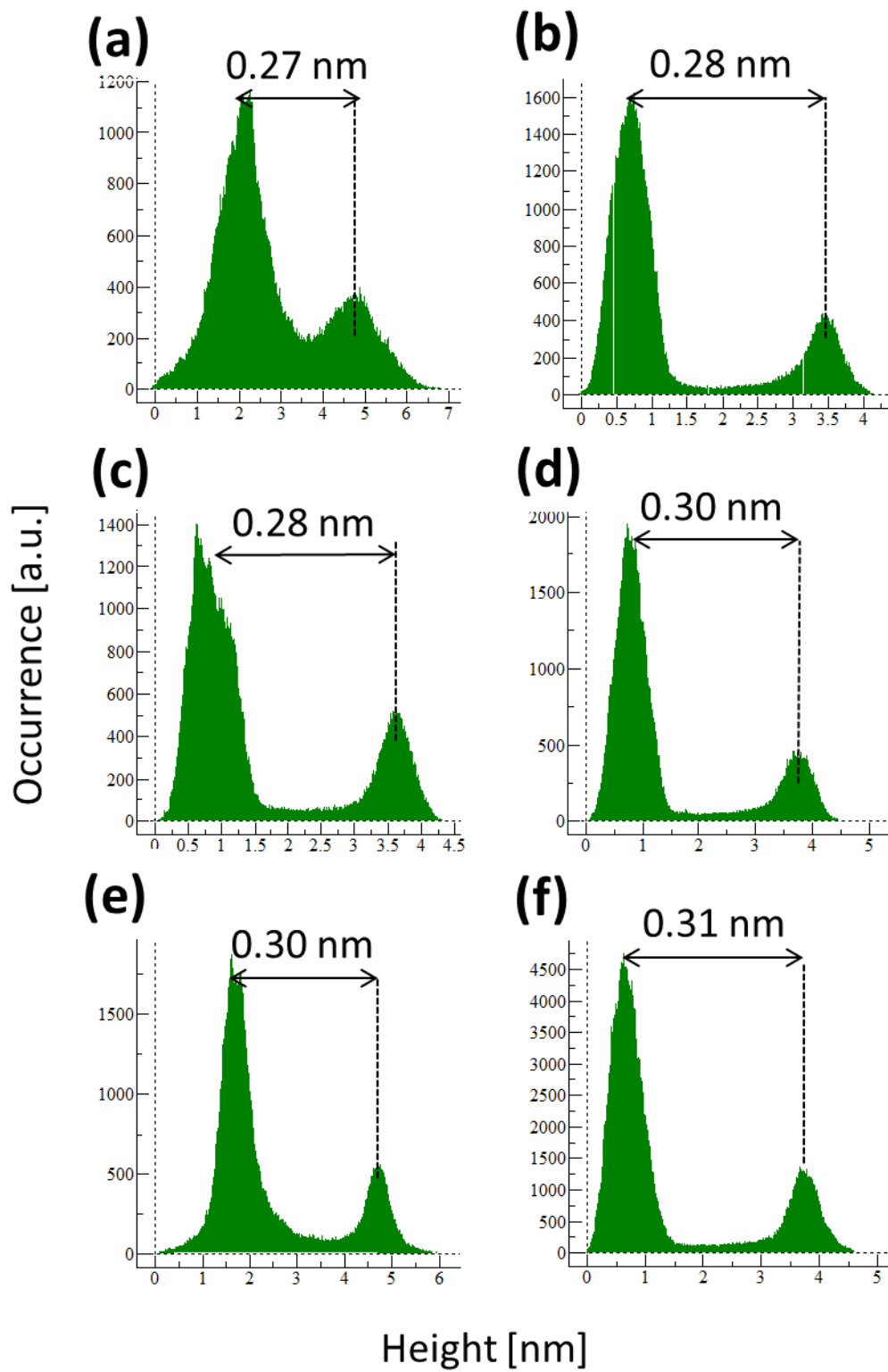


Figure 21

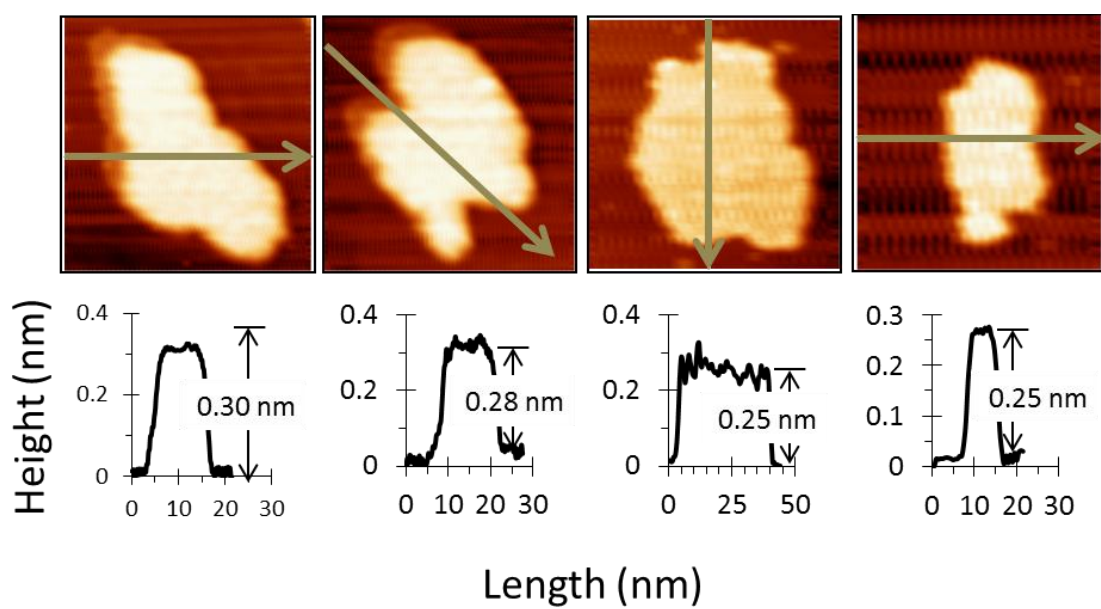


Figure 22

CHAPTER 6

A Comparison of the Ag and Au Structures on NiAl(110) using XPD and STM

Chad D. Yuen,^{1,2} Roland Widmer,⁴ Oliver Gröning,⁴ and Patricia A. Thiel^{1,2,3}

¹Ames Laboratory, Iowa State University, Ames, Iowa 50011

²Department of Chemistry, Iowa State University, Ames, Iowa 50011

³Department of Material Science and Engineering, Iowa State University, Ames, Iowa 50011

⁴EMPA Materials Science and Technology, Ueberlandstrasse 129, CH-8600 Duebendorf, Switzerland

1. Introduction

In Chapter 4, we introduced studies of Au and Ag overlayers on NiAl(110), reviewed some of our past work, and presented new results for Au/NiAl(110) using STM and XPS. In this Chapter, we present a study of both systems in which the primary technique is X-ray photoelectron diffraction (XPD), which is a powerful technique for determining short-range atomic structure. Because this technique is not available in our laboratory, we established a collaboration with the group of Dr. Roland Widmer at EMPA in Switzerland. He and his co-workers are experts in this method and they have a well-equipped laboratory for XPD studies of surfaces.

X-ray photoelectron diffraction is similar to XPS in the sense that X-rays incident on the sample cause ejection of core electrons (these are the so-called photoelectrons). The difference is that in XPS, the object of analysis is the *energy distribution* of the photoelectrons within a narrow range of emission angles. In XPD, the object of analysis

is the *spatial distribution* of the photoelectrons within a narrow window of kinetic energies, corresponding to electron emission from a specific element. The spatial distribution is inhomogeneous because the photoelectrons emitted from a single nucleus can be scattered by neighboring nuclei. When the emitted photoelectron interferes constructively with components of scattered photoelectron, diffraction conditions are met. As a result, emission from the surface is not isotropic. If the sample is single-crystal, then the emission pattern reflects local arrangements of scatterers of specific atomic identity. More details about the technique, and examples of its use in surface science, are given in a review by Woodruff and Bradshaw [1].

Our goal is to study and compare the first few monolayers of Ag and Au on NiAl (110) using XPD. Certain candidate structures were identified in past work from our group. We use single scattering cluster (SSC) calculations to generate model XPD patterns expected from these candidate structures of Ag and Au on NiAl(110), and we compare these models to our XPD results. In addition, the XPD experiments are supplemented by some XPS, STM, and low-energy electron diffraction (LEED) experiments that were performed concurrently in Dr. Widmer's laboratory.

2. Experimental Details

The XPS/XPD, STM, and LEED experiments were carried out in an Omicron ESCA ultra-high vacuum (UHV) chamber. This chamber consisted of two parts: a preparation chamber and an analysis chamber. The preparation chamber was equipped with a sputter plasma gun, room temperature STM/AFM, and rear-view LEED optics.

The analysis chamber was equipped with a VSW 125 HR electron analyzer, and an x-ray source (Al K α). The X-ray source was perpendicular to the sample plate. The base pressures of the preparation chamber and the analysis chamber were below 1×10^{-9} mbar and 1×10^{-10} mbar, respectively.

The NiAl(110) was cleaned via Ar⁺ sputtering and annealing. For sputtering, the plasma source was operated at pressures of 6×10^{-6} mbar to 8×10^{-6} mbar. The emission current was 5 mA and the accelerating voltage was 1 kV. The sputtering time was 5 to 15 minutes. The sample was heated via an electron beam. For annealing, the sample was held for 1 to 3 hours at 1200 K.

Ag and Au were deposited from a homemade two-pocket multi-evaporator, one for Ag and one for Au. Each pocket contained a W filament that had been formed into a spiral. The ends of the W wire were connected to copper feedthroughs. Ag or Au wires were placed into the middle of the spiral W filament. The evaporator was heated resistively.

All metal depositions were performed with the sample at room temperature. Between each deposition, the sample was cleaned by sputtering and annealing. In other words, no sequential depositions were performed.

In most cases, metal coverages were determined by flooding the STM images. In the case of Ag, islands often were attached to NiAl step edges, so the entire image could not be flooded. Instead, we zoomed in on individual islands and measured their areas. The fractional surface area covered by metal islands was reported in units of bilayers (BL). (Note that a unit of 1 BL here is chosen to be consistent with the units used in Ref. [2], and also with some of the structural models. In describing the experimental data, it

has the same meaning as the unit of monolayer used in other chapters, i.e., fractional surface coverage.) In one case (noted in the text), coverage was determined by comparing integrated XPS peak intensities.

In XPS and XPD, we used the photoelectron peaks of the Ni $3p_{3/2}$, Al $2s_{1/2}$, Ag $3d_{5/2}$, and Au $4f_{7/2}$ because they were most intense. XPS data were acquired by taking a survey spectrum from 0 eV to 1210 eV, followed by closer examination of individual peaks in narrower energy ranges: Ni $3p_{3/2}$ at 60 eV - 72 eV; Al $2s_{1/2}$ at 110 eV - 125 eV; Ag $3d_{5/2}$ at 362 eV - 378 eV; and Au $4f_{7/2}$ at 75 eV - 95 eV. XPD data were measured by collecting core-level photoelectron intensities over a dense grid of polar emission angles (θ) from grazing emission (90°) to normal emission (0°), and over the full 360° azimuthal angle (φ) range.

In the XPD patterns reported in this paper, the grazing emission intensities (displayed near the edges of the outer ring) represent photoelectrons emitted nearly parallel to the surface plane. Intensities near the center of the ring represent photoelectrons emitted along the surface normal. The photoelectron intensity was displayed in a linear black-and-white scale where white corresponded to maximum intensity.

All experimental data were acquired while the sample was at room temperature.

3. Experimental Results: Ag on NiAl(110)

3.1 STM, XPD, and LEED for Ag on NiAl(110)

After the surface was introduced from air, we performed cleaning cycles as described in Section 2, and checked with STM to determine when a step-terrace structure began to emerge. This structure became visible after about 12 cleaning cycles. Representative STM images of the clean surface are shown in Fig. 1. Terraces are about 100 nm wide.

At this point, we began to deposit Ag. STM images and XPD patterns for different Ag coverages are shown in Fig. 2. The STM images in Fig. 2(a) and (b) were all acquired before the XPD measurements. In STM, long rectangular islands of Ag can be identified on the surface. They grow outward from step edges. These features are quite similar to those reported by Ünal et al. [2].

In Fig. 2(a), the Ag coverage is 0.65 ± 0.03 BL. No Ag XPD pattern is seen, as shown in Fig. 2(b). It is likely that this coverage of Ag is insufficient to generate a Ag XPD pattern.

At a slightly higher coverage, 0.77 ± 0.09 BL of Ag, an almond-shaped XPD pattern begins to emerge, as shown in Fig. 2(d). It is even clearer at higher coverage, 1.2 ± 0.1 BL total coverage, as shown in Fig. 2(e). Though the XPD pattern is stronger, it does not appear to contain any different features. Note especially that there are several strong features near normal emission.

LEED patterns were also recorded right after the 1.2 BL deposition. These are shown in Fig. 3, for incident electron energies from 60 eV to 200 eV. The patterns in Fig.

3 have rectangular symmetry as would be expected for both Ag(110) and NiAl(110). These results are consistent with the LEED results of Jing et al. for Ag on NiAl(110), which showed no change in the symmetry or number of diffraction spots in the diffraction pattern when low coverages of Ag were deposited on NiAl(110) [3].

Lastly, we deposited 5 BL of Ag. (In this case, the coverage was determined by comparing the integrated XPS Ag $3d_{5/2}$ peak with that from 1.2 BL, where coverage had been established via STM.) The XPD pattern is shown in Fig. 2(g). Although weaker than at 1.2 BL, it shows the same features as the Ag XPD patterns in Fig. 2(d) and 2(f) at lower Ag coverages. No STM images or LEED patterns are available at this coverage of Ag.

Additional information from STM is available. In one experiment, we measured STM both before and after XPD, to see if XPD had any effect on the surface. Fig. 4(a) shows an STM image before XPD, at 0.65 BL of Ag. This image is taken from the same experiment as in Fig. 2(a). Fig. 4(b) shows a line profile across a Ag island, corresponding to the black arrowhead in Fig. 4(a). Based on the line profile, the island height is 0.34 nm, in agreement with the prior results [2].

An STM image of this same surface after XPD is shown in Fig. 4(c), where one can see small pits on the Ag islands. In addition, there are many protrusions or bumps on the substrate. Fig. 4(d) shows a line profile across a Ag island, corresponding to the black arrowhead in Fig. 4(c). The island height is now 0.38 nm. Overall, it appears that the Ag islands remain intact but suffer minor damage from XPD. It is well known that techniques such as XPS often produce low levels of surface contamination that are

detectable in STM, so the changes between Fig. 4(a) and Fig. 4(c) are likely due to contamination.

In addition, STM can provide information on the fine structure in the islands at high magnification. For that purpose, high-magnification STM images were also taken in the same experiment as in Fig. 2(a), at a coverage of 0.65 BL. These images are shown in Fig. 5. There are diagonal stripes or rows across the Ag islands. In Fig. 5(e), there are two types of distances between rows which are labeled DL (long) and DS (short). These two distances alternate. DL and DS have values of 1.30 ± 0.10 nm and 0.60 ± 0.07 nm, respectively. The total distance (D), which combines DL and DS, is 1.95 ± 0.06 nm. These results are not too different from those of Ünal et al., [2; 4] where DL, DS, and D were 1.2 nm, 0.8 nm, and 2.0 nm, respectively, and the lengths also alternated.

3.2 Comparing SSC Models with XPD Patterns for Ag on NiAl(110)

Our collaborators, Dr. Yong Han and Prof. Jim Evans, earlier found a number of possible stable structures for Ag on NiAl(110) that are reasonably close in energy, based on Density Functional Theory (DFT). The seven SSC models and their real structures are shown in Fig. 6 and Fig. 7, respectively. We will call these seven the 1BL, 2BL, and 3BL fcc (110) structures, the (2x1) rippled structure, the square – hex structure, the (3x1) rippled structure, and the square – square – hex structure. More information on these structures can be found in Ref. [5]. SSC calculations were done on these structures and the results are shown in Fig. 6.

It is noteworthy that some of the SSC models do not have any spots in the center of the pattern, corresponding to near-normal emission. For example, in Fig. 6, the SSC

models in (a), (d), (e), (f), and (g) do not have any spots in the center of the pattern. This is due to the fact that the models are only 1 BL coverage of Ag on the substrate. Photoelectrons which escape at grazing emission angles are more surface-sensitive than those which escape near normal angles, because in grazing emission the path length through the surface layer is longer. Hence, normal emission tends to build up as the thickness of the metal film increases.

By comparing the SSC models with the experimental XPD results, we can quickly see differences. None of the SSC models that contain a single layer or single bilayer—(110) structure, (2x1) rippled structure, square – hex structure, (3x1) rippled structure, and the square – square – hex—match the experimental XPD results (see Fig. 6 and Fig. 2). The reason that these SSC models do not match well with the XPD pattern is that in the experimental data, there are spots near the center of the experimental pattern. In the SSC models mentioned above, there are no spots near the center of the pattern. Hence, the SSC 1 BL models and the XPD result do not match.

However, there are spots in the center of the SSC model pattern of the 2 BL and 3 BL Ag (110) structures. Furthermore, the almond shape of the most intense spots in each model matches the general shape of the experimental pattern. Figure 8 shows the SSC model of the 1 BL Ag(110) structure (in green) overlaid on top of the experimental XPD pattern (in gray). We can see that certain spots in the SSC model do not overlap well with the measured XPD pattern and vice versa. Therefore, the 1 BL Ag(110) structure does not match our Ag XPD pattern. However, it is possible that small changes in the lattice constant of the model would bring the SSC model pattern in closer alignment with the experimental pattern. We see similar results with the 2 BL and the 3 BL Ag(110)

structure. These SSC models are overlaid on top of the experimental XPD pattern which is shown in Fig. 9 and Fig. 10, respectively. Again, we can see that certain spots in the SSC model (green overlay) do not overlap with spots in the measured XPD pattern (in gray) and vice versa. Again, it is possible that small changes in the lattice constant of the model would bring these spots into better alignment.

In conclusion, the measured XPD patterns do not match any of the structure models for Ag on NiAl(110). Further work is needed to establish the atomic structure of these metal islands.

4. Experimental Results: Au on NiAl(110)

4.1 STM, XPD, and LEED for Au on NiAl(110)

No STM images are available for Au deposition. LEED results show a rectangular arrangement of diffraction spots, similar to the 1.2 BL Ag coverage. The LEED images are shown in Fig. 11 ranging from 60 eV to 200 eV. After LEED, we then started XPD. The XPD results for Au showed no pattern. This is shown in Fig. 12(a). However, XPS showed Au photoelectron peaks, indicating there was Au on the surface (see Fig. 12(b)). Therefore, we concluded that there was not enough Au on the surface to generate an XPD pattern for Au. More experiments need to be performed.

4.2 SSC Models

DFT suggests four possible structures of Au on NiAl(110), which are the square – hex structure variations 1 and 2, and the square – hex – hex structure variations 1 and 2. More information on these structures can be found in Ref. [5]. SSC calculations were

done on these structures and are shown in Fig. 13 and their real structures are shown in Fig. 14.

5. Conclusions

The goal of this work was to measure XPD patterns for both Ag and Au on NiAl(110). In the case of Ag, a clear almond-shaped pattern was recorded for the Ag $3d_{5/2}$ peak, over a range of Ag coverages from 0.6 BL to 5 BL. STM and LEED were performed concurrently, and those results were consistent with prior experimental results for this system. In STM, the existence of long, rectangular islands growing outward from NiAl step edges, the heights of the Ag islands, and the existence of fine ripples on island tops, were all comparable to previous results[2]. Possible structures of Ag and Au had been determined by our colleagues, using DFT. These candidate structures served as the basis for SSC calculations of model XPD patterns. For Ag on NiAl(110), seven model patterns were generated. None of them matched well with the experimental XPD patterns of Ag, although it is possible that small changes in the lattice parameters of the structure model would result in better agreement. Only one attempt was made to deposit Au on NiAl. The results showed no XPD pattern for Au, probably indicating insufficient coverage of Au.

Acknowledgements

This work was supported by the Office of Science, Basic Energy Sciences, Materials Sciences and Engineering Division of the US Department of Energy (USDOE).

This manuscript has been authorized by Iowa State University of Science and Technology under Contract No. DE-AC02-07CH11358 with the US Department of Energy. We are indebted to the group of Dr. Roland Widmer at EMPA Materials Science and Technology, Switzerland for allowing us to collaborate by letting use their XPD system and expertise.

References

- [1] D.P. Woodruff, A.M. Bradshaw, *Rep. Prog. Phys.* 57 (1994) 1029-1080.
- [2] B. Unal, F. Qin, Y. Han, D.-J. Liu, D. Jing, A.R. Layson, C.J. Jenks, J.W. Evans, P.A. Thiel, *Physical Review B* 76 (2007) 195410.
- [3] D. Jing, *Metal thin film growth on multimetallic surfaces from quaternary metallic glass to binary crystal*, Iowa State University, Ames, 2010.
- [4] Y. Han, B. Unal, D. Jing, F. Qin, C.J. Jenks, D.-J. Liu, P.A. Thiel, J.W. Evans, *Physical Review B* 81 (2010) 115462.
- [5] T. Duguet, Y. Han, C. Yuen, D. Jing, B. Unal, J.W. Evans, P.A. Thiel, *Proceedings of the National Academy of Sciences* 108 (2011) 989-994.

Figure Captions

Figure 1

STM image of the clean NiAl (110) at 300 K. The STM parameters are (a) 50 nm x 50 nm, $I = 0.50$ nA, $V\text{-tip} = -1$ V, (b), 100 nm x 100 nm, $I = 0.5$ nA, $V\text{-tip} = +2$ V, and (c) 100 nm x 100 nm, $I = 0.50$ nA, $V\text{-tip} = -1$ V.

Figure 2

STM images (color) and XPD patterns (gray) of Ag on NiAl(110) at 300 K (a-b) 250 nm x 250 nm (0.65 BL), (c-d) 250 nm x 250 nm (0.77 BL), (e-f) 150 nm x 150 nm (1.2 BL), and (g) 5 BL. The tunneling conditions for all STM images are $I = 0.5$ nA and $V\text{-tip} = +2$ V.

Figure 3

LEED images after 1.2 BL of Ag deposition and STM, but before XPD at 300 K, (a) 60 eV, (b) 80 eV, (c) 100 eV, (d) 150 eV, and (e) 200 eV.

Figure 4

STM images of 0.65 BL Ag on NiAl(110) at 300 K, (a) before XPD, 150 nm x 150 nm, (b) line profile from the black arrowhead in (a), (c) after XPD, 150 nm x 150 nm, (d) line profile from the black arrowhead in (c). The tunneling conditions for all the STM images are $I = 0.5$ nA and $V\text{-tip} = +2$ V.

Figure 5

High magnification STM images of the Ag islands on NiAl(110) at 300 K, (a) 40 nm x 40 nm, (b) 40 nm x 40 nm, (c) FFT filter 11 nm x 11 nm, (d) line profile taken by black arrowhead in (c), (e) 13 nm x 13 nm, and (f) line profile taken by the black arrowhead in (e). The coverage is 0.65 BL Ag. The tunneling conditions for all STM images are $I = 0.5$ nA and $V\text{-tip} = +2$ V.

Figure 6

SSC calculations of the seven possible structures of Ag on NiAl(110), (a) 1 BL fcc (110) structure, (b) 2 BL fcc (110) structure, (c) 3 BL fcc (110) structure, (d) (2x1) rippled structure, (e) square – hex structure, (f) (3x1) rippled structure, and (g) square – square – hex structure.

Figure 7

Real Structure models of Ag/NiAl(110), (a) 1 BL fcc (110) structure, (b) 2 BL fcc (110) structure, (c) 3 BL fcc (110) structure, (d) (2x1) rippled structure, (e) square – hex structure, (f) (3x1) rippled structure, and (g) square – square – hex structure. The purple circles represent the silver atoms, the red circles represent the aluminum atoms, and the green circles represent the nickel atoms. The purple outlined in the top view images represent a silver atom on top of either the aluminum or nickel atom.

Figure 8

Comparing experimental XPD pattern with SSC model, (a) Experimental XPD pattern of 1.2 BL Ag, (b) SSC model of 1 BL fcc (110) structure, (c) SSC 1 BL fcc (110) structure overlaid on top of experimental XPD 1.2 BL pattern. The green model represents the SSC calculations and the gray model represents the experimental XPD pattern. The experimental XPD pattern (gray) was rotated 14° in order to overlap with the SSC model.

Figure 9

Comparing experimental XPD pattern with SSC model, (a) Experimental XPD pattern of 1.2 BL Ag, (b) SSC model of 2 BL fcc (110) structure, (c) SSC 2 BL fcc (110) structure overlaid on top of the experimental XPD 1.2 BL pattern. The green model represents the SSC calculations and the gray model represents the experimental XPD pattern. The experimental XPD pattern (gray) was rotated 14° in order to overlap with the SSC model.

Figure 10

Comparing experimental XPD pattern with SSC model, (a) Experimental XPD pattern of 1.2 BL Ag, (b) SSC model of 3 BL fcc (110) structure, (c) SSC 3 BL fcc (110) structure overlaid on top of the experimental XPD 1.2 BL pattern. The green model represents the SSC calculations and the gray model represents the experimental XPD pattern. The experimental XPD pattern (gray) was rotated 14° in order to overlap with the SSC model.

Figure 11

LEED images after Au deposition and STM, but before XPD at 300 K, (a) 60 eV, (b) 80 eV, (c) 100 eV, (d) 150 eV, and (e) 200 eV.

Figure 12

Au on NiAl(110) at 300 K, (a) XPD pattern of Au $4f_{7/2}$, and (b) survey XP spectrum.

Figure 13

SSC calculations of the four possible structures of Au on NiAl(110), (a) Square – hex (Structure 1), (b) Square – hex (Structure 2), (c) Square – hex – hex (Structure 1), and (d) Square – hex – hex (Structure 2).

Figure 14

Real Structure models of Au/NiAl(110), (a) Square – hex structure (version 1), (b) Square – hex structure (version 2), (c) Square – hex – hex structure (version 1), and (d) Square – hex – hex structure (version 2). The purple circles represent the gold atoms, the red circles represent the aluminum atoms, and the yellow circles represent the nickel atoms. The purple outlined in the top view images represent a gold atom on top of either the aluminum or nickel atom.

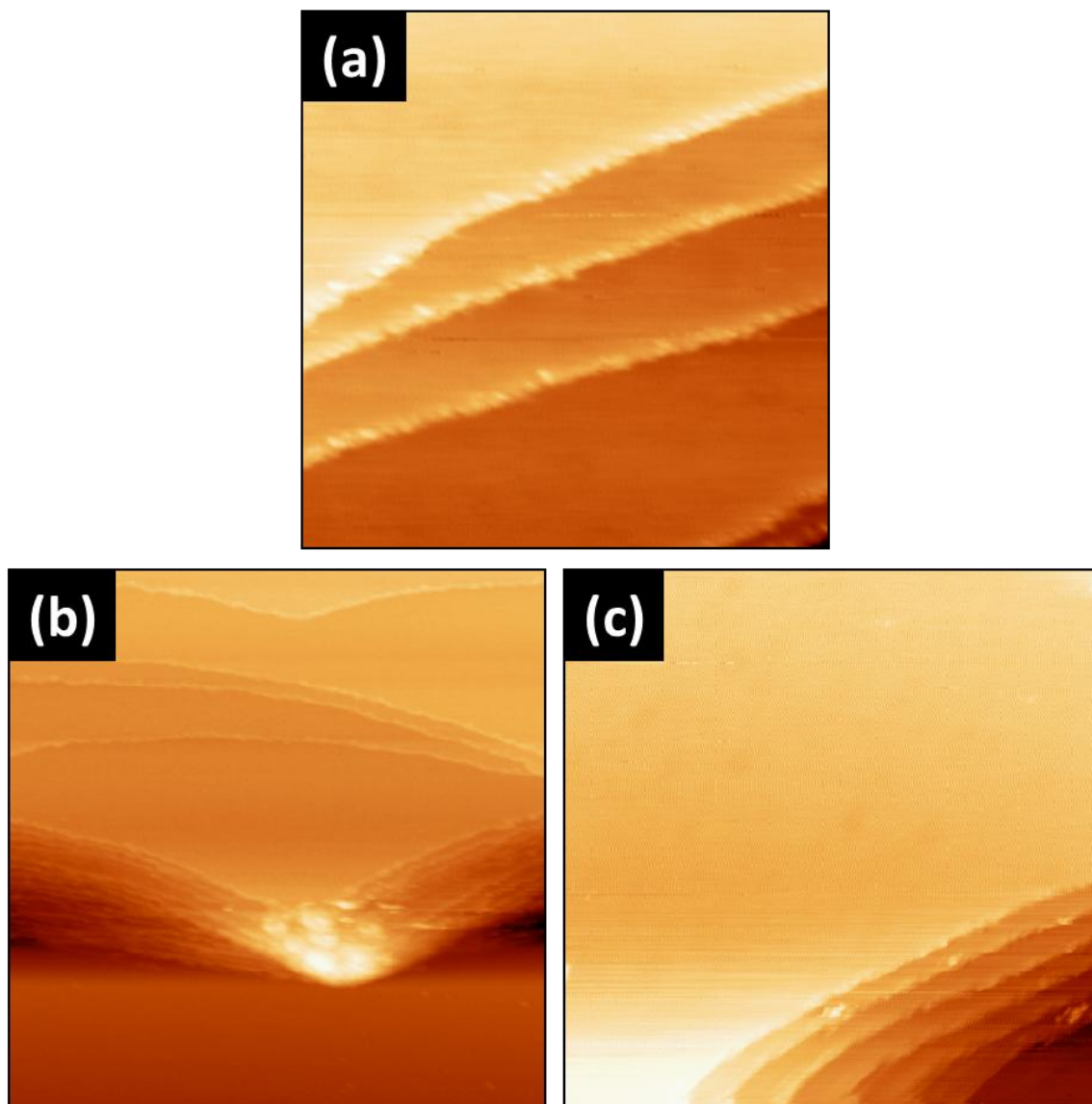


Figure 1

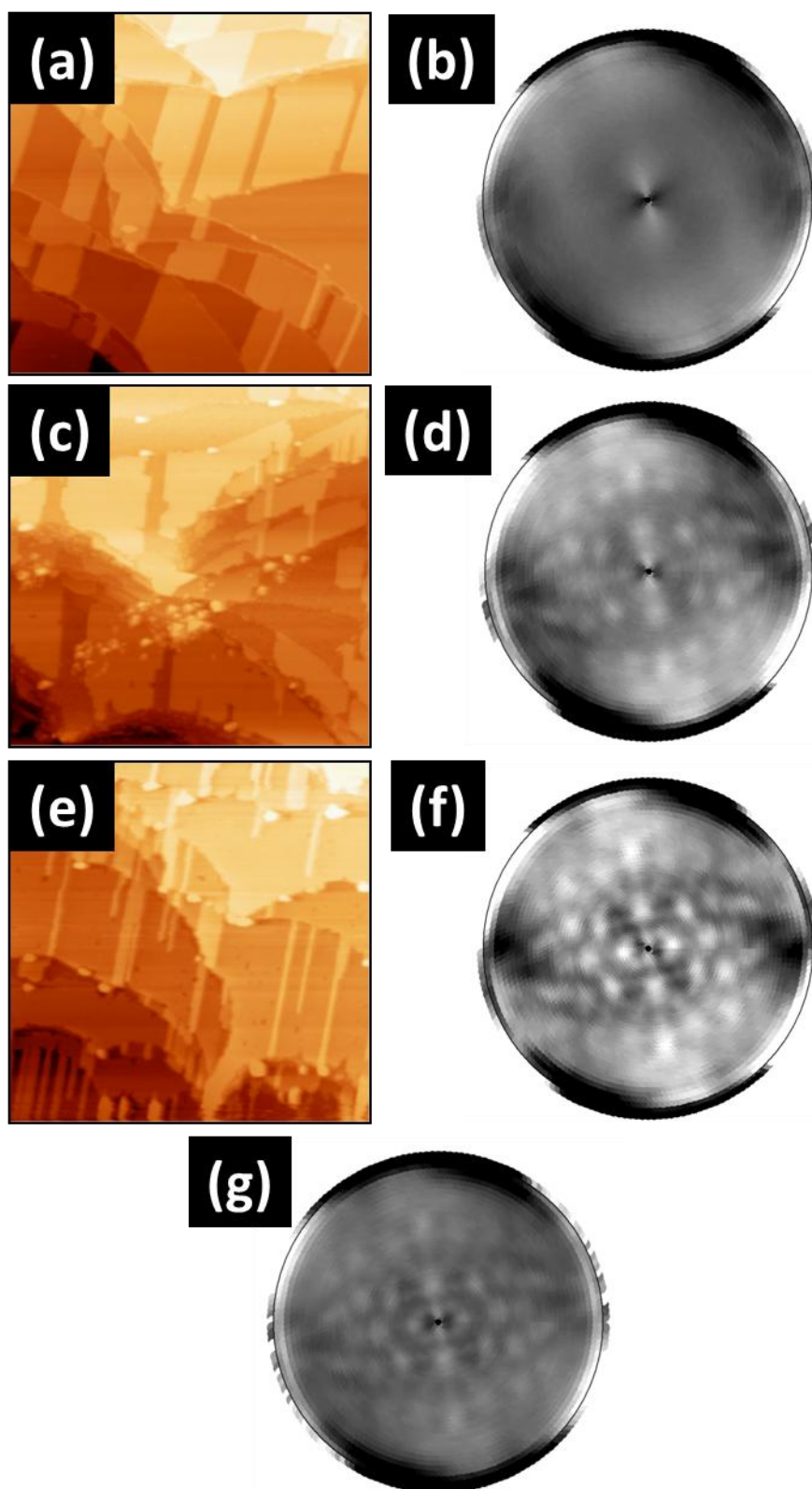


Figure 2

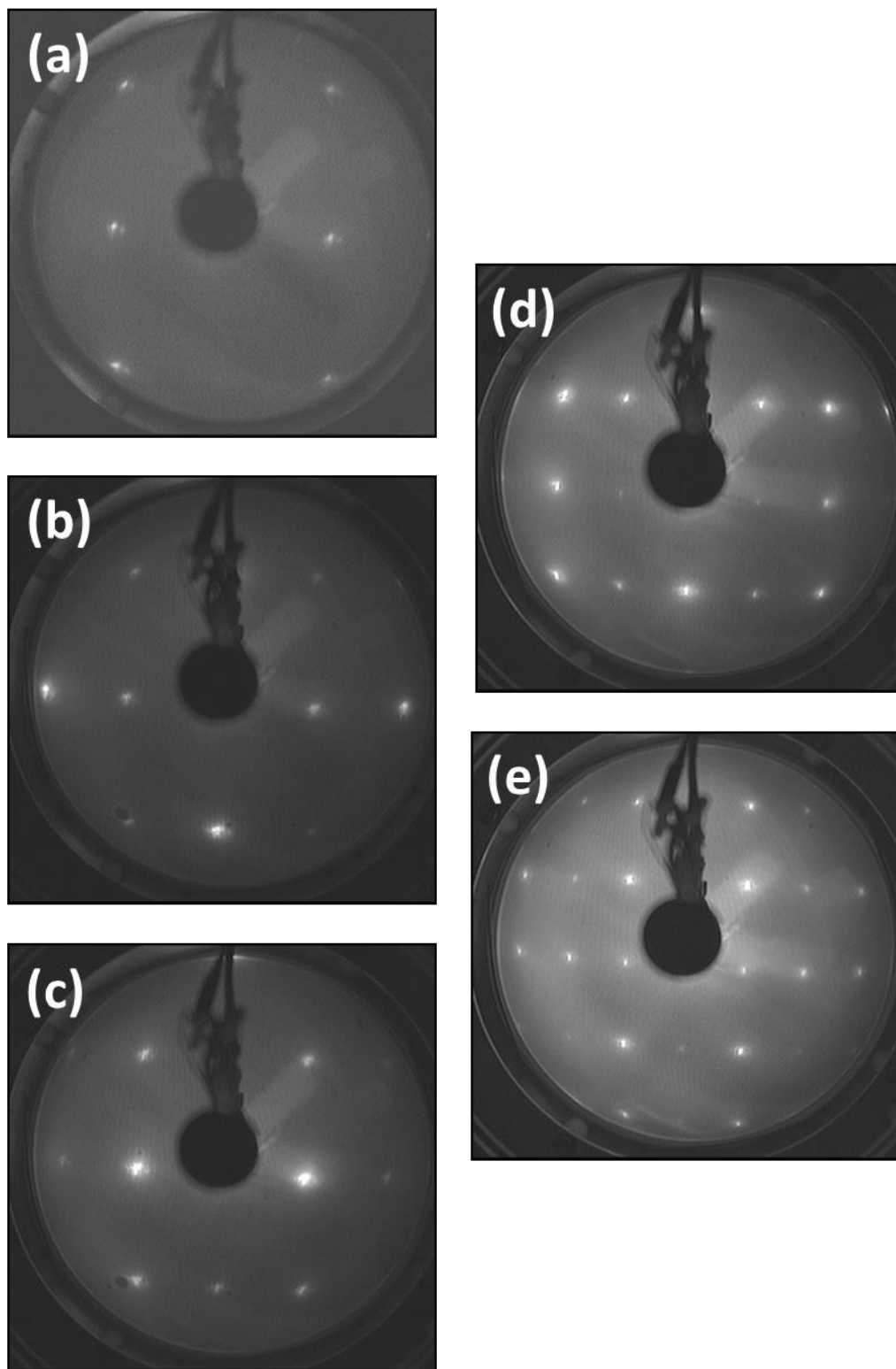


Figure 3

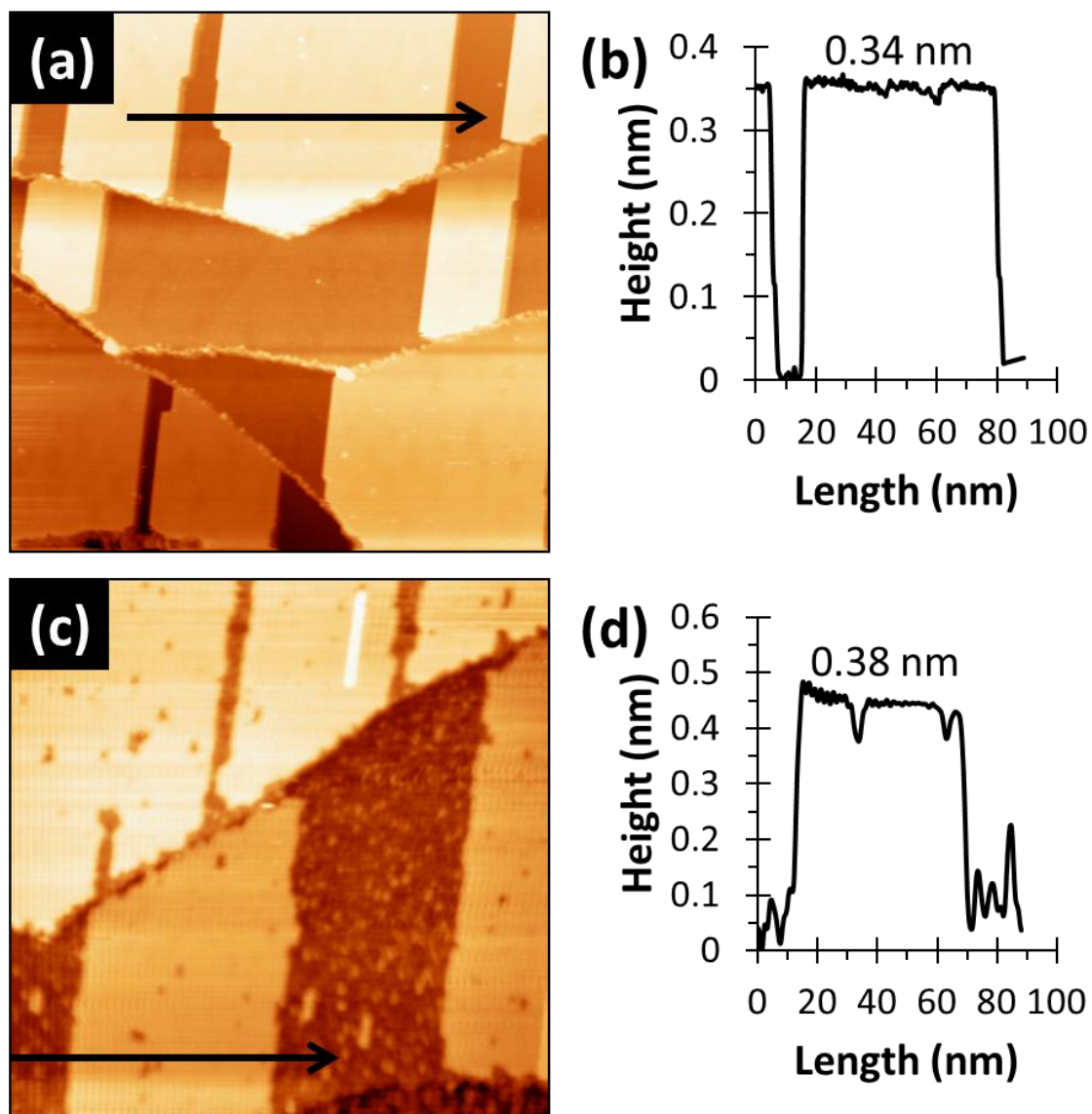


Figure 4

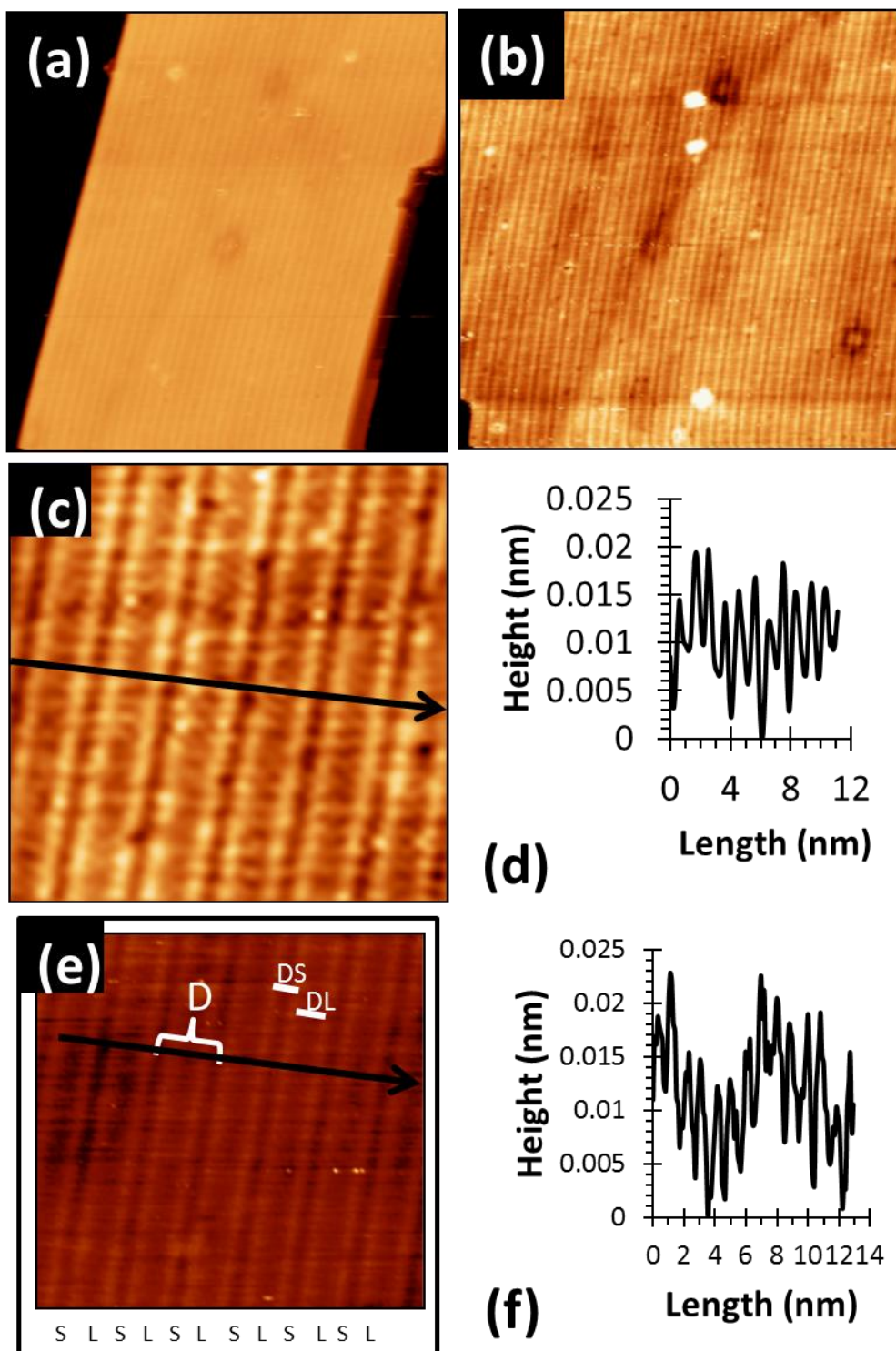


Figure 5

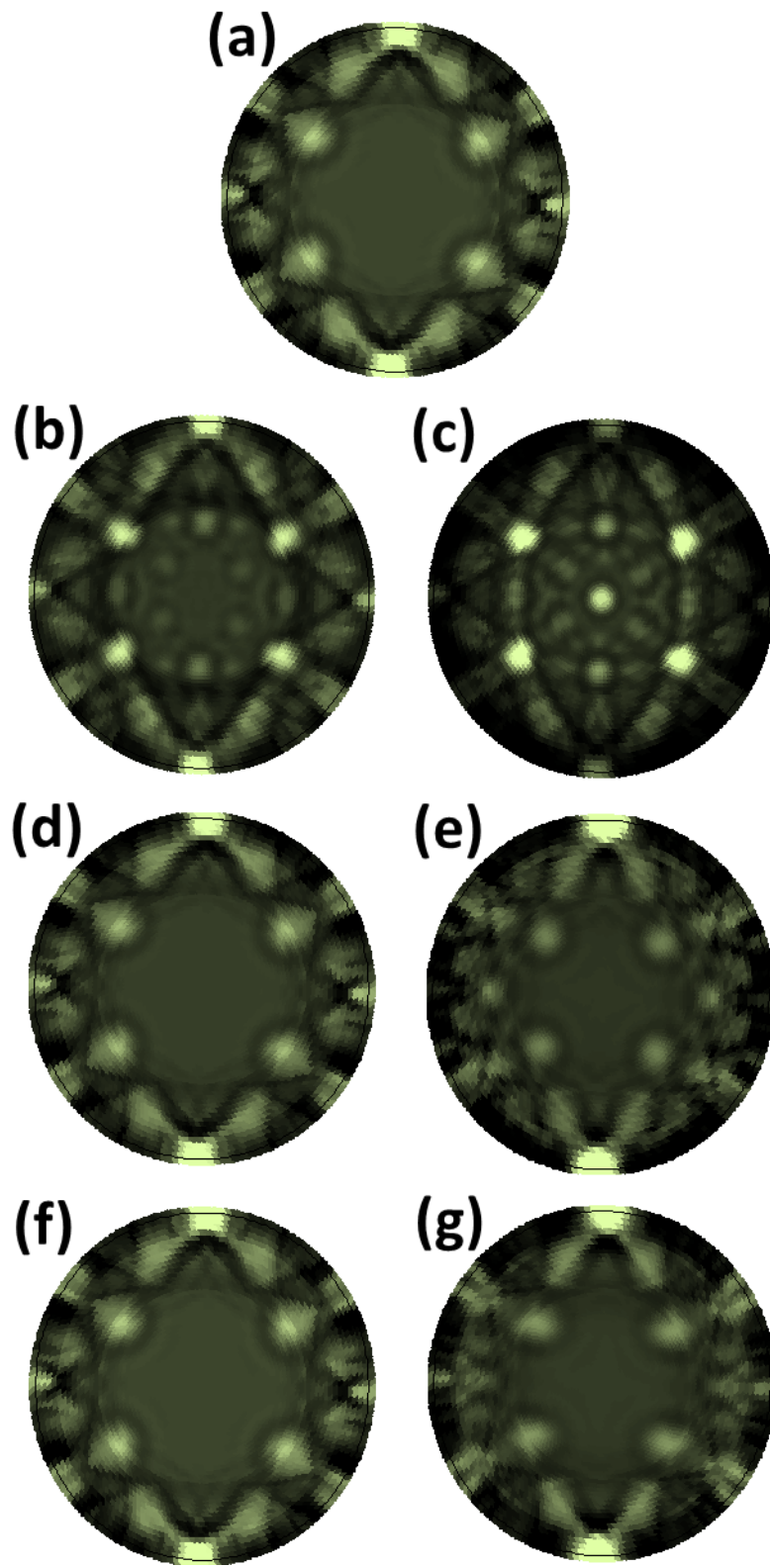


Figure 6

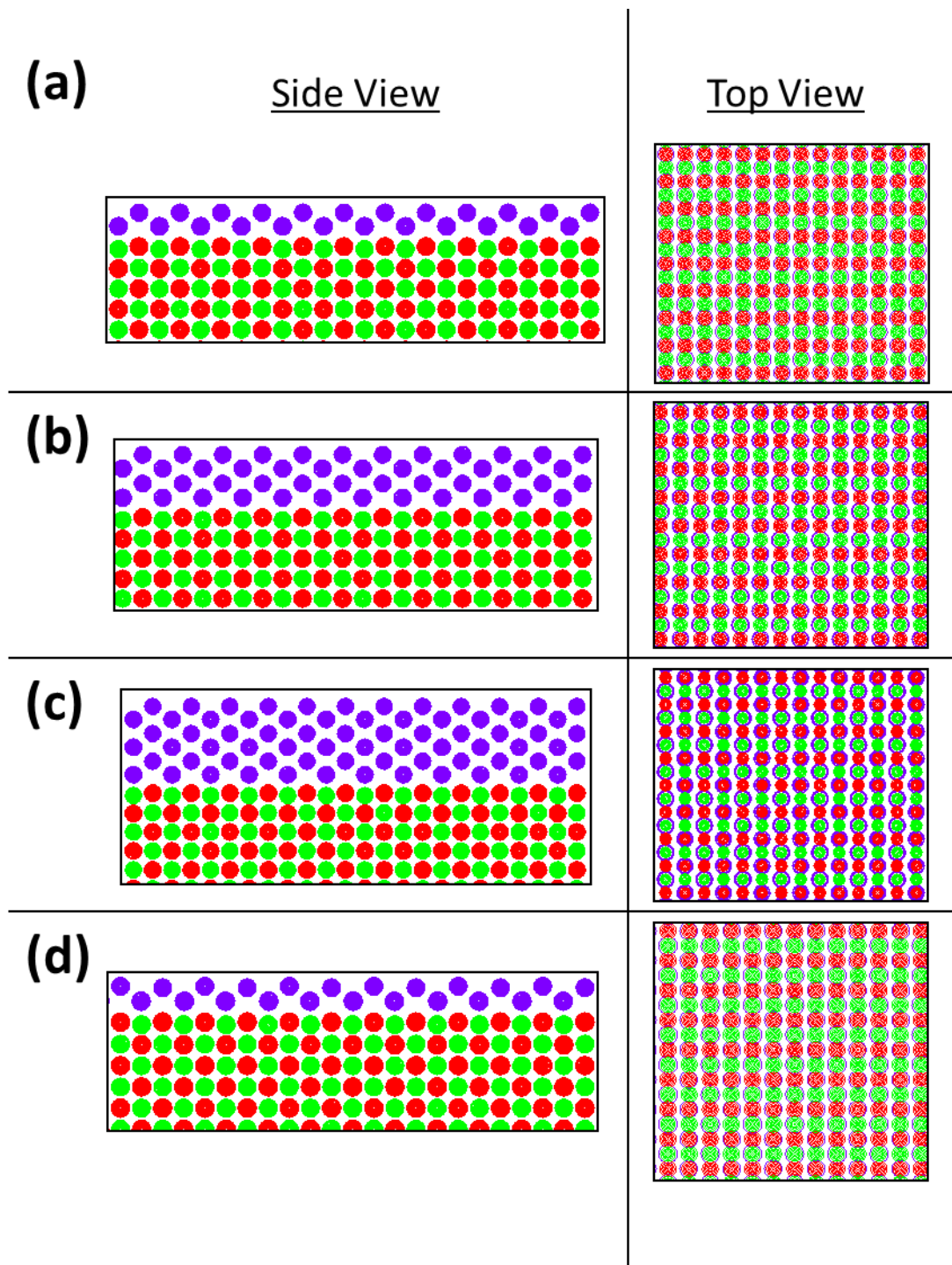


Figure 7

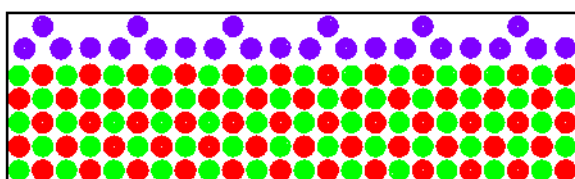
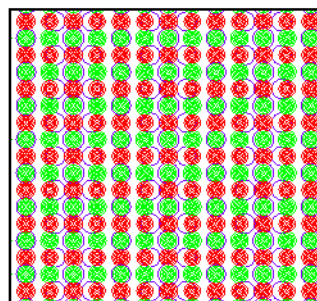
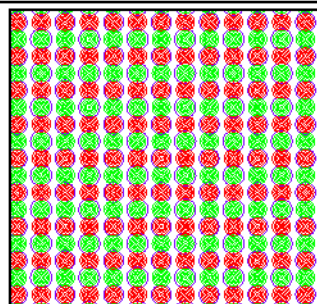
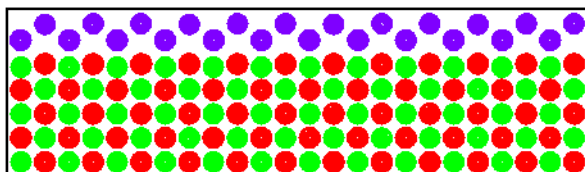
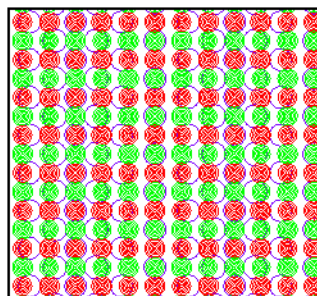
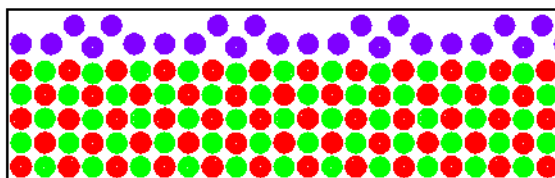
(e)Side ViewTop View**(f)****(g)**

Figure 7 (Continue)

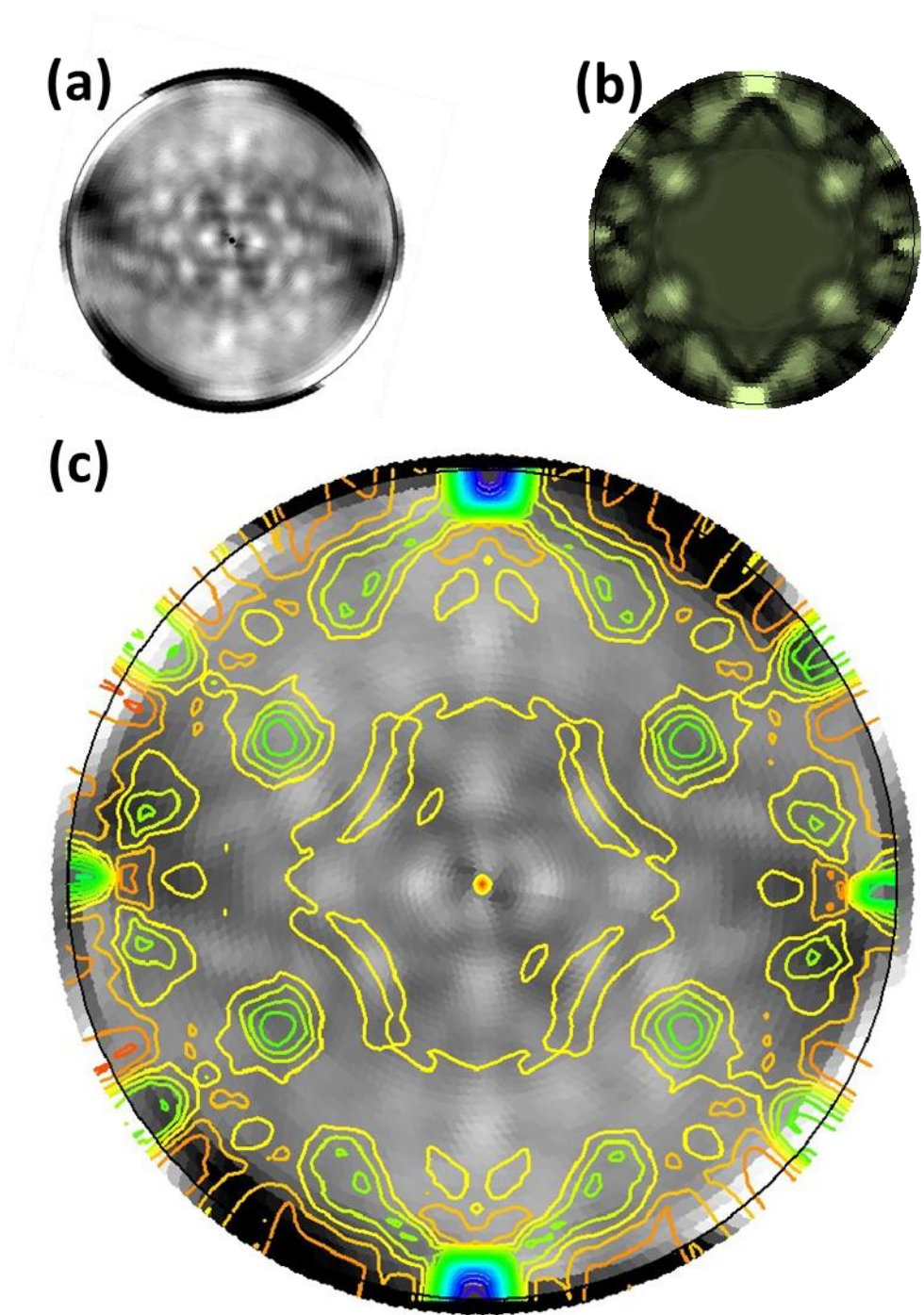


Figure 8

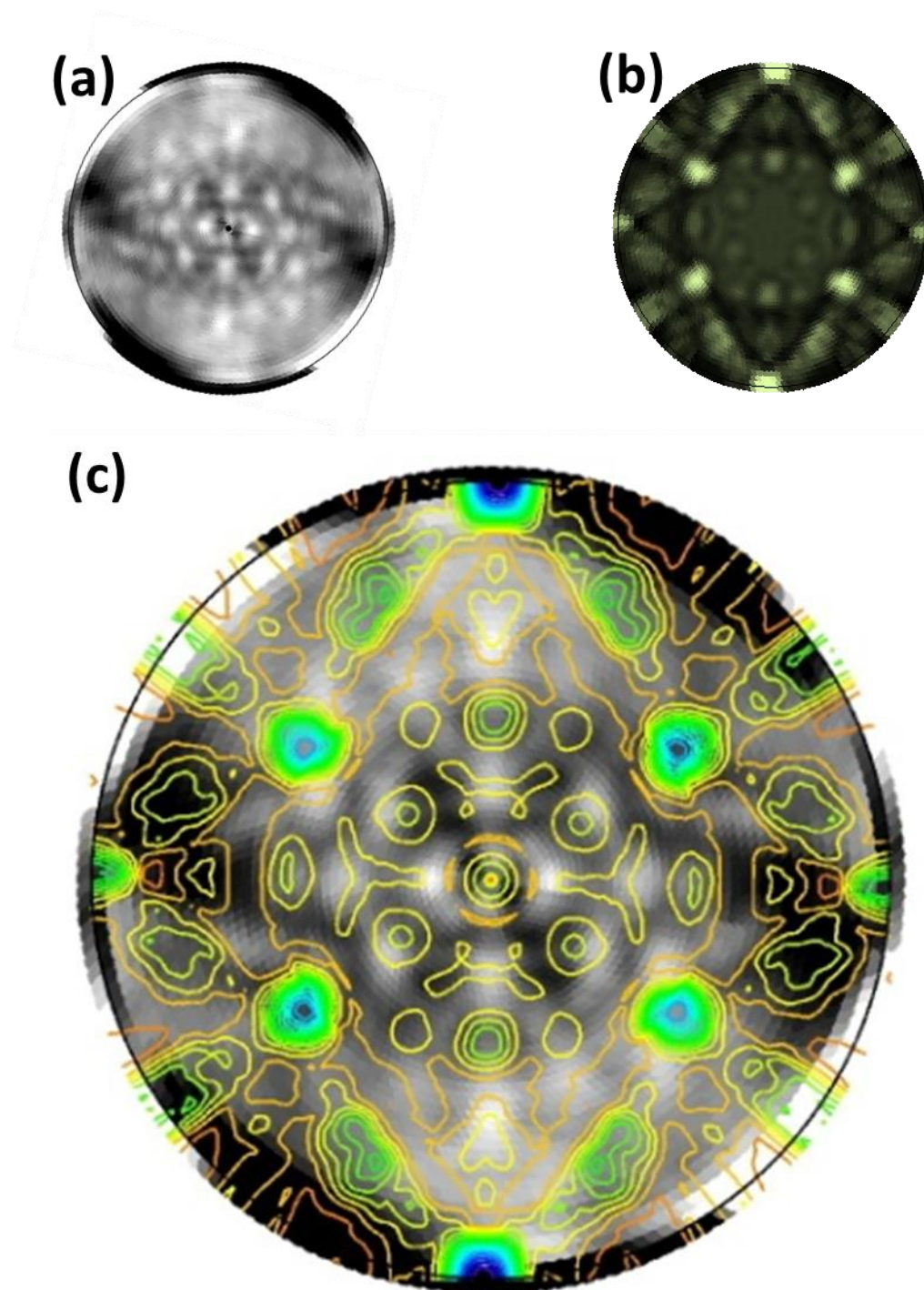


Figure 9

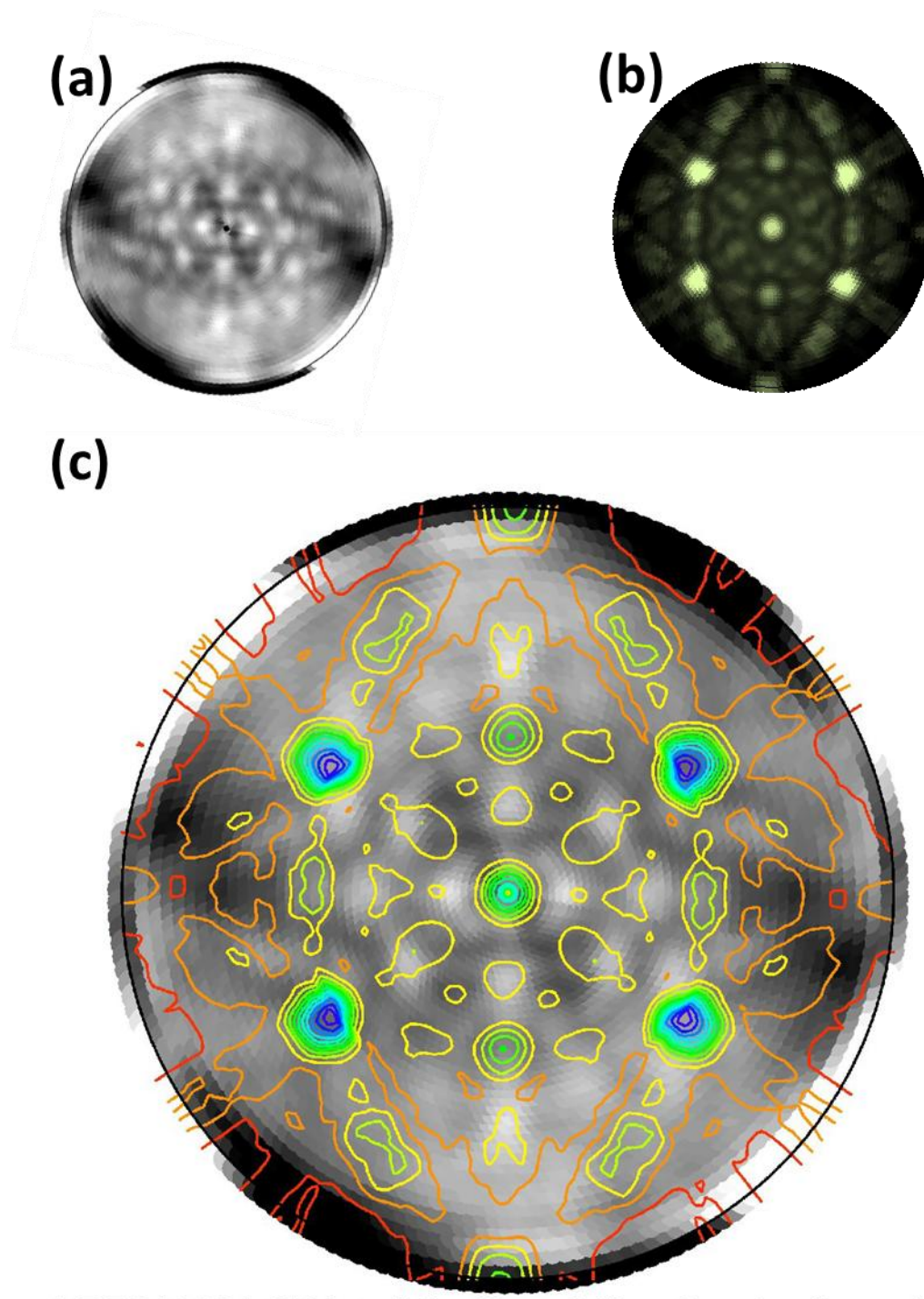


Figure 10

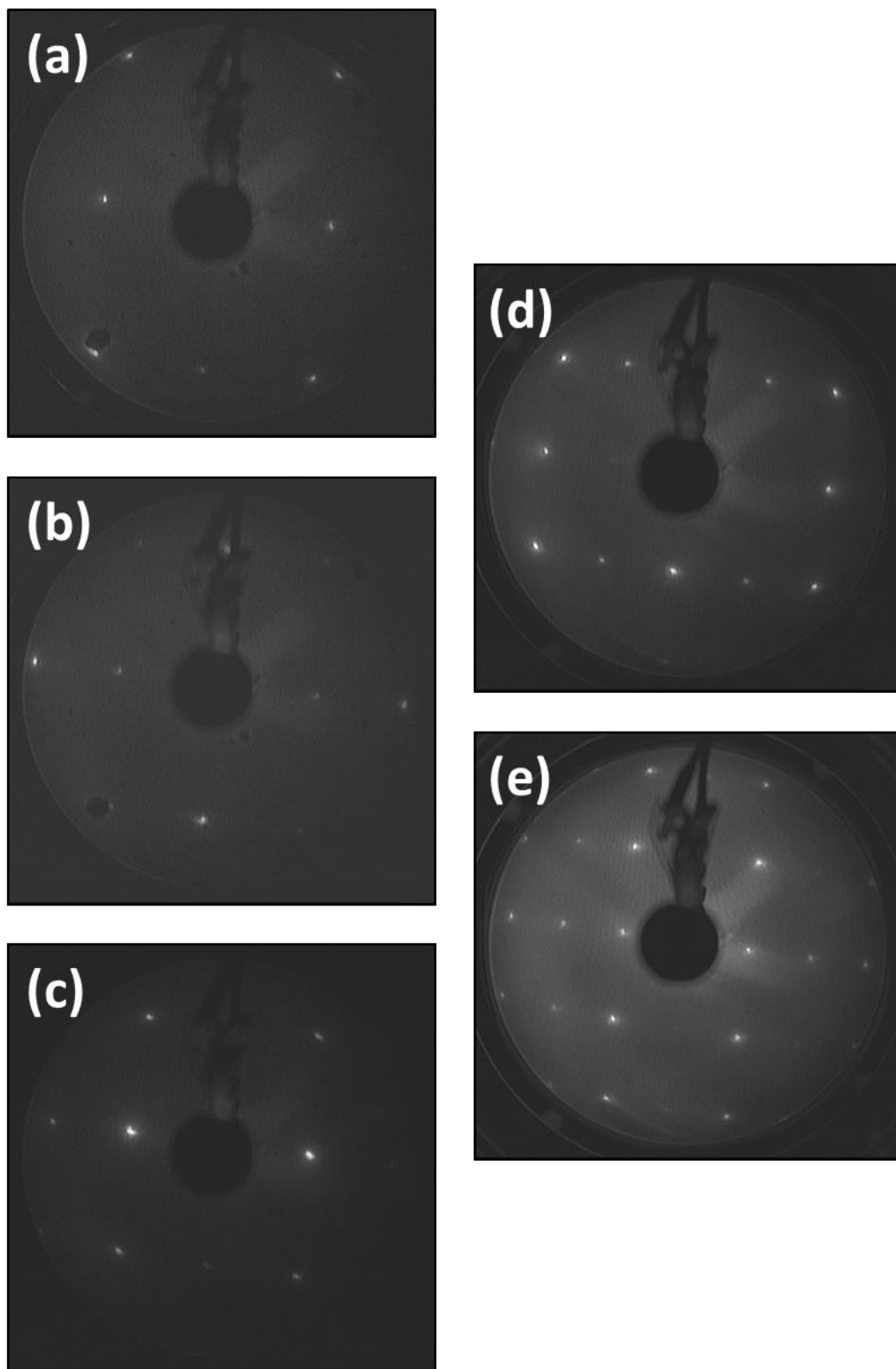


Figure 11

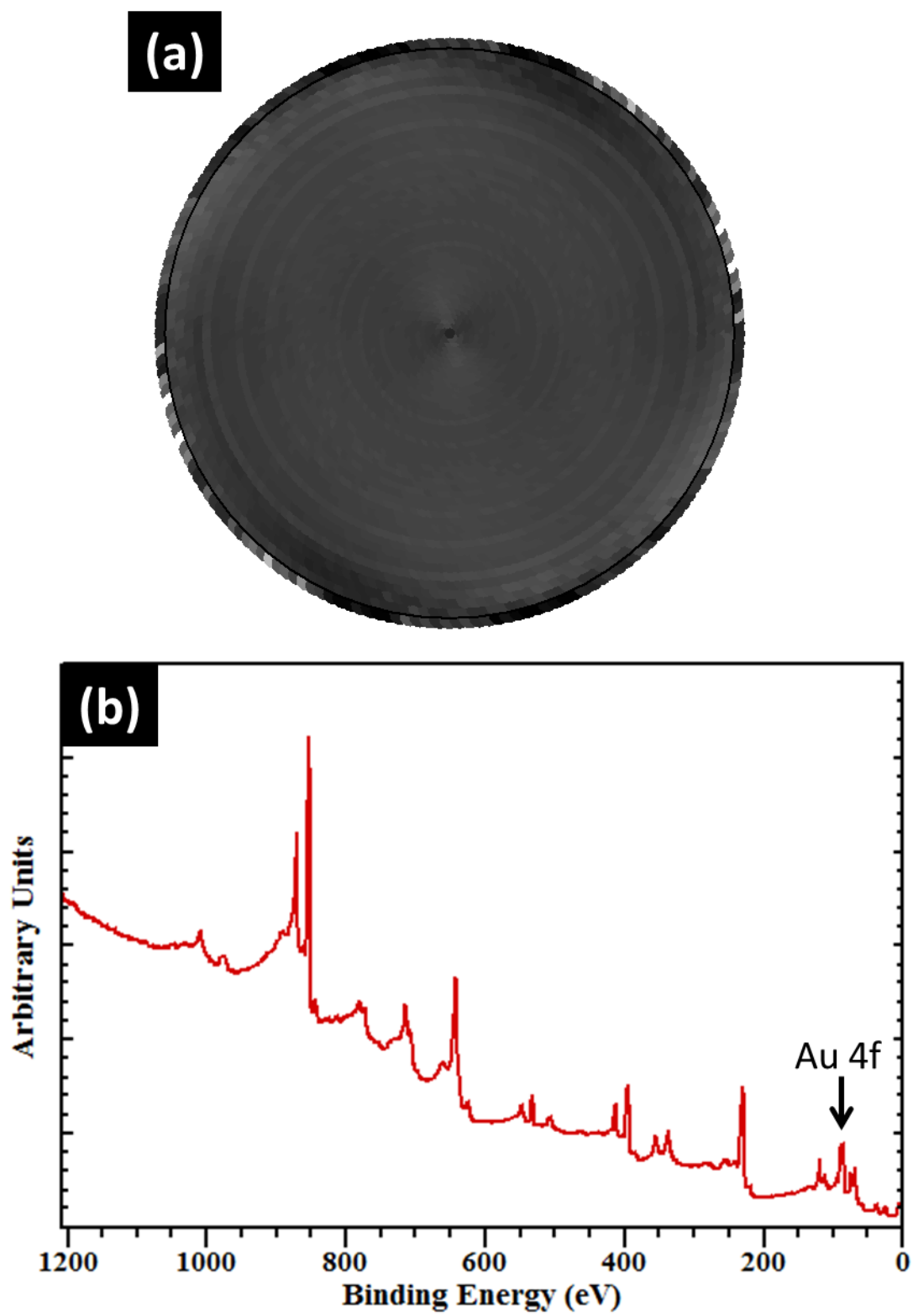


Figure 12

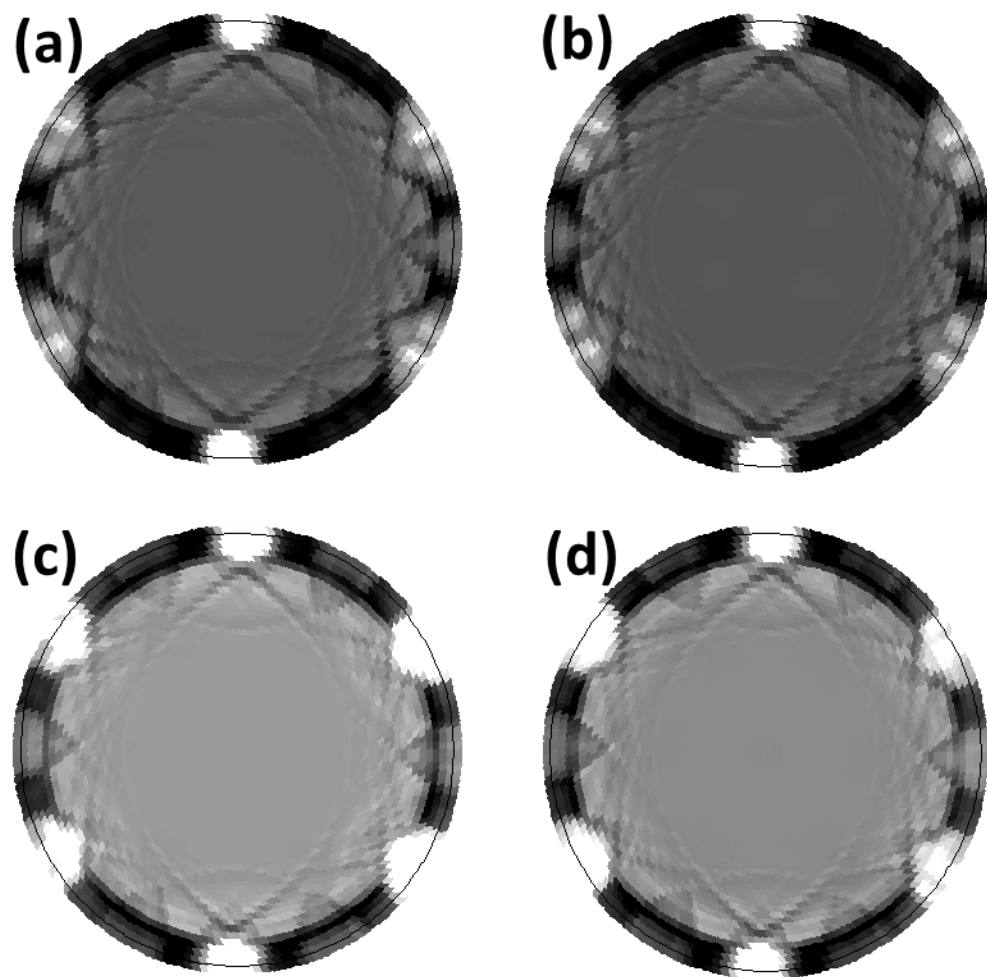


Figure 13

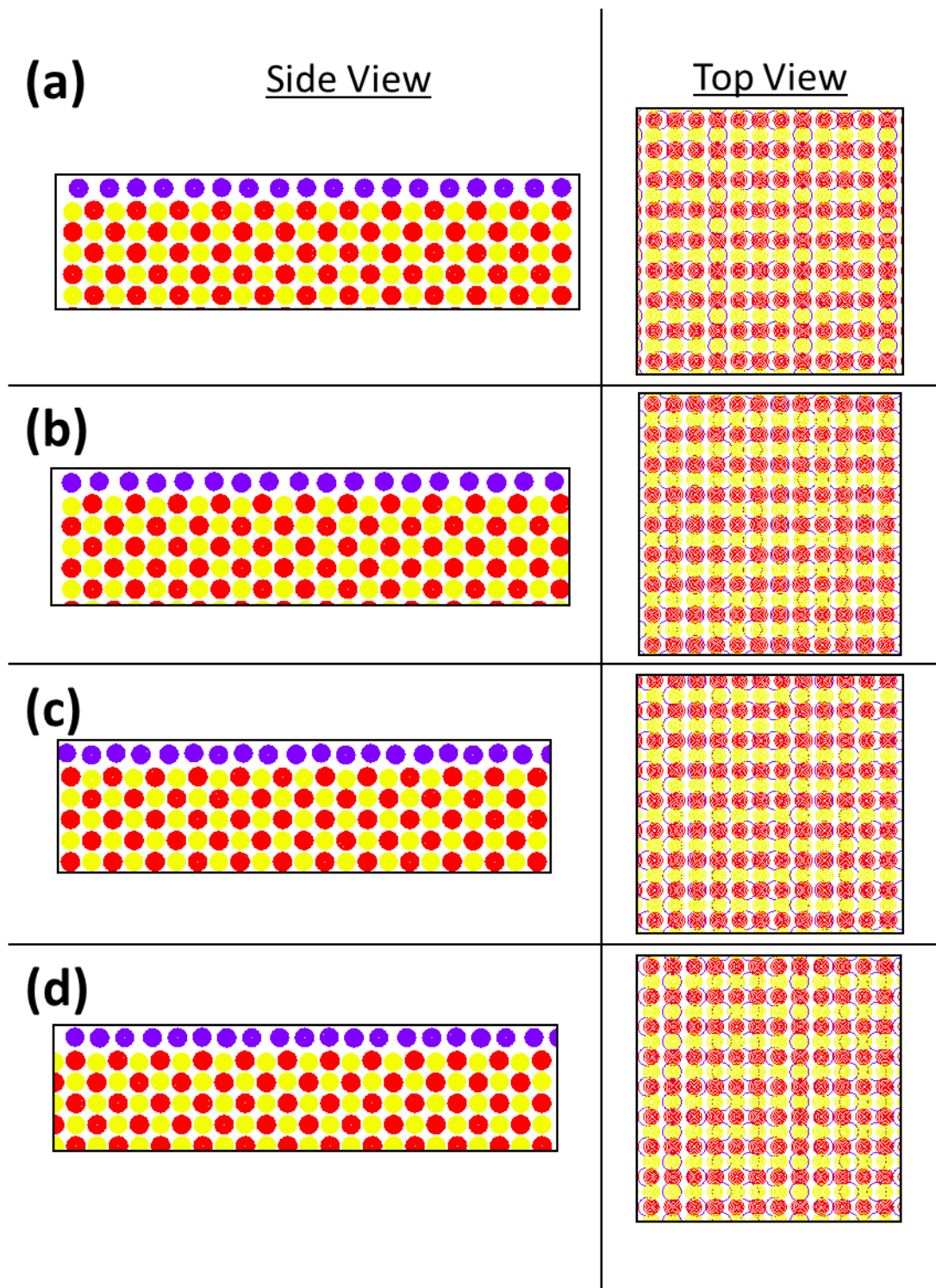


Figure 14

APPENDIX A. Using CasaXPS Software

I. File Formats

CasaXPS software only works on VAMAS file formats. Any formats with (*.aes) or (*.xps) does not work with this software (NOTE: The EIS software on the Omicron chamber in 225 Spedding can convert (*.aes) and (*.xps) formats into VAMAS formats). The procedure is as follows:

- 1) Save original data file (*.aes) or (*.xps) in the EIS program.
- 2) Once saved, go to File, export as, and then click on VAMAS.

Fortunately, you can convert some non-VAMAS formats into a VAMAS format. Listed below are the non-VAMAS formats that can be converted to VAMAS.

- SpecsLab I Files (*.exp)
- SuperESCA Files (*.allx)
- Kratos Files (*.kal)
- PHI MultiPak Files (*.spe), (*.pro), (*.ang)
- Scienta ASCII Files (*.sci)
- DS800 Files (*.mpa)
- Eclipse Files (*.dts), (*.dti)
- PCSurf Files (*.sp0)
- SSI Files (*.mrs), (*.dpr)
- PHI ASCII Files (*.asc)
- RBD ASCII Files (*.txt)
- Bristol Files (*.seq)
- Kore Files (*.lst)
- PSU Files (*.xyt)
- (*.npl)

II. Toolbar Information



Zoom In

The zoom-in icon zooms-in on your selected region of your spectrum.

1. Drag the mouse and select the region you want to zoom-in on your spectrum.



2. Click on the “Zoom-In” icon.



Zoom Out

The zoom-out icon brings back your original spectrum from your zoomed in region.



Reset

The reset icon brings back your original spectrum from either zooming-in or zooming-out.



Quantification Parameters

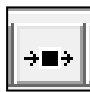
The quantification parameter icon allows you to create regions as well as calculating the atomic percent concentration, area, peak plus and peak minus values, etc.

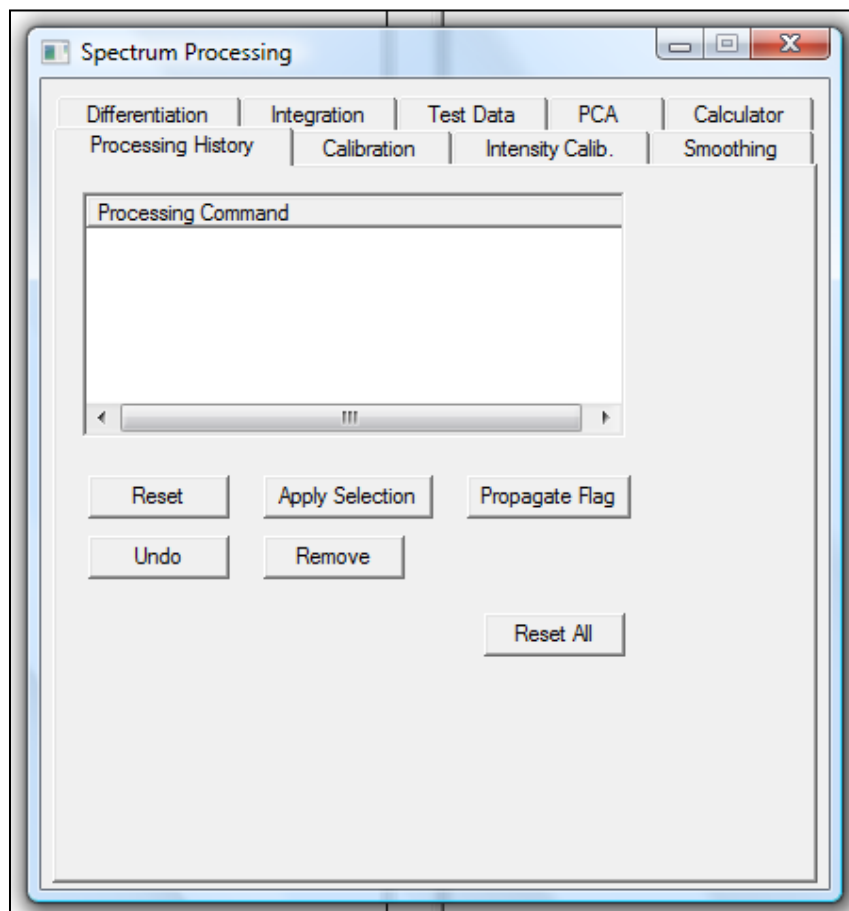


Spectrum Processing

The spectrum processing icon allows you to smooth, differentiate, and other types of data processing on your spectrum.

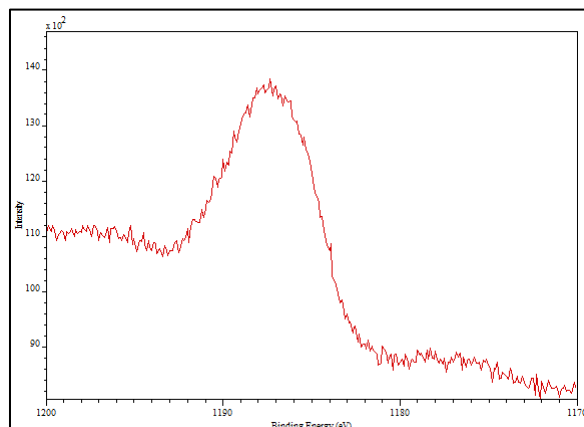


1. Click on the “Spectrum Processing”  icon.
2. A new window should appear depicted below.

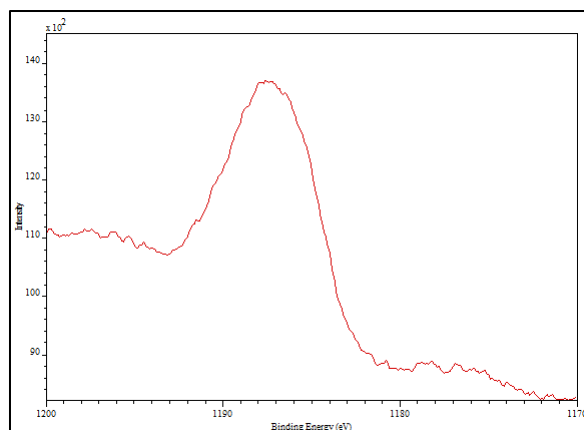


3. The “Processing History” tab tells you what you have processed from beginning to end. You can undo or reset any type of processing command that you have made.
4. The “Smoothing” tab allows you to smooth the spectrum. In the method section, there are four choices for smoothing, which are: SG Quadratic, SG Quartic, SG Linear, and Gaussian. The default is set to SG Quadratic. The smoothing width

section allows you to control the smoothness on your spectrum. The default value is set at 5. Once you have picked your preference on method and smoothing values, click on “Apply”. Below is an example on how the spectrum should look like after smoothing.

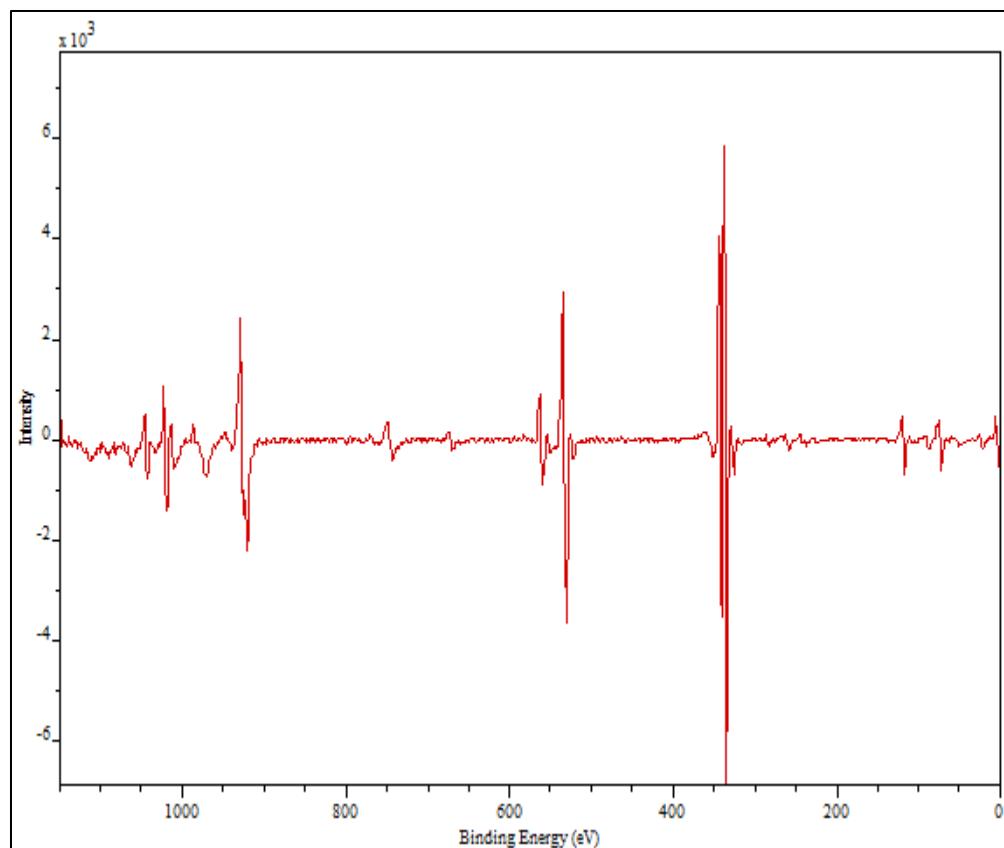


Original Spectrum



Smooth Spectrum

5. The “Differentiation” tab can take first derivatives on your spectrum. In the method section, there are two choices which are: SG Quadratic and SG Quartic. The default set is to SG Quadratic. The smoothing width section allows you to control the smoothness on your spectrum. The default value is set at 5. Once you have picked your preference on method and smoothing values, click on “Apply”. Below is an example of how the spectrum would look like after the spectrum has been differentiated.



Elemental Library

Elemental library icon allows you to easily create regions in XPS or AES analysis (**See section IV. Creating Regions B for procedures**). In addition, the library icon gives you relative sensitivity factors (RSF) for individual cross sections by doing XPS analysis. However, the elemental library does NOT give any relative sensitivity factors for AES analysis. Therefore, use the RSF values in the AES handbook for analysis.




Browser Operations

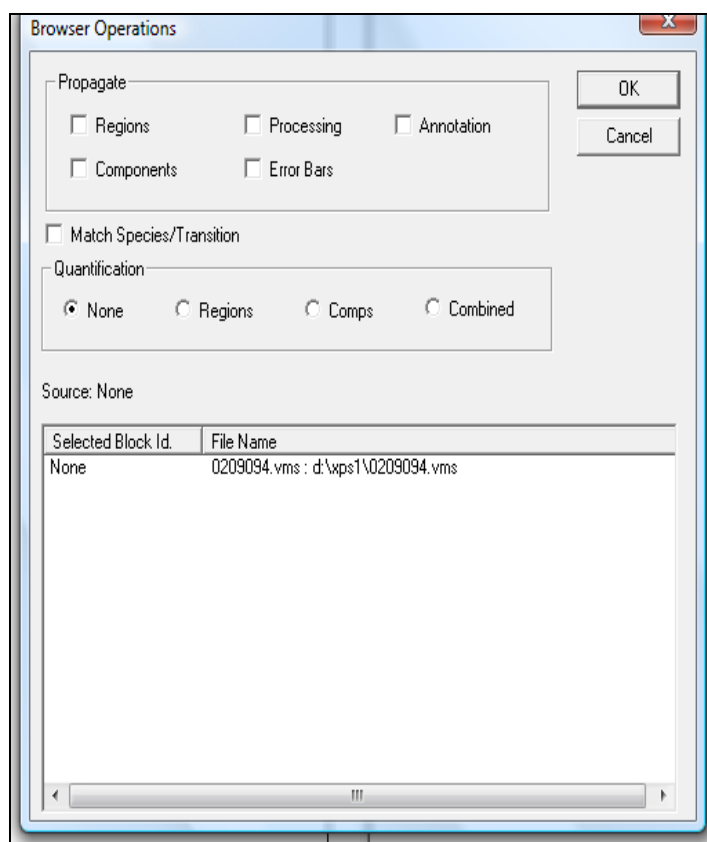
The browser operation allows you to spectrum process and editing your regions on all highlighted files at once. In other words, it can smooth, creates regions, take derivatives, and many more things to all the highlighted spectra at once.

1. Do spectrum processing (**See section II. Toolbar information under spectrum processing for procedure**) and/or creating regions (**See section III. Creating Regions A or IV. Creating Regions B for procedure**) in one of the highlight files.
2. Then highlight all the files you want to have the same process done in step 1 as shown below.

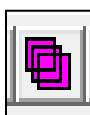
None	None
0	None
0	None
0	None
0	None



3. Click on the “Browser Operations”  icon.
4. A new window should appear depicted below.



5. Check the “Regions” and “Processing” box.
6. Click the “OK” button.



Insert Many

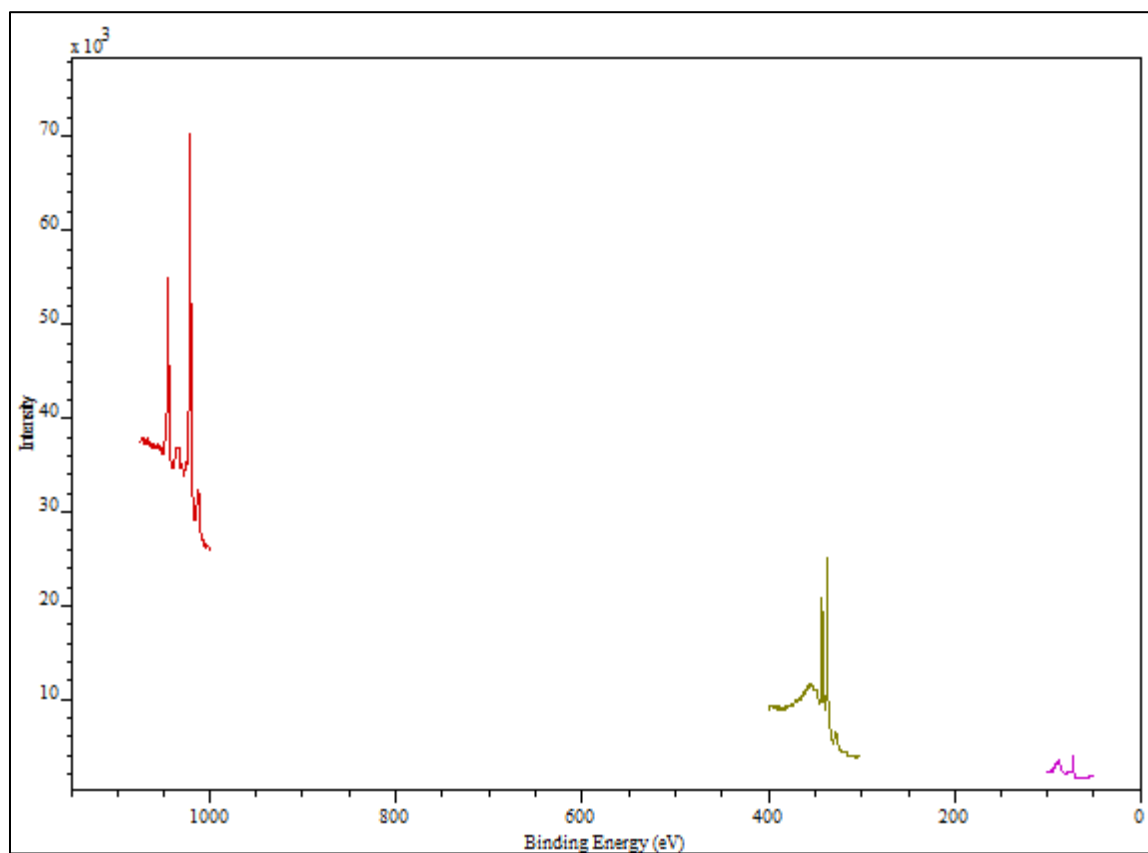
Insert many icon allows you to insert your individual peak spectra's into one spectrum.

1. Highlight the selected files on the right column. Example below.

None	None
0	None
0	None
0	None
0	None



2. Click on the “Insert Many” icon.
3. Below is an example of what the spectrum would look like.





Overlapping


The overlapping icon allows you to overlay your overview spectra or individual spectra into one graph. (NOTE: This is a great tool to do accurate quantitative analysis by making sure the start and end energy ranges are the same on every spectrum).

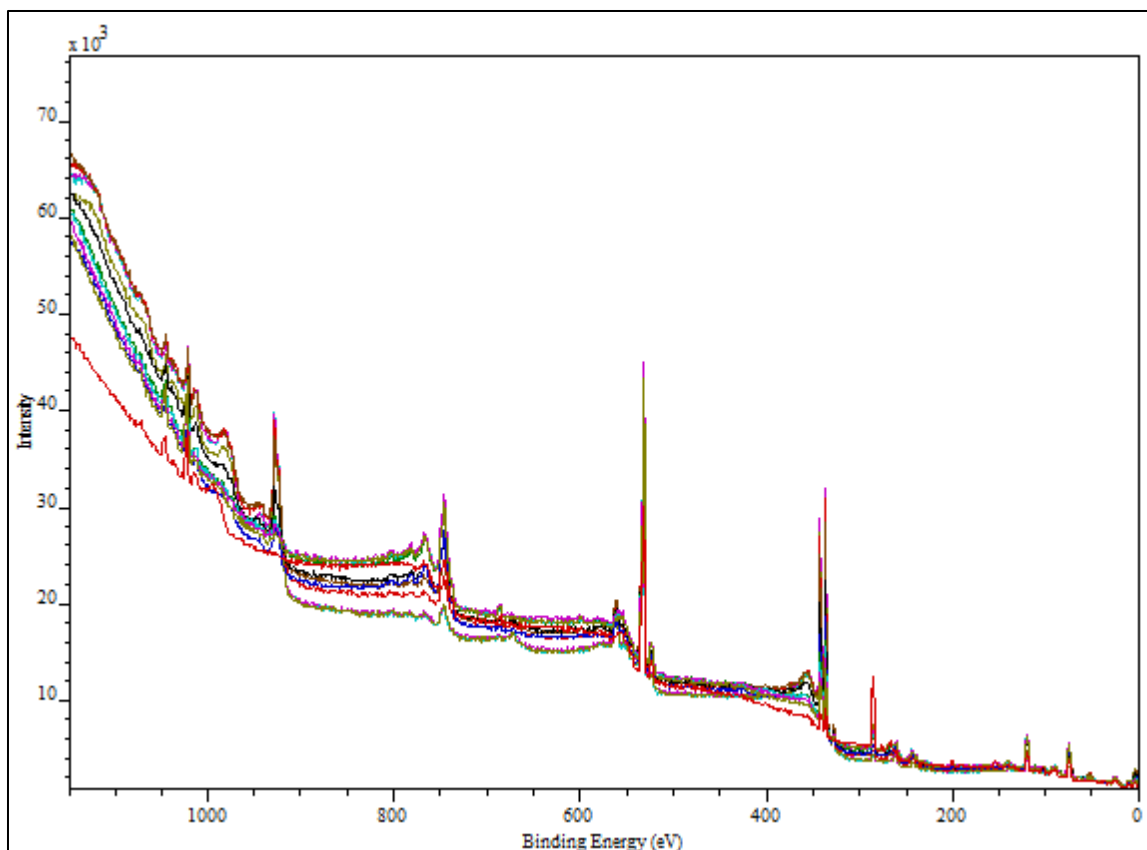
1. Highlight the selected files on the right column. Example below.

Data Set	None
0	None
1	None
2	None
3	None
4	None
5	None
6	None

2. Click on graph to activate the toolbar.



3. Click on the “Overlapping”  icon.
4. Below is an example of what the spectrum would look like.



Offset <-> No Offset


The Offset <-> No Offset icon allows you to offset your overlaid spectra.

1. Highlight the selected files on the right column. See example below.

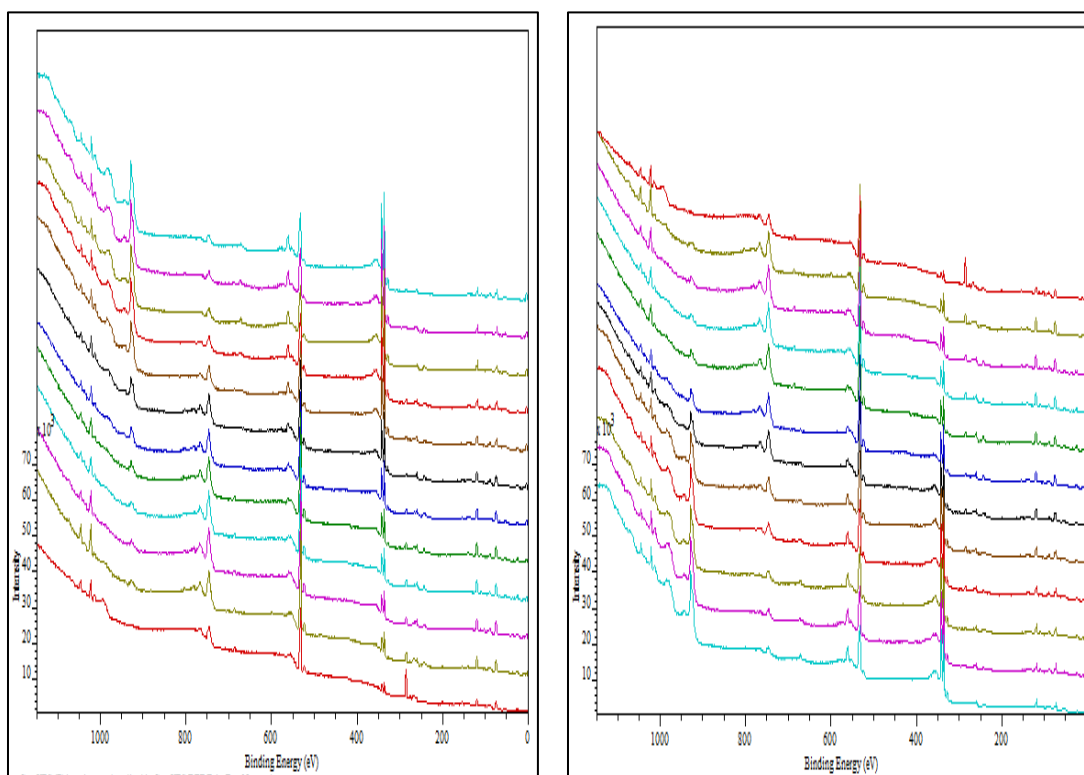
Data Set	None
0	None
1	None
2	None
3	None
4	None
5	None
6	None

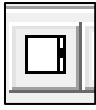
2. Click on graph to activate the toolbar.

3. Click on the “Overlying”  icon.

4. Click on the “Offset <-> No Offset”  icon.

5. Below is an example of what the spectrum would look like. There are multiple options to choose from, just continue to click on the “Offset <-> No Offset” icon until you find the one you want. The left graph is going from bottom to top and the right graph is going from top to bottom. (NOTE: the red line is your first spectrum).





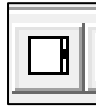
Page Layout

The page layout icon allows you to change the size of the graph.

1. Highlight the selected files on the right column. See example below.

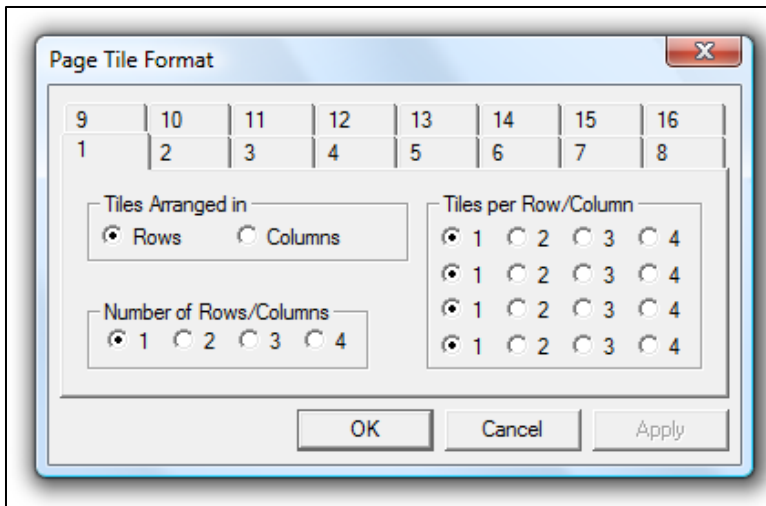
Data Set	None
0	None
1	None
2	None
3	None
4	None
5	None
6	None

2. Click on graph to activate the toolbar.



3. Click on the “Page layout” icon.

4. A “page layout” window would appear as depicted below. Play around with the settings until you are satisfied.



Display parameters

The display parameters icon allows you to “dress up” the graph. In other words, it makes it look professional for publications and presentations.

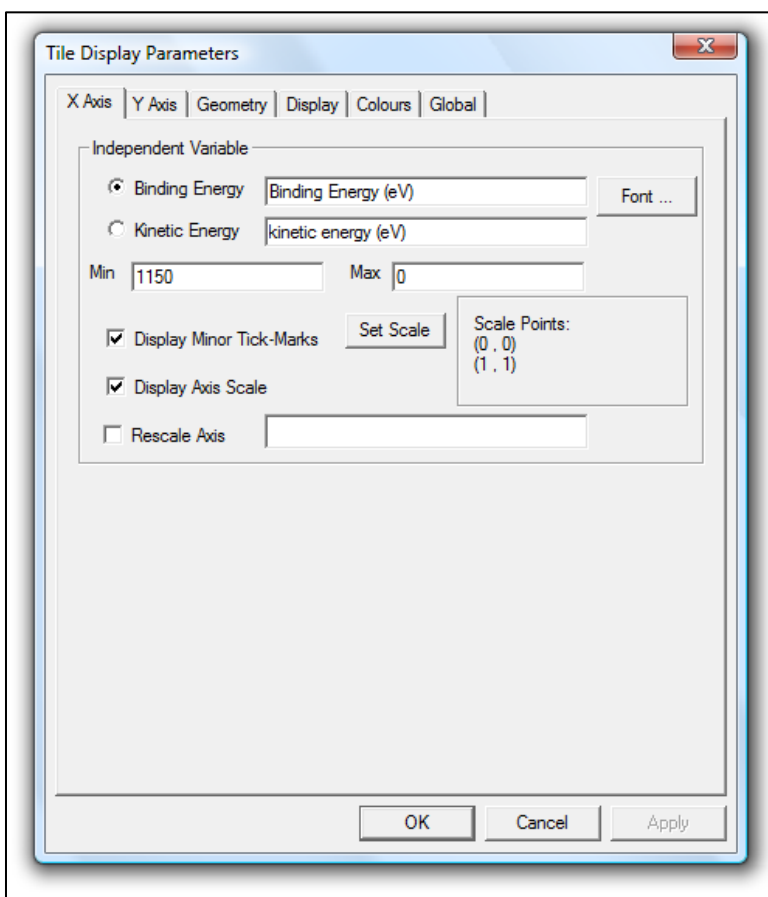
1. Highlight the selected files on the right column. See example below.

Data Set	None
0	None
1	None
2	None
3	None
4	None
5	None
6	None

2. Click on the graph to activate the toolbar.



3. Click on the “Display Parameters” icon.
4. A display parameters window would appear as depicted below. Play around with the settings until you are satisfied.



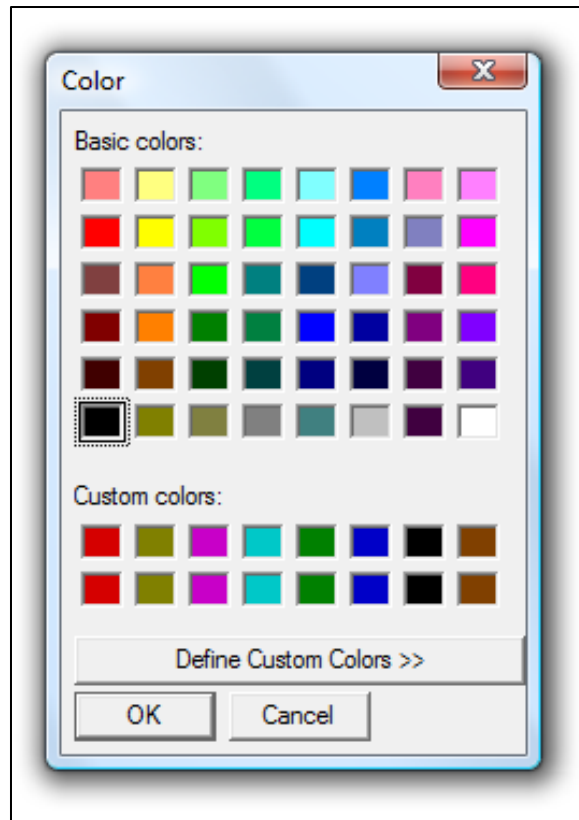
- a) X-axis tab allows you to change the font and size of the x-axis label, choosing binding energy or kinetic energy x-axis labels, change the minimum and maximum energies of your spectrum, etc.

- b) Y-axis tab allows you to change the font and size of the y-axis label, can change display y-axis parameters, can normalize your overlaid or offset spectrums, etc.

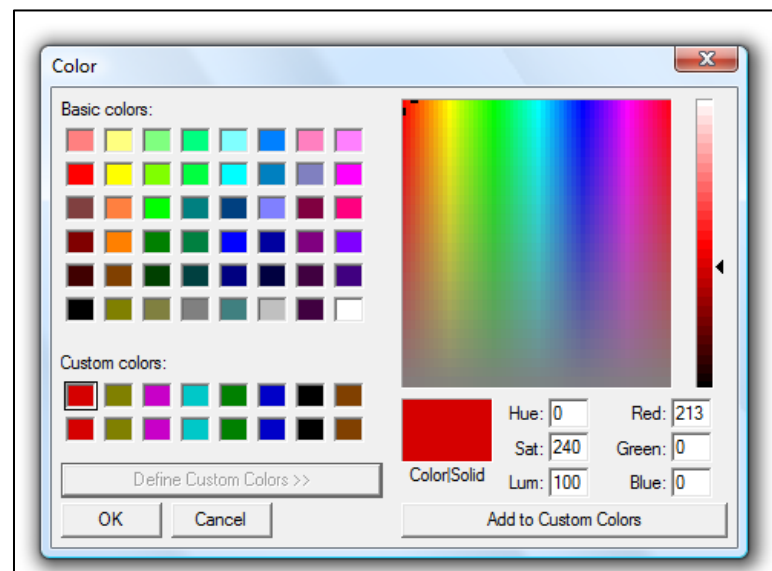
- c) Geometry tab allows you to change your spectrum graph from 2D to 3D.

- d) Display parameters allow you to display what you want or do not want on your graph. For instance, you can change the line width of the spectrum, change the axes font and size, etc.

- e) Colours tab allows you to change the color lines in your spectra and such. In order to go from color to all black, please follow these next few steps below.
 - i) Click "Spectra". A "color" window would appear as depicted below. Depending on how many spectra are in your graph, the colors would start off with red, then olive, pink, light blue, green, dark blue, black, brown, would then repeat that cycle again (see custom colors in the figure below). [Note: the first spectrum is depicted in red, the second spectrum is depicted in olive, and so forth.]



- ii) In order to change these colors, click on the color you want to change in the custom colors section. Then, click “Define Custom Colors>>”. The “color” window would now look like this.

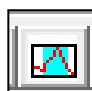


- iii) To go from red to black, drag the black arrow on the right side of the window down to black and click “Add to Custom Colors”. Then click “Ok”. Repeat steps ii) and iii) if desired.

III. Creating Regions A (Long Method)

1. Click on one of the files on the right column to work on.
2. Click on the spectrum to activate the toolbar.



3. Click on the “Quantification Parameter”  icon.
4. A “quantification parameter” window should pop up.
5. Click on the “Create” button at the bottom left of the window.
6. Type in the name of your region and press enter.
7. If this is an AES data, fill in the relative sensitivity factor in the “RSF” section. (NOTE: RSF is not given in AES analysis. You will need to plug in values from the “Handbook of Auger Electron Spectroscopy”. Make sure you multiply the sensitivity factor with the scale factor and type that into the “RSF” section). See “Handbook of Auger Electron Spectroscopy” for the surface concentration equation.
8. On the spectrum, a blue shade color appears with gray columns at the ends. This is your start and end energy ranges. Use the mouse to drag the gray columns to where you want to start and end your energy range. The blue highlighted range is your energy range being analyzed.
9. If you are doing XPS analysis, type in “Shirley” in BG type. If you are doing AES analysis, type in “Linear” in BG type.
10. You have then created your region. This is shown by annotation on the top left of the spectrum. To add more regions, repeat steps 5 through 9 again.

IV. Creating Regions B (Short Method)

1. Click on one of the files on the right column to work on.
2. Click on the spectrum to activate the toolbar.



3. Click on the “Elemental Library” icon.
4. Can either go to the “Element Table” tab (XPS analysis) or “Periodic Table” tab (XPS or AES analysis).

A. Under the “Element Table” tab, scroll down until you have reached your desired cross section. Click “create regions”. Keep doing this process until you got all the regions desired. (NOTE: If not all regions were created, meaning the annotation does not appear on the top left of the spectrum, you would then have to do the long method. **See section III. Creating Regions A for procedures.**)

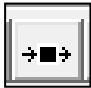
B. Under the “Periodic Table” tab, click on all the elements that you want to create regions on. Click on the “create regions” button when finished. (NOTE: If not all regions were created, meaning the annotation does not appear on the top left of the spectrum, you would then have to do the long method. **See section III. Creating Regions A for procedures.**)

5. If all the regions are created by step 4a or 4b, then close the “elemental library” window.



6. Click on the “Quantification Parameter” icon.
7. Make sure name, RSF, and start/end energy ranges are correct (NOTE: RSF is not given in AES analysis. Need to plug in values from the “Handbook of Auger Electron Spectroscopy”. Make sure you multiply the sensitivity factor with the scale factor and type that into “RSF”).
8. You have then created your region. This is shown by annotation on the top left of the spectrum.

V. Finding Atomic Percent Concentration for AES Analysis (Survey Spectra)

1. Click on one of the files to work on.
2. Click on the spectrum to activate the toolbar.
3. Click on the “Spectrum Processing”  icon.
4. Click on the “Smoothing” tab to smooth your spectrum. (See **II. Toolbar Information under Spectrum Processing for procedure**)
5. Click on the “Differentiation” tab to take the first derivative on your spectrum. (See **II. Toolbar Information under Spectrum Processing for procedure**)
6. Close the “Spectrum Processing” window.
7. Need to create regions. (See **III. Creating Regions A or IV. Creating Regions B for procedure**)
8. In the “Quantification Parameter” window, click on “Report Spec” tab.
9. Click “Regions” in the Custom Report section. A list of all of your regions should appear in the second “white box” region where it says “Names and Formulas”.
10. Click “Height Report”.
11. A new window would appear. It will give you your atomic per concentration as well as counts per second (CPS) for that file.
12. If you have more than one file and need to analyze the same regions, please see **II. Toolbar Information under Browser operations for procedure**.

VI. Finding Atomic Percent Concentration for AES Analysis (Individual Peak Spectra)

*** Unfortunately, CasaXPS cannot calculate atomic percent concentrations for individual peak spectra. However, it can calculate maximum peak heights (peak plus) and minimum peak heights (peak minus). You can use this information to calculate the atomic percent concentration manually.*


1. Follow Steps 1 through 8 and/or 12 under section **V. Finding Atomic Percent Concentration for AES Analysis (Overview Spectrum) for procedures.**
2. Click “Regions” in the “Standard Report” section.
3. A new window will appear. It shows the name, position, FWHM, raw area, $\text{area}/(T \cdot \text{MFP})$, $\text{area}/(\text{RSF} \cdot T \cdot \text{MFP})$, library RSF, peak plus, peak minus, total RSF, and atomic percent concentration.
4. Record the peak plus and peak minus values to find the atomic percent concentrations.

VII. Finding Atomic Percent Concentration for XPS Analysis (Survey Spectra)

1. Click on one of the files to work on.
2. Click on the spectrum to activate the toolbar.
3. Need to create regions (**See III. Creating Regions A or IV. Creating Regions B for procedure**)
4. In the “Quantification parameter” window, click on “Report Spec” tab.
5. Click “Regions” in the Custom Report section. A list of all of your regions should appear in the second “white box” region where it says “Names and Formulas”.
6. Click “Area Report”.
7. A new window would appear. It will give you your atomic percent concentration as well as counts per second (CPS) for that file.
8. If you have more than one file and need to analyze the same regions, please **see II. Toolbar Information under Browser operations for procedure.**

VIII. Finding Atomic Percent Concentration for XPS Analysis (Individual Peak Spectra)

*** Unfortunately, CasaXPS cannot calculate atomic percent concentrations for individual peak spectra. However, it can calculate area of the peak. You can use this information to calculate the atomic percent concentration manually.*

1. Follow steps 1 to 4 and/or 8 under section **VII. Finding Atomic Percent Concentration for XPS Analysis (Overview Spectra)**.
2. Click “Regions” in the “Standard Report” section.
3. A new window will appear. It shows the name, position, FWHM, raw area, $\text{area}/(\text{T}*\text{MFP})$, $\text{area}/(\text{RSF}*\text{T}*\text{MFP})$, library RSF, peak plus, peak minus, total RSF, and atomic percent concentration.
4. Record the raw area values to find the atomic percent concentration.
5. Below is an example on calculating the atomic percent concentration manually on Excel. This procedure also is illustrated on the next page.
 - a. Record the area values from step #4 into Excel.
 - b. Record the RSF of the individual cross section from the “Elemental Library”
icon .
 - c. Take the area and divided by the RSF of the individual cross section.
 - d. Make a third column and sum the individual cross section.
 - e. Atomic percent concentration is taking one of the (area/RSF) divided by the sum and multiplying by 100.

The screenshot shows an Excel spreadsheet with the following data:

	A	B	C	D	E	F	G	H	I	J	K
1											
2											
3				Area							
4	Step: 5a			Gd	Ge						
5				178997.3	46532.4						
6											
7				R.S.F.							
8	Step: 5b			Gd	Ge						
9				46.2	12.5						
10											
11				Area/R.S.F.							
12											
13	Step: 5c			Gd	Ge	Sum					
14				3874.4	3722.592	7596.992	Step: 5d				
15											
16											
17				Concentration							
18	Step: 5e			Gd	Ge						
19				50.99914	49.00086						
20											
21											
22											

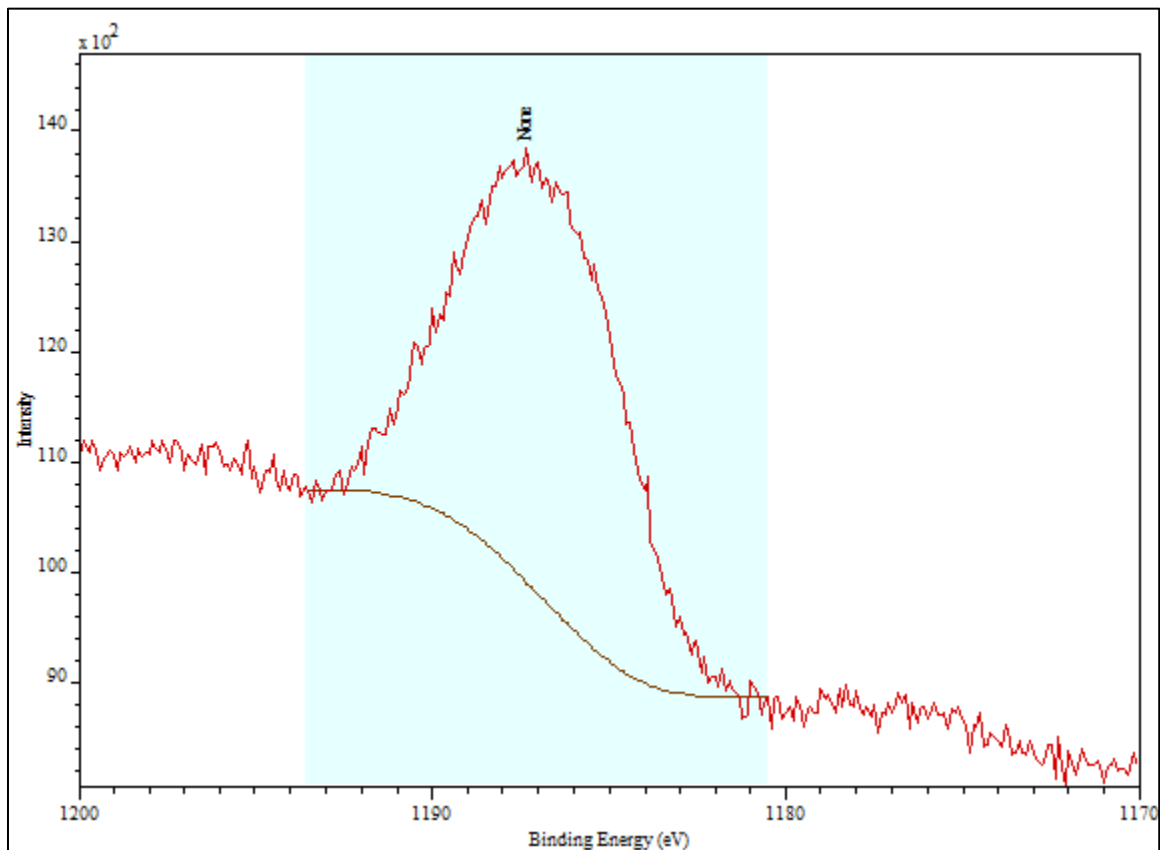
Formula box content: Gd Concentration
 $(3874.4 / 7596.992) * 100$

IX. Deconvoluting Peaks

1. Open a file that contains your standard peaks. [i.e. a spectrum of a clean surface]
2. Click on the spectrum to activate the toolbar.
3. Follow steps 1-5 in **Section III. Creating Regions A (Long Method)**.

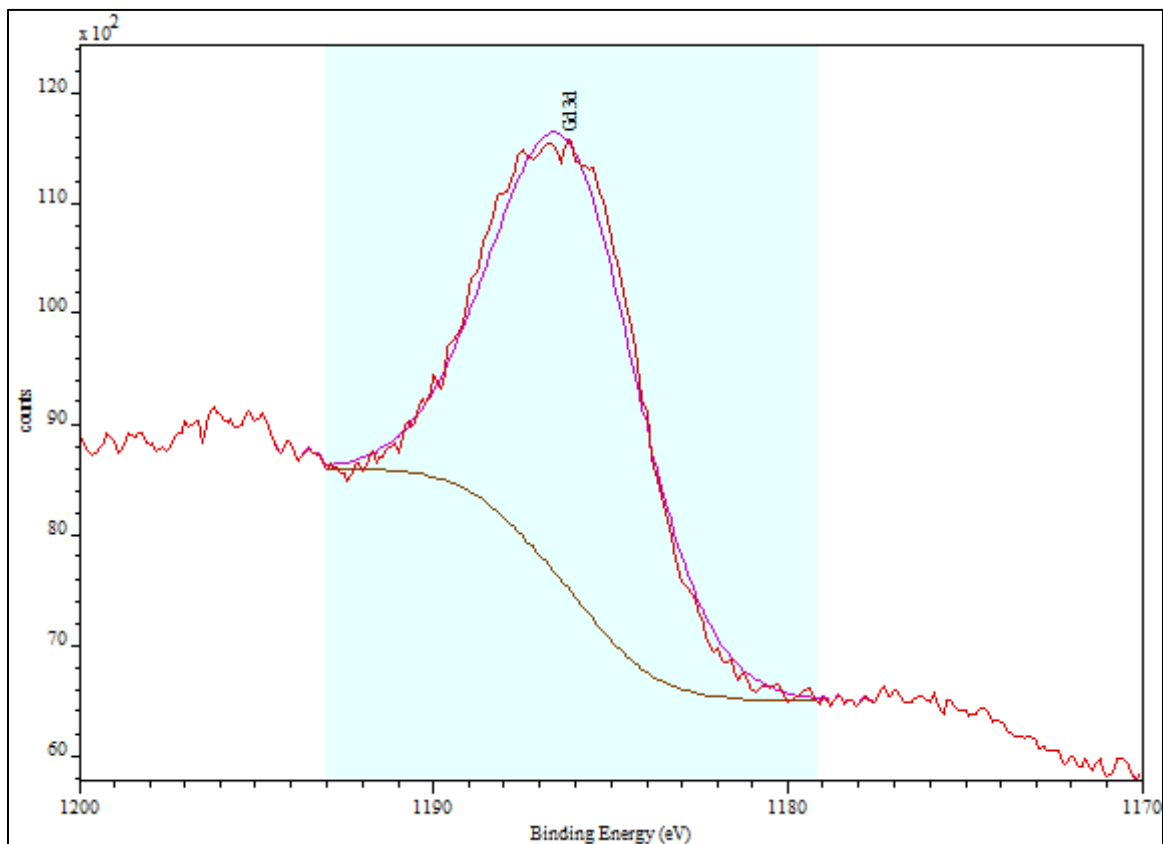


4. With the “Quantification Parameter” icon opened, select your binding energy ranges by moving the grey vertical bar in the spectrum. [NOTE: The blue highlighted area is your energy range as illustrated below].



5. In the “Quantification Parameter” window, make sure the BG (Background) Type is set to “Shirley”. If not, type it in and click “enter” to set it. A Shirley background is defined by the area underneath the curve minus from the background spectrum. It should look like an upside S-shape as shown in the figure above (See illustration in Step #4).

6. In the “Quantification Parameters” window, click on the “Components” tab.
7. Click the “Create” button.
8. A pink Gaussian curve-fit line will appear in your spectrum as depicted below. As best as you can, play around with the “Line Shape” number [i.e. GL(25)] in order to make the Gaussian line fit in your desired peak. See below. GL stands for Gaussian and Lorentzian and the number represents the percentage amount of either Gaussian or Lorentzian.

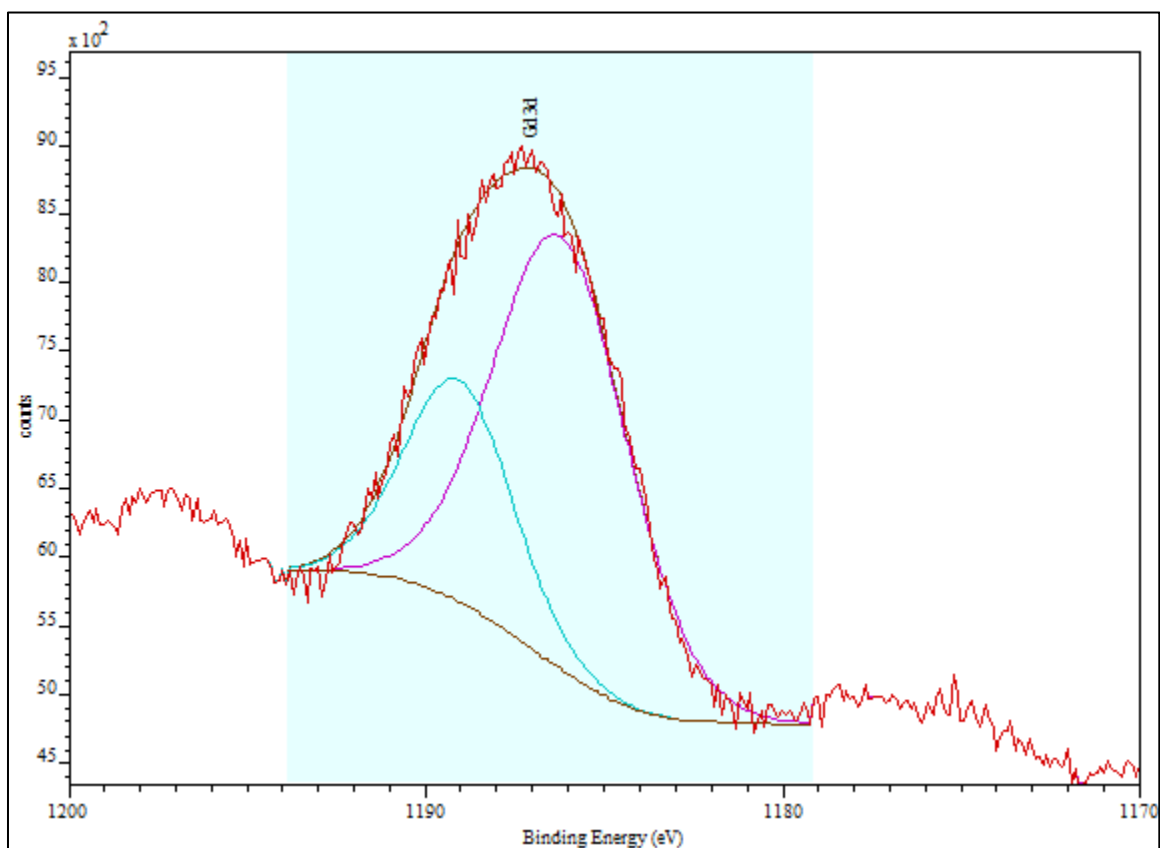


9. Once fitted, record the peak position and fwhm (full width at half maximum).
10. Then, open a file that contains your experimental peaks. [i.e. a spectrum of an oxidized surface]
11. Repeat steps #2 – 7. Make sure the binding energy ranges are constant as with your standard peak in step #4.
12. After you had created a component, a pink Gaussian curve-fit line will appear in your spectrum. Type in your standard peak position and fwhm that you had recorded in Step #9 into your component.

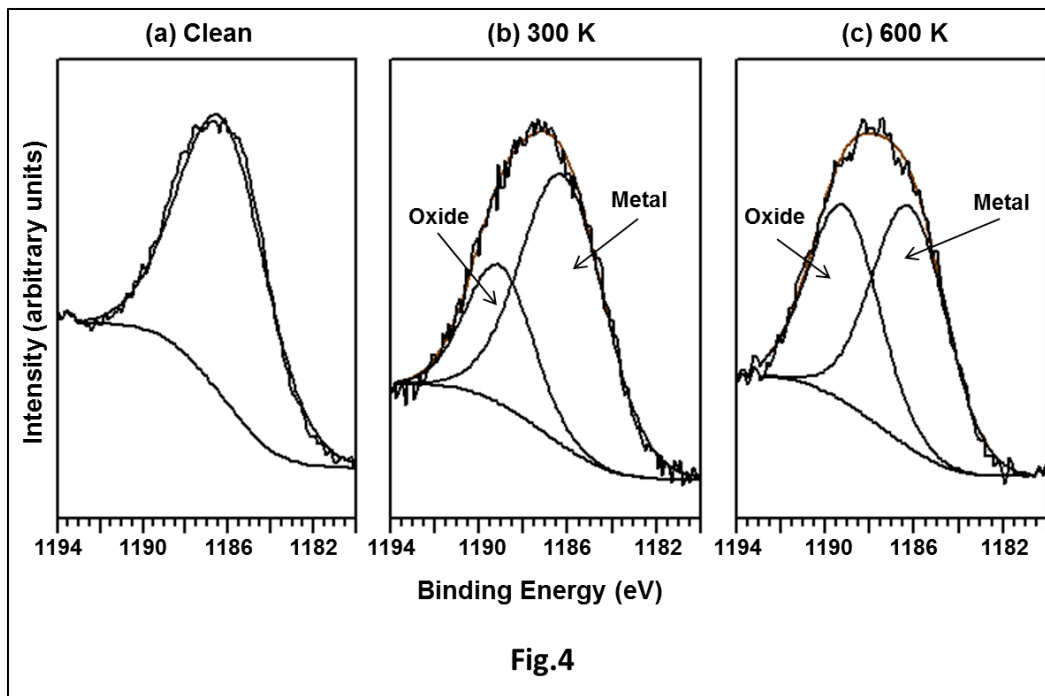
13. Once the new peak positions and fwhm have been recorded into your component, you then need to constrain it. Under “Pos. Constr.” and “fwhm Constr.”, either change the minimum or maximum or both so that the position and the fwhm are fixed. The position and fwhm should now turn the color pink.

14. Create a second component.

15. A blue Gaussian curve fit will appear as depicted below. Since, you had restrained the pure metal onto the oxidized peak, your blue Gaussian line is designated as the oxide metal and the pink Gaussian line is designated as the pure metal.



16. Below is an example of deconvoluting the Gd oxide peak in Gd_5Ge_4 .



APPENDIX B. Experimental Database

Table Captions

1. 2f Al-Pd-Zn Approximant
2. 10f Al-Pd-Zn Approximant
3. Gd₅Ge₄ (010)
 - a. Omicron Chamber (224 Spedding), performed by Chad Yuen
 - b. AES/SEM Chamber (137 Wilhelm), performed by Jim Anderegg

Sample #	Table #	Date
MPC hmd-1-73	3A	10/23/2010 – 12/12/2010
MPC-dls-7-68-2	3A 3B	4/21/2011 – 5/18/2011 7/4/2012
MPC dlw-1-97	3A	4/25/2012 – 6/28/2012
MPC dlw-1-1	3B	6/14/2011 – 8/6/2012 (except on 7/4/2012)

4. Au on NiAl (110)
5. Ag on NiAl (110) and Au on NiAl (110) [Switzerland]
6. O₂ on Ag on oxidized NiAl (110) and Ag on oxidized NiAl (110)

Table 1

2f AlPdZn Data List						
Date	Images / Spectrum	Instr.	Purpose	Lab #, Page #	File Name	Notes
1/21/2009	overview	AES	Finding a good position	Bk 1, pg 42	121090	Overview Spectrum: The whole scan range.
1/22/2009	overview	AES	Cleaning sample (sputtering only)	Bk 1, pg 42	122090 to 122092	O and C were decreasing.
1/23/2009	overview	AES	Cleaning sample (sputtering only)	Bk 1, pg 46	123090 to 123092	Shows O and C.
1/24/2009	overview	AES	Cleaning sample (sputtering only)	Bk 1, pg 48	124090	Shows O and C.
	overview	XPS	Finding a good position	Bk 1, pg 51	124090	Found Ni and Fe. It turns out the sample plate was Stainless steal and not Ta.
1/25/2009	overview	AES	Cleaning sample (sputtering only)	Bk 1, pg 51	125090 to 125091	
	overview	XPS	Finding a good position	Bk 1, pg 53	125090	
1/26/2009	overview	XPS	Using a Ag sample to help place correct position on AlPdZn	Bk 1, pg 54	126090	Showed huge Ag intensity peaks.
	overview		Using the Ag sample position for the AlPdZn	Bk 1, pg 55	126091 to 126093	File Name 126092 showed the best position.
1/27/2009	overview	AES	Cleaning sample (sputtering only)	Bk 1, pg 56	127090 to 127091	Identifying peaks.
	overview	XPS	Still searching a good position	Bk 1, pg 57	127090 to 127093	Still file name 126092 had the best position.

Table 1 (Continue)

Date	Images / Spectrum	Instr.	Purpose	Lab #, Page #	File Name	Notes
1/28/2009	overview	XPS	Playing with the CRR and Mag. to get good intensities	Bk 1, pg 59	128090 to 128096	The best intensities was making the CRR = 7 and the Mag = Medium.
	M1-M13	STM	Scanning on Site A (left grain from the fracture) on a sputtered surface	Bk 1, pg 60	12809	Surface was rough, lots of white circles (maybe oxidation), step bunching (maybe).
	M14-M20		Scanning on Site B (right grain from the fracture) on a sputtered surface	Bk 1, pg 60		Same as Site A, but appears to be smoother.
1/29/2009	overview	AES	Finding a good position	Bk 1, pg 61	129090 to 129096	File Name 129094 was the best for Frame Mode.
1/30/2009	overview	XPS	Testing to see which cathode: Al or Mg produces best intensities	Bk 1, pg 63	130090 to 130092	Mg Cathode produces the best intensities.
2/3/2009	overview	AES	Taken after sputtering	Bk 1, pg 65	203090	
	overview	XPS	Taken after sputtering	Bk 1, pg 65	203090	
	overview	AES	After sputtering again and annealing at 0.4 A	Bk 1, pg 66	203091	
	overview	XPS	After sputtering again and annealing at 0.4 A	Bk 1, pg 66	203091	

Table 1 (Continue)

Date	Images / Spectrum	Instr.	Purpose	Lab #, Page #	File Name	Notes
2/4/2009	overview	AES	After sputtering (starting the concentration vs time expt)	Bk 1, pg 67	204090 to 204091	Spot Mode shows a higher intensity than frame mode and also changed my position to file name 204090.
	overview	XPS	After sputtering (starting the concentration vs time expt)	Bk 1, pg 67	204090	
	overview	AES	After annealing at 0.4 A for 30 minutes	Bk 1, pg 68	204092	Pd decreases, Zn increases.
	overview	XPS	After annealing at 0.4 A for 30 minutes	Bk 1, pg 68	204091	Pd decreases, Zn increases (note: O 1s peak overlap one of the Pd peaks).
	overview	AES	After annealing at 0.4 A for 1 hour	Bk 1, pg 68	204093	Pd decreases, Zn increases.
	overview	XPS	After annealing at 0.4 A for 1 hour	Bk 1, pg 68	204092	Pd decreases, Zn increases.
	overview	AES	After annealing at 0.4 A for 1.5 hours	Bk 1, pg 69	204094	Zn increases, hard to find Al peak.
	overview	XPS	After annealing at 0.4 A for 1.5 hours	Bk 1, pg 69	204093	Zn increases, little oxygen (note: oxygen auger peak).
	overview	AES	After annealing at 0.4 A for 2 hours (expt. Finished)	Bk 1, pg 70	204095	Saw Pd and Zn peaks.
	overview	XPS	After annealing at 0.4 A for 2 hours (expt. Finished)	Bk 1, pg 70	204094	Little Pd peak, huge Zn peak.

Table 1 (Continue)

Date	Images / Spectrum	Instr.	Purpose	Lab #, Page #	File Name	Notes
2/5/2009	overview	AES	After sputtering (starting concentration vs temp expt)	Bk 1, pg 70	205090 to 205091	File 205091 showed better signal by changing angle on the manipulator.
	overview	XPS	After sputtering (starting concentration vs temp expt)	Bk 1, pg 71	205090	
	overview	AES	After annealing at 0.2 A for 2 hours	Bk 1, pg 71	205092	No change compared to after sputtering.
	overview	XPS	After annealing at 0.2 A for 2 hours	Bk 1, pg 71	205091	No change compared to after sputtering.
	overview	AES	After sputtering	Bk 1, pg 72	205093	
	overview	XPS	After sputtering	Bk 1, pg 72	205092	
	overview	AES	After annealing at 0.3 A for 2 hours	Bk 1, pg 73	205094	Pd decreases, Zn increases.
	overview	XPS	After annealing at 0.3 A for 2 hours	Bk 1, pg 73	205093	Zn, Ni, Fe, Pd, and O.
	overview	AES	After sputtering	Bk 1, pg 73	205095	
	overview	XPS	After sputtering	Bk 1, pg 74	205094	
	overview	AES	After annealing at 0.4 A for 2 hours	Bk 1, pg 74	205096	Pd decreases, Zn increases, possibly see Al peak.
overview	XPS	After annealing at 0.4 A for 2 hours	Bk 1, pg 74	205095	Pd decreases, Zn increases, and oxygen.	

Table 1 (Continue)

Date	Images / Spectrum	Instr.	Purpose	Lab #, Page #	File Name	Notes
2/6/2009	overview	AES	After sputtering (continue expt from 2/5/09)	Bk 1, pg 75	206090	
	overview	XPS	After sputtering (continue expt from 2/5/09)	Bk 1, pg 75	206090	
	overview	AES	After annealing at 0.5 A for 2 hours (expt finished)	Bk 1, pg 76	206091	See Pd and Zn peaks.
	overview	XPS	After annealing at 0.5 A for 2 hours (expt finished)	Bk 1, pg 76	206091	Zn, Ni, Fe, little Pd.
	M1-M13	STM	Site A (right grain from fracture)	Bk 1, pg 77	20609	See maybe step bunching, rough surface.
	M14-M21	STM	Site B (left grain from fracture)	Bk 1, pg 77		Rougher than Site A, same surface morphology as in Site A.
2/7/2009	overview	AES	Replaced sample plate and finding good position	Bk 1, pg 77	207090 to 207092	Used Ta plate instead of stainless steal plate. File 207092 had best intensity.
	overview	XPS	Replaced sample plate and finding good position	Bk 1, pg 78	207090 to 207093	Used Ta plate instead of stainless steal plate. File 207093 had best intensity.

Table 1 (Continue)

Date	Images / Spectrum	Instr.	Purpose	Lab #, Page #	File Name	Notes
2/8/2009	overview	AES	Starting Depth-Profiling Expt	Bk 1, pg 78	208090	No sputtering (found O and C).
	overview	XPS	Starting Depth-Profiling Expt	Bk 1, pg 79	208090	No sputtering (found O and C).
	overview	AES	After 5 minutes of sputtering	Bk 1, pg 79	208091	O peak decreases, no C peak.
	overview	XPS	After 5 minutes of sputtering	Bk 1, pg 79	208091	O and C peak decreasing.
	overview	AES	After 5 minutes of sputtering (10 mins total)	Bk 1, pg 80	208092	O peak decreases.
	overview	XPS	After 5 minutes of sputtering (10 mins total)	Bk 1, pg 80	208092	O and C peak decreasing.
	overview	AES	After 5 minutes of sputtering (15 mins total)	Bk 1, pg 81	208093	O peak decreases.
	overview	XPS	After 5 minutes of sputtering (15 mins total)	Bk 1, pg 81	208093	O and C peak decreasing.
	overview	AES	After 5 minutes of sputtering (20 mins total)	Bk 1, pg 81	208094	Hard to tell if there was O peak or not.
	overview	XPS	After 5 minutes of sputtering (20 mins total)	Bk 1, pg 82	208094	Shows O and C peaks, Pd increases, Al and Zn starts to decrease.
	overview	AES	After 10 minutes of sputtering (30 mins total)	Bk 1, pg 82	208095	Show Al, Pd, and Zn peaks.
	overview	XPS	After 10 minutes of sputtering (30 mins total)	Bk 1, pg 82	208095	Show Al, Pd, Zn, Ta, alittle C and O peaks.
	overview	AES	After 10 minutes of sputtering (40 mins total) [finish expt]	Bk 1, pg 82	208096	Show Al, Pd, and Zn peaks.

Table 1 (Continue)

Date	Images / Spectrum	Instr.	Purpose	Lab #, Page #	File Name	Notes
2/8/2009	overview	XPS	After 10 minutes of sputtering (40 mins total) [finish expt]	Bk 1, pg 83	208096	Show Al, Pd, Zn, Ta, alittle C and O peaks (could not get rid of C and O).
2/9/2009	overview, Zn (low energy), Pd, Al and Zn (high energy)	AES	After Sputtering (concentration vs time expt)	Bk 1, pg 84	209090	Did an overview spectrum followed by individual peak range spectrums.
	overview, Zn, Pd, and Al	XPS	After Sputtering (concentration vs time expt)	Bk 1, pg 84	209090	Did an overview spectrum followed by individual peak range spectrums.
	overview, Zn (low energy), Pd, Al and Zn (high energy)	AES	After annealing at 0.4 A for 30 minutes	Bk 1, pg 85	209091	Pd decreases, Zn increases.
	overview, Zn, Pd, and Al	XPS	After annealing at 0.4 A for 30 minutes	Bk 1, pg 85	209091	Pd decreases, Zn increases.
	overview, Zn (low energy), Pd, Al and Zn (high energy)	AES	After annealing at 0.4 A for 1 hour	Bk 1, pg 85	209092	Pd decreases, Zn increases.
	overview, Zn, Pd, and Al	XPS	After annealing at 0.4 A for 1 hour	Bk 1, pg 86	209092	Pd and Al decreases, Zn increases.

Table 1 (Continue)

Date	Images / Spectrum	Instr.	Purpose	Lab #, Page #	File Name	Notes
2/9/2009	overview, Zn (low energy), Pd, Al and Zn (high energy)	AES	After annealing at 0.4 A for 1.5 hours	Bk 1, pg 86	209093	Pd decreases, Zn increases.
	overview, Zn, Pd, and Al	XPS	After annealing at 0.4 A for 1.5 hours	Bk 1, pg 86	209093	Pd and Al decreases, Zn increases.
	overview, Zn (low energy), Pd, Al and Zn (high energy)	AES	After annealing at 0.4 A for 2 hours (finished expt)	Bk 1, pg 87	209094	Pd decreases, Zn increases.
	overview, Zn, Pd, and Al	XPS	After annealing at 0.4 A for 2 hours (finished expt)	Bk 1, pg 87	209094	Pd and Al decreases, Zn increases.

Table 1 (Continue)

Date	Images / Spectrum	Instr.	Purpose	Lab #, Page #	File Name	Notes
2/11/2009	overview, Zn (low energy), Pd, Al and Zn (high energy)	AES	After sputtering (concentration vs temperature expt)	Bk 1, pg 88	211090	
	overview, Zn, Pd, and Al	XPS	After sputtering (concentration vs temperature expt)	Bk 1, pg 88	211090	
	overview, Zn (low energy), Pd, Al and Zn (high energy)	AES	After annealing at 0.2 A for 2 hours	Bk 1, pg 89	211091	No change compared to after sputtering.
	overview, Zn, Pd, and Al	XPS	After annealing at 0.2 A for 2 hours	Bk 1, pg 89	211091	No change compared to after sputtering.

Table 1 (Continue)

Date	Images / Spectrum	Instr.	Purpose	Lab #, Page #	File Name	Notes
2/12/2009	overview, Zn (low energy), Pd, Al and Zn (high energy)	AES	After sputtering (continue expt from 2/11/09)	Bk 1, pg 89	212090	
	overview, Zn, Pd, and Al	XPS	After sputtering (continue expt from 2/11/09)	Bk 1, pg 90	212090	
	overview, Zn (low energy), Pd, Al and Zn (high energy)	AES	After annealing at 0.3 A for 2 hours	Bk 1, pg 90	212091	Pd starts to decrease.
	overview, Zn, Pd, and Al	XPS	After annealing at 0.3 A for 2 hours	Bk 1, pg 90	212091	Zn starts to increase.
2/13/2009	overview, Zn (low energy), Pd, Al and Zn (high energy)	AES	After sputtering (continue expt from 2/11/09)	Bk 1, pg 91	213090	
	overview, Zn, Pd, and Al	XPS	After sputtering (continue expt from 2/11/09)	Bk 1, pg 91	213090	
	overview, Zn (low energy), Pd, Al and Zn (high energy)	AES	After annealing at 0.4 A for 2 hours	Bk 1, pg 92	213091	Pd decreases and Zn increases.

Table 1 (Continue)

Date	Images / Spectrum	Instr.	Purpose	Lab #, Page #	File Name	Notes
2/13/2009	overview, Zn, Pd, and Al	XPS	After annealing at 0.4 A for 2 hours	Bk 1, pg 92	213091	Zn increases while Pd and Al decreases.
	overview, Zn (low energy), Pd, Al and Zn (high energy)	AES	After sputtering	Bk 1, pg 92	213092	
	overview, Zn, Pd, and Al	XPS	After sputtering	Bk 1, pg 93	213093	
	overview, Zn (low energy), Pd, Al and Zn (high energy)	AES	After annealing at 0.5 A for 2 hours (expt finished)	Bk 1, pg 93	213093	Zn increases while Pd and Al decreases.
	overview, Zn, Pd, and Al	XPS	After annealing at 0.5 A for 2 hours (expt finished)	Bk 1, pg 93	213093	Zn increases while Pd and Al decreases.
2/15/2009	M1-M82	STM	After annealing 0.5 A for 2 hours (Site A)	Bk 1, pg 95	21509	Taken at 5 areas on the surface. No step-terrace morphology, just atom clusters.
	M83-M148	STM	After annealing 0.5 A for 2 hours (Site B)	Bk 1, pg 96		Taken at 5 areas on the surface. No step-terrace morphology, just atom clusters.
	overview	AES	After STM	Bk 1, pg 96	215090	
	overview	XPS	After STM	Bk 1, pg 96	215090	

Table 1 (Continue)

Date	Images / Spectrum	Instr.	Purpose	Lab #, Page #	File Name	Notes
2/16/2009	M1-M39	STM	After sputtering and annealing at 0.3 A for 2 hours (Site A) [Temp-Independ Expt]	Bk 1, pg 97	21609	No step-terrace morphology, just atom clusters.
	M40-M78	STM	After sputtering and annealing at 0.3 A for 2 hours (Site A) [Temp-Independ Expt]	Bk 1, pg 97		No step-terrace morphology, just atom clusters.
	M79-M91	STM	After annealing at 0.3 A for 1 hour (Site B)	Bk 1, pg 98		No change in surface structure.
	M92-M103	STM	After annealing at 0.3 A for 1 hour (Site A)	Bk 1, pg 98		No change in surface structure.
	M104-M129	STM	After annealing at 0.3 A for 2.75 hours (Site A) [Finished Expt]	Bk 1, pg 98		No change in surface structure.
	M130-M155	STM	After annealing at 0.3 A for 2.75 hours (Site B) [Finished Expt]	Bk 1, pg 98		No change in surface structure.

Table 1 (Continue)

Date	Images / Spectrum	Instr.	Purpose	Lab #, Page #	File Name	Notes
2/17/2009	overview	AES	After sputtering for 20 mins	Bk 1, pg 99	217090	Just cleaning the surface.
	overview	XPS	After sputtering for 20 mins	Bk 1, pg 99	217090	Just cleaning the surface.
	overview	AES	After sputtering 10 mins (total = 30 mins)	Bk 1, pg 100	217091	
	overview	XPS	After sputtering 10 mins (total = 30 mins)	Bk 1, pg 100	217091	
	overview	AES	After sputtering 10 mins (total = 40 mins)	Bk 1, pg 100	217092	
	overview	XPS	After sputtering 10 mins (total = 40 mins)	Bk 1, pg 101	217092	
	overview	AES	After sputtering 10 mins (total = 50 mins)	Bk 1, pg 101	217093	Found out AES was not surface sensitive compared to XPS. All AES images were weird.
	overview	XPS	After sputtering 10 mins (total = 50 mins)	Bk 1, pg 101	217093	

Table 1 (Continue)

Date	Images / Spectrum	Instr.	Purpose	Lab #, Page #	File Name	Notes
2/18/2009	M1-M26	STM	After sputtering and annealing at 0.4 A for 1 hour (Site A) [Temp-Independ Expt]	Bk1, pg 102	21809	No step-terrace morphology, just atom clusters.
	M27-M52	STM	After sputtering and annealing at 0.4 A for 1 hour (Site B) [Temp-Independ Expt]	Bk 1, pg 102		No step-terrace morphology, just atom clusters.
	M53-M65	STM	After annealing at 0.4 A for 1.5 hours (Site A)	Bk 1, pg 103		No change in surface structure.
	M66-M78	STM	After annealing at 0.4 A for 1.5 hours (Site B)	Bk 1, pg 103		No change in surface structure.
	M79-M91	STM	After annealing at 0.4 A for 2 hours (Site A)	Bk 1, pg 103		No change in surface structure.
	M92-M104	STM	After annealing at 0.4 A for 2 hours (Site B)	Bk 1, pg 103		No change in surface structure.
6/2/2009	overview	XPS	Finding a good position	Bk 1, pg 105	602090 to 602092	File 602091 had the best intensity. Little Zinc peaks.

Table 1 (Continue)

Date	Images / Spectrum	Instr.	Purpose	Lab #, Page #	File Name	Notes
6/3/2009	overview, Zn, Pd, and Al	XPS	After sample was exposed to air (Depth-Profiling Expt)	Bk 1, pg 106	603090	Hardly any Zinc, probably all evaporated into chamber.
	overview, Zn, Pd, and Al	XPS	After sputtering 5 mins	Bk 1, pg 106	603091	Hardly any Zinc, probably all evaporated into chamber. Oxygen and carbon peaks were decreasing.
	overview, Zn, Pd, and Al	XPS	After sputtering 5 mins (total = 10 mins)	Bk 1, pg 107	603092	Hardly any Zinc, probably all evaporated into chamber. Oxygen and carbon peaks were decreasing.
	overview, Zn, Pd, and Al	XPS	After sputtering 5 mins (total = 15 mins)	Bk 1, pg 107	603093	Oxygen and carbon peaks were decreasing.

Table 1 (Continue)

Date	Images / Spectrum	Instr.	Purpose	Lab #, Page #	File Name	Notes
6/3/2009	overview, Zn, Pd, and Al	XPS	After sputtering 5 mins (total = 20 mins)	Bk 1, pg 108	603094	Oxygen and carbon peaks were decreasing.
	overview, Zn, Pd, and Al	XPS	After sputtering 10 mins (total = 30 mins)	Bk 1, pg 108	603095	Oxygen and carbon peaks were decreasing.
	overview, Zn, Pd, and Al	XPS	After sputtering 10 mins (total = 40 mins)	Bk 1, pg 109	603096	Oxygen and carbon peaks were decreasing.
	overview, Zn, Pd, and Al	XPS	After sputtering 10 mins (total = 50 mins) [Finished Expt]	Bk 1, pg 109	603097	No zinc peak.
	overview, Zn, Pd, and Al	XPS	After sputtering 10 mins (total = 60 mins) [Finished Expt]	Bk 1, pg 110	603908	No zinc peak.
6/4/2009	overview, Zn, Pd, and Al	XPS	After sputtering (temp-depend expt)	Bk 1, pg 111	604090	
	overview, Zn, Pd, and Al	XPS	After annealing at 0.2 A for 2 hours	Bk 1, pg 112	604091	No change in concentration.
	overview, Zn, Pd, and Al	XPS	After sputtering	Bk 1, pg 112	604092	
	overview, Zn, Pd, and Al	XPS	After annealing at 0.3 A for 2 hours (finished expt)	Bk 1, pg 113	604093	Zinc did not increase intensity. I think it all evaporated into chamber.

Table 2

10f AlPdZn Data List						
Date	Images / Spectrum	Instr.	Purpose	Lab #, Page #	File Name	Notes
6/6/2009	overview, Zn, Pd, and Al	XPS	Finding a good position	Bk 1, pg 115	606090 to 606091	File 606090 had the best intensity.
6/7/2009	overview, Zn, Pd, and Al	XPS	After exposure from air (Depth Profiling Expt)	Bk 1, pg 116	607090	Lots of oxygen and carbon.
	overview, Zn, Pd, and Al	XPS	After sputtering for 6 mins	Bk 1, pg 116	607091	Carbon starts to decrease.
	overview, Zn, Pd, and Al	XPS	After sputtering for 6 mins (total = 12 mins)	Bk 1, pg 117	607092	Carbon decreases, oxygen increases.
	overview, Zn, Pd, and Al	XPS	After sputtering for 6 mins (total = 18 mins)	Bk 1, pg 118	607093	Carbon and oxygen decreases.
	overview, Zn, Pd, and Al	XPS	After sputtering for 6 mins (total = 24 mins)	Bk 1, pg 118	607094	Carbon and oxygen decreases.
	overview, Zn, Pd, and Al	XPS	After sputtering for 15 mins (total = 39 mins)	Bk 1, pg 119	607095	Carbon and oxygen decreases.
	overview, Zn, Pd, and Al	XPS	After sputtering for 15 mins (total = 54 mins)	Bk 1, pg 120	607096	Carbon and oxygen decreases.

Table 2 (Continue)

Date	Images / Spectrum	Instr.	Purpose	Lab #, Page #	File Name	Notes
6/7/2009	overview, Zn, Pd, and Al	XPS	After sputtering for 30 mins (total = 84 mins)	Bk 1, pg 120	607097	Carbon and oxygen decreases.
	overview, Zn, Pd, and Al	XPS	After sputtering for 30 mins (total = 114 mins)	Bk 1, pg 121	607098	Oxygen decreases, carbon is gone.
	overview, Zn, Pd, and Al	XPS	Afer sputtering for 30 mins (total = 144 mins)	Bk 1, pg 122	607099	Oxygen decreases.
	overview, Zn, Pd, and Al	XPS	After sputtering for 30 mins (total = 174 mins) [finished expt]	Bk 1, pg 122	6070991	Oxygen decreases.
	overview, Zn, Pd, and Al	XPS	After sputtering for 30 mins (total = 204 mins) [finished expt]	Bk 1, pg 123	6070992	Little oxygen auger peak. Looked at Dapeng's and Baris's XPS spectras, it also shows a little oxygen auger peak.

Table 2 (Continue)

Date	Images / Spectrum	Instr.	Purpose	Lab #, Page #	File Name	Notes
6/8/2009	overview, Zn, Pd, and Al	XPS	After sputtering	Bk 1, pg 124	608090	
	overview, Zn, Pd, and Al	XPS	After annealing at 0.2 A for 2 hours	Bk 1, pg 125	608091	
	overview, Zn, Pd, and Al	XPS	After sputtering	Bk 1, pg 126	608092 to 608096	Finding good position.
	overview, Zn, Pd, and Al	XPS	After sputtering	Bk 1, pg 127	608097 to 608098	File 608095 had best intensity.
	overview	AES	After sputtering	Bk 1, pg 127	608090 to 608091	AES spectras were still weird. Should Pd had more intensity than Al and Zn. Not using AES.
6/9/2009	overview, Zn, Pd, and Al	XPS	After sputtering (temp-depend expt)	Bk 1, pg 129	609090	
	overview, Zn, Pd, and Al	XPS	After annealing at 0.2 A for 2 hours	Bk 1, pg 130	609091	Not much change in surface composition from 609090.
	overview, Zn, Pd, and Al	XPS	After sputtering	Bk 1, pg 130	609092	
	overview, Zn, Pd, and Al	XPS	After annealing at 0.3 A for 2 hours	Bk 1, pg 131	609093	Zn starts to increase and Pd starts to decrease.
	overview, Zn, Pd, and Al	XPS	After sputtering	Bk 1, pg 132	609094	
	overview, Zn, Pd, and Al	XPS	After annealing at 0.4 A for 2 hours	Bk 1, pg 132	609095	Zn increase while Pd and Al decreases.

Table 2 (Continue)

Date	Images / Spectrum	Instr.	Purpose	Lab #, Page #	File Name	Notes
6/10/2009	overview, Zn, Pd, and Al	XPS	After sputtering (continuing temp-depend expt)	Bk 1, pg 133	610090	
	overview, Zn, Pd, and Al	XPS	After annealing at 0.5 A for 2 hours (finished expt)	Bk 1, pg 134	610091	Zn increase while Pd and Al decreases.
6/11/2009	overview, Zn, Pd, and Al	XPS	After sputtering (temp-independ expt)	Bk 1, pg 135	611090	
	overview, Zn, Pd, and Al	XPS	After annealing at 0.4 A for 30 mins	Bk 1, pg 136	611091	Zn increase while Pd and Al decreases.
	overview, Zn, Pd, and Al	XPS	After annealing at 0.4 A for 30 mins (total = 1 hour)	Bk 1, pg 137	611092	Zn increase while Pd and Al decreases.
	overview, Zn, Pd, and Al	XPS	After annealing at 0.4 A for 30 mins (total = 1.5 hour)	Bk 1, pg 138	611093	Zn increase while Pd and Al decreases.
	overview, Zn, Pd, and Al	XPS	After annealing at 0.4 A for 30 mins (total = 2 hours) [finished expt]	Bk 1, pg 138	611094	Zn increase while Pd and Al decreases.
6/12/2009	overview, Zn, Pd, and Al	XPS	After sputtering (part of temp-depend expt)	Bk 1, pg 139	612090	
	overview, Zn, Pd, and Al	XPS	After annealing at 0.6 A for 10 mins	Bk 1, pg 140	612091	Zn is really high while Pd and Al are small.

Table 2 (Continue)

Date	Images / Spectrum	Instr.	Purpose	Lab #, Page #	File Name	Notes
6/15/2009	M1-M44	STM	After sputtering and annealing at 0.4 A for 15 mins (single grain)	Bk 1, pg 142	61509	No step-terrace morphology. Lots of atom clusters.
	M45-M84	STM	After sputtering and annealing at 0.4 A for 15 mins (poly grain)	Bk 1, pg 142		No step-terrace morphology. Lots of atom clusters. Cannot tell any difference between the single grain and the poly grain areas.
6/16/2009	M1-M41	STM	After sputtering and annealing at 0.5 A for 15 mins (single grain)	Bk 1, pg 145	61609	No step-terrace morphology. Lots of atom clusters.
	M42-M82	STM	After sputtering and annealing at 0.5 A for 15 mins (poly grain)	Bk 1, pg 145		No step-terrace morphology. Lots of atom clusters. Cannot tell any difference between the single grain and the poly grain areas.
	M83-M94	STM	After sputtering and annealing at 0.5 A for 15 mins (different poly grain region)	Bk 1, pg 145		No step-terrace morphology. Lots of atom clusters. Cannot tell any difference between the single grain and the poly grain areas.
6/17/2009	M1-M37	STM	After sputtering and annealing at 0.6 A for 15 mins (single grain)	Bk 1, pg 147	61709	No step-terrace morphology. Lots of atom clusters. It appears to be a lot rougher than at lower temperatures.
	M38-M68	STM	After sputtering and annealing at 0.6 A for 15 mins (poly grain)	Bk 1, pg 147		No step-terrace morphology. Lots of atom clusters. It appears to be a lot rougher than at lower temperatures. Cannot tell any difference between the single grain and the poly grain areas.

Table 2 (Continue)

Date	Images / Spectrum	Instr.	Purpose	Lab #, Page #	File Name	Notes
6/24/2009	overview	XPS	After sputtering 30 mins	Bk 1, pg 154	Did not save	Intensities were too low, due to oxide layer.
	overview	XPS	After sputtering 30 mins (total = 1 hour)	Bk 1, pg 154	624090	Lots of oxygen and carbon. Surface is getting better.
	overview	XPS	After sputtering 30 mins (total = 1.5 hour)	Bk 1, pg 155	624091	No carbon, still oxygen auger peak, but decreased a lot.
	overview, Zn, Pd, and Al	XPS	After sputtering 30 mins (total = 2 hours)	Bk 1, pg 156	624092	Have that little oxygen auger peak.
6/25/2009	overview	XPS	After sputtering	Bk 2, pg 1	625090	Cleaning sample.
	overview	XPS	After annealing at 0.4 A for 20 mins	Bk 2, pg 1	625091	Cleaning sample.
	overview, Zn, Pd, and Al	XPS	After sputtering and annealing at 0.4 A for 20 mins	Bk 2, pg 3	625092	Cleaning sample.

Table 2 (Continue)

Date	Images / Spectrum	Instr.	Purpose	Lab #, Page #	File Name	Notes
6/26/2009	overview, Zn, O, Pd, and Al	XPS	After sputtering and annealing at 0.4 A for 20 mins (oxidation expt)	Bk 2, pg 4	6260901 to 6260905	
	overview, Zn, O, Pd, and Al	XPS	After 0.2 L of oxygen	Bk 2, pg 4	6260906	
	overview, Zn, O, Pd, and Al	XPS	After 0.8 L of oxygen (total = 1 L)	Bk 2, pg 4	6260907	
	overview, Zn, O, Pd, and Al	XPS	After 9 L of oxygen (total = 10 L)	Bk 2, pg 4	6260908	
	overview, Zn, O, Pd, and Al	XPS	After 90 L of oxygen (total = 100 L)	Bk 2, pg 4	6260909	
	overview, Zn, O, Pd, and Al	XPS	After Annealing at 0.3 A for 20 mins	Bk 2, pg 4	6260910	
	overview, Zn, O, Pd, and Al	XPS	After 200 L of oxygen (total = 300 L) [finished expt]	Bk 2, pg 4	6260911	

Table 3A

Gd₅Ge₄ (010) Data List						
Date	Images / Spectrum	Instr.	Purpose	Lab #, Page #	File Name	Notes
10/27/2010	overview, Ge, Ge and Gd, Gd, O , and C	XPS	After exposure from Air (Depth Profiling Experiment)	Bk 3, pg 7	10271001	Initial composition after sample was exposed to air. Lots of carbon and oxygen.
	overview, Ge, Ge and Gd, Gd, O , and C	XPS	After 3 minutes of sputtering	Bk 3, pg 7	10271002	Carbon decreased, oxygen increased slightly.
	overview, Ge, Ge and Gd, Gd, O , and C	XPS	After 5 minutes of sputtering (total = 8 mins)	Bk 3, pg 8	10271003	Carbon decreased, oxygen decreased.
	overview, Ge, Ge and Gd, Gd, O , and C	XPS	After 10 minutes of sputtering (total = 18 mins)	Bk 3, pg 8	10271004	Carbon decreased, oxygen decreased.
	overview, Ge, Ge and Gd, Gd, O , and C	XPS	After 10 minutes of sputtering (total = 28 mins)	Bk 3, pg 8	10271005	A little amount of Carbon, oxygen decreasing.

Table 3A (Continue)

Date	Images / Spectrum	Instr.	Purpose	Lab #, Page #	File Name	Notes
10/27/2010	overview, Ge, Ge and Gd, Gd, O , and C	XPS	After 10 minutes of sputtering (total = 38 mins)	Bk 3, pg 9	10271006	No or very little C, oxygen decreasing.
	overview, Ge, Ge and Gd, Gd, O , and C	XPS	After 10 minutes of sputtering (total = 48 mins)	Bk 3, pg 9	10271007	Oxygen decreasing.
	overview, Ge, Ge and Gd, Gd, O , and C	XPS	After 15 minutes of sputtering (total = 63 mins)	Bk 3, pg 9	10271008	Huge decrease in Oxygen.
	overview, Ge, Ge and Gd, Gd, O , and C	XPS	After 15 minutes of sputtering (total = 78 mins)	Bk 3, pg 10	10271009	Oxygen decreasing.
	overview, Ge, Ge and Gd, Gd, and O	XPS	After 20 minutes of sputtering (total = 98 mins)	Bk 3, pg 10	10271010	oxygen decreasing.

Table 3A (Continue)

Date	Images / Spectrum	Instr.	Purpose	Lab #, Page #	File Name	Notes
10/28/2010	overview, Ge, Gd, and O	XPS	After 20 minutes of sputtering (total = 118 mins) [End Depth Profiling Experiment]	Bk 3, pg 11	10281001	Still have very little Oxygen, cannot get rid of it. No preferential sputtering of either Ge or Gd.
	overview, Ge, and Gd	XPS	After annealing at 400 K for 30 mins	Bk 3, pg 11	10281002	Start Depth Profiling Experiment.
	overview, Ge, and Gd	XPS	After 2 minutes of sputtering	Bk 3, pg 12	10281003	oxygen decreasing.
	overview, Ge, and Gd	XPS	After 2 minutes of sputtering (total = 4 mins)	Bk 3, pg 12	10281004	
	overview, Ge, and Gd	XPS	After 2 minutes of sputtering (total = 6 mins)	Bk 3, pg 12	10281005	
	overview, Ge, and Gd	XPS	After 2 minutes of sputtering (total = 8 mins)	Bk 3, pg 13	10281006	

Table 3A (Continue)

Date	Images / Spectrum	Instr.	Purpose	Lab #, Page #	File Name	Notes
10/28/2010	overview, Ge, and Gd	XPS	After 2 minutes of sputtering (total = 10 mins)	Bk 3, pg 13	10281007	End Depth Profiling Experiment. No preferential sputtering of either Ge or Gd.
	overview, Ge, and Gd	XPS	After annealing at 450 K for 30 mins	Bk 3, pg 13	10281008	Start Depth Profiling Experiment.
	overview, Ge, and Gd	XPS	After 2 minutes of sputtering	Bk 3, pg 14	10281009	
	overview, Ge, and Gd	XPS	After 2 minutes of sputtering (total = 4 mins)	Bk 3, pg 14	10281010	
	overview, Ge, and Gd	XPS	After 2 minutes of sputtering (total = 6 mins)	Bk 3, pg 14	10281011	
	overview, Ge, and Gd	XPS	After 2 minutes of sputtering (total = 8 mins)	Bk 3, pg 14	10281012	
	overview, Ge, and Gd	XPS	After 2 minutes of sputtering (total = 10 mins)	Bk 3, pg 15	10281013	End Depth Profiling Experiment. No preferential sputtering of either Ge or Gd.

Table 3A (Continue)

Date	Images / Spectrum	Instr.	Purpose	Lab #, Page #	File Name	Notes
10/29/2010	overview, Ge, and Gd	XPS	After annealing at 500 K for 30 mins	Bk 3, pg 15	10291001	Start Depth Profiling Experiment.
	overview, Ge, and Gd	XPS	After 2 minutes of sputtering	Bk 3, pg 15	10291002	
	overview, Ge, and Gd	XPS	After 2 minutes of sputtering (total = 4 mins)	Bk 3, pg 16	10291003	
	overview, Ge, and Gd	XPS	After 2 minutes of sputtering (total = 6 mins)	Bk 3, pg 16	10291004	
	overview, Ge, and Gd	XPS	After 2 minutes of sputtering (total = 8 mins)	Bk 3, pg 16	10291005	
	overview, Ge, and Gd	XPS	After 2 minutes of sputtering (total = 10 mins)	Bk 3, pg 17	10291006	End Depth Profiling Experiment. No preferential sputtering of either Ge or Gd.

Table 3A (Continue)

Date	Images / Spectrum	Instr.	Purpose	Lab #, Page #	File Name	Notes
11/1/2010	overview, Ge, and Gd	XPS	After annealing at 550 K for 30 mins	Bk 3, pg 17	11011001	Start Depth Profiling Experiment.
	overview, Ge, and Gd	XPS	After 2 minutes of sputtering	Bk 3, pg 17	11011002	
	overview, Ge, and Gd	XPS	After 2 minutes of sputtering (total = 4 mins)	Bk 3, pg 18	11011003	
	overview, Ge, and Gd	XPS	After 2 minutes of sputtering (total = 6 mins)	Bk 3, pg 18	11011004	
	overview, Ge, and Gd	XPS	After 2 minutes of sputtering (total = 8 mins)	Bk 3, pg 18	11011005	
	overview, Ge, and Gd	XPS	After 2 minutes of sputtering (total = 10 mins)	Bk 3, pg 19	11011006	End Depth Profiling Experiment. No preferential sputtering of either Ge or Gd.
	overview, Ge, and Gd	XPS	After annealing at 600 K for 30 mins	Bk 3, pg 19	11011007	Start Depth Profiling Experiment.
	overview, Ge, and Gd	XPS	After 2 minutes of sputtering	Bk 3, pg 19	11011008	
	overview, Ge, and Gd	XPS	After 2 minutes of sputtering (total = 4 mins)	Bk 3, pg 19	11011009	
	overview, Ge, and Gd	XPS	After 2 minutes of sputtering (total = 6 mins)	Bk 3, pg 20	11011010	
	overview, Ge, and Gd	XPS	After 2 minutes of sputtering (total = 8 mins)	Bk 3, pg 20	11011011	
	overview, Ge, and Gd	XPS	After 2 minutes of sputtering (total = 10 mins)	Bk 3, pg 20	11011012	End Depth Profiling Experiment. No preferential sputtering of either Ge or Gd.

Table 3A (Continue)

Date	Images / Spectrum	Instr.	Purpose	Lab #, Page #	File Name	Notes
11/2/2010	overview, Ge, and Gd	XPS	After annealing at 700 K for 30 mins	Bk 3, pg 21	11021001	Start Depth Profiling Experiment.
	overview, Ge, and Gd	XPS	After 2 minutes of sputtering	Bk 3, pg 21	11021002	
	overview, Ge, and Gd	XPS	After 2 minutes of sputtering (total = 4 mins)	Bk 3, pg 21	11021003	
	overview, Ge, and Gd	XPS	After 2 minutes of sputtering (total = 6 mins)	Bk 3, pg 22	11021004	
	overview, Ge, and Gd	XPS	After 2 minutes of sputtering (total = 8 mins)	Bk 3, pg 22	11021005	
	overview, Ge, and Gd	XPS	After 2 minutes of sputtering (total = 10 mins)	Bk 3, pg 22	11021006	End Depth Profiling Experiment. No preferential sputtering of either Ge or Gd.
11/9/2010	overview, Ge, and Gd	XPS	After annealing at 800 K for 30 mins	Bk 3, pg 28	11091001	Start Depth Profiling Experiment.
	overview, Ge, and Gd	XPS	After 2 minutes of sputtering	Bk 3, pg 28	11091002	
	overview, Ge, and Gd	XPS	After 2 minutes of sputtering (total = 4 mins)	Bk 3, pg 28	11091003	
	overview, Ge, and Gd	XPS	After 2 minutes of sputtering (total = 6 mins)	Bk 3, pg 29	11091004	
	overview, Ge, and Gd	XPS	After 2 minutes of sputtering (total = 8 mins)	Bk 3, pg 29	11091005	
	overview, Ge, and Gd	XPS	After 2 minutes of sputtering (total = 10 mins)	Bk 3, pg 29	11091006	End Depth Profiling Experiment. No preferential sputtering of either Ge or Gd.

Table 3A (Continue)

Date	Images / Spectrum	Instr.	Purpose	Lab #, Page #	File Name	Notes
11/11/2010	overview, Ge, and Gd	XPS	After annealing at 900 K for 30 mins	Bk 3, pg 29	11111001	Start Depth Profiling Experiment.
	overview, Ge, and Gd	XPS	After 2 minutes of sputtering	Bk 3, pg 32	11111002	XPS signal is decreasing! Something wrong with Channeltron(?)
	overview, Ge, and Gd	XPS	After 2 minutes of sputtering (total = 4 mins)	Bk 3, pg 32	11111003	
	overview, Ge, and Gd	XPS	After 2 minutes of sputtering (total = 6 mins)	Bk 3, pg 32	11111004	
	overview, Ge, and Gd	XPS	After 2 minutes of sputtering (total = 8 mins)	Bk 3, pg 33	11111005	
	overview, Ge, and Gd	XPS	After 2 minutes of sputtering (total = 10 mins)	Bk 3, pg 33	11111006	
	overview, Ge, and Gd	XPS	After 2 minutes of sputtering (total = 12 mins)	Bk 3, pg 33	11111007	
	overview, Ge, and Gd	XPS	After 2 minutes of sputtering (total = 14 mins)	Bk 3, pg 33	11111008	
	overview, Ge, and Gd	XPS	After 2 minutes of sputtering (total = 16 mins)	Bk 3, pg 34	11111009	Low Signal! Probably from the channeltron.

Table 3A (Continue)

Date	Images / Spectrum	Instr.	Purpose	Lab #, Page #	File Name	Notes
11/12/2010	overview, Ge, and Gd	XPS	After 2 minutes of sputtering (total = 18 mins)	Bk 3, pg 34	11121001 11121002	Low Signal! Probably from the channeltron.
	overview, Ge, and Gd	XPS	After 2 minutes of sputtering (total = 20 mins)	Bk 3, pg 35	11121003	Low Signal! Probably from the channeltron.
	overview, Ge, and Gd	XPS	After 2 minutes of sputtering (total = 22 mins)	Bk 3, pg 35	11121004	Low Signal! Probably from the channeltron.
	overview, Ge, and Gd	XPS	After 2 minutes of sputtering (total = 24 mins)	Bk 3, pg 35	11121005	Low Signal! Probably from the channeltron.
	overview, Ge, and Gd	XPS	After 2 minutes of sputtering (total = 26 mins)	Bk 3, pg 35	11121006	End Depth Profiling Experiment. No preferential sputtering of either Ge or Gd. Low Signal! Probably from the channeltron.
11/16/2010	M1 - M48	STM	After sputtering, room temperature = 300 K	Bk 3, pg 37	11/16/2010	Middle of sample: see step-terrace morphology, protrusions on terraces caused by sputter damaged.
	M49 - M73	STM	After sputtering, room temperature = 300 K	Bk 3, pg 37		Upper left corner of sample: see small step-terrace features.
	M74 - M86	STM	After sputtering, room temperature = 300 K	Bk 3, pg 37		Upper right corner of sample: very rough surface, small step-terrace features.
	M87 - M107	STM	After sputtering, room temperature = 300 K	Bk 3, pg 37		Lower right corner of sample: very rough surface, small step-terrace features.
	M108 - M123	STM	After sputtering, room temperature = 300 K	Bk 3, pg 38		Lower left corner of sample: very rough surface, small step-terrace features.

Table 3A (Continue)

Date	Images / Spectrum	Instr.	Purpose	Lab #, Page #	File Name	Notes
11/20/2010	M1 - M27	STM	After sputtering for 5 mins and annealing at 900 K for 2 hours	Bk 3, pg 40	11/20/2010	Middle of sample: rough surface, signs of step-terrace morphology on almost every image.
	M28 - M41	STM	After sputtering for 5 mins and annealing at 900 K for 2 hours	Bk 3, pg 40		Right of sample: step-terrace morphology, same features as in middle of sample.
	M42 - M57	STM	After sputtering for 5 mins and annealing at 900 K for 2 hours	Bk 3, pg 40		Left of sample: rough surface compared to middle of sample. Step-terrace morphology, same features as in middle of sample.
11/24/2010	M1 - M7	STM	After sputtering for 15 mins and annealing at 900 K for 2 hours	Bk 3, pg 43	11/24/2010	Middle of sample: Huge improvement in step-terrace features.
	M8 - M11	STM	After sputtering for 15 mins and annealing at 900 K for 2 hours	Bk 3, pg 43		Right of sample: surface looks worse than previous STM run. Surface is rough.
	M12 - M32	STM	After sputtering for 15 mins and annealing at 900 K for 2 hours	Bk 3, pg 43		Left of sample: see a smooth area of step-terrace features.
11/29/2010	M1 - M22	STM	After annealing at 1050 K for 15 mins	Bk 3, pg 47	11/29/2010	Middle of sample: lots of terraces.
	M23 - M33	STM	After annealing at 1050 K for 15 mins	Bk 3, pg 47		Right of sample: lots of small terraces. More rough surface compared to middle of sample.
	M34 - M70	STM	After annealing at 1050 K for 15 mins	Bk 3, pg 47		Left of sample: terraces are bigger and much smoother than middle and right side of sample.

Table 3A (Continue)

Date	Images / Spectrum	Instr.	Purpose	Lab #, Page #	File Name	Notes
12/2/2010	M1 - M26	STM	After annealing at 1100 K for 15 mins	Bk 3, pg 51	12/2/2010	Middle of sample: a new terrace starts to emerge "label as Terrace B" (looks like double step effect). See circle bumps or islands on terrace.
	M27 - M45	STM	After annealing at 1100 K for 15 mins	Bk 3, pg 51		Right of sample: same features as in the middle of the sample.
	M46 - M70	STM	After annealing at 1100 K for 15 mins	Bk 3, pg 51		Left of sample: big terraces. Same features as in the middle of the sample.
12/4/2010	M1 - M23	STM	After annealing at 1150 K for 15 mins	Bk 3, pg 54	12/4/2010	Middle of sample: "Terrace B" is a little more noticeable. Bumps or islands are on the main terrace "labeled as Terrace A".
	M24 - M47	STM	After annealing at 1150 K for 15 mins	Bk 3, pg 55		Right of sample: same features as in the middle of the sample.
	M48 - M97	STM	After annealing at 1150 K for 15 mins	Bk 3, pg 55		Left of sample: same features as in the middle of the sample.
12/6/2010	M1 - M25	STM	After annealing at 1200 K for 15 mins	Bk 3, pg 58	12/6/2010	Middle of sample: can see the difference between terrace A and terrace B. Terrace B has no islands or bumps while terrace A does. The islands or bumps changed shape from circles to squares. Noisy!
	M26 - M30	STM	After annealing at 1200 K for 15 mins	Bk 3, pg 58		Right of sample: same features as in the middle of the sample. Noisy!
	M31 - M33	STM	After annealing at 1200 K for 15 mins	Bk 3, pg 58		Left of sample: same features as in the middle of the sample. Really noisy!

Table 3A (Continue)

Date	Images / Spectrum	Instr.	Purpose	Lab #, Page #	File Name	Notes
12/8/2010	M1 - M27	STM	After annealing at 1100 K for 15 mins	Bk 3, pg 60	12/8/2010	Middle of sample: see terrace features. Still have bumps or islands on surface as well as terrace B. Similar features compared with STM images at 12/2/2010.
	M28 - M36	STM	After annealing at 1100 K for 15 mins	Bk 3, pg 60		Right of sample: step bunching, lots of bumps or islands on terraces. Terrace B also visible.
	M37 - M52	STM	After annealing at 1100 K for 15 mins	Bk 3, pg 61		Left of sample: same features as in middle right of sample.
12/10/2010	M1 - M33	STM	After annealing at 1050 K for 15 mins	Bk 3, pg 63	12/10/2010	Middle of sample: see terraces, islands or bumps on terraces, and terrace B.
	M34 - M48	STM	After annealing at 1050 K for 15 mins	Bk 3, pg 64		Right of sample: same features as in middle of surface.
	M49 - M56	STM	After annealing at 1050 K for 15 mins	Bk 3, pg 64		Left of sample: same features as in middle of sample.
12/11/2010	overview, Ge, Gd, and O	XPS	Clean surface at 300 K	Bk 3, pg 64	12111001	Beginning of Oxidation experiment.
	overview, Ge, Gd, and O	XPS	After 100 L oxygen exposure at 300 K	Bk 3, pg 65		Done at 300 K, exposed for 16 mins and 40 secs at 1.3E-7 mbar. End of Oxidation experiment.

Table 3A (Continue)

Date	Images / Spectrum	Instr.	Purpose	Lab #, Page #	File Name	Notes
12/12/2010	overview, Ge, Gd, and O	XPS	Clean surface at 300 K	Bk 3, pg 66	12121001	Beginning of Oxidation experiment.
	overview, Ge, Gd, and O	XPS	Clean surface at 600 K	Bk 3, pg 67	12121002	Small peak intensities compared to room temperature at 12121001.
	overview, Ge, Gd, and O	XPS	After 100 L oxygen exposure at 600 K	Bk 3, pg 67	12121003	Done at 600 K, exposed for 16 mins and 40 secs at 1.3E-7 mbar. Did not see any peaks. Very little peak of oxygen. Probably from the electronics.
	overview, Ge, Gd, and O	XPS	After cool down to room temperature = 300 K	Bk 3, pg 67	12121004	See peaks. Running XPS at 600 K was the problem. End of Oxidation experiment.
12/12/2010	overview, Ge, Gd, and O	XPS	Clean surface at 300 K	Bk 3, pg 69	12131002	Beginning of Oxidation experiment.
	overview, Ge, Gd, and O	XPS	After 0.5 L oxygen exposure	Bk 3, pg 69	12131003	Done at 300 K, exposed for 50 secs at 1.3E-8 mbar.
	overview, Ge, Gd, and O	XPS	After 1.5 L oxygen exposure (total exposure = 2 L)	Bk 3, pg 70	12131004	Done at 300 K, exposed for 2 mins 30 secs at 1.3E-8 mbar.
	overview, Ge, Gd, and O	XPS	After 8 L oxygen exposure (total exposure = 10 L)	Bk 3, pg 70	12131005	Done at 300 K, exposed for 2 mins 40 secs at 6.5E-8 mbar.
	overview, Ge, Gd, and O	XPS	After 90 L oxygen exposure (total exposure = 100 L)	Bk 3, pg 70	12131006	Done at 300 K, exposed for 15 mins at 1.3E-7 mbar. End of Oxidation experiment.

Table 3A (Continue)

Date	Images / Spectrum	Instr.	Purpose	Lab #, Page #	File Name	Notes
4/21/2011	overview, Ge, Gd, O, and C	XPS	After annealing at 900 K for 30 mins	Bk 3, pg 88	4211101	Start Depth Profiling Experiment.
	overview, Ge, Gd, O, and C	XPS	After 2 minutes of sputtering	Bk 3, pg 89	4211102	
	overview, Ge, Gd, O, and C	XPS	After 2 minutes of sputtering (total = 4 mins)	Bk 3, pg 89	4211103	
	overview, Ge, Gd, O, and C	XPS	After 2 minutes of sputtering (total = 6 mins)	Bk 3, pg 89	4211104	
	overview, Ge, Gd, O, and C	XPS	After 2 minutes of sputtering (total = 8 mins)	Bk 3, pg 90	4211105	
	overview, Ge, Gd, O, and C	XPS	After 2 minutes of sputtering (total = 10 mins)	Bk 3, pg 90	4211106	
	overview, Ge, Gd, O, and C	XPS	After 2 minutes of sputtering (total = 12 mins)	Bk 3, pg 90	4211107	
	overview, Ge, Gd, O, and C	XPS	After 2 minutes of sputtering (total = 14 mins)	Bk 3, pg 91	4211108	

Table 3A (Continue)

Date	Images / Spectrum	Instr.	Purpose	Lab #, Page #	File Name	Notes
4/22/2011	overview, Ge, and Gd	XPS	After 2 minutes of sputtering (total = 16 mins)	Bk 3, pg 91	4221102	Bad connection between XPS and computer on File 04221101. Had to repeat XPS.
	overview, Ge, and Gd	XPS	After 2 minutes of sputtering (total = 18 mins)	Bk 3, pg 92	4221103	
	overview, Ge, and Gd	XPS	After 2 minutes of sputtering (total = 20 mins)	Bk 3, pg 92	4221104	
	overview, Ge, and Gd	XPS	After 2 minutes of sputtering (total = 22 mins)	Bk 3, pg 92	4221105	
	overview, Ge, and Gd	XPS	After 2 minutes of sputtering (total = 24 mins)	Bk 3, pg 93	4221106	
	overview, Ge, and Gd	XPS	After 2 minutes of sputtering (total = 26 mins)	Bk 3, pg 93	4221107	
	overview, Ge, and Gd	XPS	After 2 minutes of sputtering (total = 28 mins)	Bk 3, pg 93	4221108	End Depth-Profiling experiment. No preferential sputtering of either Ge or Gd.
4/24/2011	M1 - M30	STM	After annealing 1 hour at 900 K	Bk 3, pg 94	4/24/2011	Middle of sample: see terraces and the emergence of Terrace B.
	M31 - M48	STM	After annealing 1 hour at 900 K	Bk 3, pg 95		Right of sample: see terraces, vacancy-pits, emergence of Terrace B, and high resolution images.
	M49 - M67	STM	After annealing 1 hour at 900 K	Bk 3, pg 95		Left of sample: see terraces, emergence of Terrace B, and high resolution images.

Table 3A (Continue)

Date	Images / Spectrum	Instr.	Purpose	Lab #, Page #	File Name	Notes
4/25/2011	M1 - M38	STM	After annealing 1 hour at 900 K	Bk 3, pg 96	4/25/2011	Middle of sample: see terraces, emergence of Terrace B, and high resolution images.
	M39 - M66	STM	After annealing 1 hour at 900 K	Bk 3, pg 96		Right of sample: see terraces, vacancy-pits, emergence of Terrace B, and high resolution images.
	M67 - M94	STM	After annealing 1 hour at 900 K	Bk 3, pg 97		Left of sample: see terraces, vacancy-pits, bumps on terraces, and the emergence of Terrace B.
4/27/2011	M1 - M26	STM	After annealing 1 hour at 900 K	Bk 3, pg 98	4/27/2011	Middle of sample: see terraces, vacancy-pits, emergence of Terrace B, and high resolution images.
	M27- M46	STM	After annealing 1 hour at 900 K	Bk 3, pg 99		Right of sample: see terraces, vacancy-pits, emergence of Terrace B, and high resolution images.
	M47- M54	STM	After annealing 1 hour at 900 K	Bk 3, pg 99		Left of sample: see terraces, lots of vacancy-pits, and bumps (very similar to the 1150 K data from previous sample).
	M55 - M76	STM	After annealing 1 hour at 900 K	Bk 3, pg 99		Between left and middle of sample: see terraces, vacancy-pits, and emergence of Terrace B.
4/29/2011	M1 - M28	STM	After annealing 1 hour at 900 K	Bk 3, pg 100	4/29/2011	Middle of sample: see terraces, emergence of Terrace B, and high resolution images.
	M29 - M51	STM	After annealing 1 hour at 900 K	Bk 3, pg 101		Right of sample: see terraces, vacancy-pits, emergence of Terrace B, and high resolution images.
	M52 - M88	STM	After annealing 1 hour at 900 K	Bk 3, pg 101		Left of sample: see terraces, vacancy-pits, bumps on terraces, and the emergence of Terrace B. Also see different grain boundaries at large image scales.

Table 3A (Continue)

Date	Images / Spectrum	Instr.	Purpose	Lab #, Page #	File Name	Notes
5/6/2011	overview, Ge, and Gd	XPS	After annealing 900 K for 30 mins	Bk 3, pg 106	2011-05-06-01	Start Depth Profiling Experiment.
	overview, Ge, and Gd	XPS	After 15 secs of sputtering	Bk 3, pg 107	2011-05-06-02	
	overview, Ge, and Gd	XPS	After 15 secs of sputtering (total = 30 secs)	Bk 3, pg 107	2011-05-06-03	
	overview, Ge, and Gd	XPS	After 15 secs of sputtering (total = 45 secs)	Bk 3, pg 107	2011-05-06-04	
	overview, Ge, and Gd	XPS	After 15 secs of sputtering (total = 60 secs)	Bk 3, pg 107	2011-05-06-05	
	overview, Ge, and Gd	XPS	After 15 secs of sputtering (total = 75 secs)	Bk 3, pg 108	2011-05-06-06	
	overview, Ge, and Gd	XPS	After 15 secs of sputtering (total = 90 secs)	Bk 3, pg 108	2011-05-06-07	

Table 3A (Continue)

Date	Images / Spectrum	Instr.	Purpose	Lab #, Page #	File Name	Notes
5/6/2011	overview, Ge, and Gd	XPS	After 15 secs of sputtering (total = 105 secs)	Bk 3, pg 108	2011-05-06-08	
	overview, Ge, and Gd	XPS	After 15 secs of sputtering (total = 120 secs)	Bk 3, pg 109	2011-05-06-09	
	overview, Ge, and Gd	XPS	After 15 secs of sputtering (total = 135 secs)	Bk 3, pg 109	2011-05-06-10	
	overview, Ge, and Gd	XPS	After 15 secs of sputtering (total = 150 secs)	Bk 3, pg 109	2011-05-06-11	
	overview, Ge, and Gd	XPS	After 15 secs of sputtering (total = 165 secs)	Bk 3, pg 109	2011-05-06-12	
	overview, Ge, and Gd	XPS	After 15 secs of sputtering (total = 180 secs)	Bk 3, pg 110	2011-05-06-13	
5/7/2011	overview, Ge, and Gd	XPS	After 15 secs of sputtering (total = 195 secs)	Bk 3, pg 110	2011-05-07-01	
	overview, Ge, and Gd	XPS	After 15 secs of sputtering (total = 210 secs)	Bk 3, pg 110	2011-05-07-02	
	overview, Ge, and Gd	XPS	After 15 secs of sputtering (total = 225 secs)	Bk 3, pg 111	2011-05-07-03	
	overview, Ge, and Gd	XPS	After 15 secs of sputtering (total = 240 secs)	Bk 3, pg 111	2011-05-07-04	

Table 3A (Continue)

Date	Images / Spectrum	Instr.	Purpose	Lab #, Page #	File Name	Notes
5/9/2011	M1 - M36	STM	After annealing at 1200 K for 15 mins	Bk 3, pg 113	5/9/2011	Middle of sample: see terraces, high resolution images, and faint outline areas near step edges.
	M37 - M65	STM	After annealing at 1200 K for 15 mins	Bk 3, pg 113		Right of sample: see terraces, vacancy-pits, emergence of Terrace B, and high resolution images.
	M66 - M88	STM	After annealing at 1200 K for 15 mins	Bk 3, pg 113		Left of sample: see terraces, vacancy-pits, and vacancy-voids.
5/11/2011	M1 - M18	STM	After 1 minute of sputtering	Bk 3, pg 116	2011-05-11-01	Middle of sample: see terraces, outline blobs near step edges, and lots of small pits on terraces.
	M19 - M32	STM	After 1 minute of sputtering	Bk 3, pg 116		Right of sample: see terraces, vacancy-pits, bumps on terraces, and high resolution images.
	M33 - M41	STM	After 1 minute of sputtering	Bk 3, pg 116		Left of sample: see terraces, vacancy-pits, vacancy-voids, and step edges seemed to be more choppy.
	M1 - M29	STM	After annealing at 900 K for 15 mins	Bk 3, pg 116	2011-05-11-02	Middle of sample: see terraces, outline blobs near step edges, and high resolution images indicating two structures.
	M30 - M47	STM	After annealing at 900 K for 15 mins	Bk 3, pg 117		Right of sample: see terraces, vacancy-pits, tooth shape step edges, bumps on terraces, and high resolution images.
	M48 - M65	STM	After annealing at 900 K for 15 mins	Bk 3, pg 117		Left of sample: see terraces, vacancy-pits, vacancy-voids, and high resolution images.

Table 3A (Continue)

Date	Images / Spectrum	Instr.	Purpose	Lab #, Page #	File Name	Notes
5/13/2011	M1 - M6	STM	After annealing at 1050 K for 15 mins	Bk 3, pg 120	5/13/2011	Middle of sample: see terraces, vacancy-pits, and lots of rough areas.
	M7 - M27	STM	After annealing at 1050 K for 15 mins	Bk 3, pg 120		Middle of sample (different area): see terraces and vacancy-voids.
	M28 - M54	STM	After annealing at 1050 K for 15 mins	Bk 3, pg 120		Right of sample: see terraces, vacancy-pits, bumps on terraces, and weird step edge shapes.
	M55 - M69	STM	After annealing at 1050 K for 15 mins	Bk 3, pg 120		Left of sample: see terraces, vacancy-pits, and lots of depressions on terraces.
5/17/2011	M1 - M31	STM	After annealing at 1050 K for 15 mins	Bk 3, pg 124	5/17/2011	Middle of sample: see terraces, curly step edges, bumps on terraces, and an expanded Terrace B.
	M32 - M55	STM	After annealing at 1050 K for 15 mins	Bk 3, pg 125		Right of sample: see terraces, similar to middle of sample.
	M56 - M74	STM	After annealing at 1050 K for 15 mins	Bk 3, pg 125		Left of sample: see terraces, vacancy-pits, bumps on terraces, and an expanded Terrace B.
5/18/2011	overview, Ge, and Gd	XPS	After sputtering for 15 mins	Bk 3, pg 126	2011-05-18-02	Small take-off angle with respect to analyzer (20°) - more surface sensitive.
	overview, Ge, and Gd	XPS	After annealing at 900 K for 15 mins	Bk 3, pg 126	2011-05-18-03	Small take-off angle with respect to analyzer (20°) - more surface sensitive.

Table 3A (Continue)

Date	Images / Spectrum	Instr.	Purpose	Lab #, Page #	File Name	Notes
4/25/2012	overview, Ge, Gd, and O	XPS	After sputtering for 15 mins	Bk 3, pg 139	2012-04-25-02	Surface concentration at 300 K
	overview, Ge, Gd, and O	XPS	After sputtering for 15 mins	Bk 3, pg 139	2012-04-25-03	Surface concentration at 300 K
	overview, Ge, and Gd	XPS	After annealing to 400 K for 30 mins	Bk 3, pg 140	2012-04-25-06	Surface concentration at 400 K
4/26/2012	overview, Ge, and Gd	XPS	After annealing to 400 K for 30 mins	Bk 3, pg 141	2012-04-26-01	Surface concentration at 400 K
	overview, Ge, and Gd	XPS	After annealing to 450 K for 30 mins	Bk 3, pg 141	2012-04-26-02	Surface concentration at 450 K
	overview, Ge, and Gd	XPS	After annealing to 450 K for 30 mins	Bk 3, pg 142	2012-04-26-03	Surface concentration at 450 K
	overview, Ge, and Gd	XPS	After annealing to 500 K for 30 mins	Bk 3, pg 142	2012-04-26-04	Surface concentration at 500 K
	overview, Ge, and Gd	XPS	After annealing to 500 K for 30 mins	Bk 3, pg 142	2012-04-26-05	Surface concentration at 500 K
4/27/2012	overview, Ge, and Gd	XPS	After annealing to 550 K for 30 mins	Bk 3, pg 143	2012-04-27-01	Surface concentration at 550 K
	overview, Ge, and Gd	XPS	After annealing to 550 K for 30 mins	Bk 3, pg 144	2012-04-27-02	Surface concentration at 550 K
	overview, Ge, and Gd	XPS	After annealing to 600 K for 30 mins	Bk 3, pg 144	2012-04-27-03	Surface concentration at 600 K
	overview, Ge, and Gd	XPS	After annealing to 600 K for 30 mins	Bk 3, pg 145	2012-04-27-04	Surface concentration at 600 K

Table 3A (Continue)

Date	Images / Spectrum	Instr.	Purpose	Lab #, Page #	File Name	Notes
4/28/2012	overview, Ge, and Gd	XPS	After annealing to 700 K for 30 mins	Bk 3, pg 145	2012-04-28-01	Surface concentration at 700 K
	overview, Ge, and Gd	XPS	After annealing to 700 K for 30 mins	Bk 3, pg 146	2012-04-28-02	Surface concentration at 700 K
4/29/2012	overview, Ge, and Gd	XPS	After annealing to 800 K for 30 mins	Bk 3, pg 146	2012-04-29-01	Surface concentration at 800 K
	overview, Ge, and Gd	XPS	After annealing to 800 K for 30 mins	Bk 3, pg 147	2012-04-29-02	Surface concentration at 800 K
4/30/2012	overview, Ge, and Gd	XPS	After annealing to 900 K for 30 mins	Bk 3, pg 147	2012-04-30-01	Surface concentration at 900 K
	overview, Ge, and Gd	XPS	After annealing to 900 K for 30 mins	Bk 3, pg 148	2012-04-30-02	Surface concentration at 900 K
5/1/2012	overview, Ge, and Gd	XPS	After annealing to 1050 K for 30 mins	Bk 3, pg 148	2012-05-01-01	Surface concentration at 1050 K
	overview, Ge, and Gd	XPS	After annealing to 1050 K for 30 mins	Bk 3, pg 149	2012-05-01-02	Surface concentration at 1050 K
	overview, Ge, and Gd	XPS	After annealing to 1100 K for 30 mins	Bk 3, pg 149	2012-05-01-03	Surface concentration at 1100 K
	overview, Ge, and Gd	XPS	After annealing to 1100 K for 30 mins	Bk 3, pg 149	2012-05-01-04	Surface concentration at 1100 K
	overview, Ge, and Gd	XPS	After annealing to 1150 K for 30 mins	Bk 3, pg 150	2012-05-01-06	Surface concentration at 1150 K
5/2/2012	overview, Ge, and Gd	XPS	After annealing to 1150 K for 30 mins	Bk 3, pg 150	2012-05-02-01	Surface concentration at 1150 K
5/3/2012	overview, Ge, and Gd	XPS	After annealing to 1200 K for 30 mins	Bk 3, pg 153	2012-05-03-01	Surface concentration at 1200 K
	overview, Ge, and Gd	XPS	After annealing to 1200 K for 30 mins	Bk 3, pg 153	2012-05-03-02	Surface concentration at 1200 K

Table 3A (Continue)

Date	Images / Spectrum	Instr.	Purpose	Lab #, Page #	File Name	Notes
6/25/2012	overview, Ge, and Gd	XPS	After annealing to 700 K for 30 mins	Bk 4, pg 101	2012-06-25-01	Beginning of Depth Profiling Experiment at 700 K
	overview, Ge, and Gd	XPS	After sputtering for 30 secs	Bk 4, pg 102	2012-06-25-02	
	overview, Ge, and Gd	XPS	After sputtering for 30 secs (total = 1 min)	Bk 4, pg 102	2012-06-25-03	
	overview, Ge, and Gd	XPS	After sputtering for 30 secs (total = 1.5 mins)	Bk 4, pg 102	2012-06-25-04	
	overview, Ge, and Gd	XPS	After sputtering for 30 secs (total = 2 mins)	Bk 4, pg 102	2012-06-25-05	
	overview, Ge, and Gd	XPS	After sputtering for 30 secs (total = 2.5 mins)	Bk 4, pg 102	2012-06-25-06	
	overview, Ge, and Gd	XPS	After sputtering for 30 secs (total = 3 mins)	Bk 4, pg 103	2012-06-25-07	
	overview, Ge, and Gd	XPS	After sputtering for 30 secs (total = 3.5 mins)	Bk 4, pg 103	2012-06-25-08	
	overview, Ge, and Gd	XPS	After sputtering for 30 secs (total = 4 mins)	Bk 4, pg 103	2012-06-25-09	
	overview, Ge, and Gd	XPS	After sputtering for 30 secs (total = 4.5 mins)	Bk 4, pg 103	2012-06-25-10	

Table 3A (Continue)

Date	Images / Spectrum	Instr.	Purpose	Lab #, Page #	File Name	Notes
6/25/2012	overview, Ge, and Gd	XPS	After sputtering for 30 secs (total = 5 mins)	Bk 4, pg 103	2012-06-25-11	
	overview, Ge, and Gd	XPS	After sputtering for 30 secs (total = 5.5 mins)	Bk 4, pg 103	2012-06-25-12	
	overview, Ge, and Gd	XPS	After sputtering for 30 secs (total = 6 mins)	Bk 4, pg 104	2012-06-25-13	
	overview, Ge, and Gd	XPS	After sputtering for 30 secs (total = 6.5 mins)	Bk 4, pg 104	2012-06-25-14	
	overview, Ge, and Gd	XPS	After sputtering for 30 secs (total = 7 mins)	Bk 4, pg 104	2012-06-25-15	
	overview, Ge, and Gd	XPS	After sputtering for 30 secs (total = 7.5 mins)	Bk 4, pg 104	2012-06-25-16	
	overview, Ge, and Gd	XPS	After sputtering for 30 secs (total = 8 mins)	Bk 4, pg 104	2012-06-25-17	
	overview, Ge, and Gd	XPS	After sputtering for 30 secs (total = 8.5 mins)	Bk 4, pg 104	2012-06-25-18	
	overview, Ge, and Gd	XPS	After sputtering for 30 secs (total = 9 mins)	Bk 4, pg 105	2012-06-25-19	
	overview, Ge, and Gd	XPS	After sputtering for 30 secs (total = 9.5 mins)	Bk 4, pg 105	2012-06-25-20	
	overview, Ge, and Gd	XPS	After sputtering for 30 secs (total = 10 mins)	Bk 4, pg 105	2012-06-25-21	End of Depth Profiling Experiment at 700 K

Table 3A (Continue)

Date	Images / Spectrum	Instr.	Purpose	Lab #, Page #	File Name	Notes
6/26/2012	overview, Ge, and Gd	XPS	After annealing to 900 K for 30 mins	Bk 4, pg 105	2012-06-26-01	Beginning of Depth Profiling Experiment at 900 K
	overview, Ge, and Gd	XPS	After sputtering for 30 secs	Bk 4, pg 106	2012-06-26-02	
	overview, Ge, and Gd	XPS	After sputtering for 30 secs (total = 1 min)	Bk 4, pg 106	2012-06-26-03	
	overview, Ge, and Gd	XPS	After sputtering for 30 secs (total = 1.5 mins)	Bk 4, pg 106	2012-06-26-04	
	overview, Ge, and Gd	XPS	After sputtering for 30 secs (total = 2 mins)	Bk 4, pg 106	2012-06-26-05	
	overview, Ge, and Gd	XPS	After sputtering for 30 secs (total = 2.5 mins)	Bk 4, pg 106	2012-06-26-06	
	overview, Ge, and Gd	XPS	After sputtering for 30 secs (total = 3 mins)	Bk 4, pg 107	2012-06-26-07	
	overview, Ge, and Gd	XPS	After sputtering for 30 secs (total = 3.5 mins)	Bk 4, pg 107	2012-06-26-08	
	overview, Ge, and Gd	XPS	After sputtering for 30 secs (total = 4 mins)	Bk 4, pg 107	2012-06-26-09	
	overview, Ge, and Gd	XPS	After sputtering for 30 secs (total = 4.5 mins)	Bk 4, pg 107	2012-06-26-10	

Table 3A (Continue)

Date	Images / Spectrum	Instr.	Purpose	Lab #, Page #	File Name	Notes
6/26/2012	overview, Ge, and Gd	XPS	After sputtering for 30 secs (total = 5 mins)	Bk 4, pg 107	2012-06-26-11	
	overview, Ge, and Gd	XPS	After sputtering for 30 secs (total = 5.5 mins)	Bk 4, pg 107	2012-06-26-12	
	overview, Ge, and Gd	XPS	After sputtering for 30 secs (total = 6 mins)	Bk 4, pg 108	2012-06-26-13	
	overview, Ge, and Gd	XPS	After sputtering for 30 secs (total = 6.5 mins)	Bk 4, pg 108	2012-06-26-14	
	overview, Ge, and Gd	XPS	After sputtering for 30 secs (total = 7 mins)	Bk 4, pg 108	2012-06-26-15	
	overview, Ge, and Gd	XPS	After sputtering for 30 secs (total = 7.5 mins)	Bk 4, pg 108	2012-06-26-16	
	overview, Ge, and Gd	XPS	After sputtering for 30 secs (total = 8 mins)	Bk 4, pg 108	2012-06-26-17	
	overview, Ge, and Gd	XPS	After sputtering for 30 secs (total = 8.5 mins)	Bk 4, pg 108	2012-06-26-18	
	overview, Ge, and Gd	XPS	After sputtering for 30 secs (total = 9 mins)	Bk 4, pg 109	2012-06-26-19	
	overview, Ge, and Gd	XPS	After sputtering for 30 secs (total = 9.5 mins)	Bk 4, pg 109	2012-06-26-20	
	overview, Ge, and Gd	XPS	After sputtering for 30 secs (total = 10 mins)	Bk 4, pg 109	2012-06-26-21	End of Depth Profiling Experiment at 900 K

Table 3A (Continue)

Date	Images / Spectrum	Instr.	Purpose	Lab #, Page #	File Name	Notes
6/27/2012	overview, Ge, and Gd	XPS	After annealing to 900 K for 30 mins	Bk 4, pg 109	2012-06-27-01	Beginning of Depth Profiling Experiment at 1100 K
	overview, Ge, and Gd	XPS	After sputtering for 30 secs	Bk 4, pg 110	2012-06-27-02	
	overview, Ge, and Gd	XPS	After sputtering for 30 secs (total = 1 min)	Bk 4, pg 110	2012-06-27-03	
	overview, Ge, and Gd	XPS	After sputtering for 30 secs (total = 1.5 mins)	Bk 4, pg 110	2012-06-27-04	
	overview, Ge, and Gd	XPS	After sputtering for 30 secs (total = 2 mins)	Bk 4, pg 110	2012-06-27-05	
	overview, Ge, and Gd	XPS	After sputtering for 30 secs (total = 2.5 mins)	Bk 4, pg 110	2012-06-27-06	
	overview, Ge, and Gd	XPS	After sputtering for 30 secs (total = 3 mins)	Bk 4, pg 110	2012-06-27-07	
	overview, Ge, and Gd	XPS	After sputtering for 30 secs (total = 3.5 mins)	Bk 4, pg 111	2012-06-27-08	
	overview, Ge, and Gd	XPS	After sputtering for 30 secs (total = 4 mins)	Bk 4, pg 111	2012-06-27-09	
	overview, Ge, and Gd	XPS	After sputtering for 30 secs (total = 4.5 mins)	Bk 4, pg 111	2012-06-27-10	

Table 3A (Continue)

Date	Images / Spectrum	Instr.	Purpose	Lab #, Page #	File Name	Notes
6/27/2012	overview, Ge, and Gd	XPS	After sputtering for 30 secs (total = 5 mins)	Bk 4, pg 111	2012-06-27-11	
	overview, Ge, and Gd	XPS	After sputtering for 30 secs (total = 5.5 mins)	Bk 4, pg 111	2012-06-27-12	
	overview, Ge, and Gd	XPS	After sputtering for 30 secs (total = 6 mins)	Bk 4, pg 111	2012-06-27-13	
	overview, Ge, and Gd	XPS	After sputtering for 30 secs (total = 6.5 mins)	Bk 4, pg 111	2012-06-27-14	
	overview, Ge, and Gd	XPS	After sputtering for 30 secs (total = 7 mins)	Bk 4, pg 112	2012-06-27-15	
	overview, Ge, and Gd	XPS	After sputtering for 30 secs (total = 7.5 mins)	Bk 4, pg 112	2012-06-27-16	
	overview, Ge, and Gd	XPS	After sputtering for 30 secs (total = 8 mins)	Bk 4, pg 112	2012-06-27-17	
	overview, Ge, and Gd	XPS	After sputtering for 30 secs (total = 8.5 mins)	Bk 4, pg 112	2012-06-27-18	
	overview, Ge, and Gd	XPS	After sputtering for 30 secs (total = 9 mins)	Bk 4, pg 112	2012-06-27-19	
	overview, Ge, and Gd	XPS	After sputtering for 30 secs (total = 9.5 mins)	Bk 4, pg 112	2012-06-27-20	
	overview, Ge, and Gd	XPS	After sputtering for 30 secs (total = 10 mins)	Bk 4, pg 112	2012-06-27-21	End of Depth Profiling Experiment at 1100 K

Table 3A (Continue)

Date	Images / Spectrum	Instr.	Purpose	Lab #, Page #	File Name	Notes
6/28/2012	overview, Ge, and Gd	XPS	After annealing to 900 K for 30 mins	Bk 4, pg 113	2012-06-28-01	Beginning of Depth Profiling Experiment at 1200 K
	overview, Ge, and Gd	XPS	After sputtering for 30 secs	Bk 4, pg 113	2012-06-28-02	
	overview, Ge, and Gd	XPS	After sputtering for 30 secs (total = 1 min)	Bk 4, pg 113	2012-06-28-03	
	overview, Ge, and Gd	XPS	After sputtering for 30 secs (total = 1.5 mins)	Bk 4, pg 113	2012-06-28-04	
	overview, Ge, and Gd	XPS	After sputtering for 30 secs (total = 2 mins)	Bk 4, pg 114	2012-06-28-05	
	overview, Ge, and Gd	XPS	After sputtering for 30 secs (total = 2.5 mins)	Bk 4, pg 114	2012-06-28-06	
	overview, Ge, and Gd	XPS	After sputtering for 30 secs (total = 3 mins)	Bk 4, pg 114	2012-06-28-07	
	overview, Ge, and Gd	XPS	After sputtering for 30 secs (total = 3.5 mins)	Bk 4, pg 114	2012-06-28-08	
	overview, Ge, and Gd	XPS	After sputtering for 30 secs (total = 4 mins)	Bk 4, pg 114	2012-06-28-09	
	overview, Ge, and Gd	XPS	After sputtering for 30 secs (total = 4.5 mins)	Bk 4, pg 114	2012-06-28-10	
	overview, Ge, and Gd	XPS	After sputtering for 30 secs (total = 5 mins)	Bk 4, pg 114	2012-06-28-11	

Table 3A (Continue)

Date	Images / Spectrum	Instr.	Purpose	Lab #, Page #	File Name	Notes
6/28/2012	overview, Ge, and Gd	XPS	After sputtering for 30 secs (total = 5.5 mins)	Bk 4, pg 115	2012-06-28-12	
	overview, Ge, and Gd	XPS	After sputtering for 30 secs (total = 6 mins)	Bk 4, pg 115	2012-06-28-13	
	overview, Ge, and Gd	XPS	After sputtering for 30 secs (total = 6.5 mins)	Bk 4, pg 115	2012-06-28-14	
	overview, Ge, and Gd	XPS	After sputtering for 30 secs (total = 7 mins)	Bk 4, pg 115	2012-06-28-15	
	overview, Ge, and Gd	XPS	After sputtering for 30 secs (total = 7.5 mins)	Bk 4, pg 115	2012-06-28-16	
	overview, Ge, and Gd	XPS	After sputtering for 30 secs (total = 8 mins)	Bk 4, pg 115	2012-06-28-17	
	overview, Ge, and Gd	XPS	After sputtering for 30 secs (total = 8.5 mins)	Bk 4, pg 115	2012-06-28-18	
	overview, Ge, and Gd	XPS	After sputtering for 30 secs (total = 9 mins)	Bk 4, pg 116	2012-06-28-19	
	overview, Ge, and Gd	XPS	After sputtering for 30 secs (total = 9.5 mins)	Bk 4, pg 116	2012-06-28-20	
	overview, Ge, and Gd	XPS	After sputtering for 30 secs (total = 10 mins)	Bk 4, pg 116	2012-06-28-21	End of Depth Profiling Experiment at 1200 K

Table 3B

Gd₅Ge₄ (010) Data List					
Date	Instr.	Purpose	Folder Name	File Name	Notes
6/14/2011-6/15/2011	SEM	Identifying the 5:3 thin plates on the Gd ₅ Ge ₄ (010) surface	jun1411	7-68-2a, 7-68-2b, 7-68-2c, 7-68-2d, 7-68-2001, 7-68-2003, 7-68-2004, 7-68-2006, 7-68-2008, 7-68-2011, 7-68-2013, 7-68-2014, 7-68-2015, 7-68-2018, 7-68-2019, 7-68-2021, 7-68-2023, 7-68-2026, 7-682a, 7-682b001, 7-682b003, 7-682b006, 7-682b008, 7-682b009, 7-682b010, 7-682b011	SEM images of the 5:3 thin plates on the 5:4 surface.
	SAM	Identifying the 5:3 thin plates on the Gd ₅ Ge ₄ (010) surface		7-68-2e, 7-68-2010_01, 7-68-2010_02, 7-68-2010y, 7-68-2010z, 7-68-2012_01, 7-68-2012_02, 7-682b005_01, 7-682b005_02, 7-682b005z	Gd-rich (red line) and Ge-poor (blue line) on the 5:3 thin plate.
	AES	Identifying the 5:3 thin plates on the Gd ₅ Ge ₄ (010) surface		All *.npl files	The 5:3 thin plates show the surface concentration to be Gd ₅ Ge ₃ .

Table 3B (Continue)

Date	Instr.	Purpose	Folder Name	File Name	Notes
8/2/2011-8/4/2011	SEM	What surface looks like after several cleaning cycles (Ar sputtering and 30 minute anneals at 900 K)	aug11	All *.tiff files, except a few for SAM	Lumps appeared on surface after a few cleaning cycles.
	SAM	What surface looks like after several cleaning cycles (Ar sputtering and 30 minute anneals at 900 K)		7-682d026_01, 7-682d026_02, 7-682d026i, 7-682ddaug	Did not show any surface concentration contrast between the lumps and the surface.
	AES	What surface looks like after several cleaning cycles (Ar sputtering and 30 minute anneals at 900 K)		All *.npl files	Showed the lumps to be Ge-rich and Gd-poor. Close to Gd ₃ Ge ₅ .
7/4/2012	SEM	Do we see lumps on sample # dls-7-68-2?	dls-7-68-2	All *.tiff files	No lumps on surface.
	AES	Do we see lumps on sample # dls-7-68-2?		All *.npl files	The 5:3 thin plates show the surface concentration to be Gd ₅ Ge ₃ .
8/2/2012	SEM	What surface looks like after one cleaning cycle (Ar sputtering and 30 minute anneals at 1200 K)	aug0212	All *.tiff files	More lumps appeared on surface.
	AES	What surface looks like after one cleaning cycle (Ar sputtering and 30 minute anneals at 1200 K)		All *.npl files	Showed the lumps to be Ge-rich and Gd-poor. Close to Gd ₃ Ge ₅ .

Table 3B (Continue)

Date	Instr.	Purpose	Folder Name	File Name	Notes
8/3/2012	SEM	What surface looks like after several cleaning cycles (Ar sputtering and 30 minute anneals at 1200 K)	aug0312	All *.tiff files	More lumps appeared on surface.
	AES	What surface looks like after several cleaning cycles (Ar sputtering and 30 minute anneals at 1200 K)		All *.npl files	Showed the lumps to be Ge-rich and Gd-poor. Close to Gd ₃ Ge ₅ .
8/6/2012	SEM	More cleaning cycles at 1200 K	aug0612	All *.tiff files	More lumps appeared on surface.
	AES	More cleaning cycles at 1200 K		All *.npl files	Showed the lumps to be Ge-rich and Gd-poor. Close to Gd ₃ Ge ₅ .

Table 4

Au on NiAl(110) Data List							
Date	Images / Spectrum	Instr.	Purpose	Au Coverage (Total Time)	Bk #, Page #	File Name	Notes
11/13/2009	M1 - M11	STM	Clean NiAl(110) surface	0	Bk 2, pg 23	111309	See big terraces and lots of pinning sites
	M12 - M20	STM	Au/NiAl(110) at 300 K	0.10 ML (2 mins)	Bk 2, pg 24		Elongated islands, use 4-way Mantis evaporator (filament = 1.60 A, Power = 22 W)
	M21 - M25	STM	Continuing Au deposition at 300K	0.16 ML (4 mins)	Bk 2, pg 25		Big elongated islands on terraces, see Au on step edges. The step edges are more of a scalloped pattern.
	M26 - M30	STM	Continuing Au deposition at 300K	0.54 ML (16 mins)	Bk 2, pg 25		2nd Au adlayer started to form, 1st adlayer not complete, step edges are decorated.
	M31 - M34	STM	Continuing Au deposition at 300K	(22 mins)	Bk 2, pg 25		Cannot get coverage, no good images.
	overview	XPS	Au/NiAl(110) at 300 K	(22 mins)	Bk 2, pg 25	11130901	1000 eV to -5 eV (Steps -0.5 eV, 1 Sweep)
	Au 4f _{7/2, 5/2}	XPS	Au/NiAl(110) at 300 K	(22 mins)	Bk 2, pg 25		100 eV to 75 eV (Steps -0.1 eV, 3 Sweeps)
	Ni 3p	XPS	Au/NiAl(110) at 300 K	(22 mins)	Bk 2, pg 25		80 eV to 60 eV (Steps -0.1 eV, 3 Sweeps)
	Al 2p	XPS	Au/NiAl(110) at 300 K	(22 mins)	Bk 2, pg 25		80 eV to 60 eV (Steps -0.1 eV, 3 Sweeps)

Table 4 (Continue)

Date	Images / Spectrum	Instr.	Purpose	Au Coverage (Total Time)	Bk #, Page #	File Name	Notes
11/19/2009	M1 - M6	STM	Clean NiAl(110) surface	0	Bk 2, pg 39	111909	Still have pinning sites, but better than before.
	M7 - M33	STM	Au/NiAl(110) at 300 K	0.24 ML (8 mins)	Bk 2, pg 40		Au elongated islands on terraces, decorated step edges, possible Au reconstruction happening.
	M34 - M50	STM	Continuing Au deposition at 300K	0.60 ML (16.5 mins)	Bk 2, pg 41		See possible Au reconstruction at different orientations on the islands.
	M51 - M56	STM	Continuing Au deposition at 300K	0.83 ML (24.5 mins)	Bk 2, pg 41		See no change compared to previous deposition, 2nd Au islands are more elongated while the 1st Au islands are more irregular shaped.
	M57 - M74	STM	Continuing Au deposition at 300K	1.3 ML (40.5 mins)	Bk 2, pg 41		1st adlayer is almost complete, 2nd adlayer is bigger - not as elongated as before, see possible Au reconstruction on both adlayers.

Table 4 (Continue)

Date	Images / Spectrum	Instr.	Purpose	Au Coverage (Total Time)	Bk #, Page #	File Name	Notes
11/20/2009	overview	XPS	Au/NiAl(110) at 300 K	1.3 ML (40.5 mins)	Bk 2, pg 42	11200901	1000 eV to -5 eV (Steps -0.5 eV, 1 Sweep)
	Au 4f _{7/2, 5/2}	XPS	Au/NiAl(110) at 300 K	1.3 ML (40.5 mins)	Bk 2, pg 42		100 eV to 75 eV (Steps -0.1 eV, 3 Sweeps)
	Ni 3p	XPS	Au/NiAl(110) at 300 K	1.3 ML (40.5 mins)	Bk 2, pg 42		80 eV to 60 eV (Steps -0.1 eV, 3 Sweeps)
	Al 2p	XPS	Au/NiAl(110) at 300 K	1.3 ML (40.5 mins)	Bk 2, pg 42		80 eV to 60 eV (Steps -0.1 eV, 3 Sweeps)
11/23/2009	M1 - M9	STM	Clean NiAl(110) surface	0	Bk 2, pg 49	112309	Clean surface, still see pinning sites, terraces are not huge as before but still good for experiment.
	M10 - M17	STM	Au/NiAl(110) at 300 K	0.24 ML (8 mins)	Bk 2, pg 49		
	M18 - M48	STM	Increasing temperature to 325 K	0.24 ML (8 mins)	Bk 2, pg 49		
	M49 - M75	STM	Holding temperature at 325 K	0.24 ML (8 mins)	Bk 2, pg 49		See different Au island heights at different bias conditions - indicating surface intermixing and surface alloying.
	M76 - M79	STM	Increasing temperature to 350 K	0.24 ML (8 mins)	Bk 2, pg 50		
	M80 - M115	STM	Holding temperature at 350 K	0.24 ML (8 mins)	Bk 2, pg 50		Constant Au island heights at different bias conditions - Au has already alloyed on the surface.
	M116 - M118	STM	Decreasing temperature to 300 K	0.24 ML (8 mins)	Bk 2, pg 50		

Table 4 (Continue)

Date	Images / Spectrum	Instr.	Purpose	Au Coverage (Total Time)	Bk #, Page #	File Name	Notes
11/24/2009	overview	XPS	Au/NiAl(110) at 300 K	0.24 ML (8 mins)	Bk 2, pg 51	11240901	1000 eV to -5 eV (Steps -0.5 eV, 1 Sweep)
	Au 4f _{7/2, 5/2}	XPS	Au/NiAl(110) at 300 K	0.24 ML (8 mins)	Bk 2, pg 51		100 eV to 75 eV (Steps -0.1 eV, 3 Sweeps)
	Ni 3p	XPS	Au/NiAl(110) at 300 K	0.24 ML (8 mins)	Bk 2, pg 51		80 eV to 60 eV (Steps -0.1 eV, 3 Sweeps)
	Al 2p	XPS	Au/NiAl(110) at 300 K	0.24 ML (8 mins)	Bk 2, pg 51		80 eV to 60 eV (Steps -0.1 eV, 3 Sweeps)
11/30/2009	M1	STM	Clean NiAl(110) surface	0	Bk 2, pg 61	113009	Still have some pinning sites.
	M2	STM	Clean NiAl(110) surface at 200 K	0	Bk 2, pg 61		
	M3 - M40	STM	Au/NiAl(110) at 200 K	0.24 ML (8 mins)	Bk 2, pg 61 - 62		Island density increased compared to 300 K, islands are more elongated compared to 300 K data.
12/1/2009	overview	XPS	Au/NiAl(110) at 300 K	0.24 ML (8 mins)	Bk 2, pg 62	12010901	1000 eV to -5 eV (Steps -0.5 eV, 1 Sweep)
	Au 4f _{7/2, 5/2}	XPS	Au/NiAl(110) at 300 K	0.24 ML (8 mins)	Bk 2, pg 62		100 eV to 75 eV (Steps -0.1 eV, 3 Sweeps)
	Ni 3p	XPS	Au/NiAl(110) at 300 K	0.24 ML (8 mins)	Bk 2, pg 62		80 eV to 60 eV (Steps -0.1 eV, 3 Sweeps)
	Al 2p	XPS	Au/NiAl(110) at 300 K	0.24 ML (8 mins)	Bk 2, pg 62		80 eV to 60 eV (Steps -0.1 eV, 3 Sweeps)

Table 4 (Continue)

Date	Images / Spectrum	Instr.	Purpose	Au Coverage (Total Time)	Bk #, Page #	File Name	Notes
12/4/2009	overview	XPS	Au/NiAl(110) at 300 K	0.54 ML (16 mins)	Bk 2, pg 70	12040901	1000 eV to -5 eV (Steps -0.5 eV, 1 Sweep)
	Ni 2p	XPS	Au/NiAl(110) at 300 K	0.54 ML (16 mins)	Bk 2, pg 70		880 eV to 830 eV (Steps -0.1 eV, 10 Sweeps)
	Al 2s	XPS	Au/NiAl(110) at 300 K	0.54 ML (16 mins)	Bk 2, pg 70		130 eV to 100 eV (Steps -0.1 eV, 10 Sweeps)
	Au 4f7/2, 5/2	XPS	Au/NiAl(110) at 300 K	0.54 ML (16 mins)	Bk 2, pg 70		100 eV to 75 eV (Steps -0.1 eV, 10 Sweeps)
	Ni 3p	XPS	Au/NiAl(110) at 300 K	0.54 ML (16 mins)	Bk 2, pg 70		80 eV to 60 eV (Steps -0.1 eV, 10 Sweeps)
	Al 2p	XPS	Au/NiAl(110) at 300 K	0.54 ML (16 mins)	Bk 2, pg 70		80 eV to 60 eV (Steps -0.1 eV, 10 Sweeps)
	overview	XPS	Increased temperature to 325 K and hold for XPS	0.54 ML (16 mins)	Bk 2, pg 71	12040902	1000 eV to -5 eV (Steps -0.5 eV, 1 Sweep)
	Ni 2p	XPS	Increased temperature to 325 K and hold for XPS	0.54 ML (16 mins)	Bk 2, pg 71		See shift, indicating surface intermixing and surface alloying.
	Al 2s	XPS	Increased temperature to 325 K and hold for XPS	0.54 ML (16 mins)	Bk 2, pg 71		See shift, indicating surface intermixing and surface alloying.

Table 4 (Continue)

Date	Images / Spectrum	Instr.	Purpose	Au Coverage (Total Time)	Bk #, Page #	File Name	Notes
12/4/2009	Au 4f _{7/2, 5/2}	XPS	Increased temperature to 325 K and hold for XPS	0.54 ML (16 mins)	Bk 2, pg 71	12040902	See shift, indicating surface intermixing and surface alloying.
	Ni 3p	XPS	Increased temperature to 325 K and hold for XPS	0.54 ML (16 mins)	Bk 2, pg 71		See shift, indicating surface intermixing and surface alloying.
	Al 2p	XPS	Increased temperature to 325 K and hold for XPS	0.54 ML (16 mins)	Bk 2, pg 71		See shift, indicating surface intermixing and surface alloying.
	overview	XPS	Increased temperature to 350 K and hold for XPS	0.54 ML (16 mins)	Bk 2, pg 71	12040903	Little shift change.
	Ni 2p	XPS	Increased temperature to 350 K and hold for XPS	0.54 ML (16 mins)	Bk 2, pg 71		Little shift change.
	Al 2s	XPS	Increased temperature to 350 K and hold for XPS	0.54 ML (16 mins)	Bk 2, pg 71		Little shift change.
	Au 4f _{7/2, 5/2}	XPS	Increased temperature to 350 K and hold for XPS	0.54 ML (16 mins)	Bk 2, pg 71		Little shift change.
	Ni 3p	XPS	Increased temperature to 350 K and hold for XPS	0.54 ML (16 mins)	Bk 2, pg 71		Little shift change.
Al 2p	XPS	Increased temperature to 350 K and hold for XPS	0.54 ML (16 mins)	Bk 2, pg 71	Little shift change.		

Table 4 (Continue)

Date	Images / Spectrum	Instr.	Purpose	Au Coverage (Total Time)	Bk #, Page #	File Name	Notes
12/9/2009	M1 - M11	STM	Clean surface of NiAl(110)	0	Bk 2, pg 77	120909	
	M12 - M26	STM	Au on NiAl(110) at 300 K	0.24 ML (8 mins)	Bk 2, pg 78		
	M27 - M38	STM	Increasing temperature to 310 K	0.24 ML (8 mins)	Bk 2, pg 78		
	M39 - M59	STM	Holding temperature at 310 K	0.24 ML (8 mins)	Bk 2, pg 78		Tip is dirty, island heights are constant at different bias conditions.
	M60 - M63	STM	Increasing temperature to 320 K	0.24 ML (8 mins)	Bk 2, pg 79		
	M64 - M86	STM	Holding temperature at 320 K	0.24 ML (8 mins)	Bk 2, pg 79		Island heights are constant at different bias conditions...tip not good.
	M87 - M89	STM	Increasing temperature to 330 K	0.24 ML (8 mins)	Bk 2, pg 79		
	M90 - M115	STM	Holding temperature at 330 K	0.24 ML (8 mins)	Bk 2, pg 80		Island heights are constant at different bias conditions...tip dirty/not good.
	M116 - M117	STM	Increasing temperature to 340 K	0.24 ML (8 mins)	Bk 2, pg 80		
	M118 - M142	STM	Holding temperature at 340 K	0.24 ML (8 mins)	Bk 2, pg 80		Island heights are constant at different bias conditions...tip dirty/not good.
	M143 - M144	STM	Increasing temperature to 350 K	0.24 ML (8 mins)	Bk 2, pg 81		
	M145 - M166	STM	Holding temperature at 350 K	0.24 ML (8 mins)	Bk 2, pg 81		Did not see any height difference because tip is dirty and not good quality.

Table 4 (Continue)

Date	Images / Spectrum	Instr.	Purpose	Au Coverage (Total Time)	Bk #, Page #	File Name	Notes
12/10/2009	overview	XPS	Au/NiAl(110) at 300 K	0.24 ML (8 mins)	Bk 2, pg 82	12100901	1000 eV to -5 eV (Steps -0.5 eV, 1 Sweep)
	Au 4f7/2, 5/2	XPS	Au/NiAl(110) at 300 K	0.24 ML (8 mins)	Bk 2, pg 82		100 eV to 75 eV (Steps -0.1 eV, 3 Sweeps)
	Ni 3p	XPS	Au/NiAl(110) at 300 K	0.24 ML (8 mins)	Bk 2, pg 82		80 eV to 60 eV (Steps -0.1 eV, 3 Sweeps)
	Al 2p	XPS	Au/NiAl(110) at 300 K	0.24 ML (8 mins)	Bk 2, pg 82		80 eV to 60 eV (Steps -0.1 eV, 3 Sweeps)

Table 5

Ag on NiAl(110) and Au on NiAl(110) Data List (Switzerland)						
Date	Images / Spectrum	Instr.	Purpose	Lab #, Page #	File Name	Notes
2/23/2012	overview, Ni, and Al	XPS	Sample check	Bk 4, pg 54	ARPES120223N001-004	Before XPD.
	Ni 3p, Ni AES, and Al 2s	XPD	Sample check	Bk 4, pg 54	ARPES120223N005-007	See Al and Ni patterns.
2/24/2012	overview	XPS	Sample check	Bk 4, pg 55	ARPES120224N001	After XPD.
	M1 - M18	STM	Surface Check	Bk 4, pg 56	20120224	Have step-terrace morphology, terraces are small though.

Table 5 (Continue)

Date	Images / Spectrum	Instr.	Purpose	Lab #, Page #	File Name	Notes
2/28/2012	M1 - M4	STM	After Ag deposition (e-beam) [3.08 V x 2.912 A = 9 W] for 30 secs	Bk 4, pg 58	20120228	Have step-terrace morphology. See no Ag islands.
	M5 - M9	STM	After Ag deposition (e-beam) [3.24 V x 2.767 A = 9 W] for 1 min (total = 1.5 mins)	Bk 4, pg 59		Still no Ag islands on terraces.
	M10 - end	STM	After Ag deposition (e-beam) [3.44 V x 2.872 A = 9.9 W] for 1 min (total = 2.5 mins)	Bk 4, pg 59		See Ag islands.
	overview, Ni, Al, and Ag	XPS	Prepare for XPD	Bk 4, pg 59	ARPES120228N001-008	Before XPD. See Ag intensity.
	Ni 3p, Ag 3d, and Al 2s	XPD	Running XPD experiment	Bk 4, pg 59	ARPES120228N009-011	No Ag pattern.
2/29/2012	overview	XPS	Post XPD	Bk 4, pg 59	ARPES120229N001	After XPD. See Ag intensity.

Table 5 (Continue)

Date	Images / Spectrum	Instr.	Purpose	Lab #, Page #	File Name	Notes
3/5/2012	M1 - M5	STM	After Ag deposition (7 W) for 1 min	Bk 4, pg 64	20120305	See Ag islands. Not enough for 1 BL. Need to deposit more.
	M6 - M13	STM	After Ag deposition (7.8 W) for 1 min (total = 2 mins)	Bk 4, pg 64		See Ag islands. Not enough for 1 BL.
	overview, Ni, Al, and Ag	XPS	Prepare for XPD	Bk 4, pg 64	ARPES120305N001-010	Before XPD. See Ag intensity.
	Ni 3p, Ag 3d, and Al 2s	XPD	Running XPD experiment	Bk 4, pg 64	ARPES120305N011-013	No Ag pattern.
3/6/2012	overview	XPS	Post XPD	Bk 4, pg 65	ARPES120306N001	After XPD. See Ag intensity.
	M1 - M6	STM	Post XPD	Bk 4, pg 65	20120306	See Ag islands as before. The step heights are the same as before XPD. Lots of small pits throughout surface - XPD damage.
3/7/2012	M1 - M21	STM	After Ag deposition (6.4 W) for 3 mins [0.61 ± 0.19 BL]	Bk 4, pg 66	20120307	See Ag islands, 1st BL not complete, see some 2nd BL islands as well. Ag coverage = 0.61 ± 0.19 BL.
	overview, Ni, Al, and Ag	XPS	Prepare for XPD	Bk 4, pg 66	ARPES120307N001-005	Before XPD, See Ag intensity.
	Ni 3p, Ag 3d, and Al 2s	XPD	Running XPD experiment	Bk 4, pg 66	ARPES120307N006-008	No Ag pattern.

Table 5 (Continue)

Date	Images / Spectrum	Instr.	Purpose	Lab #, Page #	File Name	Notes
3/8/2012	overview	XPS	Post XPD	Bk 4, pg 66	ARPES120308N001	After XPD. See Ag intensity.
	M1 - M12	STM	Post XPD	Bk 4, pg 67	20120308	See Ag islands as before. The step heights are the same as before XPD. Lots of small pits throughout surface - XPD damage.
3/14/2012	M1 - M14	STM	After Ag deposition (6.7 W) for 15 mins and then increased it to (7 W) for 5 mins [1.2 BL]	Bk 4, pg 69	20120314	First Ag BL completed, have lots of 2nd BL islands. Ag coverage = 1.2 BL.
	40 eV - 110 eV, 150 eV, and 200 eV	LEED	After STM	Bk 4, pg 69	20120314_AgNiAl	
	overview, Ni, Al, and Ag	XPS	Prepare for XPD	Bk 4, pg 69	ARPES120314N001-004	Before XPD. See Ag intensity.
	Ni 3p, Ag 3d, and Al 2s	XPD	Running XPD experiment	Bk 4, pg 70	ARPES120314N005-007	See Ag XPD pattern.
3/15/2012	overview	XPS	Post XPD	Bk 4, pg 70	ARPES120315N001	After XPD. See Ag intensity.

Table 5 (Continue)

Date	Images / Spectrum	Instr.	Purpose	Lab #, Page #	File Name	Notes
3/26/2012	M1 - M3	STM	After Ag deposition (5.5 W) for 10 mins	Bk 4, pg 75	20120326	See Ag islands, not enough though.
	M4 - M17	STM	After Ag deposition (7 W) for 8 mins [0.63 ± 0.28 BL]	Bk 4, pg 76		Ag coverage = 0.63 ± 0.28 BL.
	overview, Ni, Al, and Ag	XPS	Prepare for XPD	Bk 4, pg 76	ARPES120326N001-006	Before XPD. See Ag intensity.
	Ni 3p, Ag 3d, and Al 2s	XPD	Running XPD experiment	Bk 4, pg 76	ARPES120326N007-009	See Ag XPD pattern.
3/27/2012	overview	XPS	Post XPD	Bk 4, pg 76	ARPES120327N001-003	After XPD. See Ag intensity.
3/28/2012	M1	STM	After Ag deposition (5.6 W) for 30 mins	Bk 4, pg 78	20120328	Not enough Ag.
	M2 - M4	STM	After Ag depositon (6.2 W) for 30 mins	Bk 4, pg 78		Not enough Ag.
	M5	STM	After Ag depositon (6.7 W) for 30 mins	Bk 4, pg 79		Cannot tell! Having a hard time imaging.
	overview	XPS	After STM	Bk 4, pg 79	ARPES120328N001	Ag intensity was a little higher than on 3/14/12. Going to deposit more Ag.
	overview, Ni, Al, and Ag	XPS	After Ag deposition (6.7 W) for 15 mins. Prepare for XPD. [5 BL coverage, according to XPS]	Bk 4, pg 79	ARPES120328N002-005	Before XPD. See Ag intensity. Ag coverage = 5 BL.
	Ni 3p, Ag 3d, and Al 2s	XPD	Running XPD experiment	Bk 4, pg 79	ARPES120328N006-008	See Ag XPD pattern.

Table 5 (Continue)

Date	Images / Spectrum	Instr.	Purpose	Lab #, Page #	File Name	Notes
3/29/2012	overview	XPS	Post XPD	Bk 4, pg 79	ARPES120329N001-002	After XPD. See Ag intensity.
	M1 - M6	STM	After Au deposition (9.9 W) for 15 mins	Bk 4, pg 80	20120329	No Au islands.
	M7 - M8	STM	After Au deposition (10.3 W) for 15 mins	Bk 4, pg 80		No Au islands.
	M9 - M10	STM	After Au deposition (10.8 W) for 27 mins	Bk 4, pg 80		Not sure. STM is not co-operating.
	overview	XPS	After STM	Bk 4, pg 80	ARPES120329N003	No Au intensity.
	M11	STM	After Au deposition (12.1 W to 11.2 W) for 15 mins [resistance has changed]	Bk 4, pg 81	20120329	Not sure. STM is not co-operating.
	M12 - M13	STM	After Au deposition (12 W to 12.3 W) for 20 mins	Bk 4, pg 81		Not sure. STM is not co-operating.
	M14	STM	After Au deposition (12.7 W) for 15 mins	Bk 4, pg 81		Not sure. STM is not co-operating.

Table 5 (Continue)

Date	Images / Spectrum	Instr.	Purpose	Lab #, Page #	File Name	Notes
3/29/2012	overview	XPS	After STM	Bk 4, pg 81	ARPES120329N004	See a little Au intensity peak.
	M15	STM	After Au deposition (13 W to 13.5 W)	Bk 4, pg 81	20120329	Not sure. STM is not co-operating.
	40 eV - 110 eV, 150 eV, 200 eV, 250 eV, and 300 eV	LEED	After STM	Bk 4, pg 81	20120329_AuNiAl	
	overview, Ni, Au, and Al	XPS	Prepare for XPD	Bk 4, pg 82	ARPES120329N005-009	Before XPD. See Au intensity.
	Ni 3p, Au 4f, Al 2s, and Au 4d	XPD	Running XPD experiment	Bk 4, pg 82	ARPES120329N010-013	No Au pattern.
3/30/2012	overview	XPS	Post XPD	Bk 4, pg 82	ARPES120330N001-002	After XPD. See Au intensity.

Table 6

Ag on Oxidized NiAl(110) and O ₂ on Ag on Oxidized NiAl(110) Data List							
Date	Images / Spectrum	Instr.	Purpose	Ag Coverage (ML)	Bk #, Page #	File Name	Notes
5/26/2012	M1 - M20	STM	Clean NiAl(110)	0	Bk 4, pg 90	052612	Got big terraces.
	M21 - M32	STM	Oxidized NiAl(110)	0	Bk 4, pg 90		1200 L of oxygen exposure. P=1x10 ⁻⁶ mbar for 20 minutes at 600 K. Then annealed to 1200 K for 3.5 minutes.
6/2/2012	none	none	Start Ag/oxidized NiAl(110) experiment	0	Bk 4, pg 93	none	Expose 1200 L of oxygen. See 5/26/2012 for procedure.
	M1 - M26	STM	Oxidized NiAl(110)	0	Bk 4, pg 93	060212	(111) oxidized layer on NiAl(110).
	M27 - M83	STM	Finished Ag/oxidized NiAl(110) experiment	0.1 ML	Bk 4, pg 93		Mantis Evaporator, P = 17.2 W, Filament = 2.54 A for 1 minute.
6/3/2012	overview, Ag 3d, and Ag AES	XPS	Check to see if we have Ag on NiAl(110)	0.1 ML	Bk 4, pg 94	2012-06-03-01	Yes, very little peak of Ag.

Table 6 (Continue)

Date	Images / Spectrum	Instr.	Purpose	Ag Coverage (ML)	Bk #, Page #	File Name	Notes
6/5/2012	none	none	Start Ag/oxidized NiAl(110) experiment	0	Bk 4, pg 95	none	Expose 1200 L of oxygen. See 5/26/2012 for procedure.
	M1 - M24	STM	Oxidized NiAl(110)	0	Bk 4, pg 95	060512	See circular Ag islands moving from middle of terraces to the step edges or oxide channels.
	M25 - M89	STM	Finished Ag/oxidized NiAl(110) experiment	0.1 ML	Bk 4, pg 95		
6/6/2012	overview, Ag 3d, O 1s, Al 2p, and Ni 2p	XPS	Check	0.1 ML	Bk 4, pg 96	2012-06-06-01	
6/9/2012	none	none	Start O ₂ /Ag/oxidized NiAl(110) experiment	0	Bk 4, pg 96	none	Expose 1200 L of oxygen. See 5/26/2012 for procedure.
	M1 - M24	STM	Oxidized NiAl(110)	0	Bk 4, pg 96	060912	Ag islands moved quickly to the step edges.
	M25 - M107	STM	Ag deposition and another 100 L O ₂ exposure. End of experiment	0.1 ML	Bk 4, pg 98		
6/10/2012	overview, Ni 2p, O 1s, Ag 3d, and Al 2p	XPS	Check	0.1 ML	Bk 4, pg 99	2012-06-10-01	

ACKNOWLEDGEMENTS

I would like to express my sincere appreciation to Professor Patricia A. Thiel for her guidance, encouragement, tips and support throughout my graduate study. Thanking her for being a great mentor. I must also thank her for giving me the opportunity to do research in Switzerland. It was an enjoyable experience.

I would also like to thank all members, former and present, in Thiel research group, for their encouragements and advice. I especially enjoyed the friendly working environment.

I would like to thank Jim Anderegg for his technical assistance, advice, encouragements, and his collaboration. I would also like to thank Deborah L. Schlagel, William Yuhasz, and Thomas Lograsso for providing high quality intermetallic samples, including quasicrystals. Without any of them, I would not be able to complete my graduate study.

Finally, I wish to thank my parents, my brother, and my sister for their support and love they have given for boosting my confidence throughout my study.

This work was performed at the Ames Laboratory under contract number DE-AC02-07CH11358 with the U.S. Department of Energy. The document number assigned to this thesis/dissertation is IS-T3077.